

**GEOLOGY AND METAMORPHIC EVOLUTION OF THE  
INDIAN HEAD RANGE, A GRENVILLIAN INLIER  
IN WEST NEWFOUNDLAND**

**CENTRE FOR NEWFOUNDLAND STUDIES**

**TOTAL OF 10 PAGES ONLY  
MAY BE XEROXED**

**(Without Author's Permission)**

**GEE-WOONG SUNG, B.Sc.**







National Library  
of Canada

Acquisitions and  
Bibliographic Services Branch

395 Wellington Street  
Ottawa, Ontario  
K1A 0N4

Bibliothèque nationale  
du Canada

Direction des acquisitions et  
des services bibliographiques

395, rue Wellington  
Ottawa (Ontario)  
K1A 0N4

*Author: Université de*

*Author: Université de*

## NOTICE

The quality of this microform is heavily dependent upon the quality of the original thesis submitted for microfilming. Every effort has been made to ensure the highest quality of reproduction possible.

If pages are missing, contact the university which granted the degree.

Some pages may have indistinct print especially if the original pages were typed with a poor typewriter ribbon or if the university sent us an inferior photocopy.

Reproduction in full or in part of this microform is governed by the Canadian Copyright Act, R.S.C. 1970, c. C-30, and subsequent amendments.

## AVIS

La qualité de cette microforme dépend grandement de la qualité de la thèse soumise au microfilmage. Nous avons tout fait pour assurer une qualité supérieure de reproduction.

S'il manque des pages, veuillez communiquer avec l'université qui a conféré le grade.

La qualité d'impression de certaines pages peut laisser à désirer, surtout si les pages originales ont été dactylographiées à l'aide d'un ruban usé ou si l'université nous a fait parvenir une photocopie de qualité inférieure.

La reproduction, même partielle, de cette microforme est soumise à la Loi canadienne sur le droit d'auteur, SRC 1970, c. C-30, et ses amendements subséquents.

Canada

**GEOLOGY AND METAMORPHIC EVOLUTION OF THE INDIAN HEAD  
RANGE, A GRENVILLIAN INLIER IN WEST NEWFOUNDLAND**

by

© Gee-Woong Sung, B.Sc.

A thesis submitted to the school of Graduate  
Studies in partial fulfilment of the  
requirements for the degree of  
Master of Science

Department of Earth Sciences  
Memorial University of Newfoundland

February 1992

St. John's

Newfoundland





National Library  
of Canada

Acquisitions and  
Bibliographic Services Branch

395 Wellington Street  
Ottawa, Ontario  
K1A 0N4

Bibliothèque nationale  
du Canada

Direction des acquisitions et  
des services bibliographiques

395, rue Wellington  
Ottawa (Ontario)  
K1A 0N4

Author's Address

Author's Signature

The author has granted an irrevocable non-exclusive licence allowing the National Library of Canada to reproduce, loan, distribute or sell copies of his/her thesis by any means and in any form or format, making this thesis available to interested persons.

L'auteur a accordé une licence irrévocable et non exclusive permettant à la Bibliothèque nationale du Canada de reproduire, prêter, distribuer ou vendre des copies de sa thèse de quelque manière et sous quelque forme que ce soit pour mettre des exemplaires de cette thèse à la disposition des personnes intéressées.

The author retains ownership of the copyright in his/her thesis. Neither the thesis nor substantial extracts from it may be printed or otherwise reproduced without his/her permission.

L'auteur conserve la propriété du droit d'auteur qui protège sa thèse. Ni la thèse ni des extraits substantiels de celle-ci ne doivent être imprimés ou autrement reproduits sans son autorisation.

ISBN 0-315-78127-0

Canada

### ABSTRACT

The Indian Head Range (IHR), which forms an inlier in the western foreland of the Appalachian orogen in Newfoundland, is mainly underlain by an upper amphibolite facies to granulite facies metaplutonic complex. Granulite facies units have annealed, high strain fabrics and include metanorthosite, meta-lherzolite, metagabbro and noritic, dioritic, granitic and pelitic gneiss. They predate a less deformed, amphibolite facies, foliated hornblende granodiorite.

The IHR shows two distinct sets of ductile deformation fabric : (1) a relatively high strain group comprising gneissic to migmatitic rocks; and (2) a relatively lower strain group comprising foliated granitoids. This grouping is compatible with a subdivision made on the basis of grade of metamorphism, with the higher strain group possessing granulite facies assemblage and the lower strain group being characterized by amphibolite facies assemblages. Considering the relative ages of the units, it appears that two metamorphic events occurred in the IHR.

Rare aluminous-magnesian mineral assemblages, indicated by the phases sapphirine and kornerupine, occur in the pelitic gneiss, which forms km-scale inclusions in metagabbro and

screens between metagabbro and other gneissic plutonites.

Assemblages in the pelitic gneiss are subdivided into three groups. (1) Quartz-bearing assemblages consist of  $\text{qtz-opx-crd-sil-bio-pla-ilm/mt} \pm \text{spl} \pm \text{kfn} \pm \text{gnt} \pm \text{gdr} \pm (\text{crn})$ . Sapphirine-bearing assemblages are subdivided into an Al-rich assemblage (2)  $\text{spr-kfn-opx-crd-sil-bio-pla-ilm/mt} \pm \text{spl} \pm \text{rt}$ , and an Al-poor assemblage (3)  $\text{spr-opx-bio-pla-ilm/mt} \pm \text{spl} \pm \text{rt}$ . The sub-assemblage  $\text{spr-qtz}$  has not been observed. Reaction textures suggest the following metamorphic history. In quartz-bearing rocks, an early  $\text{crd-spl-high Al opx}$  (8.5-9.5 wt%  $\text{Al}_2\text{O}_3$ ) assemblage implies  $T \approx 900^\circ\text{C}$  and  $P \approx 6-8$  kbars. Subsequent breakdown of cordierite ( $\text{crd} = \text{opx-sil-qtz}$ ) and the reaction  $\text{opx-sil} = \text{gnt-qtz}$  imply  $T \approx 800^\circ\text{C}$  and  $P \approx 8-10$  kbars. In quartz-free rocks, the reaction  $\text{crd-spl} = \text{spr-opx}$  took place under similar P-T conditions. Korerupine replacement by the reaction  $\text{kfn} = \text{spr-crd-low Al opx}$  (5-7 wt%  $\text{Al}_2\text{O}_3$ ) implies much lower pressures (5-6 kbars) at similar T (750 - 800  $^\circ\text{C}$ ), indicating a quasi-isothermal synmetamorphic decompression event from 8-10 to 5-6 kbars.

Maximum P-T estimates for garnet-bearing assemblages using a variety of geothermobarometers are in the range  $8 \pm 1$  kbar and 780 - 880  $^\circ\text{C}$ , consistent with estimates from petrogenetic grids.

The P-T path inferred on the basis of petrogenetic grids



shows an initial period of cooling under isobaric (or possibly slightly increasing P) conditions from 900 to 800 °C, followed by nearly isothermal decompression from 8-10 to 5-6 kbars. One possible speculation is that such uplift may be attributed to tectonic transport during the Grenvillian orogeny.

The metamorphic conditions obtained from the IHR indicate a relatively higher P and T than results from the Long Range Inlier and the Disappointment Hill Complex, other Grenville basement inliers in western Newfoundland. However, there is a consistent increase in P and T gradually from northeast to southwestern throughout the Long Range Inlier, as pointed out by Owen and Erdmer (1989), and the data for the IHR fit this pattern.

### ACKNOWLEDGMENTS

I am grateful to Dr. Mason and Dr. Rivers, who are my supervisors, for numerous discussions and encouragement during the study. In fact, the study would not have been possible without their interest and patience.

Field work for this study was financed by a grant from Energy Mines & Resources Research (Canada) to R.A. Mason. Other support was from NSERC grants (to R.A. Mason and Toby Rivers) and from the School of Graduate Studies, Memorial University.

Finally, I wish to thank the staff of the Department of Earth Sciences, Memorial University of Newfoundland. A special thanks is extended to my friends, Mi-Jung, Steven, Gunter, Jereon and David.

# CONTENTS

	page
ABSTRACT .....	ii
ACKNOWLEDGEMENTS .....	v
CONTENTS .....	vi
LIST OF TABLES .....	x
LIST OF FIGURES .....	xi
ABBREVIATIONS.....	xviii
 CHAPTER 1 INTRODUCTION .....	 1
1.1 Purpose .....	1
1.2 Approach employed .....	4
1.3 Regional setting .....	5
1.4 Location, Previous work and General geology....	8
1.4.1 Location .....	8
1.4.2 Previous work .....	8
1.4.3 General geology .....	11
 CHAPTER 2 DESCRIPTION OF LITHOLOGIC UNITS .....	 18
2.1 Unit 1: Pelitic gneiss .....	18
2.2 Unit 2: Noritic gneiss .....	25
2.3 Unit 3: Metagabbro .....	30
2.4 Unit 4: Anorthosite .....	35
2.5 Unit 5: Dioritic gneiss .....	42



2.6	Unit 6: Lherzolite .....	47
2.7	Unit 7: Variably foliated Bt granite .....	49
2.8	Unit 8: Foliated Hb granodiorite .....	57
2.9	Unit 9: Pegmatitic dykes .....	60
2.10	Unit 10: Mafic dyke .....	62
CHAPTER 3 <b>DEFORMATION</b> .....		65
3.1	Introduction .....	65
3.2	Brittle deformation .....	66
3.3	Ductile deformation .....	68
3.4	Discussion .....	81
CHAPTER 4 <b>METAMORPHISM</b> .....		83
4.1	Metamorphic character .....	83
4.1.1	Greenschist facies metamorphism .....	84
4.1.2	Amphibolite facies metamorphism .....	84
4.1.3	Granulite facies metamorphism .....	90
4.2	Sapphirine and Kornerupine-bearing rocks .....	94
4.2.1	Introduction .....	94
4.2.2	Petrography .....	96
4.2.2.1	Sillimanite forming reaction textures...	99
4.2.2.2	Sapphirine forming reaction textures...	102
4.2.2.3	Garnet forming reaction textures .....	107
4.2.2.4	Kornerupine replacement reaction textures...	110
4.2.3	Mineral chemistry .....	113
4.2.4	Metamorphic reactions and projections...	130

4.2.5	P-T conditions during mineral	
	reactions	....140
CHAPTER 5	INDEPENDENT GEOTHERMOBAROMETRY	.....151
5.1	Introduction	.....151
5.2	Mineral assemblage	.....153
5.2.1	Orthopyroxene-Clinopyroxene	.....153
5.2.2	Garnet-Biotite	.....156
5.2.3	Garnet-Plagioclase- $\text{Al}_2\text{SiO}_5$ -Quartz	.....159
5.2.4	Garnet-Orthopyroxene	.....166
5.2.5	Garnet-Hornblende	.....167
5.3	Geothermometry	.....170
5.3.1	Garnet-Biotite Geothermometry	.....170
5.3.2	Clinopyroxene-Orthopyroxene	
	Geothermometry	.....171
5.3.3	Garnet-Orthopyroxene Geothermometry	.....172
5.3.4	Garnet-Hornblende Geothermometry	.....173
5.4	Geobarometry	.....174
5.4.1	Garnet-Plagioclase- $\text{Al}_2\text{SiO}_5$ -Quartz	
	Geobarometry	.....175
5.4.2	Garnet-Orthopyroxene-Plagioclase-quartz	
	Geobarometry	.....175
5.5	Results of Geothermobarometry	.....177
5.5.1	Geothermometry	.....177
5.5.2	Geobarometry	.....184

CHAPTER 6 DISCUSSION AND TECTONIC IMPLICATIONS .....	189
6.1 Discussion .....	189
6.2 Tectonic implications of the P-T path.....	194
6.3 Correlation with the Long Range Inlier .....	197
REFERENCE .....	200
APPENDIXES .....	211
Appendix 1 Staining Method.....	211
Appendix 2 Microprobe Analytical Procedure	
and Mineral Analyses ...	214
2-1 Biotite .....	216
2-2 Clinopyroxene .....	221
2-3 Hornblende .....	226
2-4 Plagioclase .....	230
2-5 Orthopyroxene .....	234
2-6 Garnet .....	243
Appendix 3 Geothermobarometry .....	253



## TABLES

	Page
Table 1 : Representative microprobe analyses and structural formulae of sapphirine.....	115
Table 2 : Representative microprobe analyses and structural formulae of kornerupine.....	118
Table 3 : Representative microprobe analyses and structural formulae of orthopyroxene.....	120
Table 4 : Representative microprobe analyses and structural formulae of cordierite.....	122
Table 5 : Representative microprobe analyses and structural formulae of spinel and sillimanite..	124
Table 6 : Representative microprobe analyses and structural formulae of additional minerals.....	126
Table 7 : Temperature estimates from the opx-cpx thermometer in metagabbro and dioritic gneiss of the Indian Head Range.....	178
Table 8 : Temperature estimates (for 8 kbar) from garnet-orthopyroxene thermometer in mafic rocks of the Indian Head Range.....	180
Table 9 : Temperature estimates (for 8 kbar) from garnet-biotite thermometers in the noritic gneiss of the Indian Head Range.....	181
Table 10: Temperature estimates from garnet-hornblende thermometer in the metagabbro of the Indian Head Range.....	183
Table 11: Pressure estimates (for 800°C) from garnet-sillimanite-plagioclase-quartz barometer in the pelitic gneiss of the Indian Head Range....	185
Table 12: Compositional parameters and pressure estimates (for 800°C) from orthopyroxene-garnet-plagioclase-quartz barometers in pelitic gneiss of the Indian Head Range.....	187

# FIGURES

	Page
Figure 1. Map shows distribution of Grenville basement inliers in the Appalachian orogen (after Hatcher, 1983).....	2
Figure 2. Simplified geological map of part of western Newfoundland showing that basement rocks in the IHR were involved in Paleozoic thrusting (after Cawood and Williams, 1988).....	6
Figure 3. Topography of the southern part of the Indian Head Range looking towards St. Georges Bay from middle of the range.....	9
Figure 4. Topography of the Indian Head area looking east from the western side of Port Harmon.....	9
Figure 5. Simplified geological sketch map of the southern part of the Indian Head Range.....	13
Figure 6. Field photograph of sapphirine and the kornerupine-bearing pelitic gneiss showing concentration of kornerupine (brown) and sapphirine (blue color) in folded pelitic layer .....	19
Figure 7. Field photograph of the sapphirine-bearing pelitic gneiss showing sapphirine aggregates (blue) associated with leucosomes.....	19
Figure 8. Photomicrograph showing aggregate of fine grained sapphirine (center and bottom left of photomicrograph) in biotite-rich pelitic gneiss.....	23
Figure 9. Photomicrograph showing porphyroblast of kornerupine enclosed by fine-grained sillimanite and orthopyroxene.....	23
Figure 10. Field photograph showing outcrop of strongly deformed noritic gneiss.....	26
Figure 11. Photograph of representative hand specimen of noritic gneiss showing well-developed gneissic	

texture.....	28
Figure 12. Photomicrograph showing representative texture of noritic gneiss.....	28
Figure 13. Field photograph showing an outcrop of the metagabbro.....	31
Figure 14. Photomicrograph showing granoblastic-polygonal texture of the metagabbro.....	31
Figure 15. Field photograph showing a xenolith of noritic gneiss in metagabbro. The xenolith is rimmed by a selvage composed of fine grained orthopyroxene.....	34
Figure 16. Field photograph showing the quarry in the anorthosite body looking east from Indian Head Park.....	36
Figure 17. Photograph of hand specimen of anorthosite showing grey subrounded plagioclase megacrysts in recrystallized fine grained milky plagioclase.....	38
Figure 18. Photomicrograph of thin section of specimen shown in Fig.17, showing plagioclase phenocryst with bent lamellar twinning and undulose extinction, surrounded by subgrains of recrystallized plagioclase with mortar texture.	38
Figure 19. Field photograph showing orthopyroxene megacrysts up to 7 cm diameter in the anorthosite.....	41
Figure 20. Field photograph of the dioritic gneiss showing subhorizontal high strain layering.....	43
Figure 21. Photograph showing hand specimen of the dioritic gneiss from outcrop in Fig. 20.....	44
Figure 22. Photomicrograph showing recrystallized granoblastic-polygonal texture of melanocratic part in the dioritic gneiss.....	44
Figure 23. Field photograph showing part of a large ultramafic boudin of lherzolitic composition that occurs in the high strain zone composed principally of the dioritic gneiss.....	48



Figure 24.	Modal Quartz-K-feldspar-Plagioclase plot (Streckeisen, 1976) of the granitoid lithologies in the Indian Head Range.....	50
Figure 25.	Field photograph showing weakly foliated biotite granite.....	51
Figure 26.	Field photograph showing outcrop of the strongly deformed biotite granite with a single straight layering .....	51
Figure 27.	Photomicrograph showing mesoperthite (stained yellow) and biotite (center of photograph) in a recrystallized sample of the variably foliated biotite granite.....	54
Figure 28.	Photomicrograph of the variably foliated biotite granite showing a variety of textures..	54
Figure 29.	Field photograph showing Fe-Ti oxide rich bands (principally ilmenite) in the variably foliated biotite granite.....	56
Figure 30.	Photograph of a hand specimen of hornblende granodiorite showing anastomosing foliation defined by hornblende.....	58
Figure 31.	Photomicrograph of representative hornblende granodiorite.....	58
Figure 32.	Photomicrograph of hand specimen of pegmatitic dike showing graphic texture which consists of coarse K-feldspar and quartz.....	61
Figure 33.	Field photograph showing undeformed mafic dike with columnar jointing cutting the anorthosite.....	63
Figure 34.	Photomicrograph of mafic dike showing subophitic olivine grains and small laths of plagioclase.....	63
Figure 35.	Field photograph showing the effects of late brittle fractures in the metagabbro.....	67
Figure 36.	Simplified structural map of the southern Indian Head Range showing the distribution of units, orientation of foliation and location of high strain zones.....	70

- Figure 37. Field photograph showing continuous compositional layering and streaked-out mafic tectonic augen in straight dioritic gneiss.....73
- Figure 38. Field photograph showing streaked-out boudin of pegmatitic dike in strongly deformed biotite granite.....73
- Figure 39. Stereonet plots.  
 A : Stereogram showing lower hemisphere equal area projection of contoured poles to foliations from two shear zones in the southern part of the Indian Head Range.  
 B : Stereogram showing lower hemisphere equal area projection of stretching lineations from two shear zones in the southern part of the Indian Head Range.....76
- Figure 40. A: Field photograph demonstrating sinistral shear sense of ductile deformation in the noritic gneiss from the shape of elongated orthopyroxene porphyroclasts.  
 B: Photograph demonstrating shear sense of ductile deformation in the anorthosite from deformed orthopyroxene aggregates.....79
- Figure 41. Field photograph showing greenschist facies chlorite-epidote assemblage on fractures in the anorthosite.....85
- Figure 42. Photomicrograph showing partial corona of amphibole around clinopyroxene in the dioritic gneiss.....87
- Figure 43. Photomicrograph showing orthopyroxene partly replaced by amphibole in noritic gneiss.....87
- Figure 44. Photomicrograph showing amphibolite facies mineral assemblage in the metagabbro.....89
- Figure 45. Photomicrograph of the metagabbro showing typical granoblastic polygonal texture exhibited by plagioclase.....91
- Figure 46. Photomicrograph of the variably foliated biotite granite showing granoblastic texture with sutured grain boundaries.....91
- Figure 47. Photomicrograph showing mineral reaction

texture of cordierite breakdown to (orthopyroxene + sillimanite) symplectite and quartz.....	100
Figure 48. Photomicrograph showing replacement of cordierite + spinel by (orthopyroxene + sillimanite)symplectite.....	100
Figure 49. Photomicrograph showing corona texture of fine grained sapphirine in plagioclase surrounding a porphyroblast of orthopyroxene.....	103
Figure 50. Photomicrograph showing sapphirine corona around orthopyroxene with magnetite and orthopyroxene.....	103
Figure 51. Photomicrograph showing orthopyroxene and Fe-spinel(hercynite-magnetite) reaction to produce Mg-spinel and sapphirine.....	105
Figure 52. Photomicrograph showing orthopyroxene and sapphirine symplectite produced by reaction of cordierite-spinel assemblage. ....	105
Figure 53. Photomicrograph showing various inclusion phases (sillimanite, magnetite/ilmenite, spinel, orthopyroxene and biotite) in garnet poikiloblast in pelitic gneiss.....	108
Figure 54. Photomicrograph showing garnet poikiloblast with various inclusion phases (sillimanite, orthopyroxene and ilmenite/ilmenite).....	108
Figure 55. Photomicrograph showing replacement of porphyroblast of kornerupine by orthopyroxene andsapphirine.....	111
Figure 56. Photomicrograph showing kornerupine reacting to the assemblage orthopyroxene, cordierite, andsapphirine.....	111
Figure 57. Mineral compositions of pelitic gneiss in the Indian Head Range plotted on the (Mg.Fe)O -Al <sub>2</sub> O <sub>3</sub> -SiO <sub>2</sub> diagram.....	114
Figure 58. Molecular proportions of Al vs. Si (per 10 oxygen formula unit) in sapphirines from pelitic gneiss in the Indian Head Range.....	116

- Figure 59. Representative biotite compositions from the pelitic gneiss in the Indian Head Range plotted in  $\text{Al}+\text{Fe}^{3+}+\text{Ti} - \text{Mg} - \text{Fe}^{2+}+\text{Mn}$  diagram...128
- Figure 60. (F.M)-A-S and AFM diagrams constructed from measured mineral compositions showing reactions involving cordierite deduced from textural relationships.....132
- Figure 61. AFM diagram constructed using measured mineral compositions showing phase relations for sapphirine forming reaction (4).....134
- Figure 62. (F.M)-A-S and AFM diagrams constructed from measured mineral compositions showing phase relations for garnet forming reactions.....136
- Figure 63. AFM diagrams constructed from measured mineral compositions showing phase relations for kornerupine replacement reactions.....139
- Figure 64. Partial P-T grid for phase relations in the FMAS system for high  $f\text{O}_2$  conditions (after Hensen 1986).....143
- Figure 65. Comparison of the stability field of Boron-free kornerupine (after Seifert 1975) with the  $\text{Al}_2\text{SiO}_5$  phase diagram (after Holdaway 1971)....147
- Figure 66. Partial P-T path in the reaction grid.....148
- Figure 67. Photomicrograph showing equilibrium textural relationships between orthopyroxene, clinopyroxene and plagioclase in the dioritic gneiss.....154
- Figure 68. Partial ternary diagram of orthopyroxene compositions from different mineral assemblages plotted in  $(\text{Fe.Mg})\text{O}$ ,  $\text{CaO}$ ,  $\text{Al}_2\text{O}_3$  composition space.....155
- Figure 69. Compositions of coexisting orthopyroxene-clinopyroxene in the metagabbro and dioritic gneiss.....155
- Figure 70. Photomicrograph showing garnet porphyroblast wrapped by the biotite matrix in noritic gneiss.....157

Figure 71. Photomicrograph showing equilibrium textural relationship between garnet and biotite in noritic gneiss.....	157
Figure 72. Core to rim compositional profiles for Fe in garnet coexisting with biotite and orthopyroxene from noritic gneiss in the Indian Head Range.....	160
Figure 73. Core to rim compositional profiles for Mg in garnet coexisting with biotite and orthopyroxene from noritic gneiss in the Indian Head Range.....	161
Figure 74. Core to rim compositional profiles of the ratio $Mg/(Mg+Fe)$ in garnet coexisting with biotite and orthopyroxene from noritic gneiss in the Indian Head Range.....	162
Figure 75. Feldspar ternary diagram showing the range of plagioclase compositions from the pelitic gneiss and dioritic gneiss in the Indian Head Range.....	163
Figure 76. Photomicrograph showing the textural relationship between garnet with blebby inclusions of sillimanite and adjacent orthopyroxene.....	164
Figure 77. Photomicrograph showing garnet porphyroblast with orthopyroxene corona in plagioclase matrix.....	164
Figure 78. Garnet compositions from the Indian Head Range plotted on 10Ca-Mg-Fe and 10Mn-Mg-Fe ternary diagrams.....	168
Figure 79. P-T-time trajectory from reaction grids showing successive metamorphic conditions.....	193
Geological Map and Sample Location Map.....	in pocket

# ABBREVIATIONS

The following abbreviations are used in this study.

ab	: albite component in plagioclase
alm	: almandine component in garnet
an	: anorthite component in plagioclase
bt	: biotite
crd	: cordierite
crn	: corundum
cpx	: clinopyroxene
en	: enstatite
fs	: ferrosilite
ged	: gedrite
gr	: grossular component in garnet
gnt	: garnet
hbl	: hornblende
IHR	: Indian Head Range
ilm	: ilmenite
Kfs	: K-feldspar
krr	: kornepurine
mag	: magnetite
or	: orthoclase
opx	: orthopyroxene
pl	: plagioclase
prp	: pyrope component in garnet
qtz	: quartz
spr	: sapphirine
sil	: sillimanite
sps	: spessartine component in garnet
spil	: spinel
wo	: wollastonite
$a_j$	: activity of component j in phase i
$\gamma_j$	: activity coefficient (component j in phase i)
$x_j$	: molar proportion of component j in phase i
$X_{Mg}$	: $Mg/Mg+Fe$
$X_{Fe}$	: $Fe/Mg+Fe$
$X_{Ca}$	: $Ca/Ca+Fe+Mg+Mn$
Fe	: total Fe as $Fe^{2+}$

## CHAPTER 1

### INTRODUCTION

#### 1-1 PURPOSE

The study is concerned with the bedrock geology of the Indian Head Range in western Newfoundland, and with the estimation of the metamorphic conditions and metamorphic history of the principal lithologies.

The Indian Head Range is an inlier of Precambrian crystalline rocks in western Newfoundland, and is one of several such bodies which form a prominent chain of massifs along the western margin of the Appalachian Orogen (Hatcher 1983) (Fig. 1). The inliers are generally considered to be the southern extension of the Grenville Province, which is situated along the southeastern margin of the exposed Canadian Shield. Several Grenvillian basement inliers occur in western Newfoundland and they form a topographic high known as the Long Range Mountains. The largest of these inliers, the Long Range Inlier (Fig. 1) exposes a high grade plutono-metamorphic complex that has recently been shown to have a prolonged and complex geological history (Owen 1991), and it

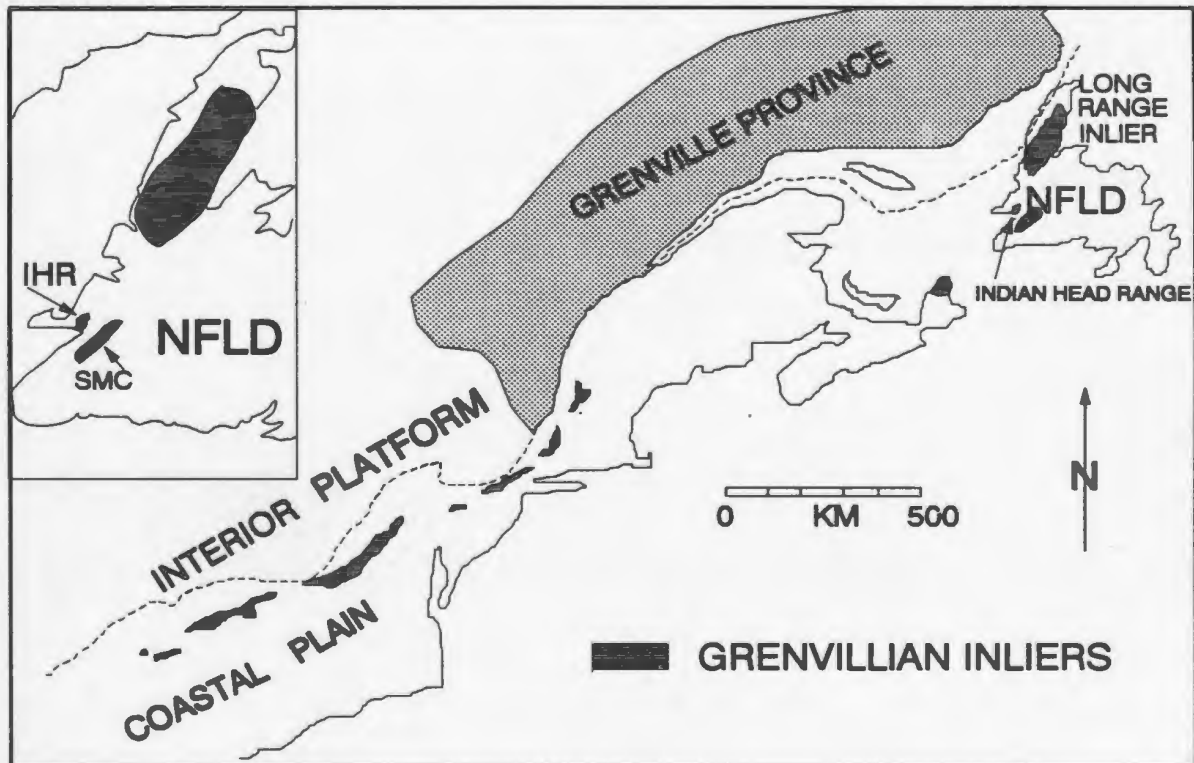


Figure 1. Map shows distribution of Grenville basement inliers in the Appalachian orogen (after Hatcher, 1983).

Dashed line: northwest limit of the Appalachian orogen.

IHR: Indian Head Range, SMC: Steel Mountain Complex



is the aim of this study to provide comparable data for the Indian Head Range.

Recently, several studies of the Precambrian inliers in the Appalachian orogen have shed light on the metamorphic and deformational effects of the Grenvillian and earlier orogenic events, and also on the later effects of the Appalachian orogeny. Presumed Grenvillian basement has recently been identified in several areas of the southwestern Long Range Mountains in Newfoundland (e.g. the Disappointment Hill complex within the Steel Mountain terrane, see van Berkel 1987, Currie 1987) and, also in northern Cape Breton Island, Nova Scotia (Barr et al., 1987). These studies have demonstrated that each inlier is individually distinct in terms of lithology, age, structural history and grade of metamorphism.

This thesis is subdivided in the following manner. Chapter 1 gives an overview of the regional setting and general geology of the Indian Head Range. Description and discussion of the lithological and structural character of the map units are presented in detail in chapters 2 and 3. Chapter 4 is concerned with metamorphism of the study area. Special attention is paid to the sapphirine and kornerupine-bearing assemblages from aluminous magnesian pelitic gneisses,

which preserve evidence of the mineral reactions that took place during the metamorphic evolution of the area, and these are described and discussed in detail. Metamorphic conditions are constrained through use of available petrogenetic grids on the basis of the interpretation of the mineral reactions. In Chapter 5, independent estimates of pressure and temperature are made by geothermobarometry utilizing the analyzed compositions of coexisting minerals, and the results are compared with the estimates made from the petrogenetic grid. In Chapter 6, an attempt is made to integrate the geology and metamorphic conditions to infer a synmetamorphic P-T path for the Indian Head Range. Finally, comparisons with adjacent inliers, including the Long Range Inlier and the Disappointment Hill complex, are made.

#### 1-2 APPROACH EMPLOYED

The study area was mapped at a 1:12,500 scale during the summer of 1990, with an additional short field season in 1991 to check critical outcrops. Most mapping was done by foot traverse. About 400 representative samples from different rock types were collected and 200 thin sections were made for petrographic study, mineral analysis with the electron microprobe and geothermobarometric calculations. About 40 hand

specimens and 30 thin sections were stained for K-feldspar with sodium cobaltinitrite following the method recommended by Bailey and Stevens (1960) and Norman (1974) in order to aid lithological classification. Quantitative P-T estimates of metamorphic conditions are based on various published geothermobarometers in the computer program P-T Calc of Mengel (1987).

### 1-3 REGIONAL SETTING

The Indian Head Range, which is considered a part of the Long Range Mountains of western Newfoundland, is situated along the western margin of the Appalachian orogen, and is interpreted as an inlier of Grenvillian crystalline basement rocks reworked during the Appalachian orogen.

In terms of its structural relationships with the surrounding younger Paleozoic rocks, the inlier occupies the core of an anticline that developed in the hanging-wall of a west-directed Acadian thrust, and the eastern margin of the inlier is marked by an east-directed back thrust (Cawood and Williams, 1988) as shown in the simplified cross-section in Fig. 2.

The interpretation that the inlier is a part of the

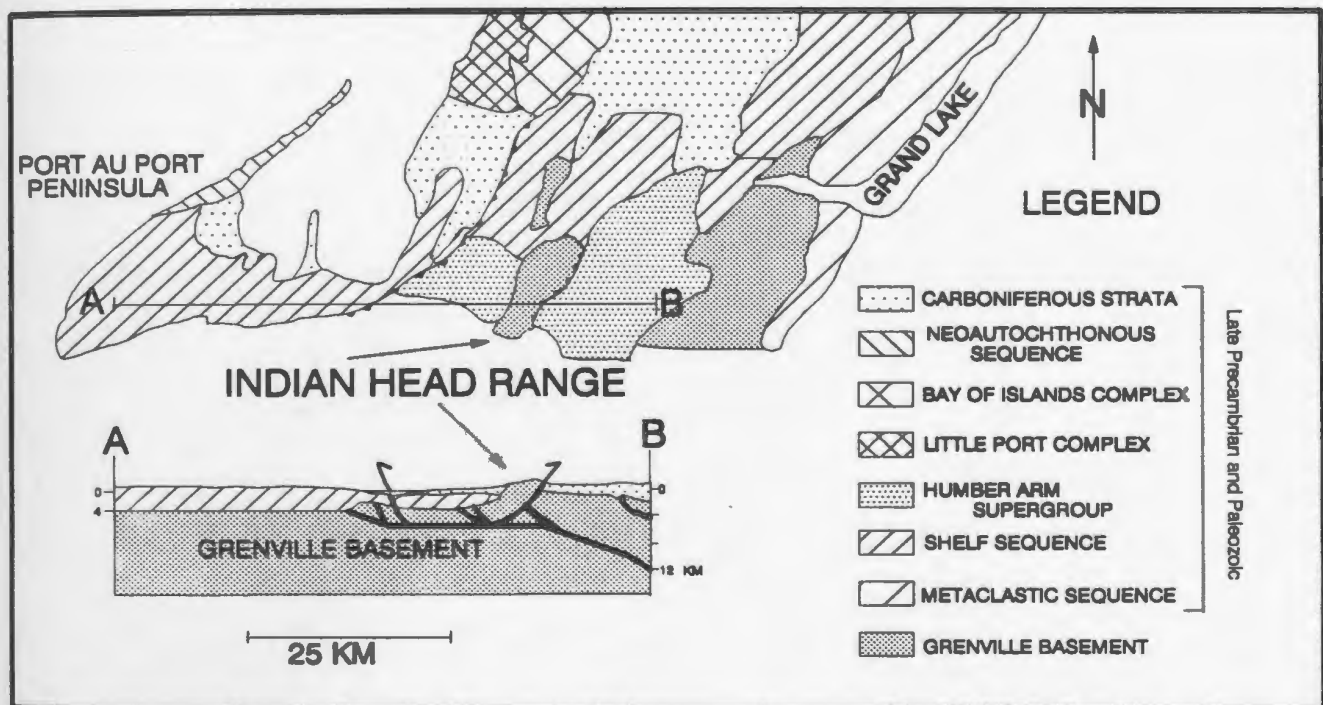


Figure 2. Simplified geological map of part of western Newfoundland (after Cawood and Williams 1988) showing that basement rocks in the IHR were involved in Paleozoic thrusting. Unexposed faults shown in cross-section were inferred from seismic data.

Grenville basement is based on the general lithological, deformational and metamorphic similarities with rocks of the Grenville Province in southern Labrador and with other inliers in the western margin of the Appalachian orogen (see Fig. 1). A Grenvillian age is supported by available K/Ar and Ar/Ar radiometric age dates of 825-900 Ma from rocks of the Indian Head Range (Lowden 1961, Lowden et al. 1963, Dallmeyer 1978). However, it is not clear which units in the area were dated and, in any case, it is likely that these are minimum ages, dating the time of cooling through the closure temperature of argon loss from the host minerals. This interpretation is reinforced by the recently reported U/Pb zircon ages of  $\approx$  1,500 Ma from granitoid rocks of the adjacent inlier, the Disappointment Hill complex (Owen and Currie 1991). Owen (1991) has also provided data indicating a 1550 Ma age from quartzfeldspathic gneiss of presumed igneous origin in the Long Range Inlier. Thus the available absolute age data for the study area are insufficient to constrain the geological history in terms of timing.

Therefore, for more detailed comparison with other inliers and with the Grenville Province itself, absolute age determinations are indispensable. U/Pb geochronological work is in progress for five of the units outlined in this study, in collaboration with Dr G.R. Dunning of Memorial University.

The results will be published separately.

#### **1-4 LOCATION, PREVIOUS WORK AND GENERAL GEOLOGY**

##### **1-4-1 Location**

The Indian Head Range is located approximately 6 km east of Stephenville, western Newfoundland and is bounded by latitudes  $48^{\circ}30'$  and  $48^{\circ}39'$  N, and longitudes  $55^{\circ}24'$  and  $55^{\circ}32'$  W. The range forms a ridge rising to approximately 600 m running inland in a NNE direction from St. George's Bay (Fig 3). A prominent valley occupied by Long Gull Pond divides the range into northern and southern portions. Indian Head, a promontory from which the range takes its name, extends about 2 km into St. George's Bay (Fig. 4). This thesis is concerned with the southern portion of the range, south of Long Gull Pond.

##### **1-4-2 Previous work**

There has been very little previous mapping and few reported geological studies in the Indian Head Range. Several mining companies conducted prospecting programmes for magnetite deposits prior to 1941. The Geological Survey of Newfoundland mapped the area and investigated the economic potential for

Figure 3. Topography of the southern part of the Indian Head Range looking towards St. Georges Bay from middle of the range.

Figure 4. Topography of the Indian Head area looking east from the western side of Port Harmon.





renewed iron mining in 1942, but the work was not published until after World War II (Heyl and Ronan 1954). Clifford and Baird (1962) also briefly noted the relationship between the Indian Head Range and the younger Paleozoic rocks. Colman-Sadd (1969) undertook an M.Sc. study on the genesis of the iron deposits (the Indian Head Mine, the Upper Drill Brook Mine, the Cliff Mine and the Skindles Mine) and the petrology of the country rocks in the area. Apart from the collection of samples for K/Ar and Ar/Ar age determination noted previously, there has been no further geological study since that date.

#### 1-4-3 General geology

The Indian Head Range consists principally of granulite facies rocks, and as with several other granulite facies terranes of the Grenville Province, it is dominated by the "anorthosite suite" (anorthosite and associated gabbroic/noritic gneiss and pyroxene-bearing granitoids), and contains volumetrically minor amounts of other rock types, in this case, pelitic gneiss. Even though the study area is relatively small, the range of lithological and metamorphic features of each unit in the Indian Head Range is similar to those of much larger granulite facies terranes associated with anorthosite suites elsewhere in terms of both mineral assemblages and metamorphic and deformational characters.

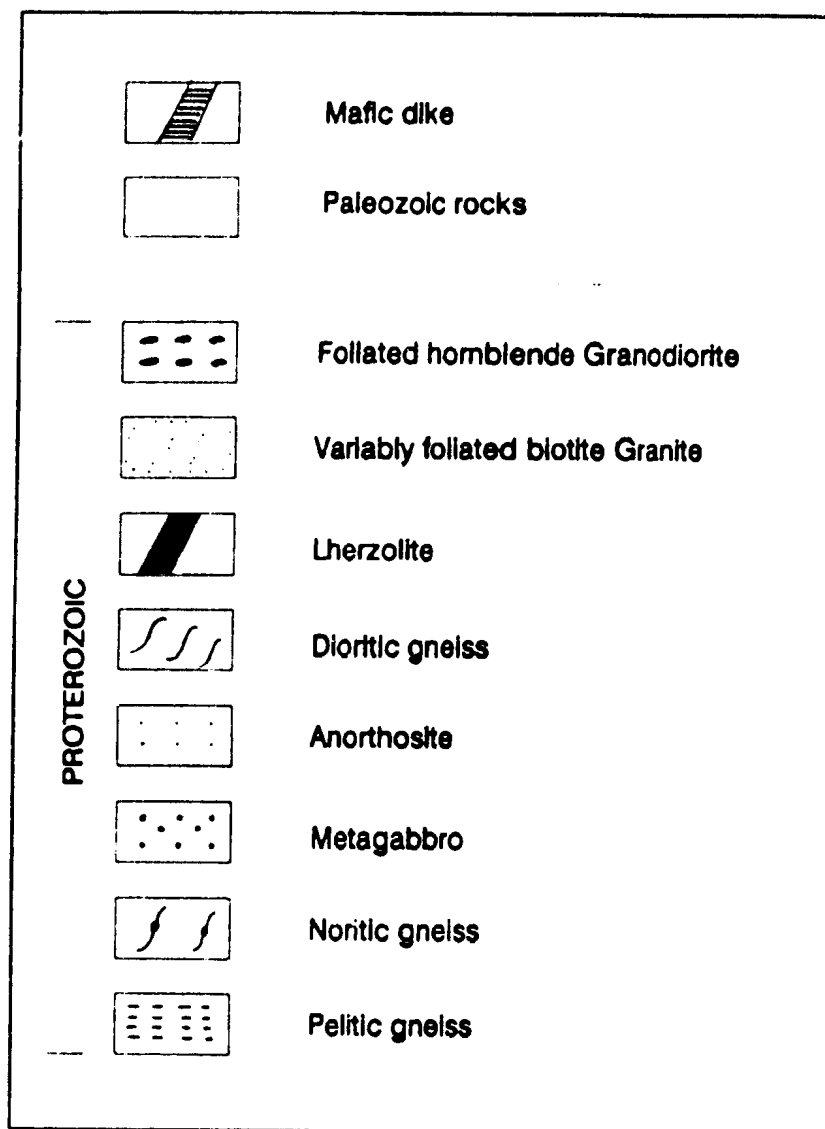
The geology of the southern part of the Indian Head Range is summarized in the geological sketch map (Fig. 5) and is shown in more detail on the accompanying 1: 12,500 scale map (in the pocket at the back of the thesis). Map units which are described in this study are defined on the basis of both their lithologic and structural character.

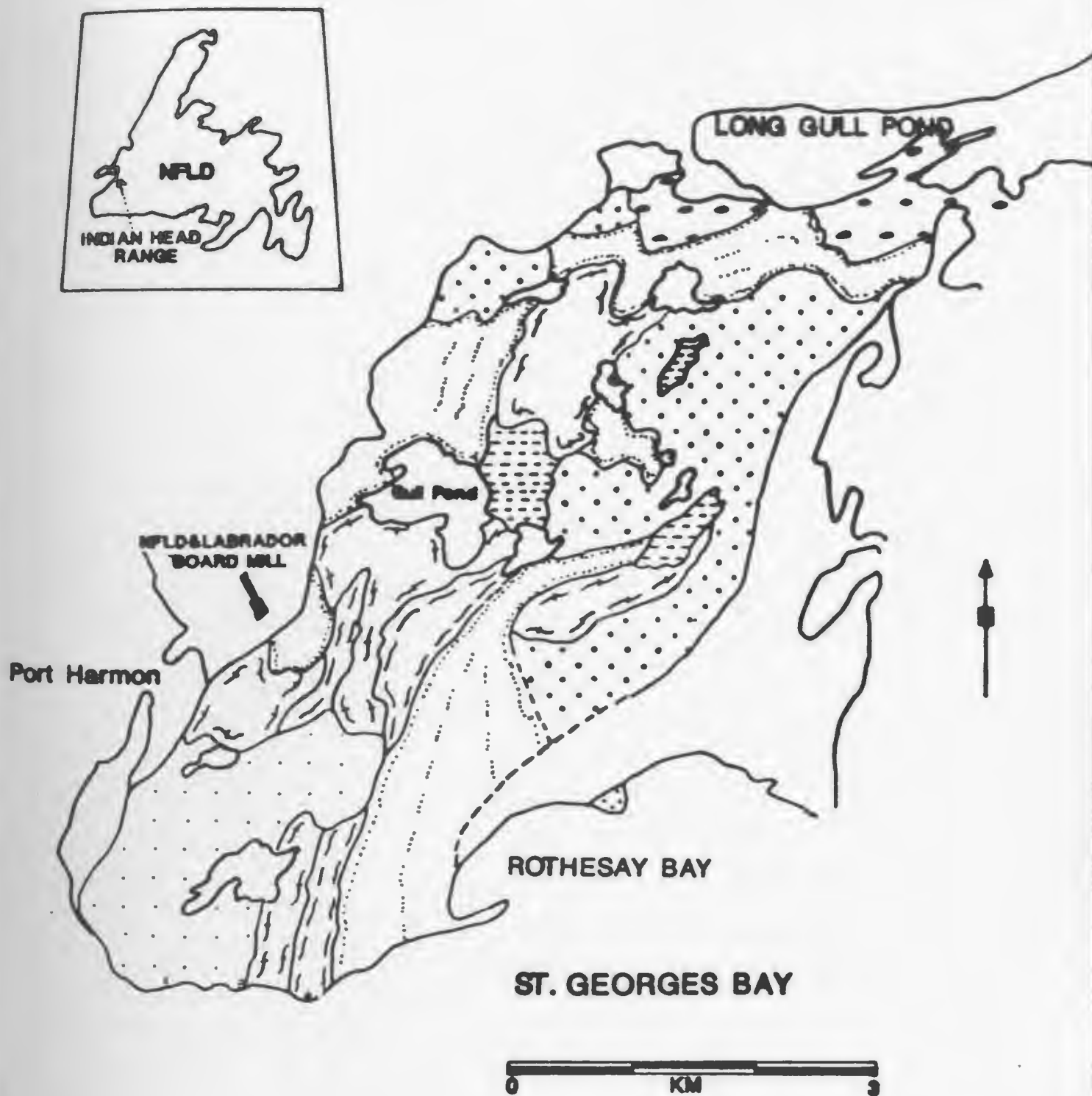
The study area consists of a variety of orthogneisses, including anorthosite, noritic gneiss, metagabbro, dioritic gneiss and meta-granitoids of two types: variably foliated biotite granite and foliated hornblende granodiorite. Minor areas of paragneiss (mostly metapelite) are exposed between the metagabbro and variably foliated biotite granite in the middle part of the study area and as lenses within the metagabbro. Lherzolite is exposed as a large (decimetric) scale boudin in the dioritic gneiss.

Paleozoic sedimentary cover rocks are locally exposed at the contact with the metagabbro and variably foliated biotite granite in the eastern part of the study area. The unconformable relationship between the Paleozoic sedimentary rocks and older high grade metamorphosed rocks has been described by others (see Cawood and Williams 1988).

The Indian Head Range forms a large (10's of km) scale elongate dome, of which the longer axis trends northeast, with

Figure 5. Simplified geological map of the southern part of the Indian Head Range.





the anorthosite body located near its center (Heyl and Ronan 1954). The dome is an Acadian (?) feature which is interpreted to have developed as the crystalline basement rocks became involved in west-directed thrusting. Imbrication of basement horses is interpreted to have caused the formation of a ramp anticline, which was later cut by easterly-directed back-thrusts that locally elevated the basement rocks into the level of the surrounding cover (Cawood and Williams 1988) (Figure 2). Outcrop scale effects of this Acadian deformation are manifest as widespread brittle fractures. In outcrop it can clearly be observed that the brittle fractures cut older ductile deformation fabrics in the Precambrian units. This ductile deformation is expressed as gneissosity, migmatitic layering and foliation. Although locally folded, the predominant trend of the ductile fabrics is also NNE, subparallel to the long axis of the dome, but it is not clear whether the fabric orientations in the basement controlled the orientation of superimposed structures during the Acadian(?) thrusting.

Two types of ductile deformation fabric can be distinguished. Gneissosity and migmatitic layering, developed mainly in mafic gneisses, are associated with granulite facies mineral assemblages and evidence of high strain is widespread. Foliated fabrics, on the other hand, occurring principally in the foliated hornblende granodiorite unit, formed under

relatively lower strain and are characterized by amphibolite facies mineral assemblages. The most prominent deformational features in the study area are two high strain zones up to 200 m wide formed in various types of mafic gneiss, hornblende and granitoid rocks adjacent to the anorthosite, that are interpreted as major shear zones. One is particularly well exposed along the coast line east of the anorthosite body, where it strikes NNE-SSW. The other shear zone, on the northwestern side of the anorthosite, strikes NE-SW.

In terms of relative age relationships as determined from field observations, the metagabbro, noritic gneiss and anorthosite are younger than the pelitic gneiss: enclaves of the latter occur locally in the metagabbro and noritic gneiss. The noritic gneiss is older than the metagabbro because xenoliths of the noritic gneiss are observed within the weakly deformed metagabbro. The relative age relationship between the variably foliated biotite granite and the mafic gneisses (including anorthosite) is obscured by deformation. However, a boudin (2-3 m length) of granitic composition, which is considered to be a deformed dike, is included in the dioritic gneiss. This relationship suggests that the mafic gneisses may be older than the variably foliated biotite granite. The foliated hornblende granodiorite is distinguished from other units in being significantly less deformed and also by its

amphibolite facies mineral assemblages. Contact relationships establish that this unit is younger than the metagabbro, noritic gneiss and variably foliated biotite granite. Small undeformed medium- to very coarse-grained pegmatitic dikes and sills of alkali feldspar granite composition (not shown in Fig. 5) are ubiquitous throughout the area and younger than all the other intrusive units except the Paleozoic mafic dikes. The latter are in part tentatively correlated with the Long Range dyke swarm, and are thus interpreted to have been emplaced about 615 Ma (Kamo et al. 1989). However, some bodies may be much younger (Jurassic ?) and associated with the opening of the present Atlantic.

The Indian Head Range has several small scale iron deposits noted above. Some of them were exploited commercially earlier this century. The Upper Drill Brook Mine and Skindles Mine, which are located north and east of Gull Pond, occur at the edge of the pelitic gneiss (unit 1). The Cliff Mine, which is located immediately to the north of Gull Pond, and the Indian Head Mine, which is located approximately 50 m east of the Newfoundland & Labrador Board Mill occur within the noritic gneiss (unit 2), near the contact with the variably foliated biotite granite (unit 7).

## CHAPTER 2

### DESCRIPTION OF LITHOLOGIC UNITS

This chapter includes field and hand sample descriptions of the map units, and chemical compositions for major mineral phases in all units except the pelitic gneiss. The mineral chemistry of the pelitic gneiss unit is discussed in detail in Chapter 4.

#### 2-1 Unit 1: Pelitic gneiss

This unit is exposed as several bodies in the study area, the largest of which occurs between the noritic gneiss and the variably foliated biotite granite in the northern central part of the area (Fig. 5). Several small inclusions and lenses of biotite psammite (1-2 cm in width) in the metagabbro and noritic gneiss are also assigned to this unit.

This unit comprises heterogeneous leucocratic to mesocratic pelitic (locally) to quartzofeldspathic gneisses.

The unit is commonly pale green or pale grey in outcrop and variable from porphyroblastic to granoblastic in texture. Segregations (from a few cm to tens cm of wide) into leucosome



Figure 6. Field photograph of sapphirine and the kornerupine-bearing pelitic gneiss showing concentration of kornerupine (brown) and sapphirine (blue color) in folded pelitic layer. Lens cap is 5 cm in diameter. Sample# : SA-B-1.

Figure 7. Field photograph of the sapphirine-bearing pelitic gneiss showing sapphirine aggregates (blue) associated with leucosomes. Brown mineral defining foliation is orthopyroxene. Sample# : SA-C.



and melanosome are generally developed, in particular, in quartzofeldspathic gneiss. The melanosomes consist mainly of orthopyroxene, biotite, plagioclase and rarely (in pelitic layers), sapphirine and coarse kornerupine (Fig. 6). Biotite is generally developed with sapphirine as fine-grained aggregates in the melanosomes. The leucosomes consist of quartz (in quartz-bearing rocks), fine-grained plagioclase, orthopyroxene and cordierite. Garnetiferous biotite-bearing gneiss is observed in a few outcrops. Fine-grained garnet, orthopyroxene and biotite show well developed layerings.

Sapphirine- and /or kornerupine-bearing assemblages occur in well-defined layers in some gneissic rocks (Fig. 6), presumably reflecting an (original sedimentary ?) layering of appropriate composition. Elsewhere, however, sapphirine forms nodules ranging from 2 to 5 cm in width and lacking preferred orientation. The origin of these features is not certain, but they appear to have been enhanced by leucosome segregations (Fig. 7).

The major minerals of this unit are quartz, plagioclase ( $An_{50}$ ), antiperthite, cordierite, sillimanite, biotite and orthopyroxene. Fresh plagioclase occurs locally, but cloudy, saussuritized grains are ubiquitous. Distorted twin lamellae of plagioclase are also observed. Green spinel, which is

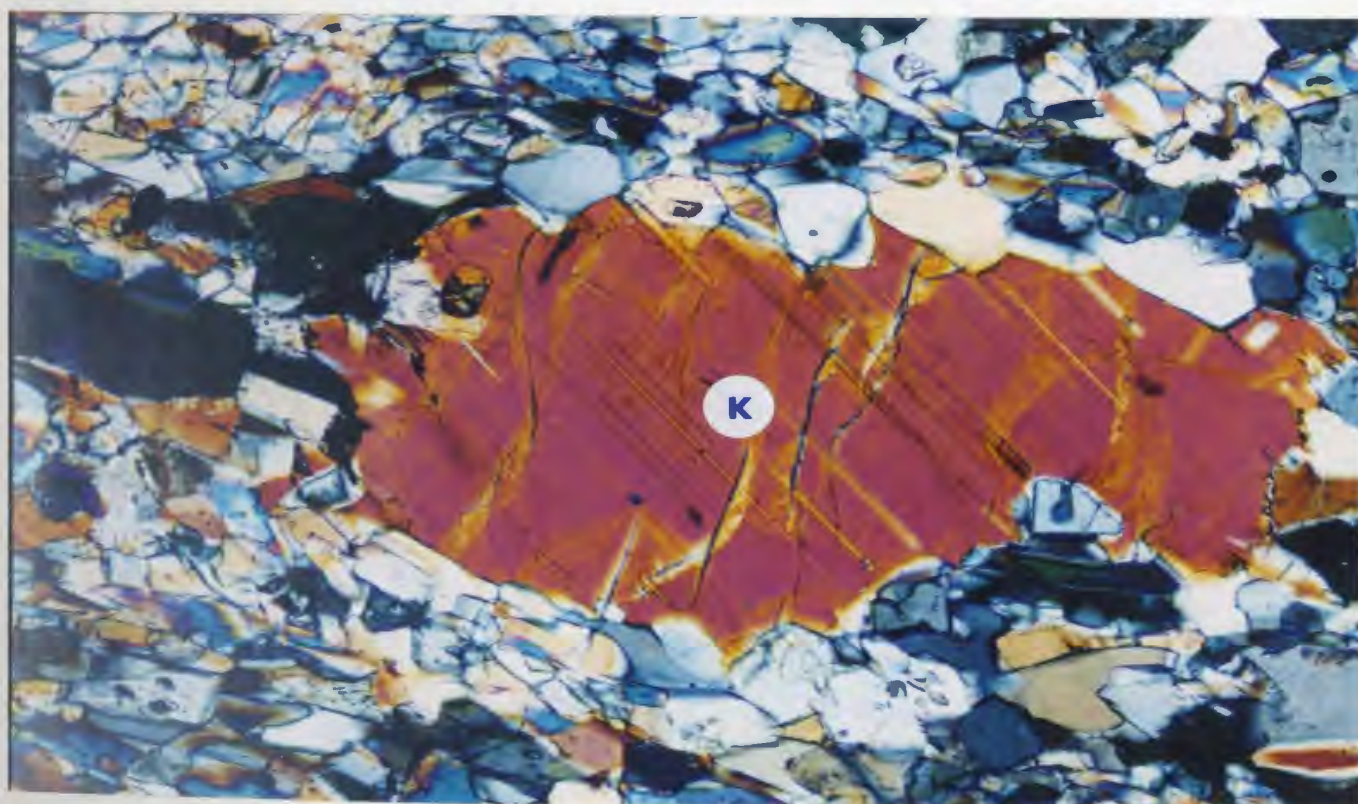
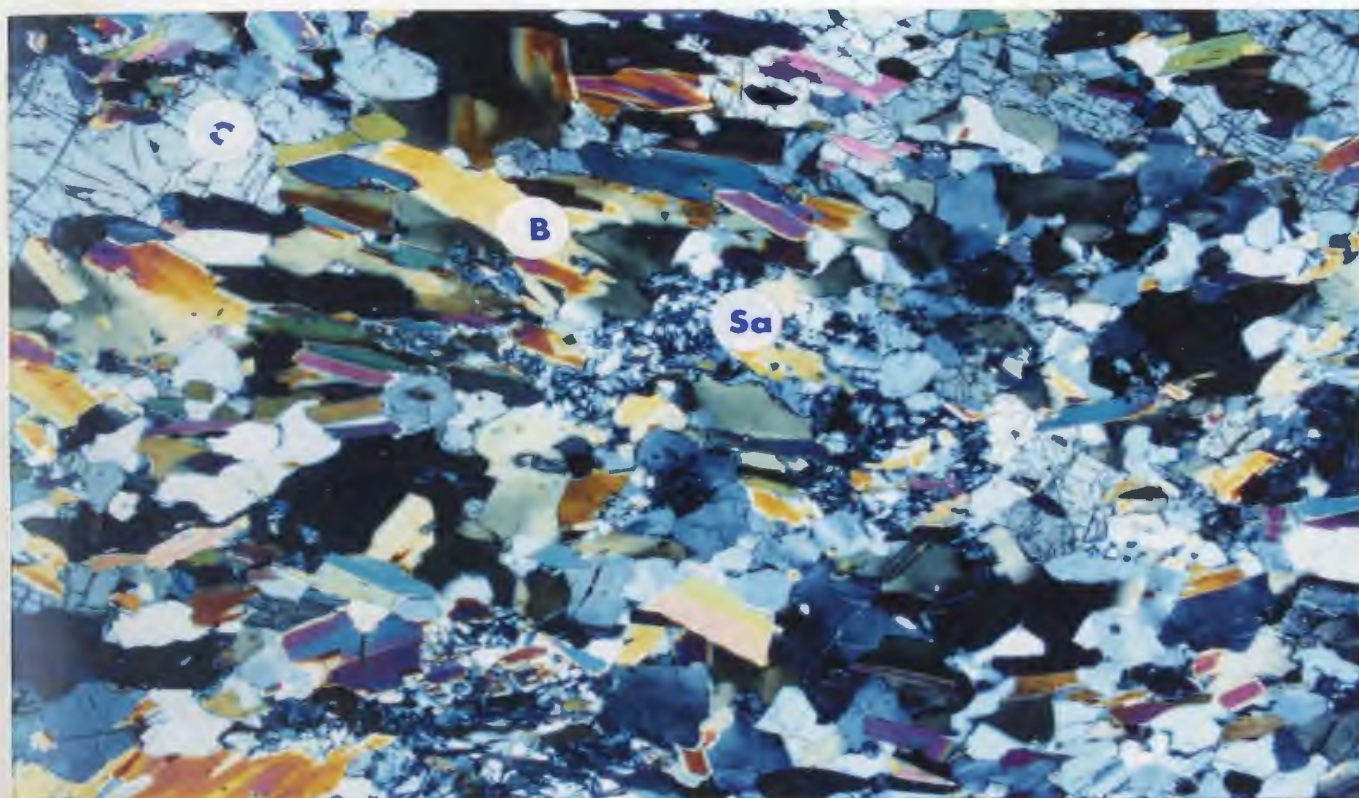
exsolved from Fe-Ti oxide, is found in sapphirine-bearing samples and is generally accompanied by accessory prismatic and fibrous sillimanite. Sillimanite is also present as rhombs and needles, and as coronas around composite magnetite/ilmenite grains. Cordierite occurs as relatively coarse grains which are associated with sillimanite and orthopyroxene. Sillimanite and orthopyroxene locally occur as symplectic intergrowths around cordierite. Sapphirine in some specimens consists entirely of intimately intergrown fine grains (Fig. 8), whereas in others there are isolated larger crystals (0.5 - 1 cm). The sapphirine is generally associated with orthopyroxene, kornerupine, magnetite/ilmenite and spinel either as corona phases or in symplectic intergrowth. Kornerupine occurs as porphyroblastic grains (Fig. 9) and is partially replaced by symplectites of sapphirine and orthopyroxene. Quartz does not develop in contact with sapphirine, but does occur with orthopyroxene, kornerupine and spinel.

It is difficult to determine the protolith of these rocks due to the lack of many primary features and whole rock chemical data. However, the presence of compositional layering in some outcrops, together with aluminous mineral assemblages including sapphirine, kornerupine, sillimanite and cordierite is consistent with a sedimentary origin.

Figure 8. Photomicrograph showing aggregate of fine grained sapphirine (center and bottom left of photomicrograph) in biotite-rich pelitic gneiss. Width of photomicrograph : 5.4 mm. Crossed polarized light. Sample# : S-22.  
O: orthopyroxene, B: biotite, Sa: sapphirine.

Figure 9. Photomicrograph showing porphyroblast of kornerupine enclosed by fine-grained sillimanite and orthopyroxene. Width of photomicrograph : 2.9 mm. Crossed polarized light. K: kornerupine.  
Sample# : SA-B-1.





### Age relations

Contacts between the pelitic gneiss and adjacent units have not been seen. However, several exposures in the noritic gneiss and metagabbro have the form of thin lenses, which are considered to be inclusions in these units, implying that the pelitic gneiss predated the noritic gneiss and metagabbro.

### 2-2 Unit 2: Noritic Gneiss

Noritic gneiss is mainly distributed around the anorthosite body in the southern part of the study area and is associated with metagabbro (unit 3) in the middle and northern part of the study area as shown in Fig. 5.

The unit is a strongly deformed meta-norite with gneissose fabric (Figs. 10 and 11). This dark to buff coloured rock shows compositional layering with layers of ultramafic composition ranging in width from a few mm to 20-30 cm alternating with leucocratic layers of anorthositic composition (Fig. 11). The ultramafic layers consist of elongate and subrounded deep-brown orthopyroxene, composite ilmenite/magnetite grains, and (locally) fine-grained pinkish brown garnet and biotite. Where magnetite/ilmenite and





Figure 10. Field photograph showing outcrop of strongly deformed noritic gneiss.



orthopyroxene are abundant, the rock has a light-brown weathering surface with well developed layering. The leucocratic bands consist of fine- to medium-grained plagioclase and fine-grained orthopyroxene, biotite and composite ilmenite/magnetite. The plagioclase occurs as both dark grey crystals up to a few mm across and as milky grey, finer grains. The milky grains appear to be recrystallized.

Plagioclase porphyroblasts have a wide range of composition (An <sub>42-63</sub>), commonly exhibit bent twin lamellae, and are set in a fine-grained granoblastic matrix apparently resulting from high strain deformation. The fine-grained plagioclase shows a similar variable range of composition (An <sub>38-60</sub>). Retrograde hornblende and biotite are locally developed around relatively coarse orthopyroxene grains. Orthopyroxene is bronzite (En <sub>82-75</sub>) in composition and shows reddish brown to deep green pleochroism (Fig. 12). Where present, garnet (almandine: 50-57, pyrope: 43-50) occurs principally as poikiloblastic weakly zoned crystals associated with orthopyroxene and biotite, and contains abundant biotite inclusions.

Amphibolite, consisting essentially of green hornblende and plagioclase, occurs locally in this unit as irregularly

Figure 11. Photograph of representative hand specimen of noritic gneiss showing well-developed gneissic texture. Brown bands consist of orthopyroxene and light colored bands consist principally of recrystallized fine grained plagioclase. Scale in cm. Sample# : S-63B.

Figure 12. Photomicrograph showing representative texture of noritic gneiss. Elongated coarse-grained orthopyroxene with typical brown-green pleochroism in the central part of the photomicrograph and fine-grained biotite in plagioclase rich-layers in the lower part of the photomicrograph. Width of photomicrograph : 8.8 mm. Plane polarized light. Sample# : S-63B.



shaped enclaves up to 20-30 cm in size. These have subangular forms in areas of relatively low strain. The foliation of the amphibolite is parallel to that of the surrounding noritic gneiss.

### Age relations

In the contact zone between the anorthosite and the noritic gneiss, intercalations of one into the other are common. They are interpreted to be the result of deformation. Igneous cross-cutting relationships have not been observed, and so the age relations between the two units has not been established.

### 2-3 Unit 3: Metagabbro

This unit mainly occupies the eastern part of the study area, with small bodies also being exposed in northwestern margin of the study area.

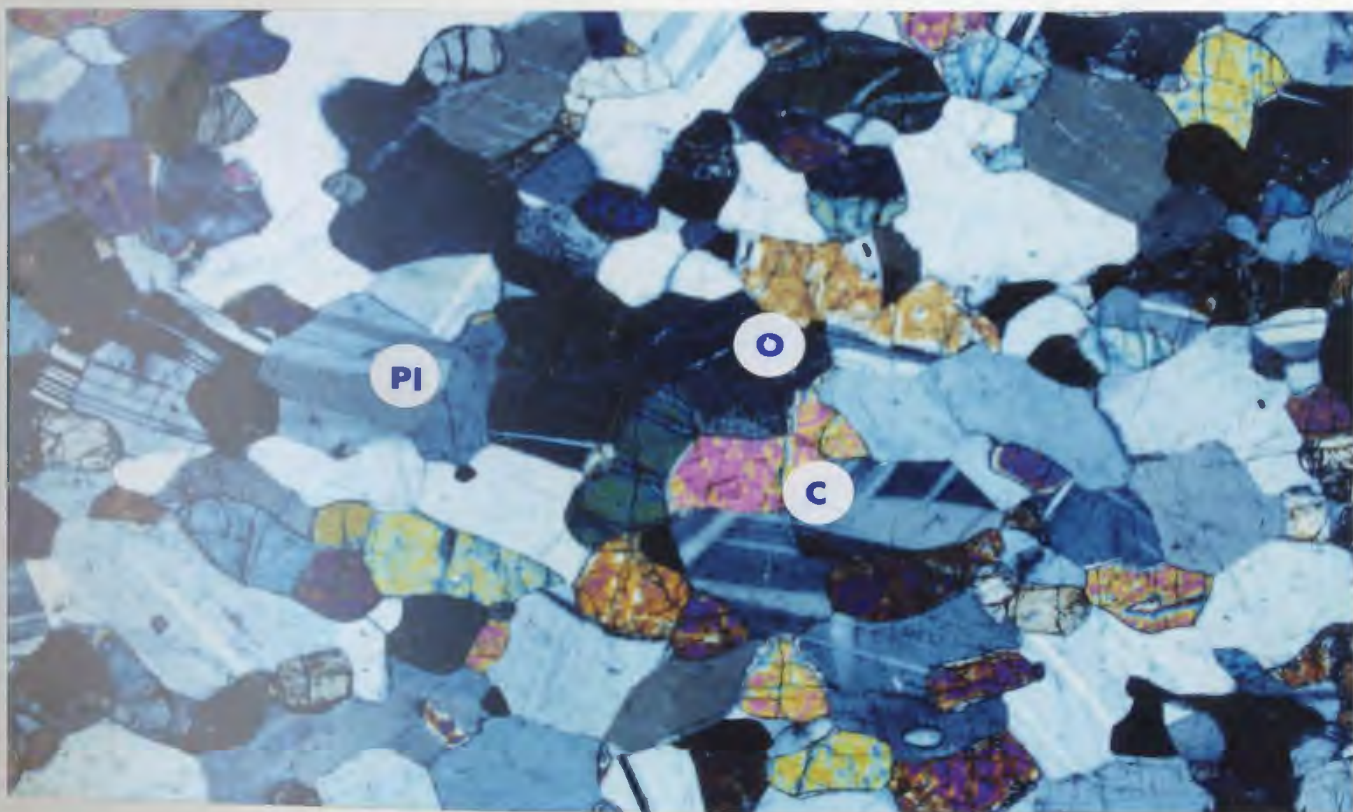
This unit differs from the noritic gneiss (unit 2) in being massive, having a fine grain size (1-3 mm) and containing abundant clinopyroxene. It represents a recrystallized and relatively homogeneous leucocratic gabbroic rock (Fig. 13). However, locally, fine compositional layering (up to few mm in width) consisting mainly of orthopyroxene and

Figure 13. Field photograph showing an outcrop of the metagabbro. Note: red weathering along fracture surfaces.

Figure 14. Photomicrograph showing granoblastic-polygonal texture of the metagabbro. Note : abundance of  $120^\circ$  triple point grain boundaries and recrystallized orthopyroxene, clinopyroxene and plagioclase. Width of photomicrograph : 5.4 mm. Crossed polarized light.

O: orthopyroxene, C: clinopyroxene, Pl: plagioclase. Sample# : S-7.





clinopyroxene is recognized on weathered surfaces. The unit is locally strongly fractured and stained red by oxidation along superimposed (presumably Paleozoic) fracture surfaces.

Microscopically, the metagabbro has a granoblastic-polygonal texture due to recrystallization, which appears to have eliminated any original igneous textures (Fig. 14). The dominant mineral assemblage is orthopyroxene + clinopyroxene + plagioclase with the ratio clinopyroxene/ (clinopyroxene + orthopyroxene) being about 0.4. Plagioclase, which is present as homogeneous equant grains, ranges in composition from An<sub>42-74</sub>. Orthopyroxene occurs as xenoblastic grains and is hypersthene (En<sub>64-56</sub>) in composition with pink to green pleochroism. Clinopyroxene occurs as both isolated crystals and as grains coexisting with orthopyroxene. Clinopyroxene ranges from Wo<sub>30</sub> En<sub>37</sub> Fs<sub>13</sub> to Wo<sub>44</sub> En<sub>28</sub> Fs<sub>28</sub> in composition. The pyroxenes are locally partly replaced by Ca-rich amphibole, but are usually fresh. Biotite and magnetite/ilmenite are common minor phases. The biotite contains a relatively high Ti content ( TiO<sub>2</sub> : up to 4.5 wt.%). Locally the apparently retrograde assemblage hornblende + garnet is developed. However, although two-pyroxene and hornblende + garnet assemblages occur, neither two-pyroxene-garnet nor





Figure 15. Field photograph showing a xenolith of noritic gneiss in metagabbro. The xenolith is rimmed by a selvage composed of fine grained orthopyroxene.



clinopyroxene-garnet occurrences are observed in this unit. Quartz (2-3 %) is relatively rare, but is common in samples from the contact zone with the granitoids, where it occurs as small anhedral crystals along plagioclase grain boundaries.

#### Age relations

The boundary between the noritic gneiss and metagabbro is gradational in the field so that the relative age relationship is obscure. However, xenoliths of the noritic gneiss within the undeformed metagabbro were observed at one locality (Fig. 15), implying that the unit postdates the noritic gneiss.

#### 2-4 Unit 4: Anorthosite

The anorthosite body forms the southwestern tip of the Indian Head Range. The best exposures are in the quarry which is located at the end of Indian Head (Fig. 16).

Coarse (up to 10-15 cm) to medium-grained, white to deep grey plagioclase of approximately An<sub>50-63</sub> composition accounts for more than 90 percent by the volume of this unit. Although the rocks generally exhibit a massive texture in outcrop, they also show evidence of significant ductile deformation, with



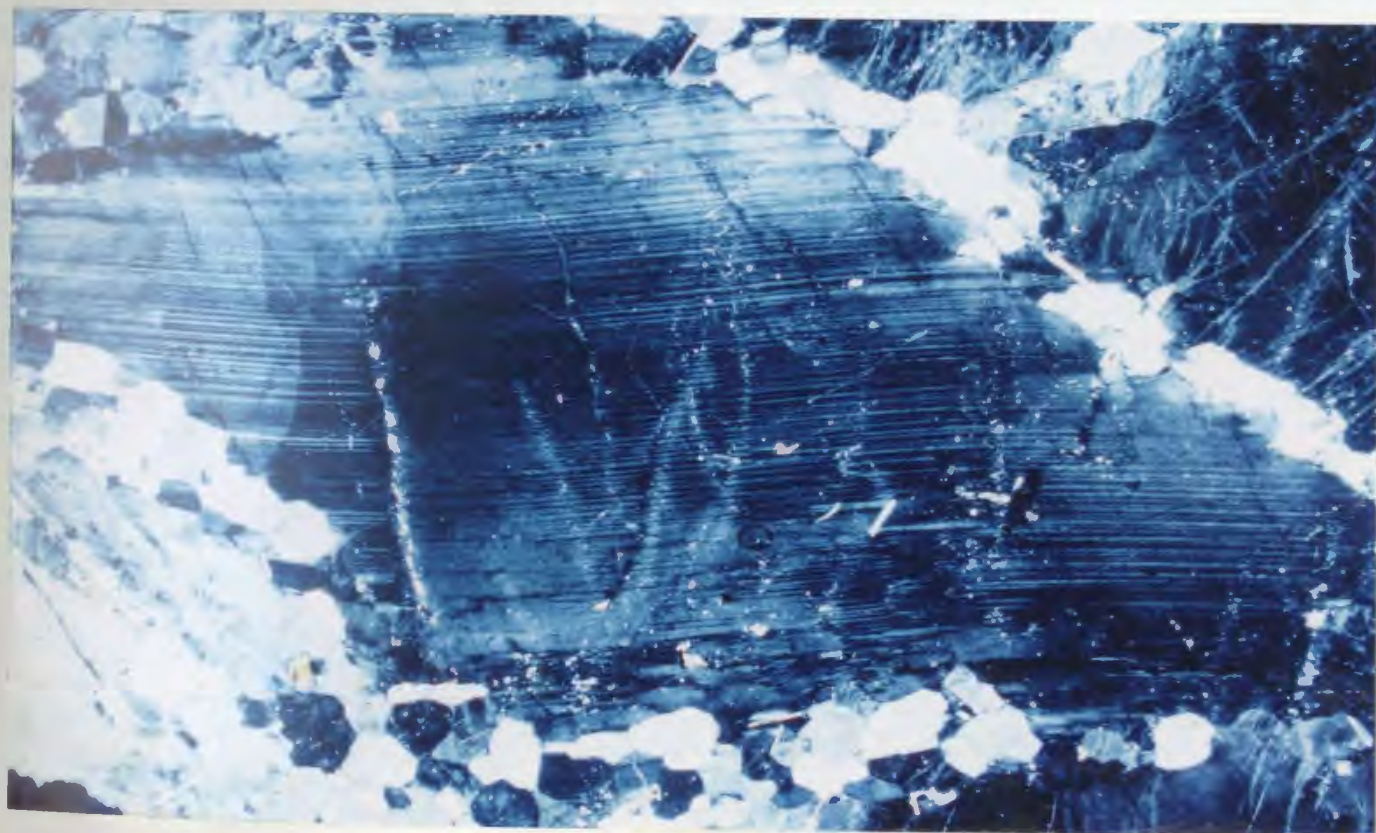
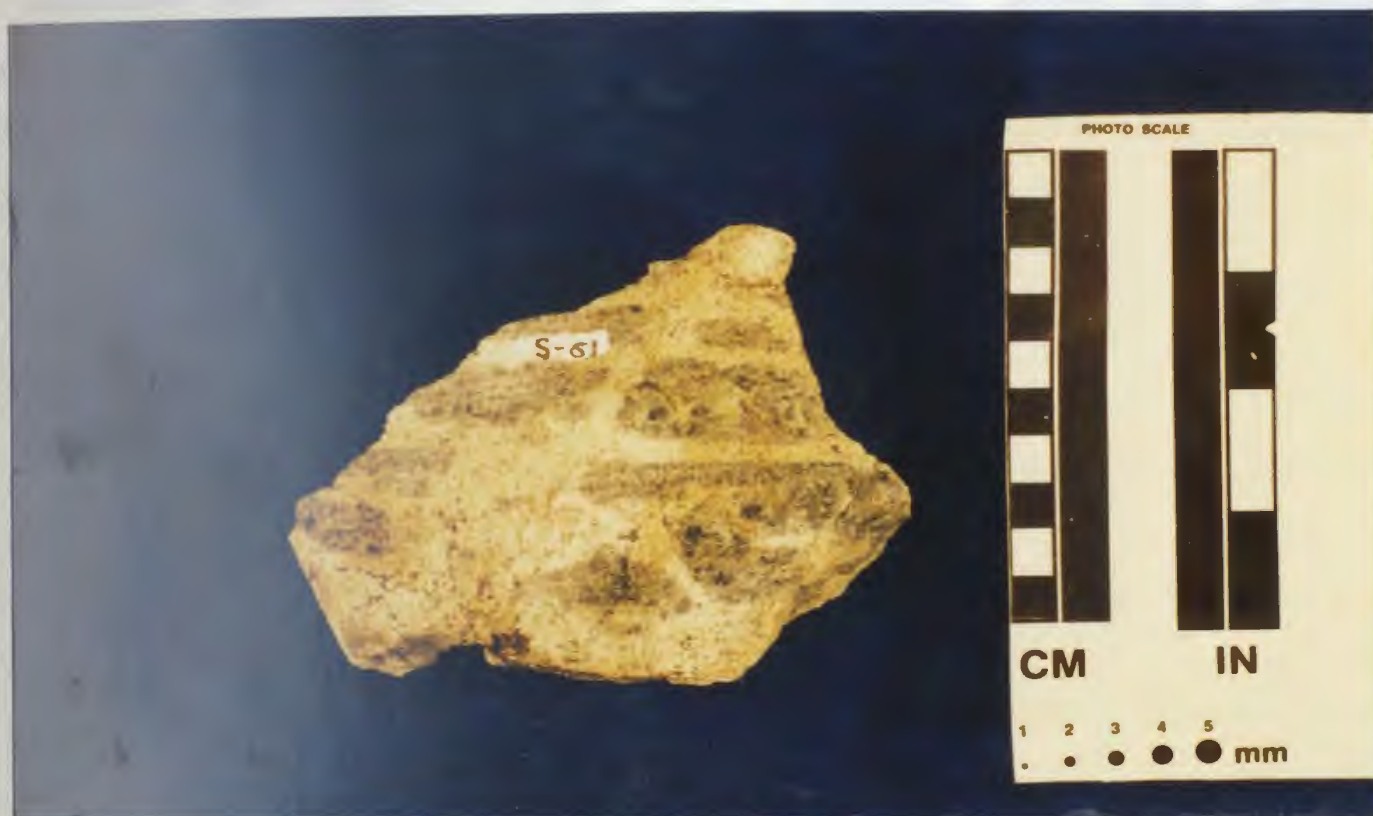
Figure 16. Field photograph showing the quarry in the anorthosite body looking east from Indian Head Park.

primary deep purple-grey plagioclase crystals up to 15 cm in size surrounded by haloes of smaller secondary milky white grains (Fig. 17). Accessory phases include apatite, rutile, magnetite and ilmenite. Secondary epidote and chlorite are common on fracture surfaces. The grain size of the plagioclase gradually becomes reduced and homogeneous toward the boundary of the unit where it grades into the noritic gneiss. Locally, in the marginal parts of this unit where orthopyroxene is relatively abundant, the rocks show narrow compositional banding (1-3 cm) defined by strongly deformed orthopyroxene similar to that in the noritic gneiss. In the contact zone between the anorthosite and the noritic gneiss (Unit 2) intercalations of one into the other are common. The anorthosite locally preserves a weak compositional layering considered to be igneous in origin, which is between 30-50 cm in width and consists mainly of concentrations of undeformed orthopyroxene phenocrysts. The orthopyroxenes occur as crystals ranging from a few mm to giant crystals with dimensions in excess of 30 cm (Fig. 19). These megacrysts of orthopyroxene have sub-round to irregular shape and occur singly or in aggregates in this unit. Locally, the orthopyroxenes are rimmed by green hornblendes.

On the microscopic scale, deformed igneous plagioclase porphyroclasts with peripheral plagioclase neoblasts in mortar

Figure 17. Photograph of hand specimen of anorthosite showing grey subrounded plagioclase megacrysts in recrystallized fine grained milky plagioclase. Sample# : S-61.

Figure 18. Photomicrograph of thin section of specimen shown in Fig.17, showing plagioclase phenocryst with bent lamellar twinning and undulose extinction, surrounded by subgrains of recrystallized plagioclase with mortar texture. Width of photomicrograph : 5.4 mm. Crossed polarized light.



texture are typical (Fig. 18). Twinned, bent and broken porphyroclasts of plagioclase of An<sub>50-67</sub> composition are common. In some sections from relatively highly deformed areas, granoblastic texture dominates. The plagioclase neoblasts have a similar composition to porphyroclasts and are generally saussuritized along grain boundaries or cracks. Orthopyroxene (En<sub>63-67</sub>) is the dominant mafic mineral. The composition of orthopyroxene in the unit is quite similar to that of metagabbro unit, but considerably more Fe rich than that in the noritic gneiss. The orthopyroxene megacrysts are internally recrystallized, and the crystals may contain inclusions of plagioclase as blebs and lamellae which are considered to be formed by exsolution. Thus, texturally, the orthopyroxene megacrysts (Fig. 19) in the anorthosite appear to belong to category 1 of Emslie (1975), characteristic of crystallization within the mantle and at deep crustal level. Minor biotite and hornblende are observed around orthopyroxene. Magnetite and/or ilmenite are locally intergrown with orthopyroxene.

#### Age relations

Anorthosite dikes with coarse grained pegmatitic orthopyroxene and plagioclase are observed in the anorthosite body and in





Figure 19. Field photograph showing orthopyroxene megacrysts up to 7 cm diameter in the anorthosite.

the surrounding noritic gneiss. They imply that the anorthosite is younger than the noritic gneiss. A variety of granitoid dikes ranging from alkali feldspar granite to granite also intrude the anorthosite body. Based on composition, these granitoid dikes appear to be related to the variably foliated biotite granite (Unit 7) which is distributed in the eastern and northern part of the study area. Anorthosite dikes have not been observed within the variably foliated biotite granite, so these observations may imply that the anorthosite is older than the variably foliated biotite granite.

#### 2-5 Unit 5: Dioritic gneiss

This unit principally occurs adjacent to the anorthosite body (Unit 4) between the noritic gneiss and the variably foliated biotite granite in the southern part of the area, and it comprises a conspicuous part of the high strain zone in the study area.

The unit exhibits continuous melanocratic and leucocratic layering ranging from a few mm to tens of cm in width (Figs. 20 and 21). The melanocratic layers consist of amphibole, orthopyroxene, clinopyroxene and plagioclase, and the leucocratic layers contain principally fine-grained



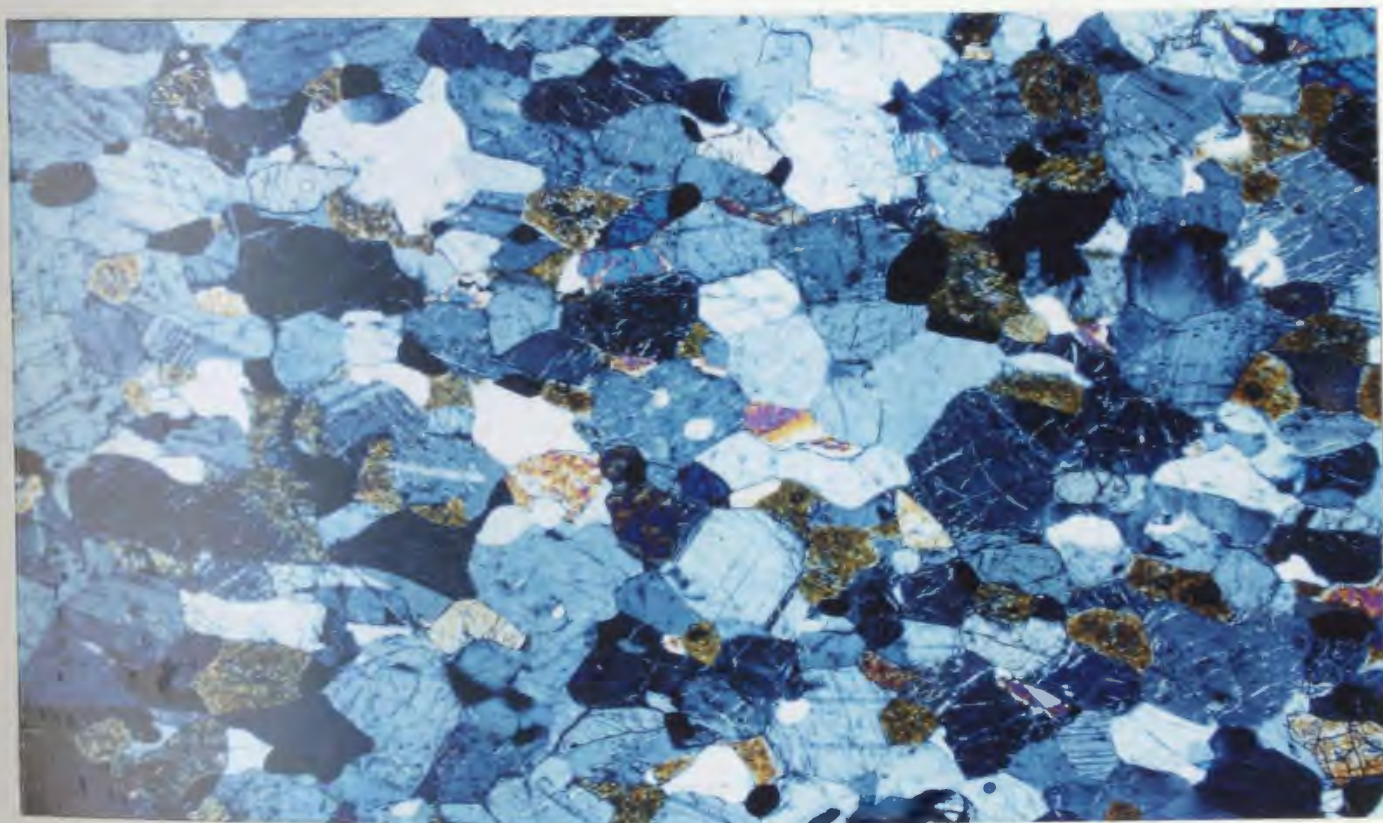
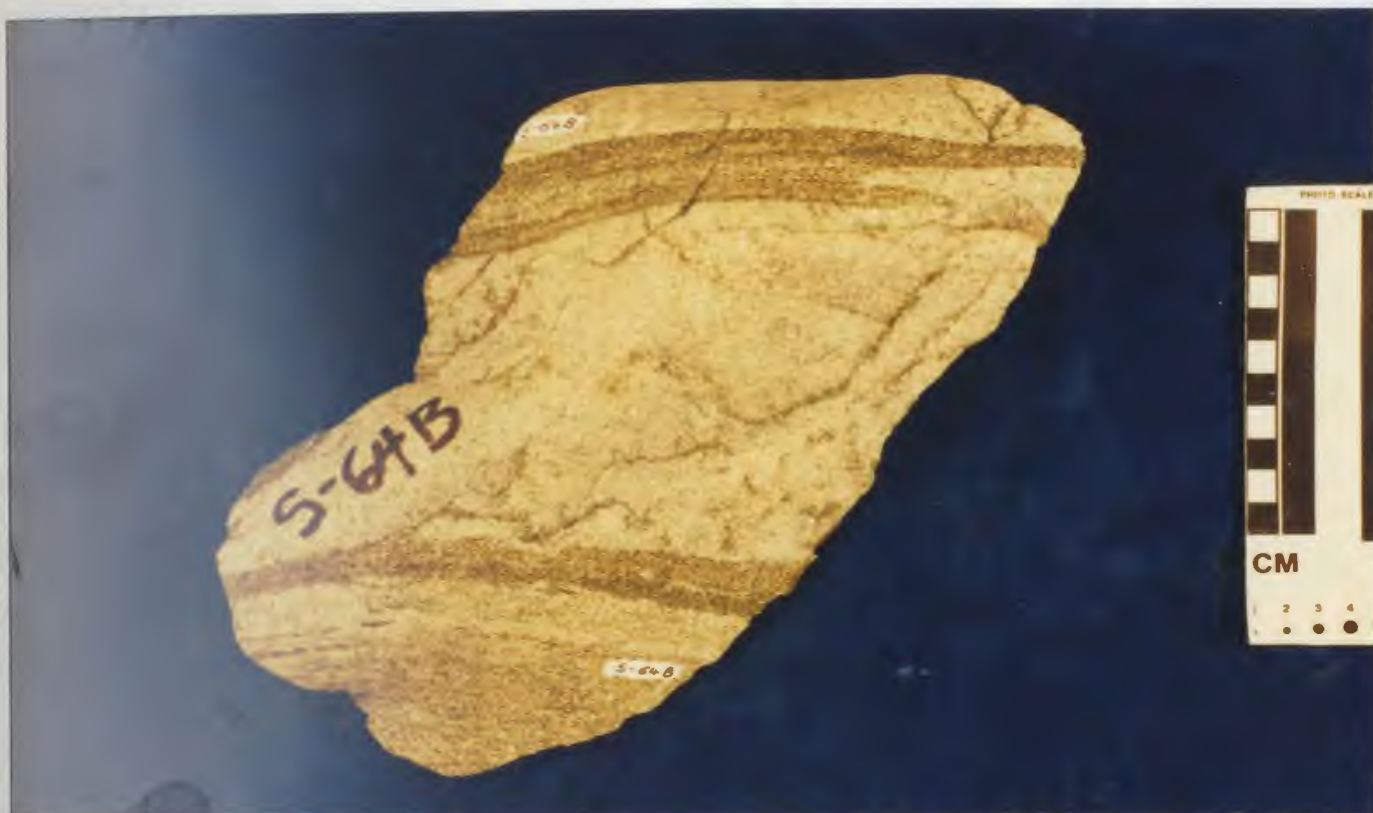


Figure 20. Field photograph of the dioritic gneiss showing subhorizontal high strain layering.

Figure 21. Photograph showing hand specimen of the dioritic gneiss from outcrop in Fig. 20. Note strongly developed banding defined by variable concentration of felsic and mafic phases. Sample# : S-64B.

Figure 22. Photomicrograph showing recrystallized granoblastic-polygonal texture of melanocratic part in the dioritic gneiss. Note retrograde amphibole formed from orthopyroxene and clinopyroxene. Width of photomicrograph : 5.4 mm. Crossed polarized light. Sample# : S-103B.





plagioclase and minor quartz and K-feldspar. Well developed and clearly exposed layering is preserved on the southeastern shore in the Indian Head area. The effects of penetrative ductile deformation are widespread and characterize the unit.

On the microscopic scale, this unit generally has a fine grained granoblastic-polygonal texture (Fig. 22). Its constituent mineralogy is quartz (<10 %), plagioclase ( $\approx$  65 %), hornblende ( $\approx$  20 %), orthopyroxene ( $\approx$  3 %), clinopyroxene ( $\approx$  2 %) and minor biotite.

Plagioclase has a relatively narrow range of composition (An <sub>44-56</sub>) and is partially altered to sericite and epidote. Quartz grains in plagioclase rich layers are xenomorphic. Orthopyroxene and clinopyroxene are ubiquitous and locally show mutually stable contact relations. Their compositions are very similar to those from metagabbro (Unit 3). They are partially replaced by hornblende, which may be entirely retrograde in origin. Ilmenite is the most common oxide and is very abundant in places, and apatite is generally an important minor constituent.

#### Age relations

The contacts with noritic gneiss, anorthosite and variably

foliated biotite granite are highly deformed so that relative age relationships are difficult to interpret. However, the existence of ellipsoidal masses (20-30 cm width, 2-3 m length) of granitic composition interpreted to be deformed dikes within the dioritic gneiss, implies that the unit is older than the variably foliated biotite granite.

#### 2-6 Unit 6: Lherzolite

This unit forms a megaboudin several tens of meters in length and several meters in width within the highly strained dioritic gneiss in the southern part of the study area (Fig. 23). The lherzolite is deep brown in color in outcrop and is, in part, altered to serpentine. The contact with the dioritic gneiss is concordant with the main foliation of the high strain zone.

The lherzolite principally consists of olivine ( $\approx 60\%$ ), orthopyroxene ( $\approx 30\%$ ) and clinopyroxene ( $\approx 10\%$ ) and typically shows granoblastic and relict hypidiomorphic-granular texture. Olivine is commonly interlaced with serpentine and magnetite. Orthopyroxene and clinopyroxene generally occur as xenoblastic grains.





Figure 23. Field photograph showing part of a large ultramafic boudin of lherzolitic composition that occurs in the high strain zone composed principally of the dioritic gneiss. Note partial alteration to serpentine (white cracks in lower left hand side of photo).

### 2-7 Unit 7: Variably foliated biotite granite

The variably foliated biotite granite is widely distributed across the Indian Head Range, but the best exposed body occurs in the northwestern part of the study area.

The predominant rock type of this unit is a fine to medium grained leucocratic biotite granite but a granodiorite facies is developed in the contact zone with noritic gneiss and metagabbro. These two lithologies can be distinguished on the basis of their modal compositions of quartz, K-feldspar and plagioclase (Fig. 24), but are otherwise similar.

On fresh surfaces, the rocks are characteristically buff or olive brownish, but weather to a dirty pink color. The texture varies from granular to strongly foliated to weakly gneissic and partially migmatitic (Figs. 25 and 26). The foliation is defined by elongated quartz and the preferred orientation of biotite. The gneissic texture is mainly observed in the contact zone with other units. The presence of flattened alkali feldspar granite dykes and quartz veins parallel to the foliation reinforces the gneissic texture.

The granitic facies of the unit is generally characterized by approximately 55% mesoperthite, 30% quartz,

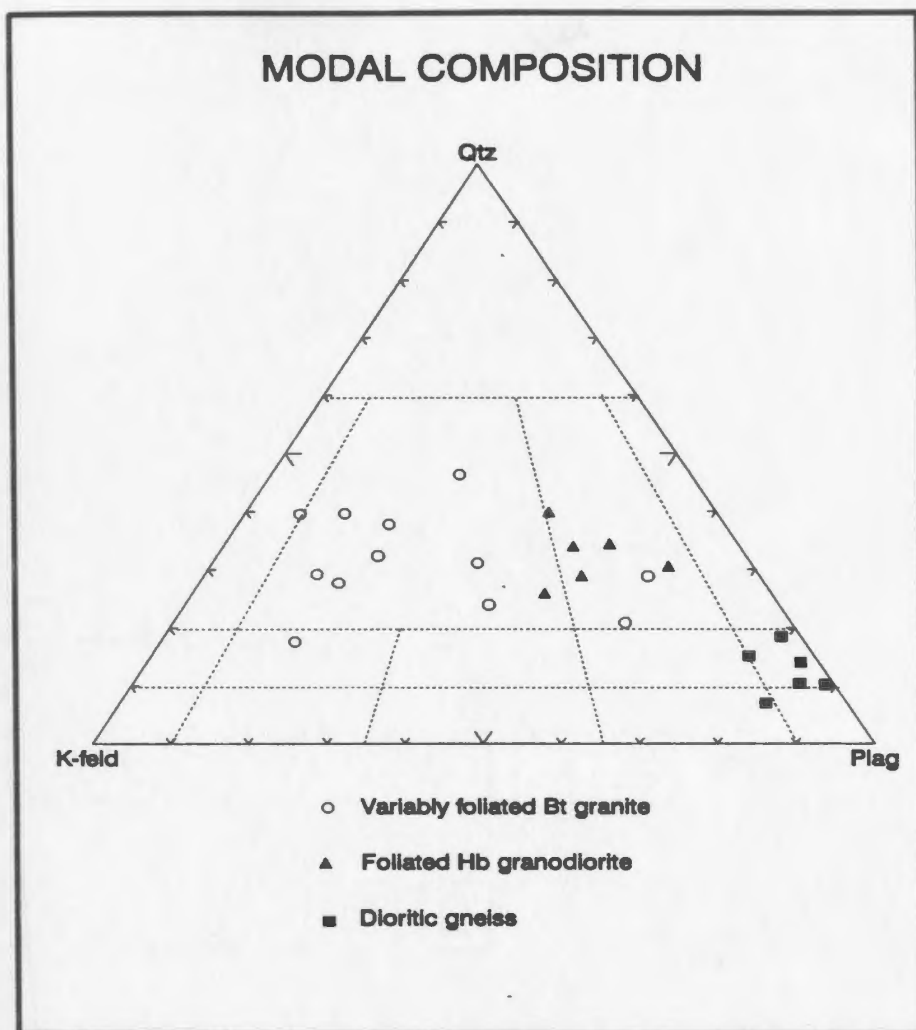


Fig. 24. Modal Qtz-K-feld-Plag plot (Streckeisen 1976) of granitoid lithologies in the Indian Head Range.



Figure 25. Field photograph showing weakly foliated biotite granite.

Figure 26. Field photograph showing outcrop of the strongly deformed biotite granite with a single straight layering (E-W in photograph). White bands consist mainly of quartz.



10% plagioclase. Most of the rocks exhibit a granoblastic texture but some grain boundaries are irregularly sutured (Fig. 27). In strongly deformed examples, quartz forms lenticular grain aggregates that are interpreted to be recrystallized quartz ribbons (Fig. 28). Patch and plume mesoperthite are common, but string types also occur. Plagioclase with composition of An<sub>25.33</sub> occurs as equant grains. Orthopyroxene occurs locally and is partially altered to amphibole. Biotite is ubiquitous and has a relatively high Ti contents (TiO<sub>2</sub> 3.5-5 wt. %). Magnetite, ilmenite and apatite occur as accessory minerals. Secondary epidote, sphene and chlorite are common.

The unit also locally includes Fe-Ti oxide layers (Fig. 29), ranging in width up to 30-40 cm in contact zones with the pelitic gneiss (Unit 1) and noritic gneiss (Unit 2). These layers consist mainly of ilmenite.

#### Age relations

Contacts with units other than the hornblende granodiorite are zones of high strain, and unsuitable for determination of age relationships. The contact with the foliated hornblende granodiorite shows clearly that the latter postdates this

Figure 27. Photomicrograph showing mesoperthite (stained yellow) and biotite (center of photograph) in a recrystallized sample of the variably foliated biotite granite. Width of photomicrograph : 1.6 mm. Crossed polarized light. Sample# : IH-31.

Figure 28. Photomicrograph of the variably foliated biotite granite showing a variety of textures. Note elongated quartz grains parallel to the main foliation, K-feldspar (stained yellow) and bimodal grain size due to deformation and subsequent partial recrystallization. Width of photomicrograph : 5.4 mm. Crossed polarized light. Q: quartz. Sample# : S-79.



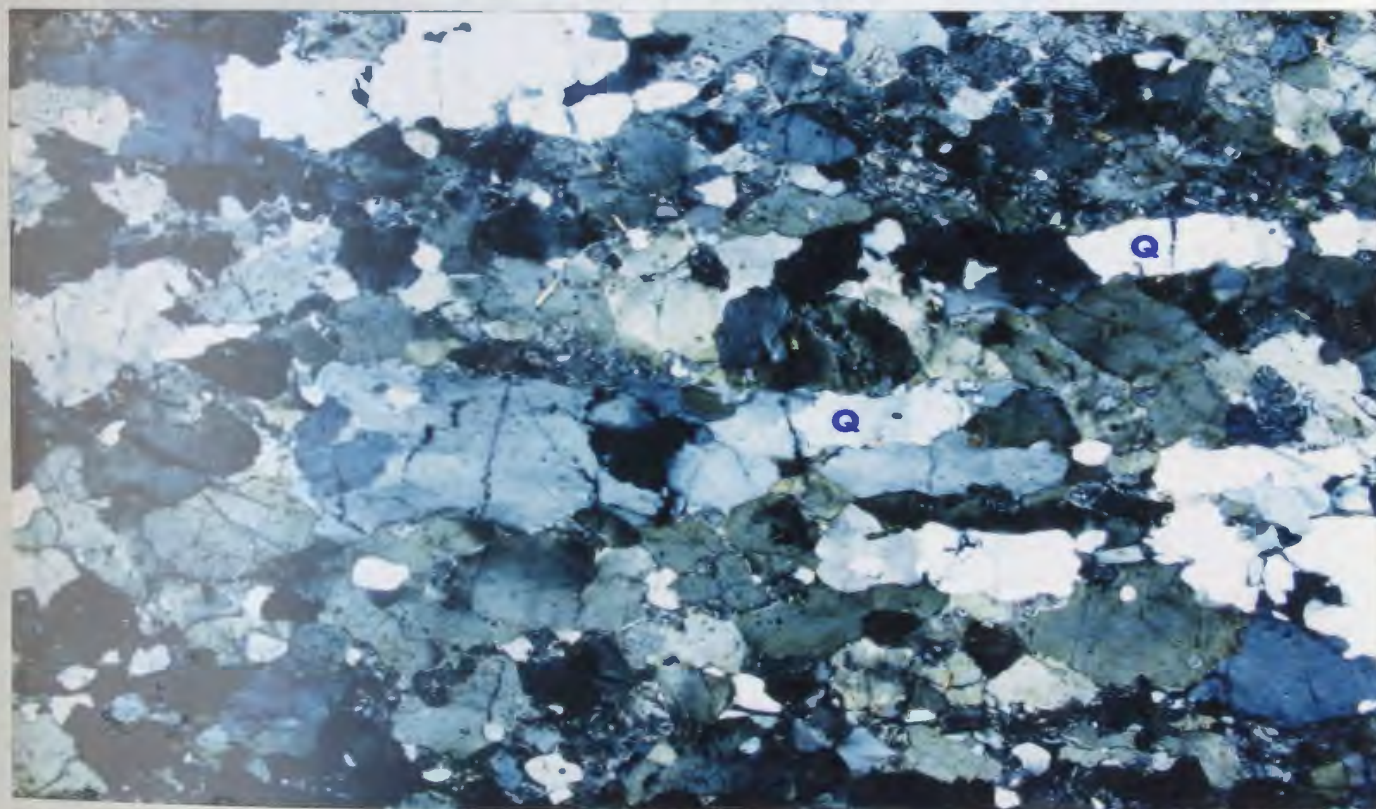
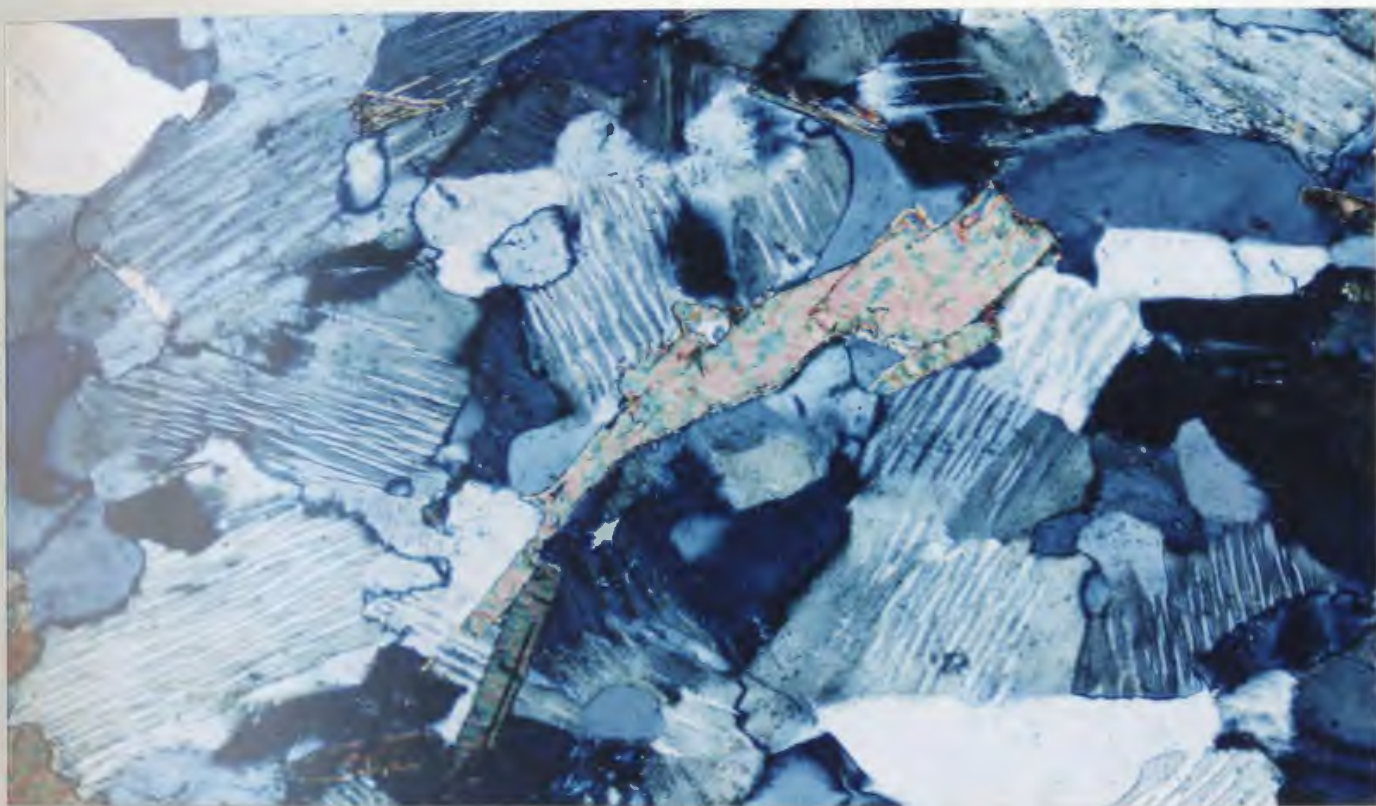






Figure 29. Field photograph showing Fe-Ti oxide rich bands (principally ilmenite) in the variably foliated biotite granite. Lens cap is 5 cm in diameter.

unit.

**2-8 Unit 8: Foliated hornblende granodiorite**

This unit outcrops around Long Gull Pond in the northern part of the study area and is easily distinguished from the variably foliated biotite granite (Unit 7) on the basis of mineralogy and texture.

This unit is a coarse grained, locally well foliated, hornblende granodiorite with composite augen of salmon pink microcline and quartz up to 3 cm in length, around which is an anastomosing fabric defined by the porphyroblasts of hornblende and locally fine grained biotite (Fig. 30). The unit shows neither gneissic texture nor continuous compositional layering. However, mafic-rich parts, in which hornblende is dominant, are locally present.

On the microscopic scale, the groundmass is medium grained and granodioritic in composition (Fig. 24). Microcline comprises 10 % to 30 % of the rock (Fig. 31). Plagioclase (An<sub>60-65</sub>) generally occurs as medium-grained untwinned subidioblastic crystals and is altered in part to chlorite and

Figure 30. Photograph of a hand specimen of hornblende granodiorite showing anastomosing foliation defined by hornblende. Sample# : S-82.

Figure 31. Photomicrograph of representative hornblende granodiorite. Note : microcline in center of left hand side of photomicrograph and coarse grained hornblende. Width of photomicrograph : 5.4 mm. Crossed polarized light. Sample# : S-109.





epidote. Quartz, which composes from 20% to 30% of the rock, forms equant xenoblastic grains and shows undulatory extinction. Mesoperthite is observed near the contact with variably foliated biotite granite. Green hornblende is the dominant ferromagnesian phase in the unit. The predominant pleochroic scheme of these hornblendes is green-yellow but brown-green also occurs. High  $\text{TiO}_2$  (3-4 wt %) biotite is a ubiquitous minor phase. Magnetite, ilmenite and sphene are present as accessory minerals. Small amounts of chlorite and epidote occur as retrograde phases.

#### Age relations

This unit clearly crosscuts variably foliated biotite granite and metagabbro unit, implying that it is younger than the anorthosite, metagabbro, noritic gneiss and variably foliated biotite granite. The contact with other units is well exposed at several places.

#### 2-9 Unit 9: Pegmatitic dykes

The medium- to very coarse-grained pegmatitic dikes (Fig. 32), which consist of coarse pink K-feldspar, quartz and (rarely)

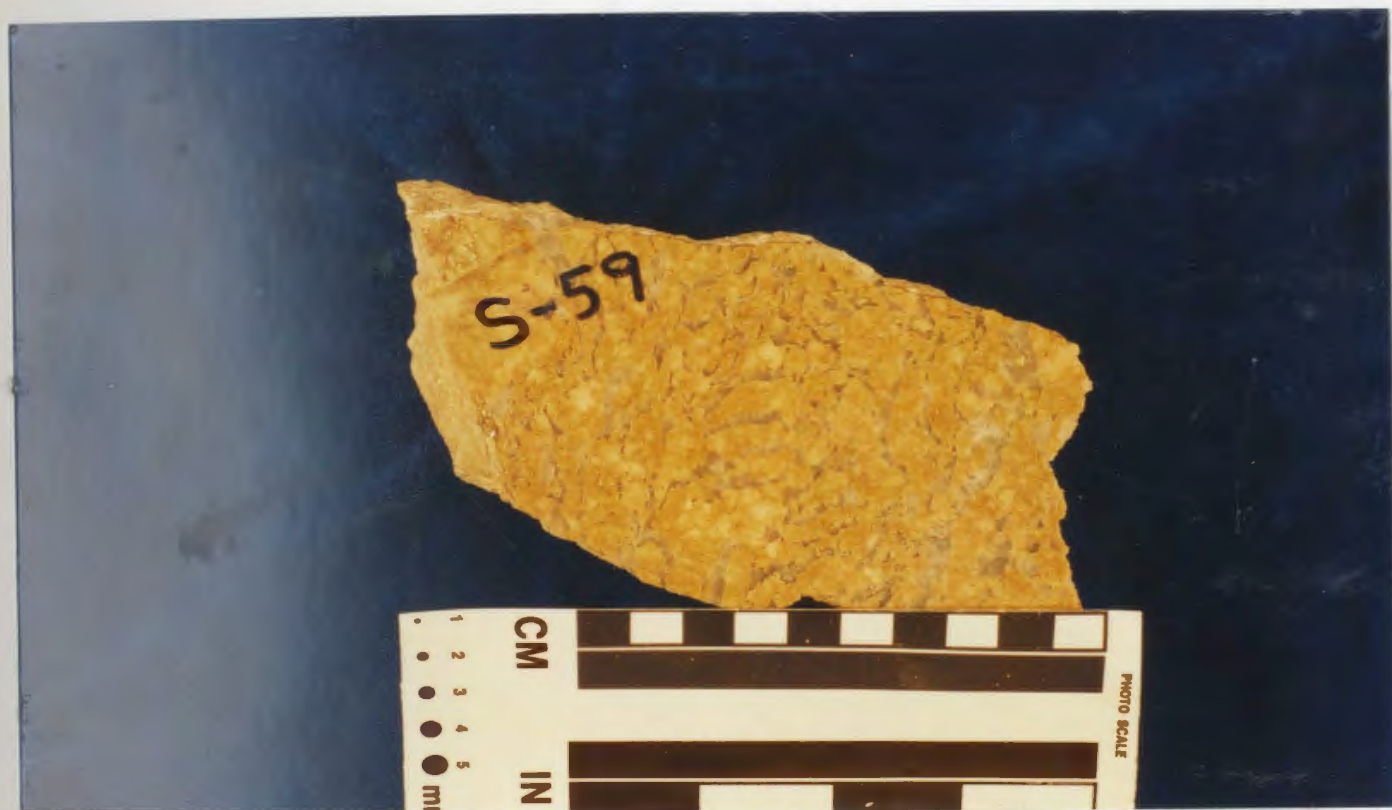


Figure 32. Photograph of hand specimen of pegmatitic dike showing graphic texture which consists of coarse K-feldspar and quartz. Sample# : S-59.

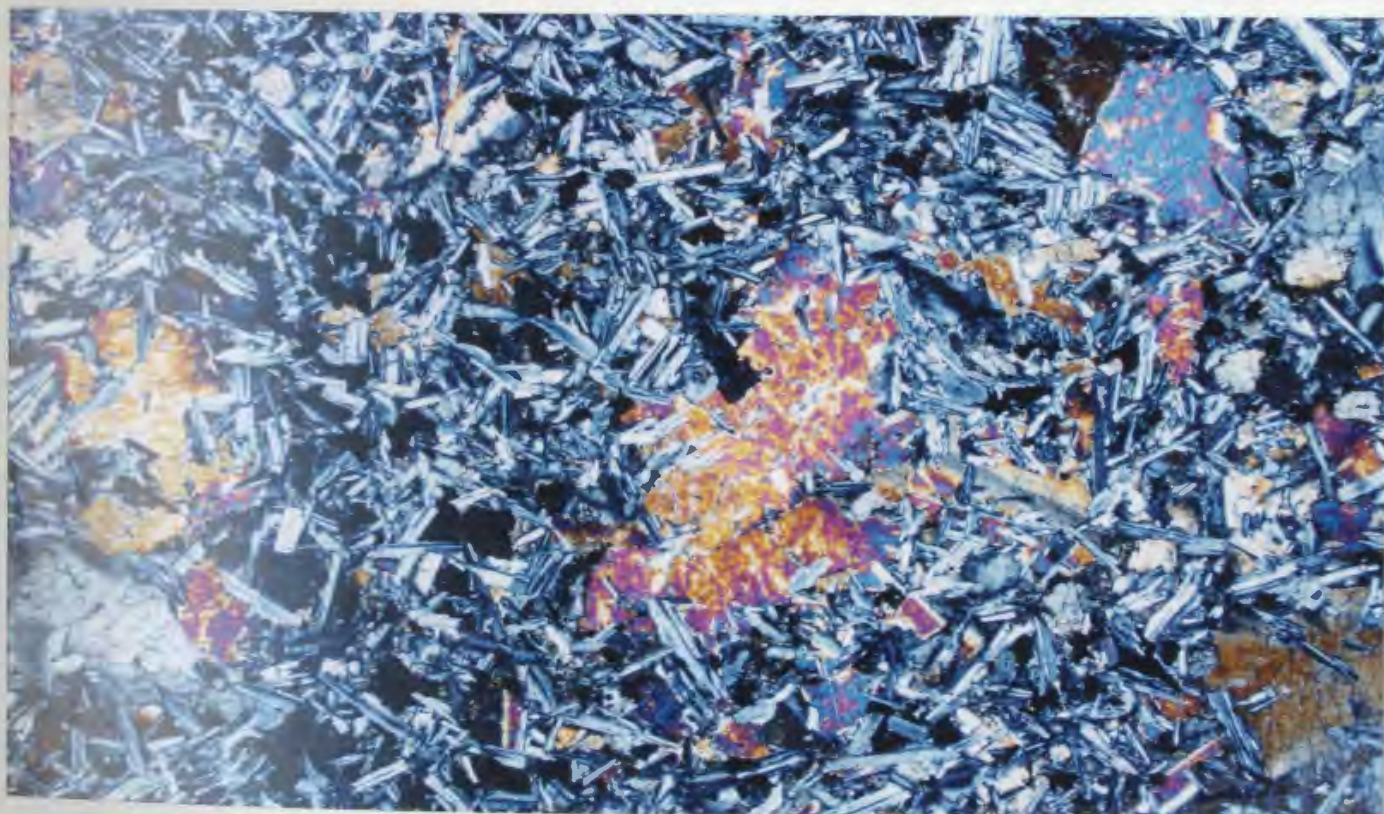
biotite and Fe-Ti oxides, are common in all units described above.

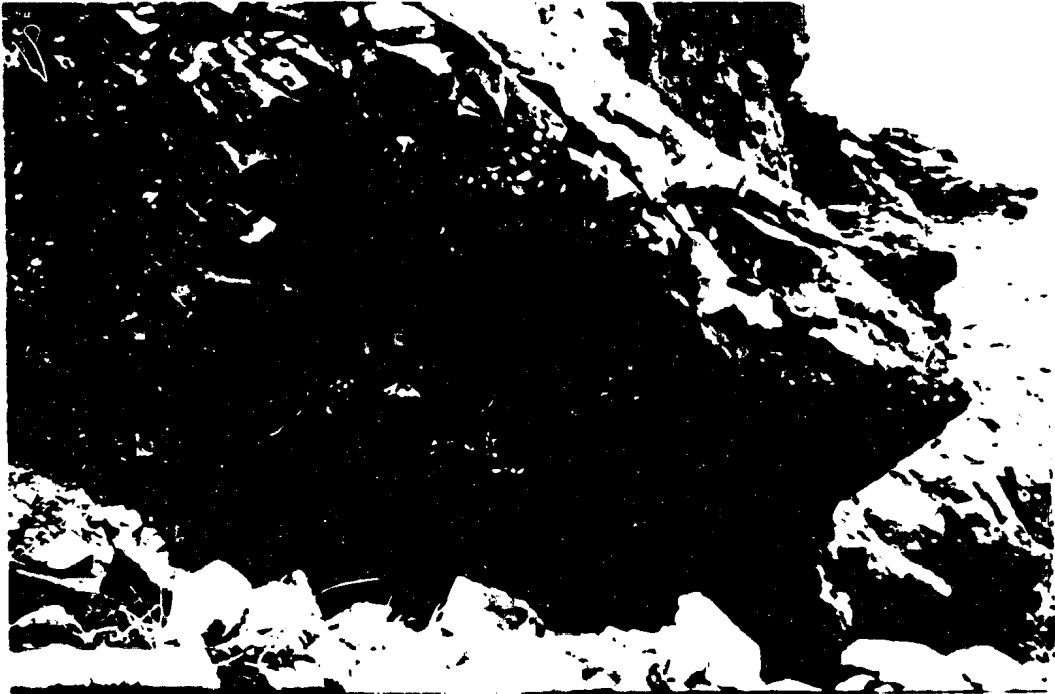
The dikes generally crosscut all units but are parallel to the major foliations and compositional banding in the high strain zone, indicating that they predate movement along the latter. Locally, pegmatitic dikes are seen to cut each other, suggesting that there is more than one generation.

#### 2-10 Unit 10: Mafic dykes

Olivine-diabase dykes, with well preserved ophitic texture (Figs. 33, 34), occur at several localities, especially along the coast line of the southern part in the study area. These undeformed dykes crosscut the anorthosite, the noritic gneiss and the high strain zone, and their lack of deformation or alteration characters implies that they postdate all other units. Although the Long Range dike swarm (Kamo et al. 1989) is known to intrude other Grenvillian inliers in west Newfoundland, the pristine appearance of these dikes may indicate the post-dated Early Paleozoic orogeny, and these are part of a younger, unrelated dike swarm.







## CHAPTER 3

### DEFORMATION

#### 3-1 Introduction

The Indian Head Range, like several other Grenvillian inliers in the Appalachian orogen, including the adjacent Long Range Inlier, contains evidence of an early ductile deformation that occurred at high metamorphic grade, and a later brittle deformation that occurred at low metamorphic grade. However, the ages of these deformational events are not well constrained due to paucity of geochronologic data. The very limited radiometric age data available (K/Ar and  $^{40}\text{Ar}/^{39}\text{Ar}$ ) have yielded essentially late Grenvillian ages (825 to 900 Ma) (Lowden 1961, Lowden et al. 1963, Dallmeyer 1978), which likely represent cooling ages following the Grenvillian orogeny.

On the basis of current understanding of the Paleozoic geology of the western Newfoundland, it is likely that the brittle structures were formed during the Acadian orogeny, and are therefore Silurian in age (Cawood and Williams 1988). These structures are only discussed briefly in this study.



It is well known that ductile structures such as those in the Indian Head Range are widespread in the Grenville Province proper, but it cannot be assumed on that basis that they therefore formed during the Grenvillian orogeny. For instance, a recent integrated structural/ metamorphic/ geochronic study of high grade gneisses in Lac Joseph terrane in the Grenville Province of western Labrador has shown that these gneisses formed at about 1,650 Ma, and were only very slightly reworked during the Grenvillian orogeny at about 1,010 Ma (Connelly 1991).

This chapter is concerned principally with the description of ductile deformational features in the Indian Head Range and with the qualitative distribution of strain in the high grade units of the map area. Particular emphasis is paid to two previously unrecognized high strain zones which are first order structural features with important tectonic implications.

### 3-2 Brittle deformation

The principal effect of the late low grade deformation in the Indian Head Range is the development of brittle fractures. Rocks close to these features are fractured, partly oxidized to hematite and fracture surfaces are coated by greenschist



Figure 35. Field photograph showing the effects of late brittle fractures in the metagabbro.

facies minerals such as chlorite and epidote (Fig. 35). These features cut older structures and occur in all units except the mafic dikes.

Fractures are generally steep, and have mainly northerly to northeasterly trends. Fracture planes show no evidence of vertical or horizontal displacement. Thus, these brittle fractures appear to have formed as a result of the release of residual stresses following thrusting of the Indian Head Range during Acadian orogeny.

### 3-3 Ductile deformation

Ductile deformation is expressed as gneissosity, migmatitic layering and foliation and is developed in the Precambrian units of the Indian Head Range. These fabrics are assumed to have formed either during the Grenvillian orogeny or during a pre-Grenvillian orogeny and to have been variably reworked during the Grenvillian orogeny.

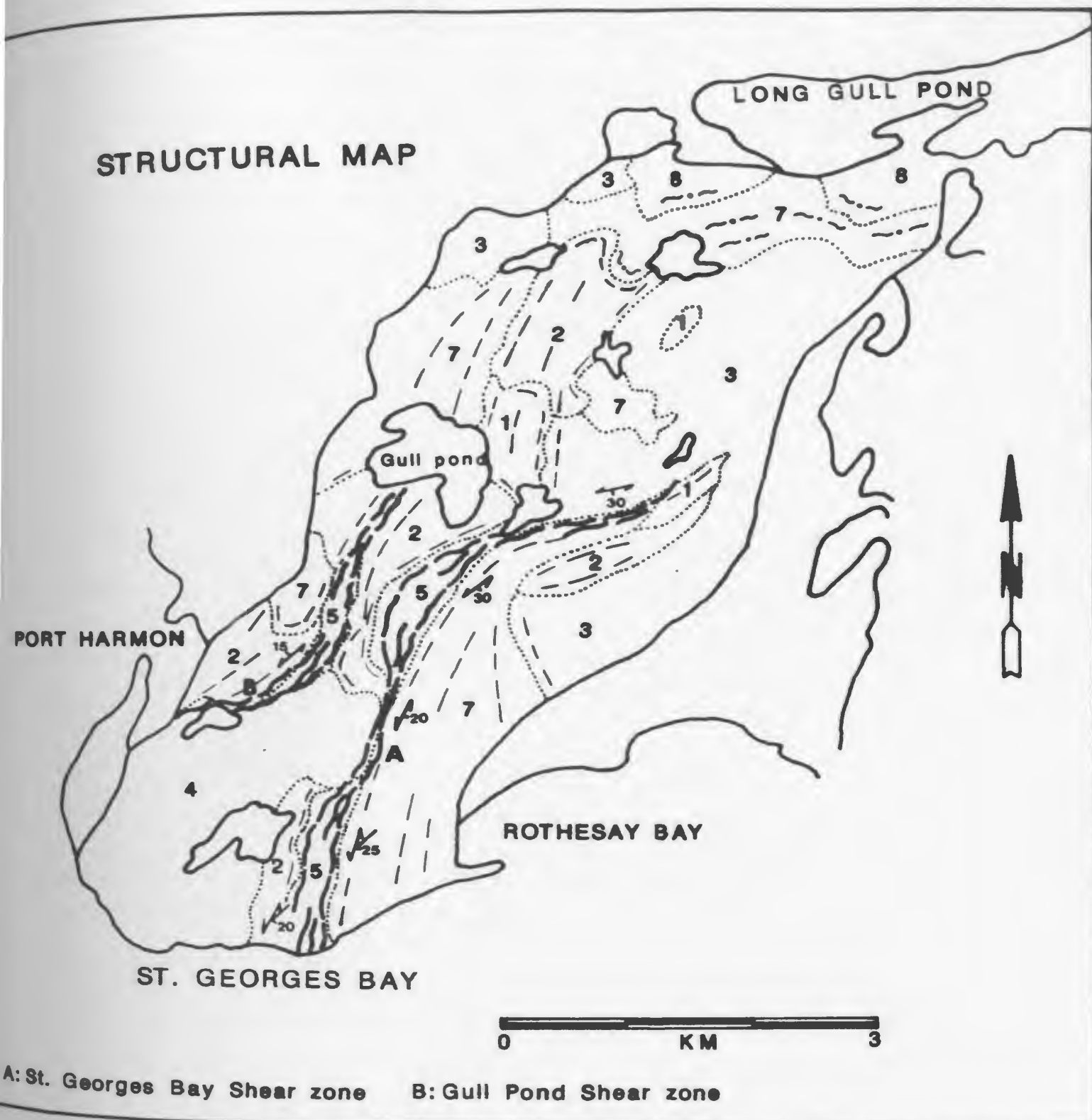
A clear distinction can be made in the field between units with strongly developed gneissic and migmatitic fabrics, typically associated with granulite facies (or retrograded granulite facies) mineral assemblages, and units with foliated fabrics defined by amphibolite facies mineral assemblages. Granulite facies gneissic to migmatitic fabrics are present in

the pelitic gneiss (Unit 1), noritic gneiss (Unit 2), dioritic gneiss (Unit 5) and some of the variably foliated biotite granite (Unit 7) in the study area. On the other hand, much of the variably foliated biotite granite (Unit 7) in the northern part of the map area, and all of the foliated hornblende granodiorite (Unit 8) immediately south of Long Gull Pond show variable but less intense deformation. Also both are characterized by amphibole rather than pyroxene.

The metagabbro (Unit 3) does not fit easily into this scheme, however, as it does not superficially show much evidence of high strain, yet exhibits granulite facies mineralogy. On the basis of the general fine grain size and annealed microstructure, and age relations, it has been assigned to the older high grade group.

A common feature of the ductile deformation in the study area is that the intensity of strain increases towards the margins of the units, and that the orientation of the fabric is generally parallel to unit boundaries. This suggests that unit boundaries may have been rotated into subparallelism with the gneissosity or foliation during the deformation.

The most prominent structural features in the study area are two ductile high strain zones (mylonite zones) which occur in dioritic gneiss, noritic gneiss and variably foliated



//: Trend of foliation in shear zone    //: Trend of gneissosity  
 //: Trend of foliation    ○: Unit boundaries

Figure 36. Simplified structural map of the southern Indian Head Range showing the distribution of units, orientation of foliation and location of high strain zones.

biotite granite adjacent to the anorthosite. They are informally referred to as the St. Georges Bay (SGB) and Gull Pond (GP) shear zones (Fig. 36). The St. Georges Bay shear zone is particularly well exposed along the shore line on the eastern side of the anorthosite body where it strikes NNE-SSW and dips gently towards the SE. The Gull Pond shear zone, on the northwestern margin of the anorthosite, strikes NE-SW to almost east-west and dips shallowly towards the north-northwest. Although the two shear zones approach each other near the northern end of the anorthosite, they appear to diverge further north and to be two separate structures.

#### Description of fabrics

As already noted, gneissic and migmatitic fabrics are generally developed in the high grade rocks. These fabrics are characterized by alternating leucocratic and melanocratic layers which vary from planar, lenticular to discontinuous in form. The leucocratic layers typically consist of feldspar and quartz, with the melanocratic layers being composed mainly of orthopyroxene and clinopyroxene, and minor amphibole and biotite. Where present, foliation defined by the preferred orientation of biotite is subparallel with the gneissic layering. The gneissic fabrics are generally stronger along the margins of the units and are oriented approximately



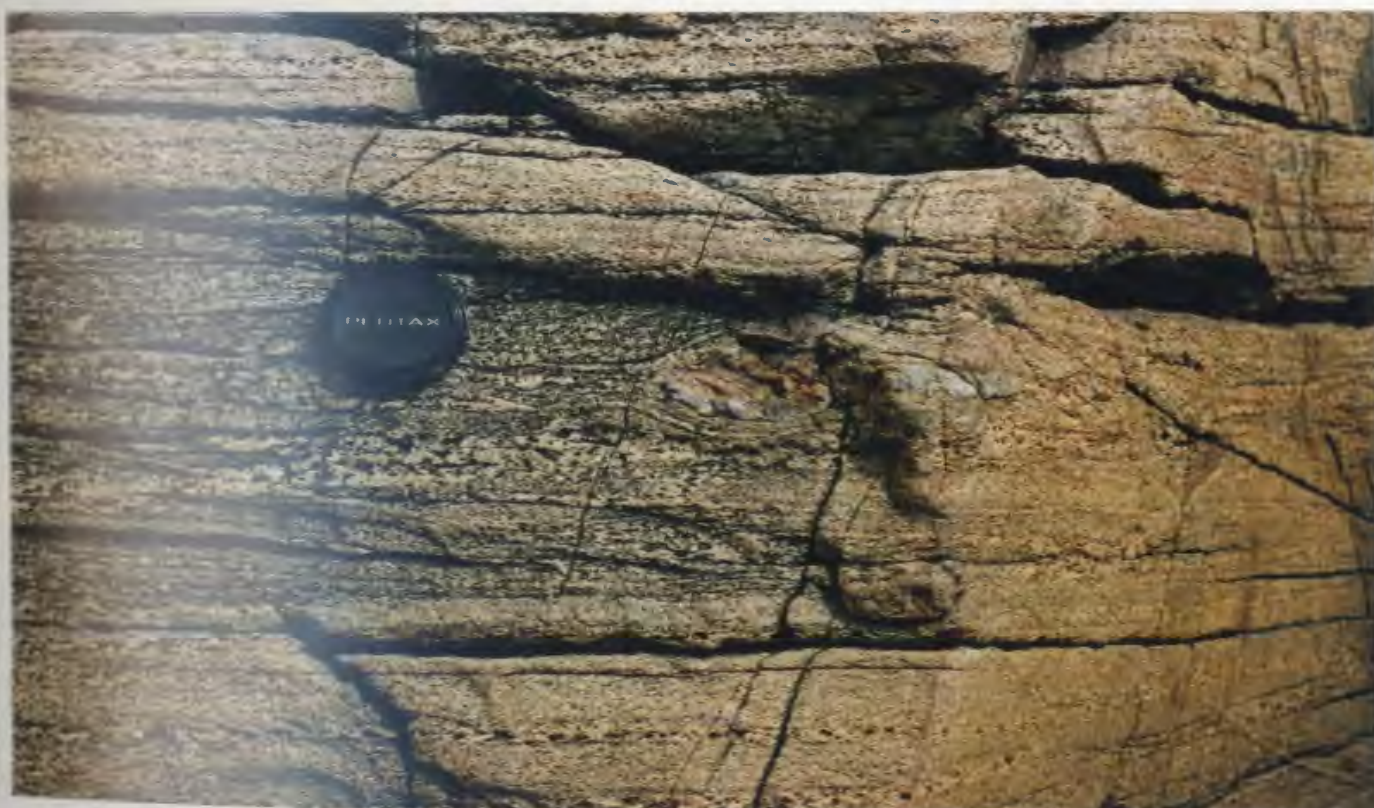
northeast with a shallow dip towards the SE or NW.

On the other hand, the predominantly foliated fabrics which are developed in some of the variably foliated biotite granite and throughout the foliated hornblende granodiorite units, are distinguished from gneissic and migmatitic fabric by the absence of high grade mineral assemblage and pervasive gneissic (layering) fabrics. Textures are variable, from weak to strongly foliated fabrics, the latter being defined by lenticular biotite and hornblende flakes and aggregates. The orientation pattern of the foliated fabrics is characterized by predominantly east-west strikes and moderate northerly dips.

Close to the SGB and GP shear zones, gneissic fabrics in the high grade gneisses become stronger and layering more continuous. A typical feature of the high strain zones is the development of continuous compositional layering ranging from several mm to tens of cm in width (Fig. 37). Such layering has been referred to as "straight gneiss" by some authors (e.g. Davidson et al. 1984, Hanmer 1987) and has been shown to be of tectonic origin. The melanocratic layers consist mainly of orthopyroxene, clinopyroxene, amphibole and plagioclase, with the leucocratic layers being composed principally of fine-grained plagioclase. In granitic rocks compositional layering is defined by the planar segregation of quartz and feldspars

Figure 37. Field photograph showing continuous compositional layering and streaked-out mafic tectonic augen in straight dioritic gneiss. Lens cap is 5 cm in diameter.

Figure 38. Field photograph showing streaked-out boudin of pegmatitic dike in strongly deformed biotite granite. Lens cap is 5 cm in diameter.



and by the subparallel orientation of many leucocratic veins with the main mylonitic fabric.

Several lithologies in the high strain zones also show other criteria indicative of extreme ductile deformation, such as the presence of augen of mafic minerals and granitic pegmatites (Figs. 37, 38) and, as already noted with the occurrence of a large discrete tectonic enclave of lherzolite (Unit 6), a lithology not seen elsewhere in the study area. The occurrence of the lherzolite enclave in the high strain zone suggests the possibility of substantial tectonic transport along the SGB high strain zone.

Another characteristic feature of the high strain zones is significant reduction in both the grain size and thickness of layering compared to rocks elsewhere in the study area.

A stretching lineation, which is developed in the planar fabric as a mineral alignment (biotite) or elongate mineral aggregates (orthopyroxene, plagioclase and quartz), is locally observed in the shear zones in the noritic gneiss, dioritic gneiss and variably foliated biotite granite.

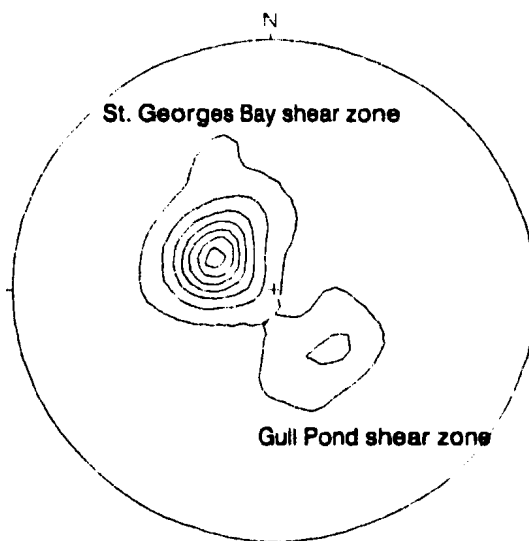
The orientation of planar and linear structures in the shear zones is summarized in a stereonet plot (Fig. 39 A). For the St. Georges Bay shear zone, the diagram shows maxima of planar structures which indicate northeast structural trends, with moderate to shallow southeasterly dips (20-30°). On the

Figure 39. Steronet plots.

A : Stereogram showing lower hemisphere equal area projection of contoured poles to foliations from two shear zones in the southern part of the Indian Head Range.

B : Stereogram showing lower hemisphere equal area projection of stretching lineations from two shear zones in the southern part of the Indian Head Range.

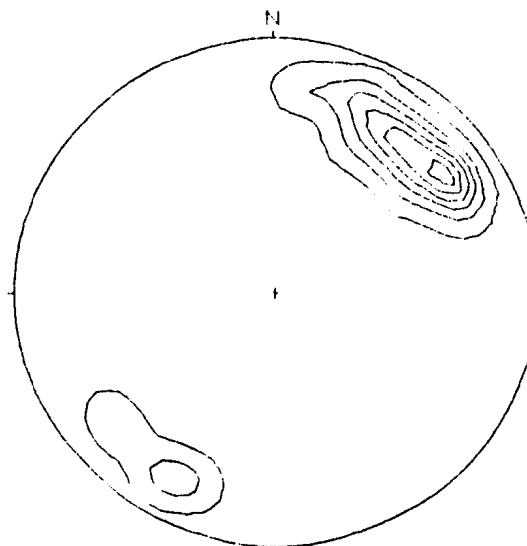
Max. value counted:  
31.6 times uniform  
at 120/24



Contours:  
1 5 10 15 20 25 30 per 1% area

N = 85  
Poles to Planes

Max. value counted:  
28.1 times uniform  
at 52/21



Contours:  
1 5 10 15 20 25 per 1% area

N = 21  
Lineations



other hand, the Gull Pond shear zone has shallow northwesterly dips ( $10-30^\circ$ ). The few measured stretching lineations show a restricted orientation plunging approximately 10 degree towards  $040^\circ-060^\circ$  (Fig. 39 B).

As should be apparent from the foregoing text, most rocks in the Indian Head Range are moderately to extensively recrystallized, implying the existence of an important annealing event after the main deformation. As a result, rocks in the shear zones rarely preserve any indications of the shear sense of the ductile movement, although a few examples have been found (Fig. 40 a,b). Even though these kinematic indicators are insufficient to unambiguously determine shear sense in the shear zones, the few observed asymmetrical boudins and rotated winged orthopyroxene porphyroclasts from both shear zones indicate a consistent top-side towards the northeast sense of movement parallel to the trend of the lineation. However the regional significance of this observation is not apparent, although it is noted that a N to NW sense of tectonic transport is widespread along many shear zones in the Grenville Province (Rivers et al., 1989).

Figure 40. A: Field photograph demonstrating sinistral shear sense of ductile deformation in the noritic gneiss from the shape of elongated orthopyroxene porphyroclasts.

B: Photograph demonstrating shear sense of ductile deformation in the anorthosite from deformed orthopyroxene aggregates.

Displacement sense is top side to left.

Sample# : S-111B



Figure 41. Field photograph showing greenschist facies chlorite-epidote assemblage on fractures in the anorthosite.

### 3-4 Discussion

The Indian Head Range shows two distinct sets of ductile deformation features. On the basis of qualitative estimates of the intensity of ductile strain, it is possible to divide the rocks of the Indian Head Range into two groups; (1) a relatively high strain group comprising the gneissic to migmatitic rocks; and (2) a relatively lower strain group comprising the foliated granitoids. The grouping fits well with a subdivision made on the basis of grade of metamorphism, with the high strain group possessing granulite ( or relict granulite ) facies assemblages, whereas the lower strain group is characterized by amphibolite facies assemblages.

Considering the relative ages of the units (chapter 2), which indicate that the foliated granitoid rocks are younger than the gneissic units, it appears that there is evidence of two metamorphic events in the Indian Head Range, an early granulite facies event associated with high strain and a later lower strain amphibolite facies event. In the shear zones, granulite facies assemblages are retrograded to amphibolite facies. This implies that the shearing postdated an early granulite facies event. However, the relationship between the amphibolite facies shearing event (which affected granulite facies rocks) and the amphibolite facies metamorphism of the

foliated granitoid rocks (which were not apparently previously metamorphosed) is not clear from this study and awaits the results of a geochronological study (in progress).

In the units with granulite facies gneissic and migmatitic fabrics, the increasing intensity of strain is consistent with the subparallel arrangement of the unit boundaries, which are interpreted to be tectonic. The two high strain zones are distributed around the anorthosite body. The trend of increasing strain along unit boundaries appears to be related to strain concentrations between rock types of different competence. The competency contrasts were largest around the anorthosite body and thus resulted in the strong deformation in the dioritic gneiss, noritic gneiss and variably foliated biotite granite which appear to have had relatively low competence compared to the anorthosite. Similar strain features have been well documented from the Cape Caribou River allochthon in Labrador (Wardle and Ash, 1984).

## CHAPTER 4

### METAMORPHISM

#### 4-1 Metamorphic character

Rocks of the Indian Head Range show evidence of three distinct metamorphic events characterized by different textures and mineral assemblages. A knowledge of these metamorphisms in the study area is a key to understanding the evolution of the Indian Head Range, which is the aim of this thesis.

In this chapter, the character of each of the metamorphisms is introduced with respect to distribution, mineral assemblages and textures. Subsequent sections concentrate on the sapphirine-and kornepine-bearing rocks in the pelitic gneiss (Unit 1) which preserve abundant evidence of mineral reactions from which the metamorphic conditions and P-T path of the granulite facies units of the Indian Head Range can be inferred.

Metamorphic mineral assemblages in the study area mostly belong to the granulite facies, with upper amphibolite facies assemblages developed in a few units. The granulite facies mineral assemblages are dominant in all Precambrian units



except the foliated hornblende granodiorite (Unit 8). Locally, granulite and upper amphibolite facies mineral assemblages are intermingled in the high strain zones and in the metagabbro (unit 3). Retrograde greenschist facies mineral assemblages are developed along late brittle fractures throughout all units except the Paleozoic mafic dikes.

#### 4-1-1 Greenschist facies metamorphism

The local effects of the greenschist facies metamorphic event are widely developed on fracture surfaces in all Precambrian units in the map area (Fig. 41). They have not been studied in detail, but are noted here briefly for the sake of completion. Chlorite and epidote are dominant minerals. Uralitization of pyroxene and sericitization of plagioclase are also considered to be an effect of the greenschist facies metamorphism. This metamorphic event is presumably part of the Acadian orogeny (see Cawood and Williams, 1988) as noted in chapter 3.

#### 4-1-2 Amphibolite facies metamorphism

Amphibolite facies mineral assemblages occur throughout the foliated hornblende granodiorite (Unit 8) and evidence of a partial amphibolite facies retrograde overprint on an earlier granulite facies metamorphism can be locally found in the

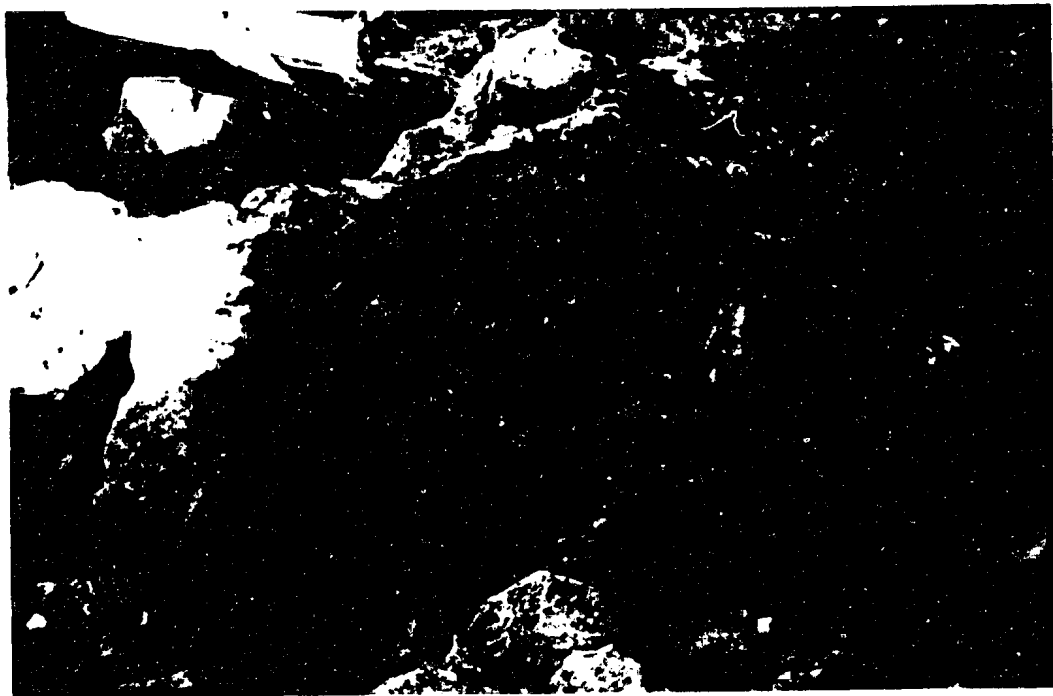


Figure 41. Field photograph showing greenschist facies chlorite-epidote assemblage on fractures in the anorthosite.

dioritic gneiss (Unit 5), noritic gneiss (Unit 2) in the high strain zones and in the metagabbro (Unit 3).

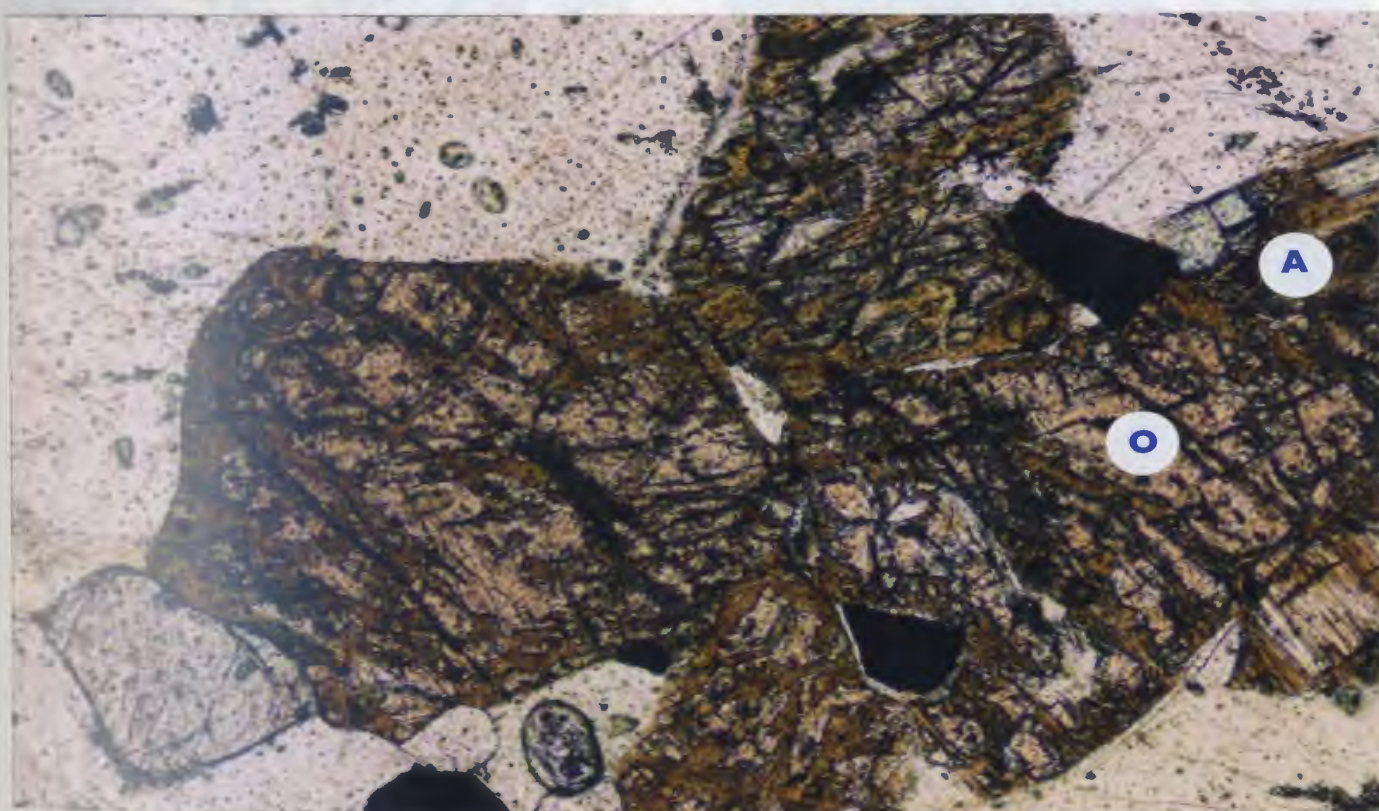
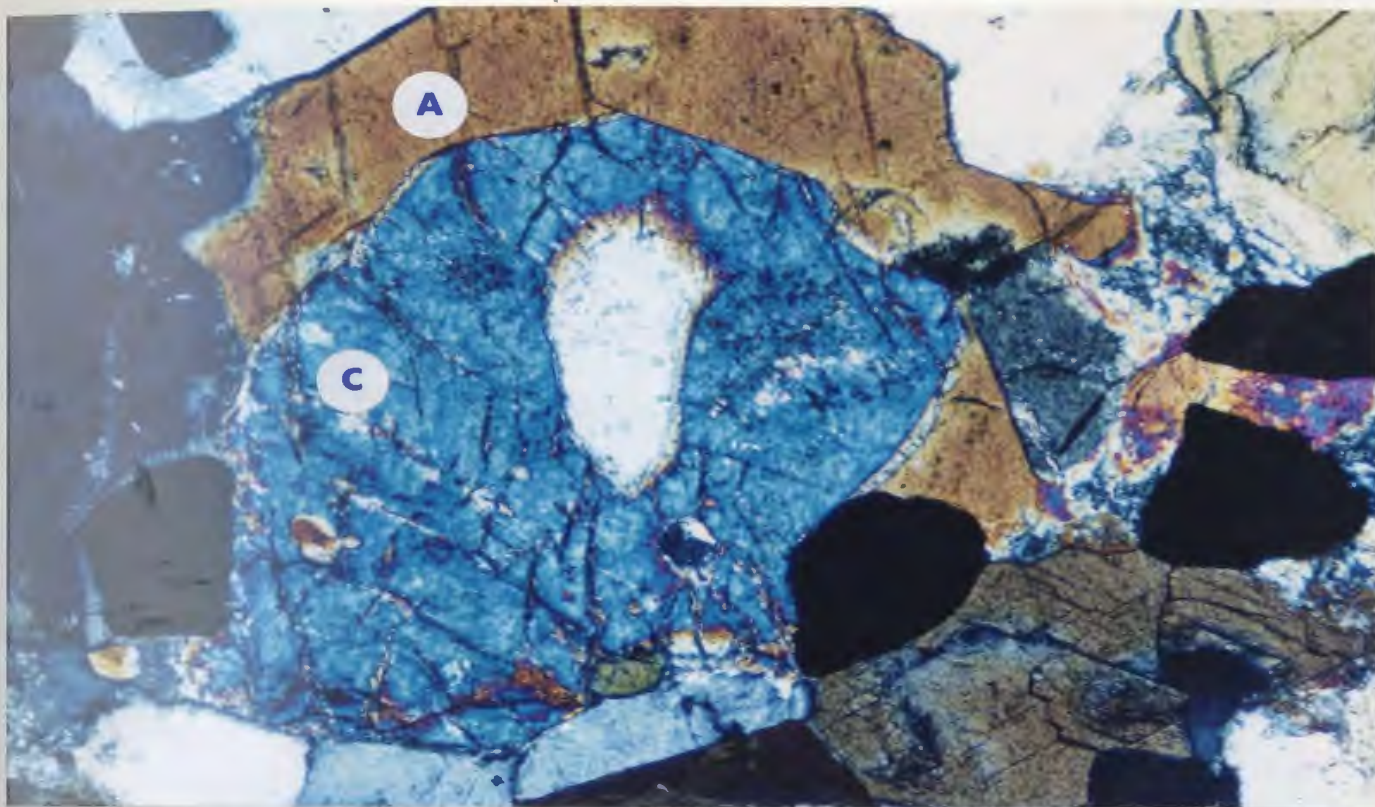
The foliated hornblende granodiorite, which is characterized by dominant amphibolite facies mineral assemblages, is distinguished from the granulite facies rocks by the presence of green hornblende and microcline, and by the absence of mesoperthite and pyroxenes.

In the granulite facies rocks, the most obvious effect of the retrograde amphibolite facies metamorphism is evidence of reactions involving hydration of pyroxenes to amphibole. Amphibole is present as partial coronas (Fig. 42) and as a replacement product of orthopyroxene and clinopyroxene (Fig. 43) in the dioritic gneiss and noritic gneiss. Biotite also overgrows the mafic minerals. The hornblende + garnet subassemblage is locally developed in metagabbro (Unit 3) and interpreted to be a result of reaction under amphibolite facies conditions (Fig. 44).

Thus, textural relations suggest that the amphibolite facies metamorphism postdated the granulite facies metamorphism. However, it is not obvious whether the amphibolite facies metamorphic event indicated by the foliated hornblende granodiorite and that indicated by the retrograde amphibolite facies overprint in granulite facies rocks are related; as these amphibolite facies rocks are widely separated in the field. Resolution of this problem must await

Figure 42. Photomicrograph showing partial corona of amphibole wrapping around clinopyroxene in the dioritic gneiss. Width of photomicrograph : 1.6 mm. Crossed polarized light. A: amphibole, C: clinopyroxene. Sample# : S-36A.

Figure 43. Photomicrograph showing orthopyroxene partly replaced by amphibole in noritic gneiss. Width of photomicrograph : 1.6 mm. Plane polarized light. A: amphibole, O: orthopyroxene. Sample# : S-16.





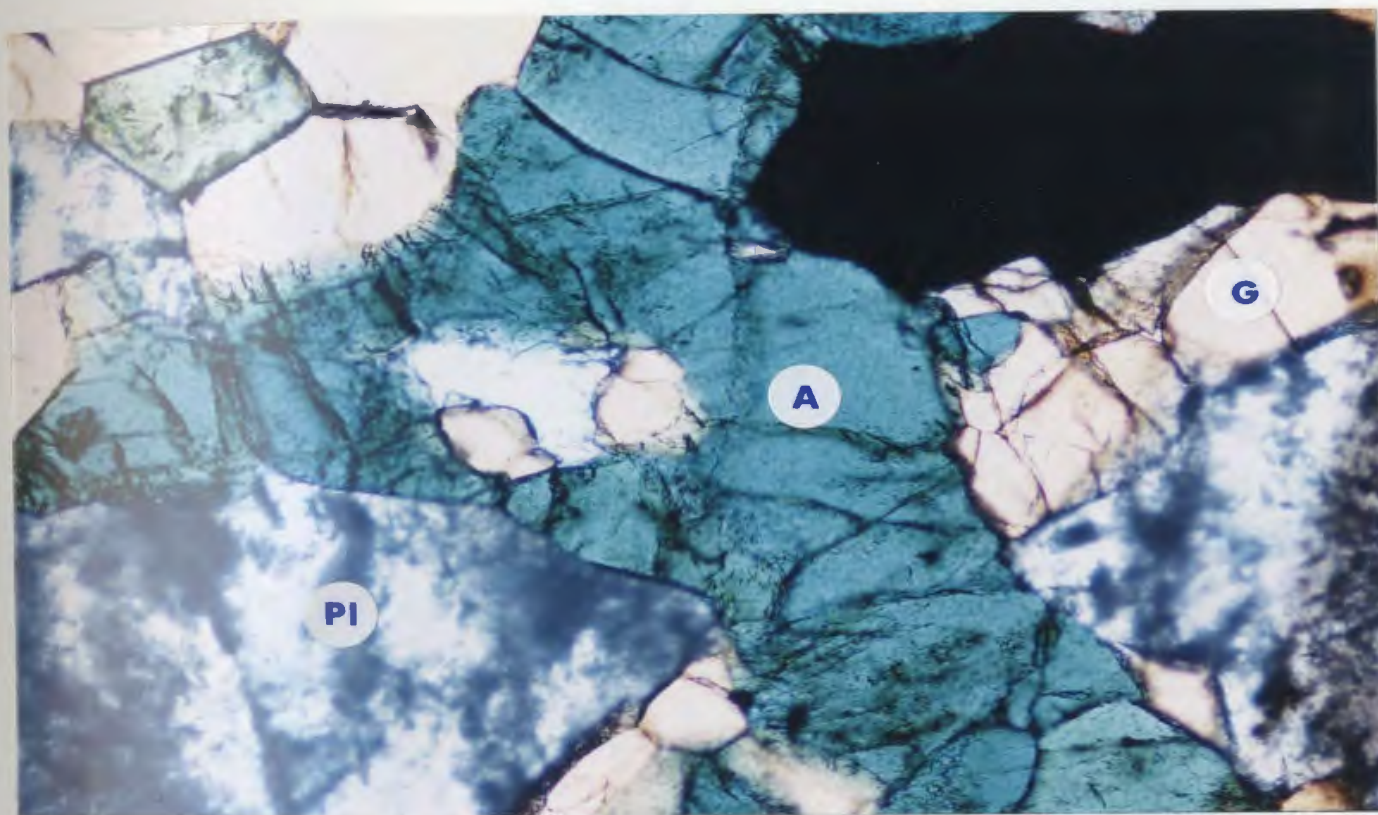


Figure 44. Photomicrograph showing amphibolite facies mineral assemblage in the metagabbro. Note : Ca- amphibole, garnet (pink-buff) and plagioclase (grey-white). Width of photomicrograph : 2.9 mm. Plane polarized light.

G: garnet, A: Ca-amphibole, Pl: plagioclase.

Sample# : S-77.



geochronological work.

#### 4-1-3 Granulite facies metamorphism

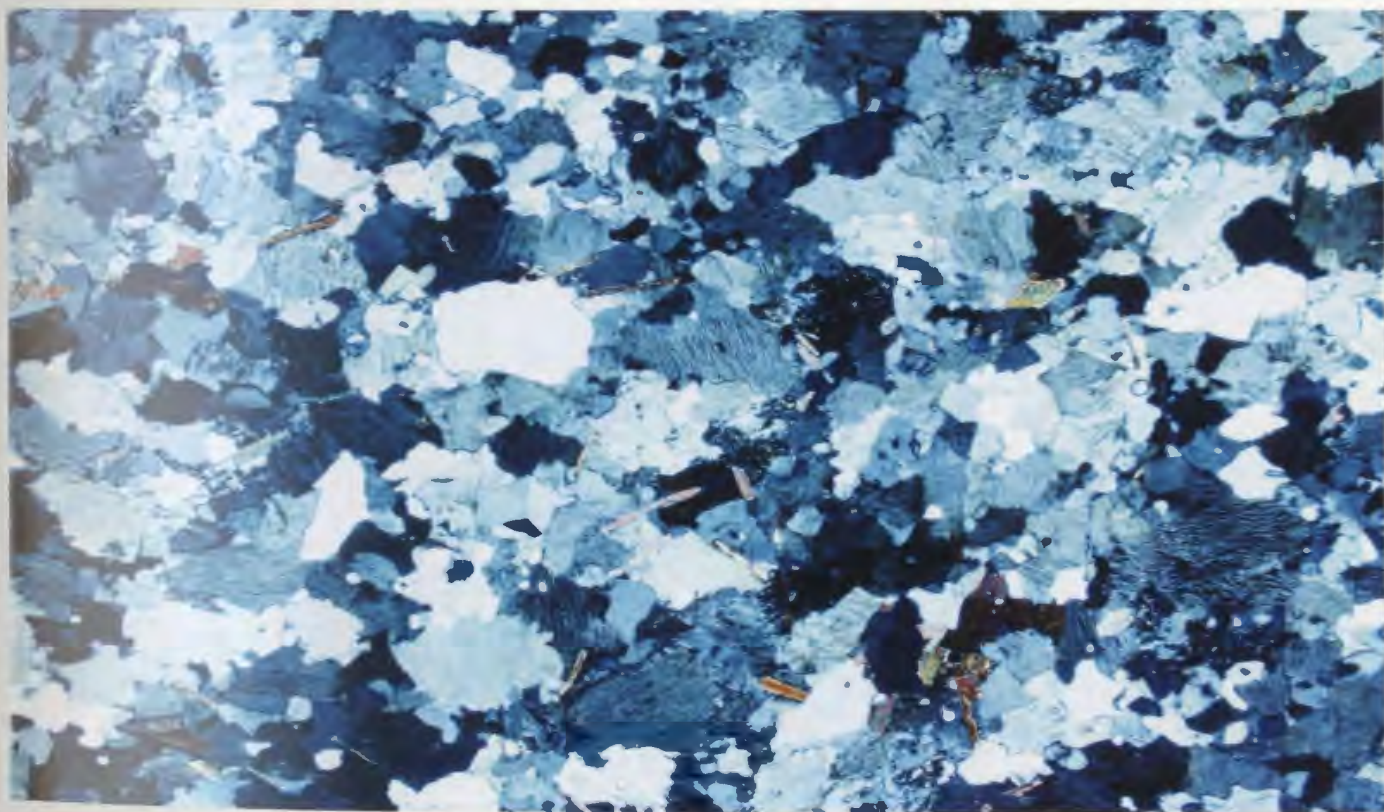
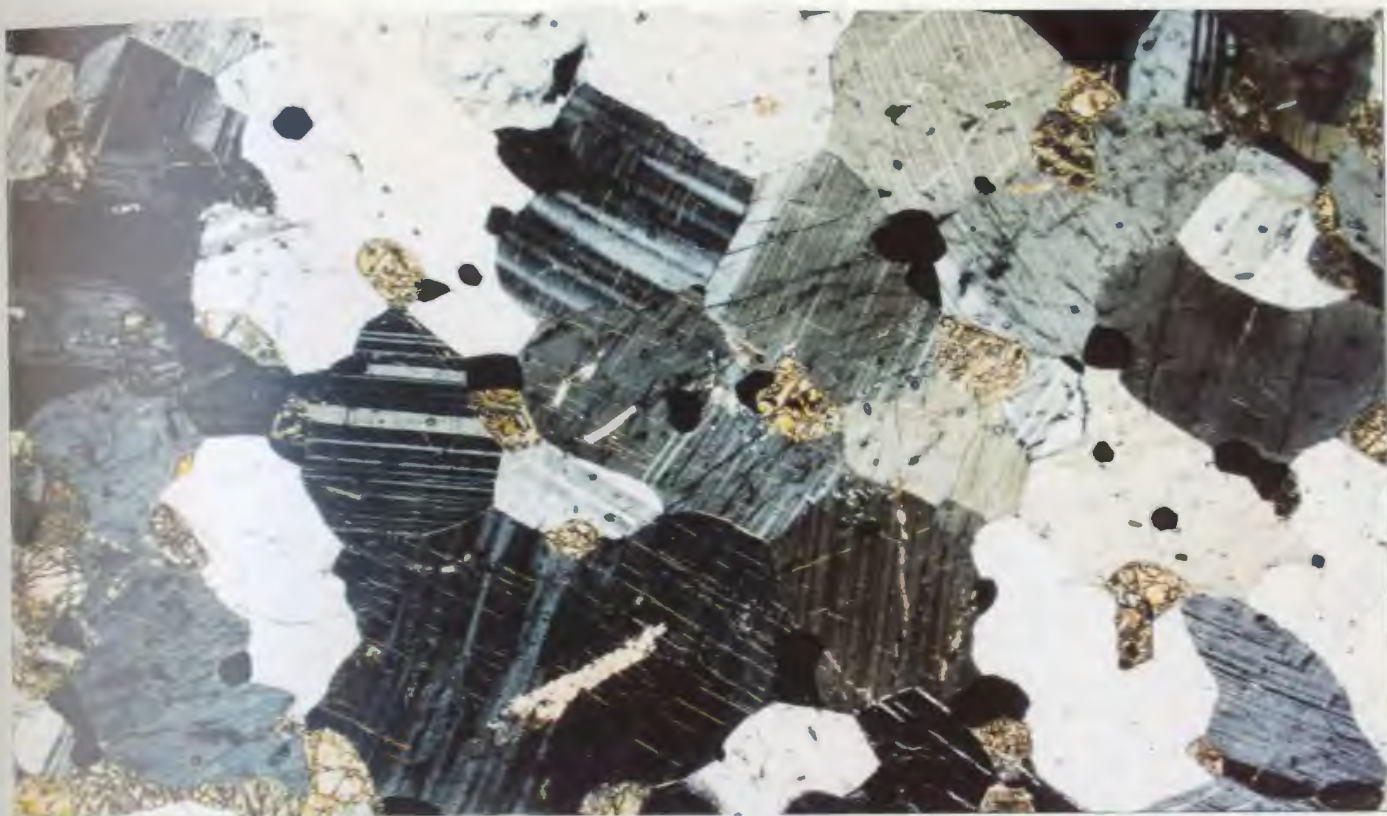
The remaining Precambrian units in the study area are characterized by granulite facies mineral assemblages. Critical minerals in mafic rocks of this area are orthopyroxene, clinopyroxene, plagioclase, rutile and locally garnet.

They typically exhibit granoblastic polygonal textures with straight grain boundaries, and 120° triple-point junctions are common between plagioclase grains (Fig. 45). This is consistent with extensive annealing after the granulite facies event, as noted previously. In the variably foliated biotite granite (Unit 7), alkali feldspar is characterized by irregular patchy submesoperthitic to mesoperthitic intergrowths, quartz, biotite and rare orthopyroxene. This unit also shows granoblastic textures with sutured grain boundaries as shown in Fig. 46.

With respect to physical conditions of metamorphism, clear evidence for the attainment of high-grade metamorphism throughout this area is shown by the widespread coexistence of orthopyroxene and clinopyroxene in mafic rocks and of the sillimanite-orthopyroxene-quartz and sapphirine-orthopyroxene

Figure 45. Photomicrograph of the metagabbro showing typical granoblastic polygonal texture exhibited by plagioclase. Note generally straight grain boundaries and triple-point junction between recrystallized plagioclase crystals. Width of photomicrograph : 2.9 mm. Crossed polarized light. Sample# : S-65.

Figure 46. Photomicrograph of the variably foliated biotite granite showing granoblastic texture with sutured grain boundaries. Note fine grained quartz and perthite with irregular patchy intergrowths. Width of photomicrograph : 5.4 mm. Crossed polarized light. Sample# : S-70.



assemblage in pelitic gneiss (Unit 1). Representative examples of these assemblages have been used for geothermobarometry (chapter 5) and are discussed further there.

## 4-2 Sapphirine- and kornerupine-bearing rocks

### 4-2-1 Introduction

Sapphirine and kornerupine-bearing rocks occur locally within the pelitic gneiss unit of the southern Indian Head Range. They preserve abundant evidence of mineral reactions in the form of symplectic and corona textures.

The relatively rare minerals sapphirine and kornerupine have attracted much attention in the last few years because their mineral assemblages are very sensitive to pressure and temperature, and they are comparatively unreactive during decompression and cooling or subsequent metamorphic events (Droop 1989).

Occurrences of sapphirine have been reported from several regional high grade terranes, e.g., Antarctic Shield, Limpopo Mobile Belt, Grenville Province ( Horrocks 1983, Windley et al. 1984, Arima et al. 1986, Herd et al. 1986, Herd et al. 1987, Currie and Gittins 1988, Droop 1989, Grant 1989 ). However, occurrences of kornerupine are relatively rarer and the mineral has been reported from the Archaean of western Greenland, in southern India and in the Limpopo Mobile Belt (see Schreyer and Abraham 1976, Windley et al. 1984, Droop 1989). In the Grenville Province, sapphirine has been

reported from pelitic rocks of Wilson Lake and St-Maurice (Morse and Talley 1971, Leong and Moore 1972, Herd et al. 1986, Herd et al. 1987, Currie and Gittins 1988), but kornepine is less well-known and has been relatively rarely reported from the Grenville Province proper.

The pelitic gneiss of the southern Indian Head Range has many similarities to sapphirine/kornepine-bearing rocks from other granulite terranes in terms of both mineral assemblages and textural relations. These similarities may imply analogous metamorphic conditions including metamorphic pressure, temperature and mechanisms of formation. Thus comparison of results with those from other granulite facies terranes bearing sapphirine/kornepine is likely to be useful.

In order to estimate metamorphic P-T conditions of the Indian Head Range and to make comparisons with other areas in which sapphirine and/or kornepine occur, petrography and mineral chemistry of the pelitic gneisses are described in detail in this chapter. Then, estimates of metamorphic P-T conditions are made by comparison with petrogenetic grids established by experimental petrologists (Schreyer and Seifert 1969; Chatterjee and Schreyer 1972; Newton 1972; Seifert 1974; Bishop and Newton 1975; Bertrand et al. 1989).



#### 4-2-2 Petrography

The pelitic gneiss (s.l.) unit in the study area shows a heterogeneous character, and varies from quartzofeldspathic to metapelitic (s.s.) in composition. Quartzofeldspathic gneiss, which is generally associated with well developed quartz segregations, is the more common type. Outcrops of sapphirine-bearing rocks are relatively rare, and are more or less massive, coarse-grained and dark-coloured in contrast to quartzofeldspathic gneisses. Sapphirine occurs in both discrete medium grained aggregates (2-5 cm in width) and as scattered fine grains. The contacts between sapphirine-bearing layers and surrounding quartzofeldspathic gneiss are gradational and concordant with the main foliation in the unit.

Mineral assemblages in the pelitic gneiss unit of the study area can be subdivided into three groups based firstly on the presence or absence of quartz and secondly on the basis of phases coexisting with sapphirine.

The three mineral assemblages are discussed below.

(1) **Quartz-bearing assemblages**, characteristic of quartzofeldspathic gneiss, do not contain sapphirine, and are

characterized by :

quartz + orthopyroxene + cordierite + sillimanite + biotite  
+ plagioclase + ilmenite/magnetite ± spinel ± kornerupine ±  
garnet ± gedrite ± (corundum).

Sapphirine-bearing assemblages do not occur with quartz,  
and are subdivided on the basis of the presence or absence of  
kornerupine and other Al-rich phases.

(2) **Al-rich sapphirine bearing assemblages** consist of  
sapphirine + kornerupine + orthopyroxene + cordierite +  
sillimanite + biotite + plagioclase ± garnet +  
magnetite/ilmenite ± spinel ± rutile.

(3) **Al-poorer sapphirine bearing assemblages** do not  
contain kornerupine, sillimanite and cordierite, and consist  
of sapphirine + orthopyroxene + biotite + plagioclase +  
magnetite/ilmenite ± spinel ± rutile.

Textural relations observed in these mineral assemblages can  
be used to infer several distinct stages of mineral reaction,  
are described below.

Several textural features indicate that orthopyroxene,  
cordierite and spinel were stable together at an early stage.

These include : in the **quartz-bearing assemblage (1)**, (a) the observation that orthopyroxene is the most abundant porphyroblastic phase and appears to be related to later reactions; (b) the observation that spinel exists only as relics in ilmenite and garnet; (c) the observation that cordierite ( Mg-rich, see Section 4-2-3) commonly occurs as large porphyroblasts embayed by sillimanite - orthopyroxene - quartz intergrowths which are considered to have formed later.

In the **Al-rich sapphirine bearing assemblages (2)**, the reaction of cordierite and spinel to produce later assemblages such as orthopyroxene and sillimanite is widespread.

In the **Al-poorer sapphirine bearing assemblage (3)**, orthopyroxene occurs as a porphyroblastic phase. Biotite is abundant and two types can be distinguished, an early prograde biotite (brown color) and a later retrograde biotite (reddish color). Spinel, which was exsolved from composite magnetite/ilmenite, is replaced by a corona of sapphirine.

Although gedrite and corundum (as a relic in ilmenite) appear to be phases of an early stage in the **quartz-bearing assemblages (1)**, it has not been possible to infer a reaction sequence from textural relations. Furthermore plagioclase and biotite are ubiquitous in all assemblages discussed above, but these minerals do not show textural evidence for involvement in any reactions that are proposed below.

#### 4-2-2-1. Sillimanite forming reaction textures

In quartz-bearing assemblages (1), textural relations indicating the formation of a fine grained sillimanite-orthopyroxene-quartz intergrowth replacing cordierite porphyroblasts are common. Opx-sil symplectites surround and invade cordierite porphyroblasts and large strain-free quartz grains occur adjacent to the margin of the symplectite (Fig.47). This texture implies operation of the reaction



In the Al-rich sapphirine bearing assemblages (2) in which quartz is absent, symplectites of orthopyroxene and sillimanite are observed around cordierite and spinel (Fig. 48). Textural relations indicate that the symplectite was formed by the reaction of cordierite and spinel. The inferred reaction is

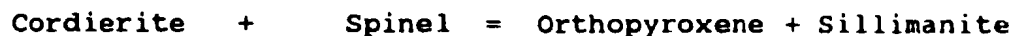
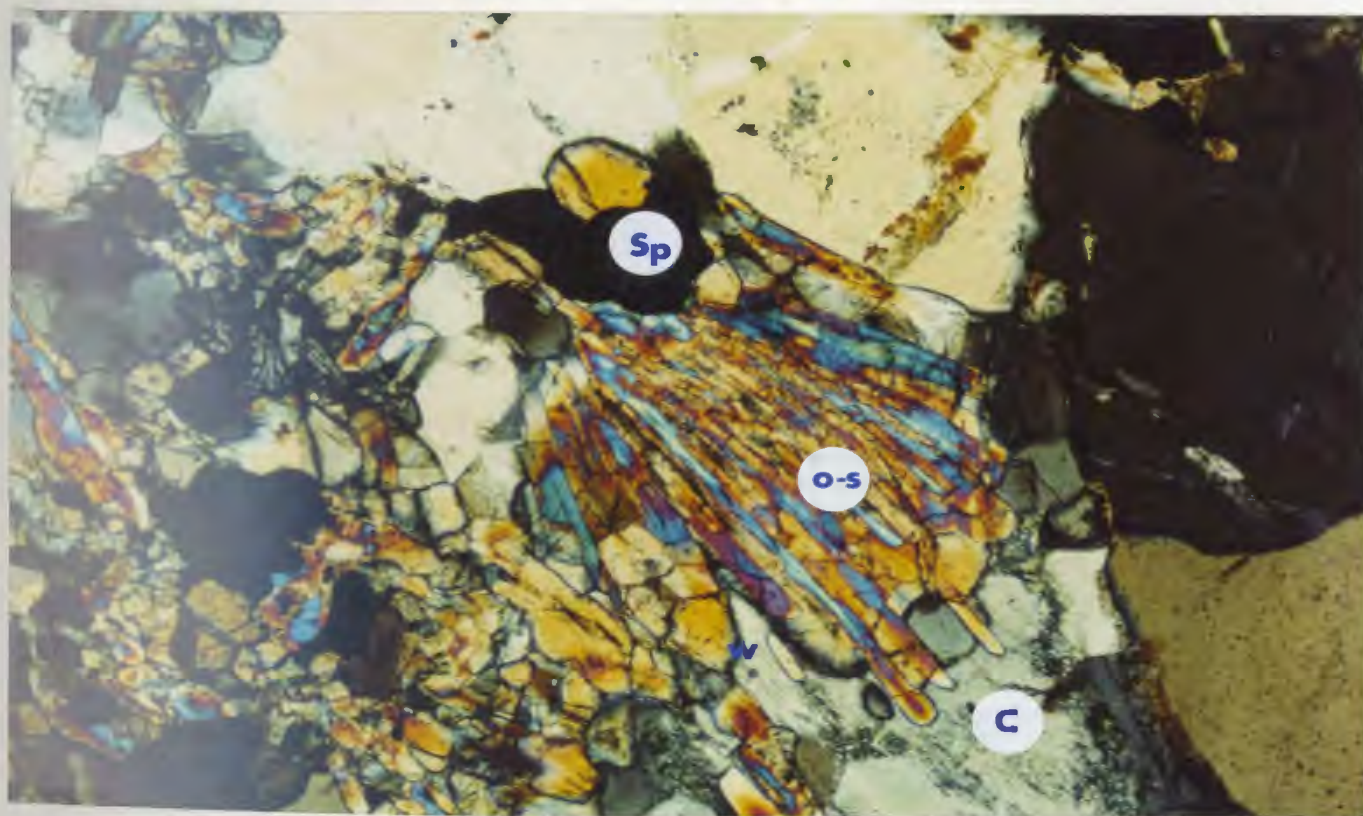
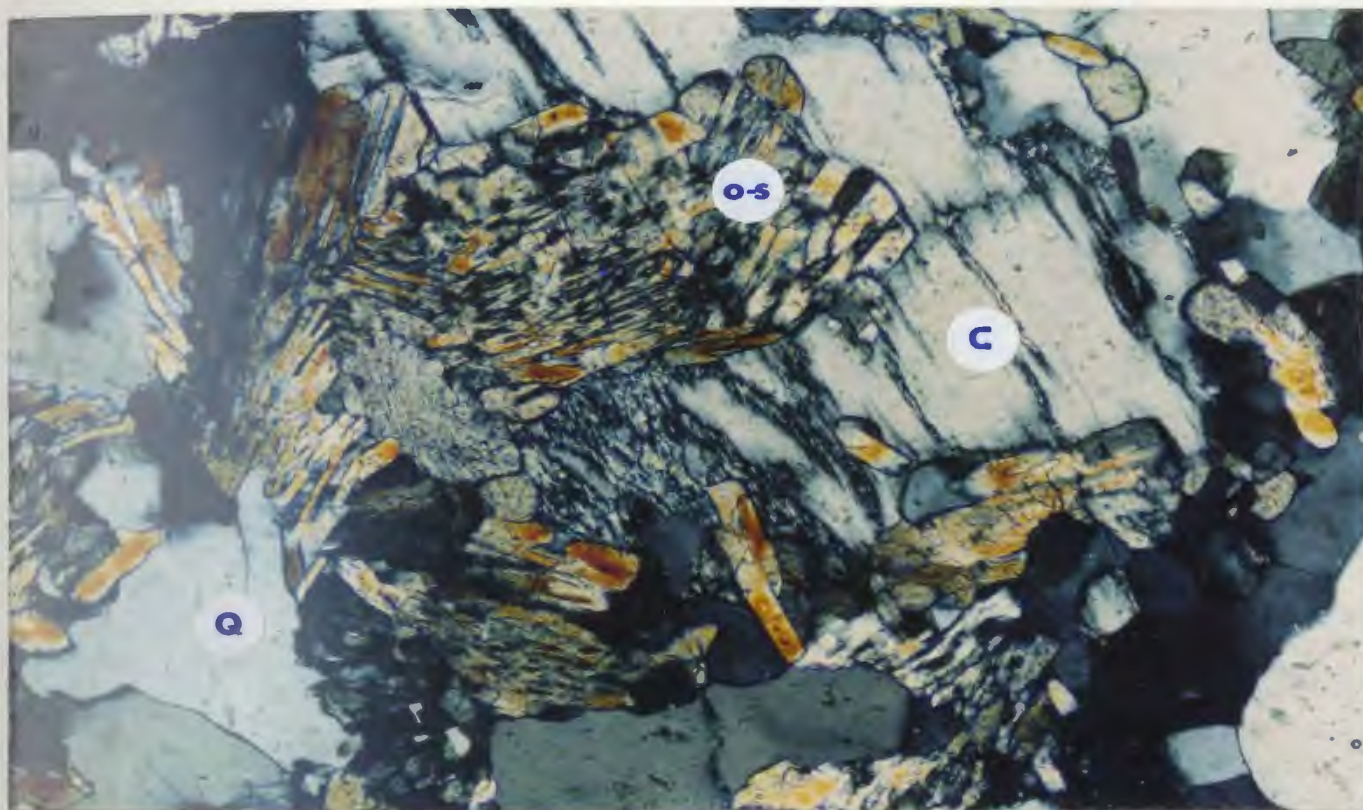


Figure 47. Photomicrograph showing mineral reaction texture of cordierite breakdown to (orthopyroxene + sillimanite) symplectite and quartz. Width of photomicrograph : 2.9 mm. Crossed polarized light. C: cordierite, Q: quartz. O-S: opx-sil symplectite. Sample# : S-68.

Figure 48. Photomicrograph showing replacement of cordierite + spinel by (orthopyroxene + sillimanite) symplectite. Width of photomicrograph : 1.6 mm. Crossed polarized light. Sp: spinel, C: cordierite. O-S: opx-sil symplectite. Sample# : SA-A-1.





#### 4-2-2-2. Sapphirine forming reaction textures

Sapphirine in the mineral assemblages (2) and (3) is present in several distinct forms including symplectic intergrowths with orthopyroxene and as coronas with orthopyroxene porphyroblasts and magnetite (Figs. 49, 50). Two types of spinel occur with green and grey colors in these assemblages. The grey spinel is present as a corona phase with sapphirine rimming ilmenite in the **Al-poorer sapphirine bearing assemblages** (3). The green spinel is also present as isolated inclusions in ilmenite/magnetite oxide in assemblages (2). Cordierite rarely displays contact with sapphirine in assemblage (2).

It is difficult to deduce the sapphirine forming reactions because of the variety of minerals involved. However, textural relations suggest that sapphirine has formed by reaction of orthopyroxene and spinel in **Al-poorer sapphirine bearing assemblages** (3) (Fig. 51) and by reaction of cordierite and spinel already replaced by magnetite in **Al-rich sapphirine-bearing assemblage** (2) (Fig. 52).

The inferred reactions for sapphirine formation are

$$\text{Fe-spinel} + \text{Orthopyroxene} + \text{O}_2 = \text{Mg-spinel} + \text{Magnetite} + \text{Sapphirine}$$

Figure 49. Photomicrograph showing corona texture of fine grained sapphirine in plagioclase surrounding a porphyroblast of orthopyroxene. Width of photomicrograph : 5.4 mm. Crossed polarized light. O: orthopyroxene, Sa: sapphirine. Sample# : S-22.

Figure 50. Photomicrograph showing sapphirine corona around orthopyroxene with magnetite and orthopyroxene. Width of photomicrograph : 1.6 mm. Plane polarized light. O: orthopyroxene, Sa: sapphirine, M: magnetite. Sample# : SA-B-3.

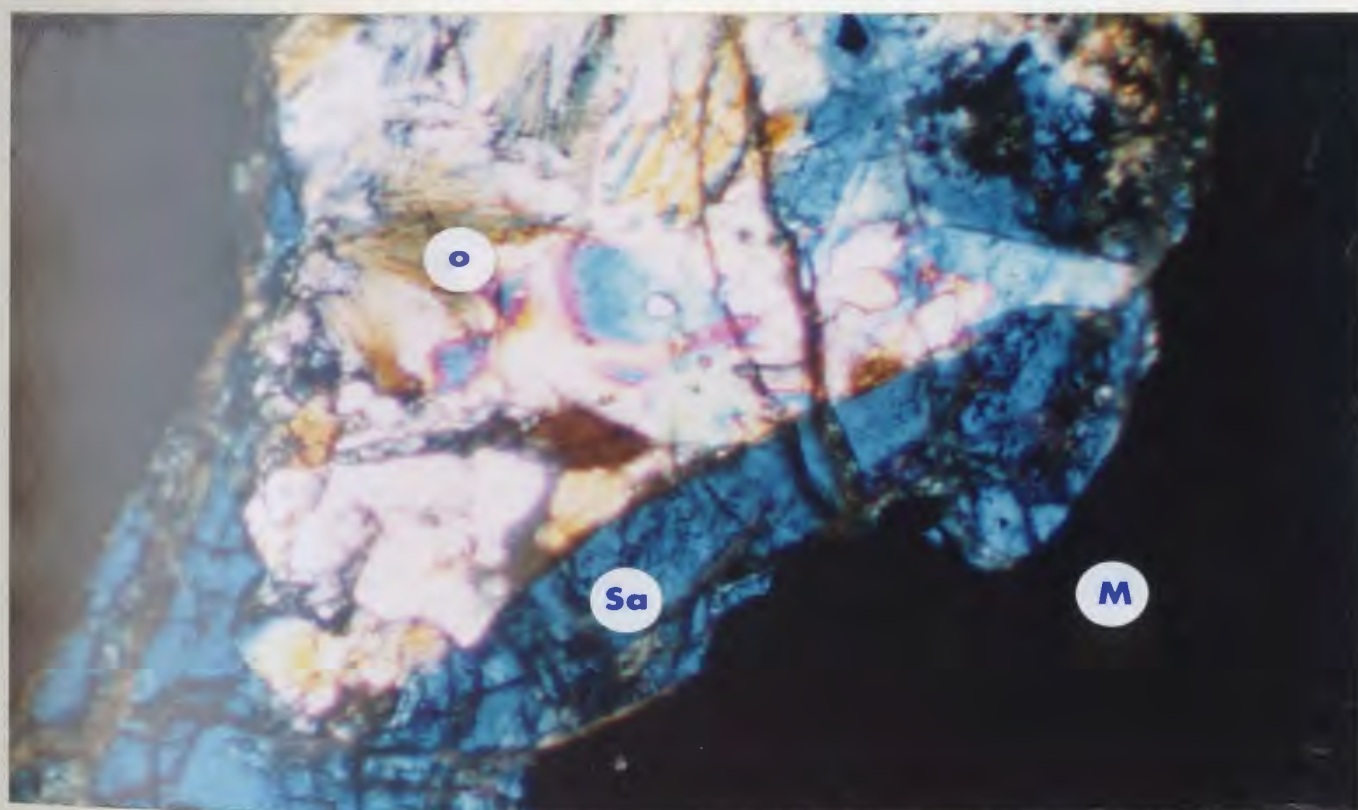
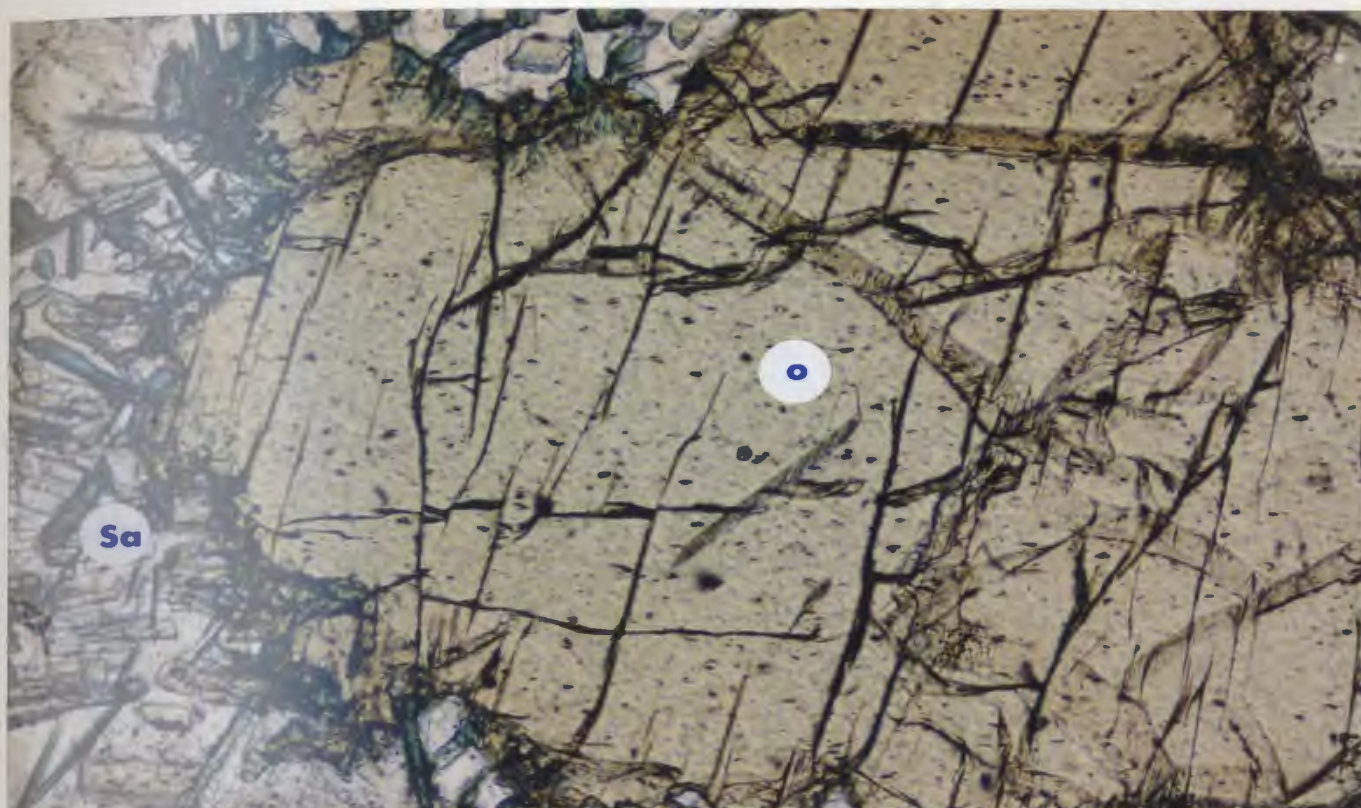


Figure 51. Photomicrograph showing orthopyroxene and Fe-spinel (hercynite-magnetite) reaction to produce Mg-spinel and sapphirine. Width of photomicrograph : 1.6 mm. Plane polarized light.

O: orthopyroxene, Sp: Mg-spinel, Sa: sapphirine.

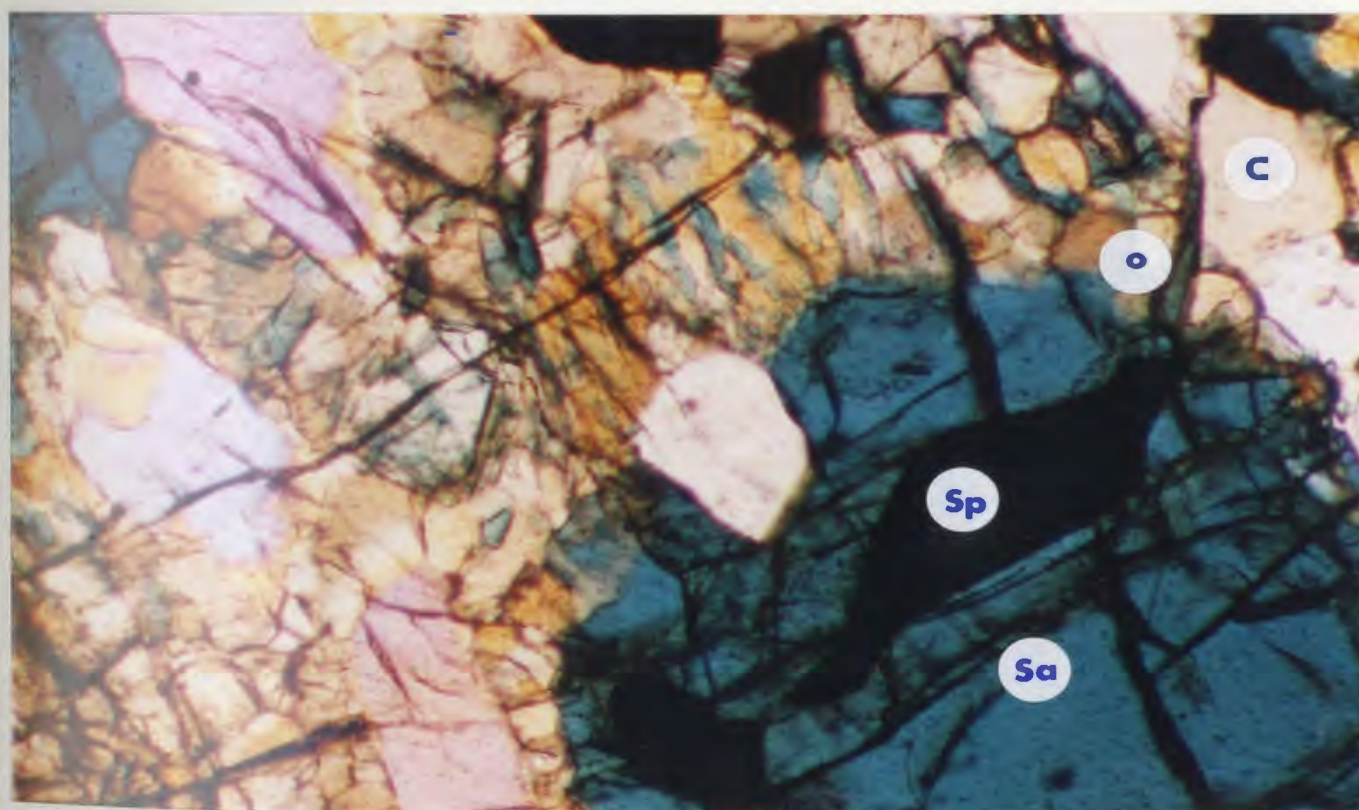
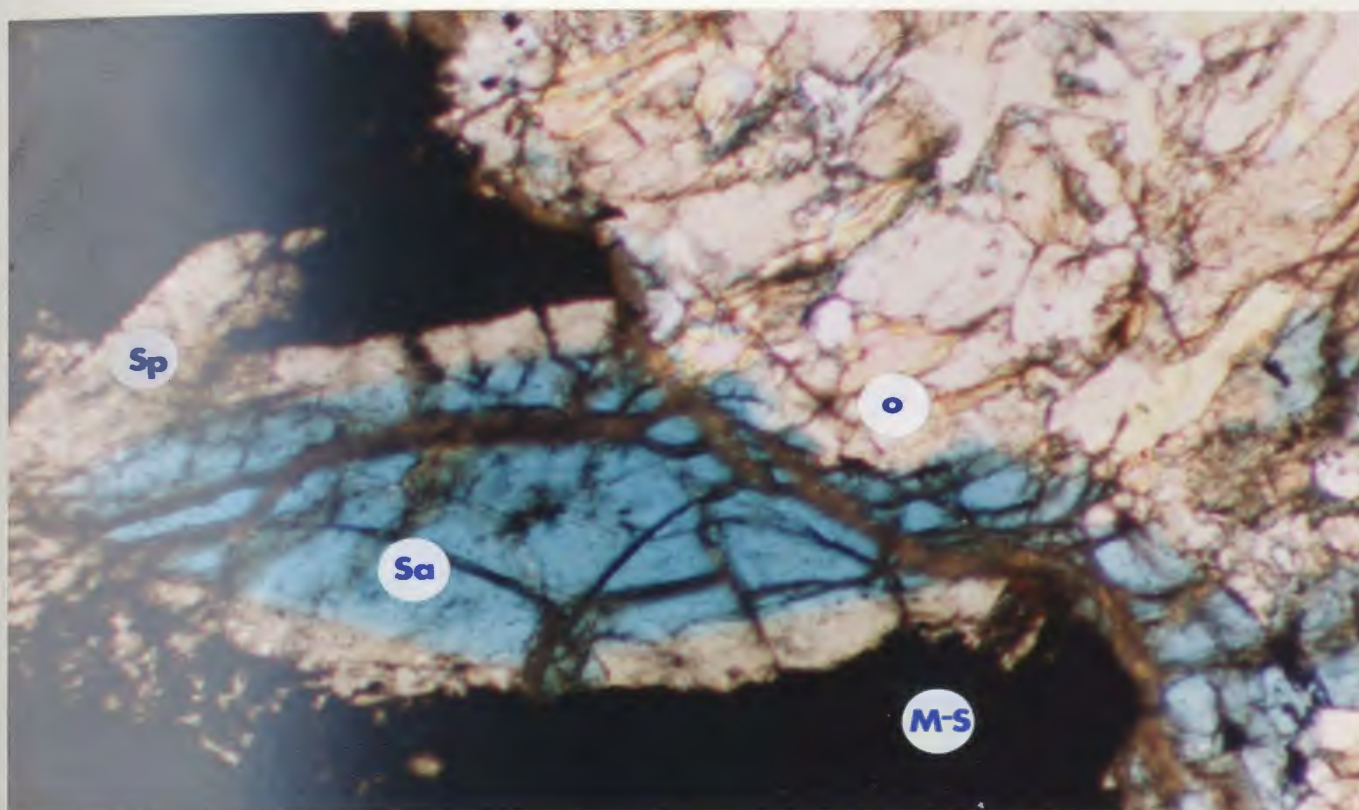
M-S: Magnetite-Hercynite. Sample# : SA-B-2.

Figure 52. Photomicrograph showing orthopyroxene and sapphirine symplectite produced by reaction of cordierite-spinel assemblage. Width of photomicrograph : 2.9 mm. Plane polarized light.

O: orthopyroxene, C: cordierite, Sp: Fe-spinel.

Sa: sapphirine. Sample# : SA-A-1.





Cordierite + Spinel = Orthopyroxene + Sapphirine.

#### 4-2-2-3. Garnet forming reaction textures

Garnet is present as large poikiloblasts that include abundant biotite, spinel, sillimanite and magnetite/ilmenite in the quartz-bearing assemblage (1), implying that it developed later than the assemblage of included phases (Fig. 53). Plagioclase occurs as a matrix around orthopyroxene. Stable contact relations with orthopyroxene are observed in thin sections. Where present, quartz shows a partial corona texture around garnet (Fig. 54). Garnet does not show contacts with cordierite.

Textural relations suggest that garnet was formed by the reaction of orthopyroxene, plagioclase and inclusions including sillimanite, spinel and/or magnetite. Possible reactions are written below :

Orthopyroxene + Sillimanite = Garnet + Quartz

Orthopyroxene + Plagioclase = Garnet + Quartz

Orthopyroxene + Sillimanite + Fe-Spinel = Garnet

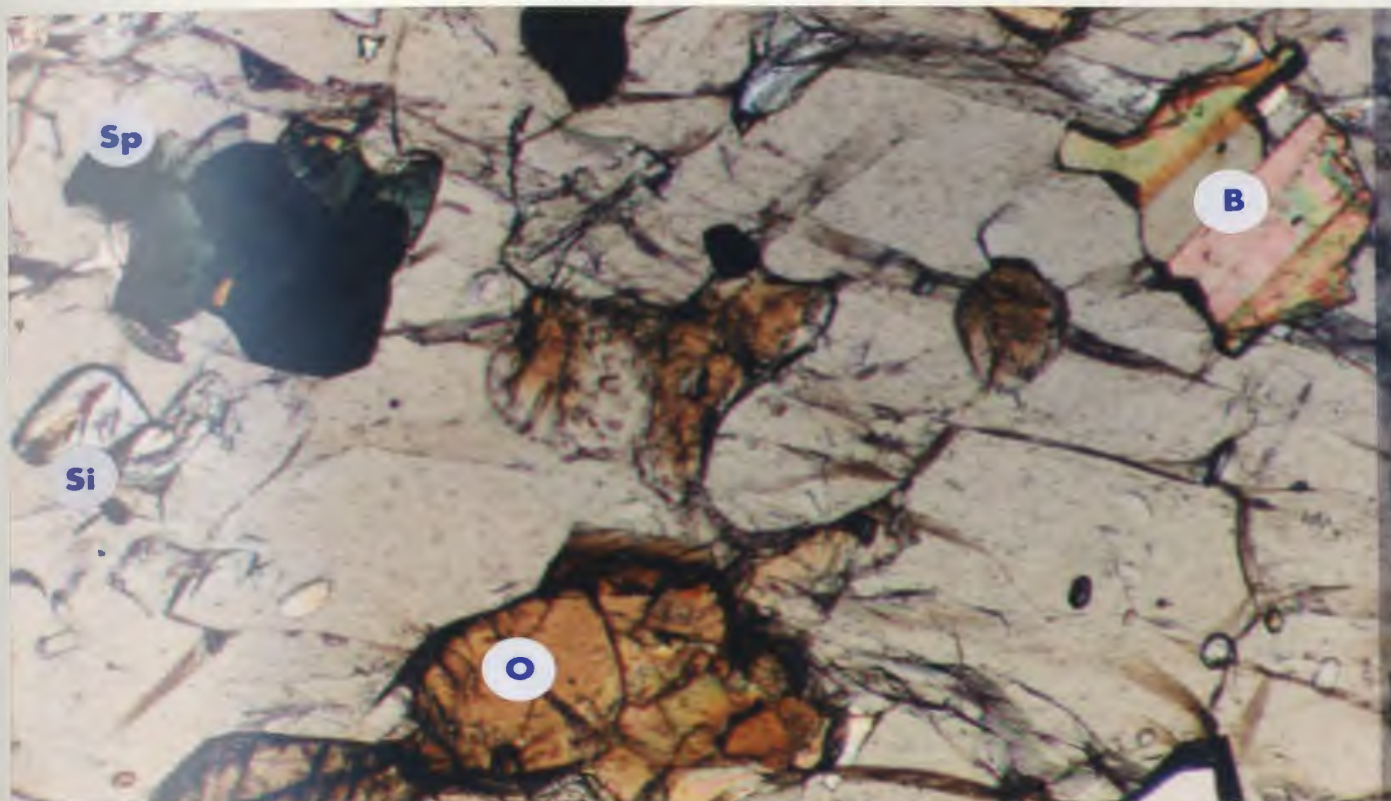


Figure 53. Photomicrograph showing various inclusion phases (sillimanite, ilmenite, spinel, orthopyroxene and biotite) in garnet poikiloblast in pelitic gneiss. Width of photomicrograph : 1.6 mm. Plane polarized light.

O: orthopyroxene, Sp: spinel, B: biotite, Si: sillimanite. Sample# : S-90-1.

Figure 54. Photomicrograph showing garnet poikiloblast with various inclusion phases (sillimanite, orthopyroxene, ilmenite). Note quartz partial corona texture wrapping around garnet poikiloblast. Width of photomicrograph : 5.4 mm. Crossed polarized light.

Q: quartz. Sample# : S-88-1.



#### 4-2-2-4. Kornerupine replacement reaction textures

In Al-rich sapphirine bearing assemblages (2) kornerupine occurs as porphyroblasts (1-2 cm) which show abundant evidence of reaction with other minerals in the assemblage. The kornerupine porphyroblasts record evidence of reactions involving the breakdown of kornerupine, but reactions leading to formation of this mineral are not clear from textural relations.

In these samples, sapphirine and orthopyroxene occur as replacement products formed from kornerupine (Fig. 55). The presence of symplectic and corona textures around kornerupine also indicates that assemblages such as kornerupine and kornerupine + spinel were replaced by the assemblages including sapphirine, orthopyroxene and cordierite (Fig. 56). Textural relations suggest the following possible reactions listed below :

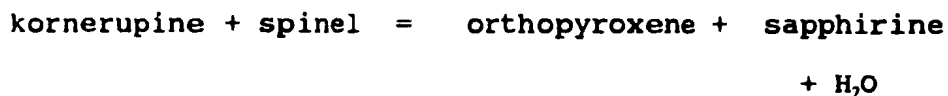
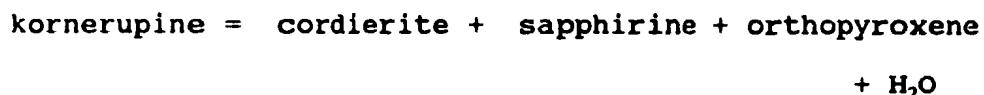
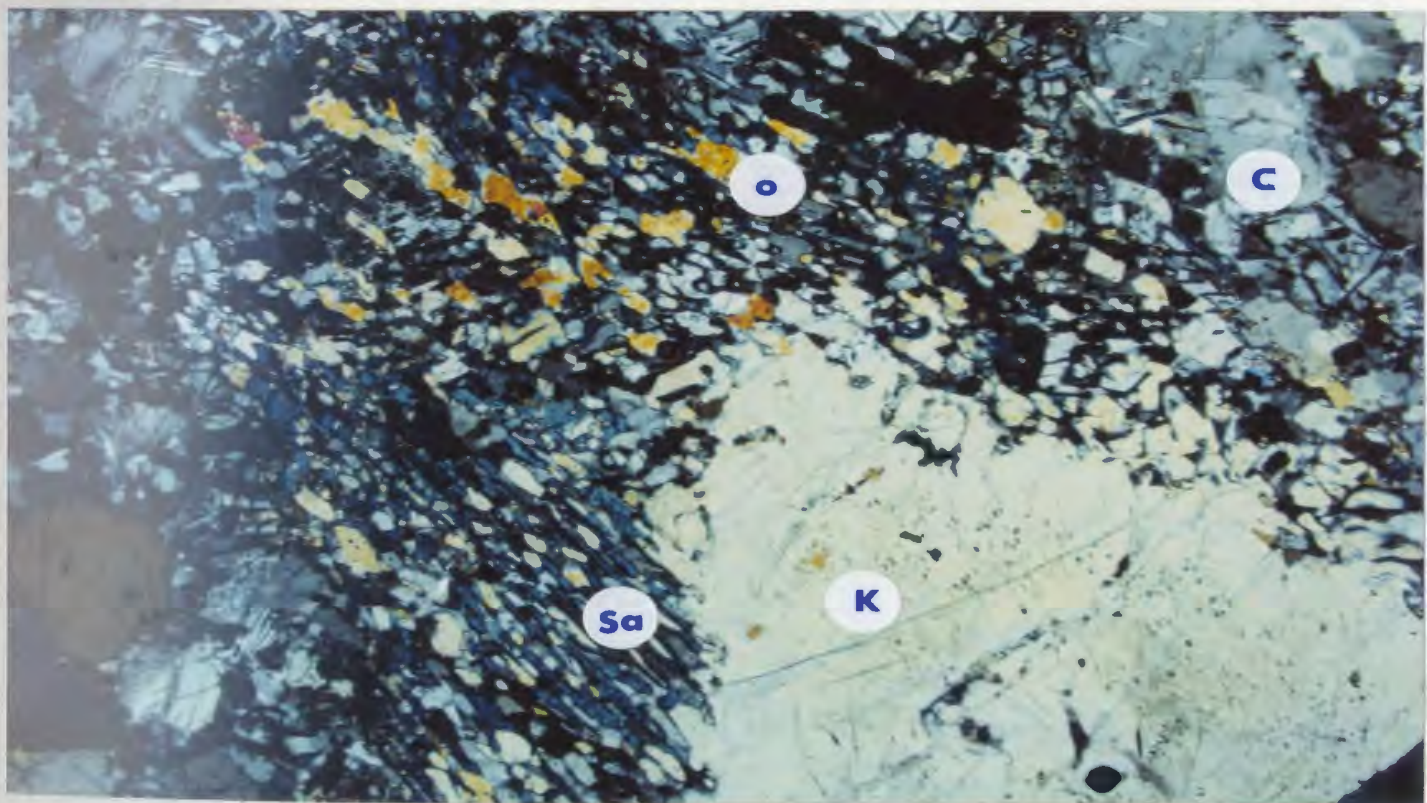
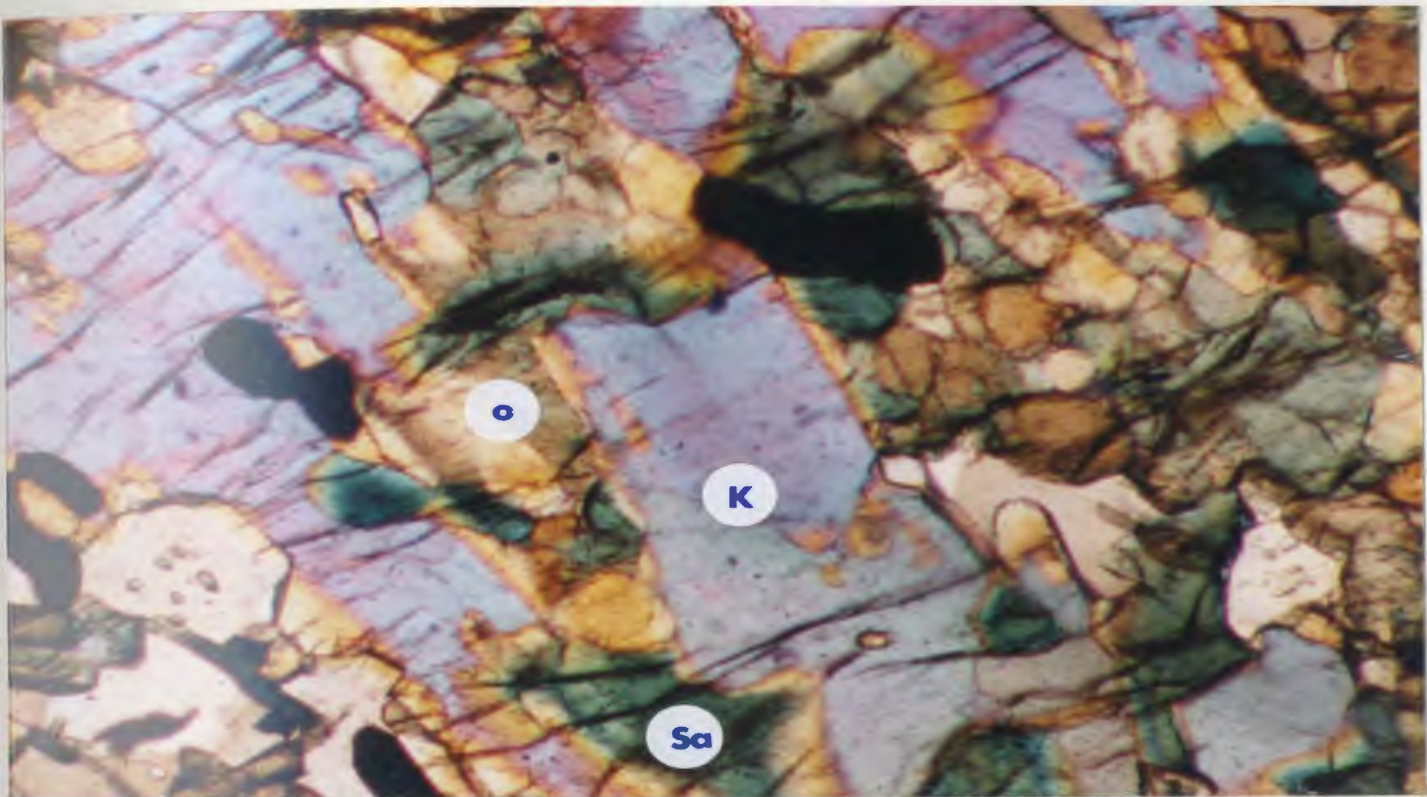


Figure 55. Photomicrograph showing replacement of porphyroblast of kornerupine by orthopyroxene and sapphirine. Width of photomicrograph : 2.9 mm. Plane polarized light.  
K: kornerupine, O: orthopyroxene, Sa: sapphirine.  
Sample# : SA-C-3.

Figure 56. Photomicrograph showing kornerupine reacting to the assemblage orthopyroxene, cordierite, and sapphirine. Width of photomicrograph : 2.9 mm. Crossed polarized light.  
O: orthopyroxene, C: cordierite, K: kornerupine, Sa: sapphirine. Sample# : SA-B-3.





#### 4-2-3 Mineral Chemistry

Electron microprobe mineral analyses were performed on phases occurring in the reaction relationships discussed above. Microprobe operating conditions and standards for the analytical data are presented in Appendix 2. All phases were analyzed for Na, Mg, Al, Si, K, Ca, Ti, Mn and Fe. Analyses are tabulated, and chemical compositions of minerals are presented graphically in the (Fe,Mg)O - Al<sub>2</sub>O<sub>3</sub> - SiO<sub>2</sub> (F.M-A-S system) of Figure 57, and where appropriate in AFM diagram.

**Sapphirine** : Six representative analyses of sapphirine are listed in Table 1. The ideal structural formula of sapphirine was given by Moore (1968) as  $M_7(M)O_2[T_6O_{18}]$  where M and T are (Al,Mg) in octahedral and (Al,Si) in tetrahedral sites respectively. In order to compare the data with sapphirines analysed from other areas, the sapphirines analyzed here were recalculated on the basis of 20 oxygens. The calculated excess of cations over 14 for all the analyzed samples is compatible with the analyses from Wilson Lake in the Grenville Province (Herd et al. 1987) and indicates the presence of a considerable amount of Fe<sup>3+</sup> (Ellis 1980, Grew 1980). For



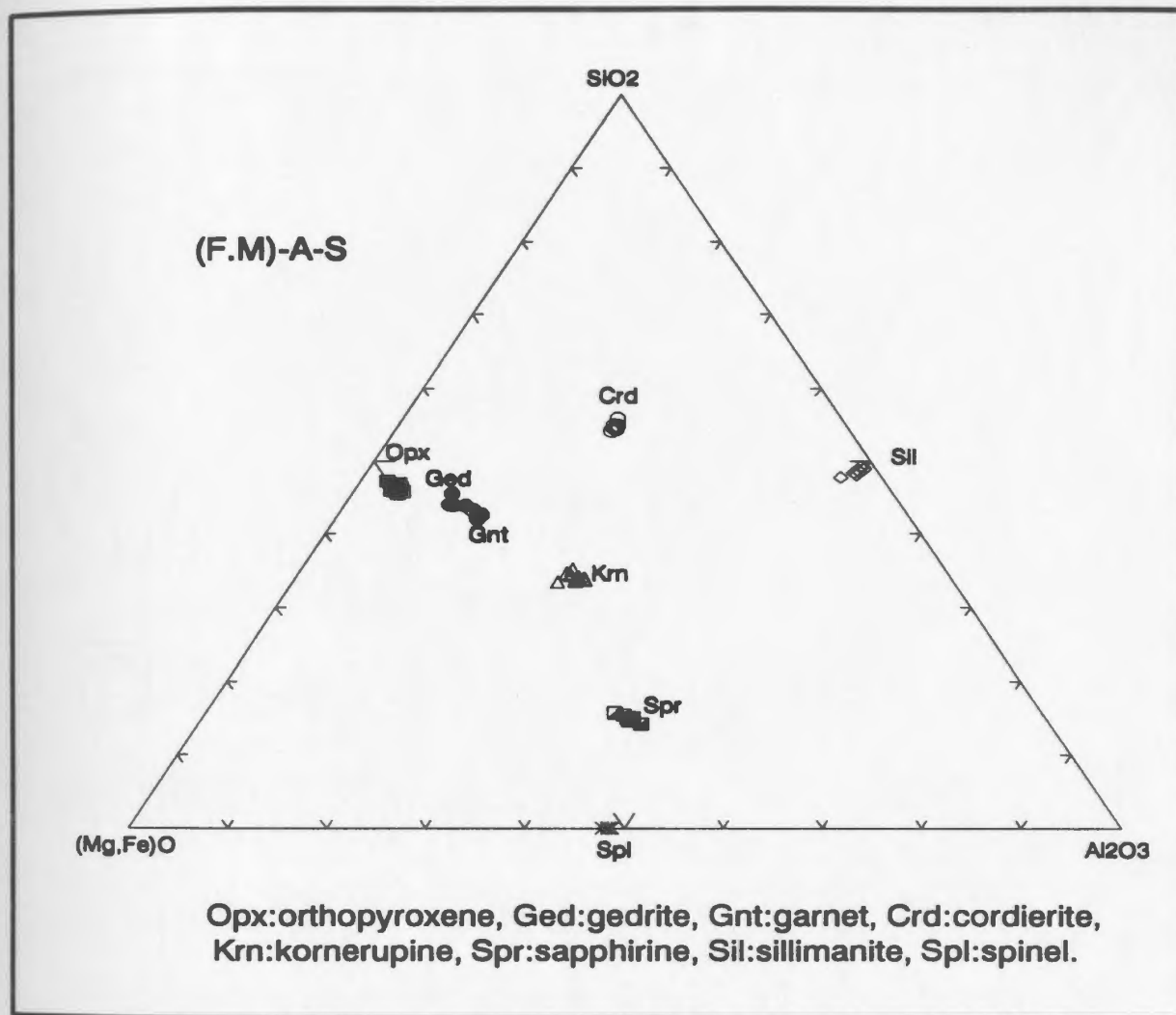


Figure 57. Mineral compositions of pelitic gneiss in the I.H.R. plotted on the (Mg,Fe)-Al<sub>2</sub>O<sub>3</sub>-SiO<sub>2</sub> diagram.

Table 1. Representative microprobe analyses and structural formulae of Sapphirine

SAMPLE MIN CODE	SA-B-1 Spr Core	SA-B-1 Spr Fine	SA-B-2 Spr Core	SA-B-2 Spr Core	SA-B-2 Spr Core	SA-C Spr Fine	SA-A-1 Spr Core	SA-C-3 Spr SY-OPX	SA-C-3 Spr Core	S-22 Spr R-OPX
SiO <sub>2</sub>	13.06	12.25	12.34	13.00	12.67	12.33	12.24	12.02	12.46	11.55
TiO <sub>2</sub>	0.00	0.00	0.00	0.00	0.00	0.00	0.00	0.00	0.00	0.00
Al <sub>2</sub> O <sub>3</sub>	58.02	60.87	60.21	59.40	59.42	60.72	60.43	60.30	60.30	62.00
FeO	9.55	8.11	8.33	9.23	9.04	7.85	8.81	8.15	8.16	8.11
MnO	0.00	0.00	0.00	0.00	0.10	0.00	0.07	0.00	0.00	0.09
MgO	18.60	18.64	18.49	18.66	18.32	18.62	18.12	18.65	18.79	18.02
CaO	0.00	0.00	0.00	0.00	0.00	0.00	0.00	0.00	0.00	0.00
Na <sub>2</sub> O	0.01	0.03	0.00	0.01	0.01	0.01	0.01	0.02	0.01	0.02
K <sub>2</sub> O	0.00	0.00	0.00	0.00	0.00	0.00	0.00	0.00	0.00	0.00
Total	99.24	99.90	99.38	100.30	99.57	99.53	99.68	99.14	99.73	99.79
Structural formulae based on 20 oxygens										
Si	1.59	1.47	1.49	1.56	1.53	1.48	1.48	1.45	1.50	1.39
Ti	0.00	0.00	0.00	0.00	0.00	0.00	0.00	0.00	0.00	0.00
Al	8.32	8.61	8.57	8.41	8.47	8.61	8.59	8.60	8.54	8.78
Fe	0.97	0.81	0.84	0.93	0.91	0.79	0.89	0.82	0.82	0.81
Mn	0.00	0.00	0.00	0.00	0.01	0.00	0.01	0.00	0.00	0.01
Mg	3.37	3.33	3.33	3.34	3.30	3.34	3.26	3.36	3.37	3.23
Ca	0.00	0.00	0.00	0.00	0.00	0.00	0.00	0.00	0.00	0.00
Na	0.00	0.01	0.00	0.00	0.00	0.00	0.00	0.00	0.00	0.00
K	0.00	0.00	0.00	0.00	0.00	0.00	0.00	0.00	0.00	0.00
Total	14.25	14.23	14.23	14.24	14.23	14.22	14.23	14.25	14.23	14.22
Structural formulae based on 14 cations										
Si	1.56	1.45	1.47	1.53	1.51	1.46	1.45	1.43	1.47	1.37
Ti	0.00	0.00	0.00	0.00	0.00	0.00	0.00	0.00	0.00	0.00
Al	8.17	8.47	8.43	8.27	8.33	8.48	8.46	8.45	8.41	8.64
Fe	0.95	0.80	0.83	0.91	0.90	0.78	0.87	0.81	0.81	0.80
Mn	0.00	0.00	0.00	0.00	0.01	0.00	0.01	0.00	0.00	0.01
Mg	3.31	3.28	3.27	3.28	3.25	3.29	3.21	3.30	3.31	3.18
Ca	0.00	0.00	0.00	0.00	0.00	0.00	0.00	0.00	0.00	0.00
Na	0.00	0.01	0.00	0.00	0.00	0.00	0.00	0.00	0.00	0.00
K	0.00	0.00	0.00	0.00	0.00	0.00	0.00	0.00	0.00	0.00
Total	14.00	14.00	14.00	14.00	14.00	14.00	14.00	14.00	14.00	14.00
Fe/(Fe+Mg+Ca+Mn(%))	22.37	19.62	20.18	21.73	21.63	19.13	21.40	19.69	19.59	20.12
Mg/FMCM(%)	77.63	80.38	79.82	78.27	78.12	80.87	78.43	80.31	80.41	79.66
Ca/FMCM(%)	0.00	0.00	0.00	0.00	0.00	0.00	0.00	0.00	0.00	0.00
Mn/FMCM(%)	0.00	0.00	0.00	0.00	0.24	0.00	0.17	0.00	0.00	0.23
Si+Al	9.91	10.08	10.06	9.97	10.00	10.09	10.07	10.06	10.04	10.17
Fe+Mg+Mn+Ca	4.34	4.15	4.17	4.27	4.23	4.13	4.15	4.19	4.19	4.05
Fe/(Fe+Mg)	0.22	0.20	0.20	0.22	0.22	0.19	0.21	0.20	0.20	0.20

Spr-sapphirine; Fe-Total Fe; Fine- Fine grained; SY-OPX-Symplectite with Opx; R-OPX-Rim with Opx.

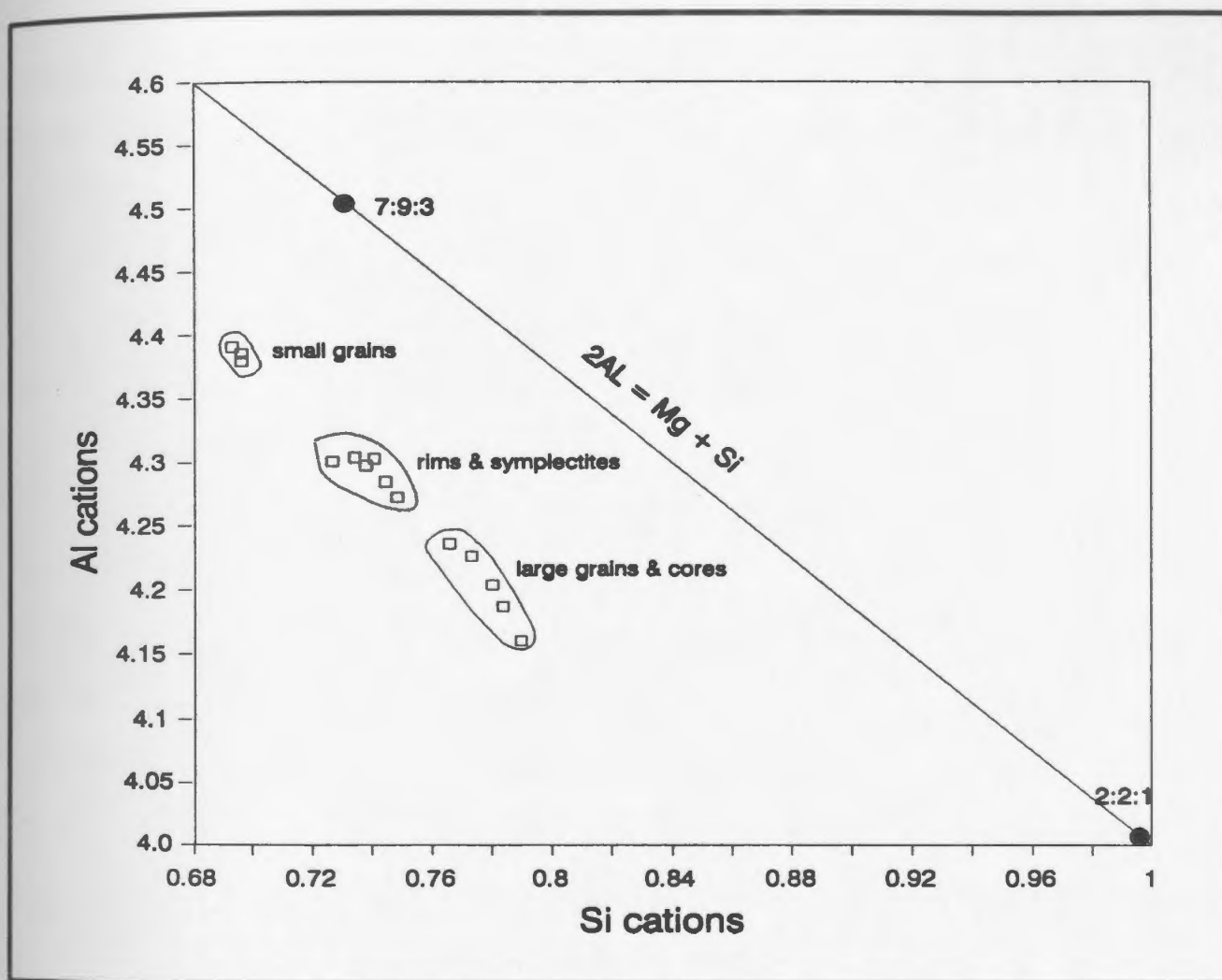


Fig. 58. Molecular proportions of Al vs. Si (per 10 oxygen formula unit) in sapphirines from pelitic gneiss in the Indian Head Range. Diagonal line represents the ideal substitution.

estimation of  $\text{Fe}^{3+}$  the structural formulae were recalculated on the basis of fourteen cations as suggested by Moore (1968). This results in a relatively high amount of  $\text{Fe}^{3+}$  (0.27-0.14 atoms). Zoning was not detected in most grains, except for sapphirines adjacent to orthopyroxene, in which the rims tend to be higher in Al and poorer in Si than the cores. Grains of sapphirine associated with other minerals do not show chemical variation.  $X_{\text{Mg}}$  ranges from 0.77 - 0.80. The total FeO content ranges between 7.9 and 9.6 wt.%, and is relatively high compared to other areas (see Arima et al. 1984, Droop 1989, Grant 1989, Windley et al. 1984). The compositions of sapphirines from the study area are closer to a  $(\text{Mg}, \text{Fe})\text{O} : \text{Al}_2\text{O}_3 : \text{SiO}_2$  ratio of 7:9:3 than to a ratio of 2:2:1 implying operation of the Tschermak substitution  $(\text{Mg}(\text{Fe}^{2+}))\text{Si} = (\text{Al}(\text{Fe}^{3+}))\text{Al}$ . In a Si versus Al plot, they lie below the ideal Tschermak substitution trend, confirming the presence of about 0.2  $\text{Fe}^{3+}$  cations as shown in Fig. 58.

**Kornerupine** : Analyses of kornerupine (excluding B and  $\text{H}_2\text{O}$ ) are presented in Table 2. The general structural formula for kornerupine was first given by Moore and Bennett (1968) as  $\text{Mg}_2\text{MgAl}_6[\text{Si}_2\text{O}_7][(\text{Al}, \text{Si})_2\text{SiO}_{10}]\text{O}_4(\text{OH})$ . Schreyer and Seifert (1969) proposed two possible stoichiometric ratios, either  $4\text{MgO} \cdot 3\text{Al}_2\text{O}_3 \cdot 4\text{SiO}_2 \cdot \text{H}_2\text{O} = (4:3:4)$  or  $3.5\text{MgO} \cdot 3.5\text{Al}_2\text{O}_3 \cdot 3.5\text{SiO}_2 \cdot \text{H}_2\text{O} =$

Table 2. Representative microprobe analyses and structural formulae of Komerupine

SAMPLE MIN CODE	SA-B-3 Km R-OPX	SA-B-3 Km CORE	SA-C-3 Km CORE	SA-C-3 Km CORE	SA-C-1 Km CORE	SA-C-1 Km R-SIL	SA-C-1 Km R-SPR	SA-C-1 Km CORE	IH-45 Km CORE	SA-B-2 Km CORE	SA-C Km R-SIL	SA-C Km CORE
SiO <sub>2</sub>	30.13	29.75	30.08	29.16	30.03	29.31	29.12	29.72	29.48	29.59	29.17	30.03
TiO <sub>2</sub>	0.02	0.05	0.05	0.05	0.04	0.04	0.07	0.07	0.00	0.02	0.03	0.04
Al <sub>2</sub> O <sub>3</sub>	41.03	42.30	40.47	42.41	39.83	41.59	41.73	41.43	43.27	41.54	42.53	39.65
FeO	5.29	4.98	7.27	6.47	6.11	6.47	6.78	6.07	5.66	6.12	5.83	6.46
MnO	0.00	0.00	0.00	0.00	0.00	0.00	0.00	0.00	0.00	0.00	0.00	0.00
MgO	19.42	19.54	18.83	18.05	18.12	18.00	18.23	18.65	18.46	18.64	18.15	18.66
CaO	0.00	0.00	0.00	0.00	0.00	0.00	0.00	0.00	0.00	0.00	0.00	0.00
Na <sub>2</sub> O	0.13	0.00	0.17	0.06	0.13	0.11	0.12	0.12	0.08	0.11	0.06	0.10
K <sub>2</sub> O	0.00	0.16	0.00	0.00	0.00	0.00	0.00	0.00	0.00	0.00	0.00	0.00
Total	96.02	96.78	96.88	96.21	94.26	95.52	96.05	96.07	96.95	96.02	95.56	94.93
Structural formulae based on 21 oxygens												
Si	3.89	3.81	3.89	3.78	3.97	3.83	3.79	3.85	3.78	3.84	3.79	3.95
Ti	0.00	0.00	0.00	0.00	0.00	0.00	0.01	0.01	0.00	0.00	0.00	0.00
Al	6.25	6.39	6.18	6.48	6.20	6.41	6.41	6.33	6.54	6.36	6.52	6.15
Fe	0.57	0.53	0.79	0.70	0.67	0.71	0.74	0.66	0.61	0.66	0.61	0.71
Mn	0.00	0.00	0.00	0.00	0.00	0.00	0.00	0.00	0.00	0.00	0.00	0.00
Mg	3.74	3.73	3.63	3.49	3.57	3.50	3.54	3.60	3.52	3.61	3.52	3.66
Ca	0.00	0.00	0.00	0.00	0.00	0.00	0.00	0.00	0.00	0.00	0.00	0.00
Na	0.03	0.00	0.04	0.02	0.03	0.03	0.03	0.03	0.02	0.03	0.02	0.03
K	0.00	0.03	0.00	0.00	0.00	0.00	0.00	0.00	0.00	0.00	0.00	0.00
Total	14.49	14.50	14.54	14.48	14.45	14.48	14.51	14.49	14.46	14.49	14.45	14.49
Fe/Fe+Mg+Ca+Mn(%)	13.26	12.51	17.81	16.75	15.91	16.79	17.27	15.44	14.68	15.56	14.83	16.27
Mg/FMCM(%)	86.74	87.49	82.19	83.25	84.09	83.21	82.73	84.56	85.32	84.44	85.17	83.73
Ca/FMCM(%)	0.00	0.00	0.00	0.00	0.00	0.00	0.00	0.00	0.00	0.00	0.00	0.00
Mn/FMCM(%)	0.00	0.00	0.00	0.00	0.00	0.00	0.00	0.00	0.00	0.00	0.00	0.00
Si+Al	10.15	10.20	10.07	10.27	10.17	10.23	10.20	10.19	10.31	10.20	10.31	10.09
Fe+Mg+Mn+Ca	4.31	4.27	4.42	4.19	4.24	4.21	4.28	4.26	4.13	4.27	4.13	4.37
Fe/(Fe+Mg)	0.13	0.13	0.18	0.17	0.16	0.17	0.17	0.15	0.15	0.16	0.15	0.16

Km : Komerupine, FeO : Total FeO, R-OPX : Rim of Km adjacent to Opx, R-SPR : Rim of Km adjacent to sapphirine, R-SIL : Rim of Km adjacent to sillimanite.

(1:1:1). Kornerupine analyzed in the study has  $(\text{Mg,Fe})\text{O} : \text{Al}_2\text{O}_3 : \text{SiO}_2$  ratios close to the 4:3:4 kornerupine synthesized by Seifert (1975). All analyses for kornerupine generally have totals between 95 wt.% and 96 wt.%, indicating relatively high water or/and boron contents. Total FeO is relatively high compared with kornerupine from other areas (see Windley et al. 1984) with a limited range from 5.5 to 7 wt.%.  $X_{\text{Mg}}$  (0.82-0.87) in kornerupine is much higher than in sapphirine and orthopyroxene from the same assemblage. No zoning or chemical variation was detected throughout the grains.

**Orthopyroxene :** Orthopyroxene occurs in all 3 mineral assemblage groups. Orthopyroxenes analyzed in this study are essentially solid solutions in  $\text{FeO-MgO-Al}_2\text{O}_3\text{-SiO}_2$  (FMAS), with only very limited CaO and MnO, and correspond to hypersthene - bronzite in composition (Table 3). The  $\text{Al}_2\text{O}_3$  content falls in the range 5.5 to 9.5 wt.percent and is similar to that of aluminous orthopyroxenes from other sapphirine-bearing granulite areas (Arima and Barnett 1984, Lal et al. 1987, Harley et al. 1990). The  $\text{Al}_2\text{O}_3$  content of porphyroblastic orthopyroxene generally decreases from core to rim with increasing MgO, and orthopyroxene symplectite with sapphirine and fine grained orthopyroxene shows the lowest content of  $\text{Al}_2\text{O}_3$  (5.5-6 wt.%). These differences imply that each



Table 3. Representative microprobe analyses and structural formulae of Orthopyroxene

SAMPLE MIN CODE	S-90-1 OPX R-GNT	S-90-1 OPX C-GNT	S-68 OPX CORE	S-68 OPX RIM	SA-B-1 OPX CORE	SA-B-1 OPX FINE	SA-C-1 OPX SY-SIL	IH-45 OPX CORE	SA-B-2 OPX CORE	SA-B-2 OPX SY-SPR	S-74B OPX CORE	S-74B OPX F-SIL	SA-A-2 OPX CORE	SA-C OPX F-KRN
SiO <sub>2</sub>	50.31	49.72	48.08	48.55	49.87	50.24	50.83	47.48	49.92	50.45	46.79	47.49	50.14	50.94
TiO <sub>2</sub>	0.05	0.07	0.11	0.12	0.01	0.00	0.03	0.00	0.02	0.01	0.10	0.08	0.00	0.02
Al <sub>2</sub> O <sub>3</sub>	4.86	5.61	7.89	7.05	8.80	8.17	6.95	8.67	8.89	7.31	8.62	7.50	7.75	7.24
FeO	20.60	21.31	21.89	21.86	12.21	12.37	11.89	11.58	11.58	12.06	22.56	22.77	12.90	11.34
MnO	0.15	0.16	0.09	0.11	0.04	0.03	0.07	0.05	0.03	0.04	0.43	0.47	0.44	0.05
MgO	24.06	23.46	21.78	21.97	29.52	29.51	30.53	30.46	30.07	30.09	20.90	21.40	28.76	30.52
CaO	0.01	0.01	0.01	0.02	0.02	0.01	0.01	0.00	0.63	0.02	0.02	0.02	0.00	0.01
Na <sub>2</sub> O	0.02	0.01	0.03	0.01	0.00	0.01	0.00	0.03	0.01	0.01	0.01	0.01	0.01	0.00
K <sub>2</sub> O	0.00	0.00	0.00	0.00	0.00	0.00	0.00	0.00	0.00	0.00	0.00	0.00	0.00	0.00
Total	100.05	100.34	99.87	99.69	100.47	100.35	100.31	100.27	100.54	99.99	99.42	99.73	100.00	100.13
Structural formulae based on 8 oxygens														
Si	1.86	1.84	1.79	1.81	1.76	1.78	1.80	1.77	1.76	1.79	1.76	1.78	1.79	1.80
Ti	0.00	0.00	0.00	0.00	0.00	0.00	0.00	0.00	0.00	0.00	0.00	0.00	0.00	0.00
Al	0.21	0.24	0.35	0.31	0.37	0.34	0.29	0.36	0.37	0.31	0.38	0.33	0.33	0.30
Fe	0.84	0.66	0.68	0.68	0.36	0.37	0.35	0.34	0.34	0.36	0.71	0.72	0.39	0.34
Mn	0.00	0.01	0.00	0.00	0.00	0.00	0.00	0.00	0.00	0.00	0.01	0.01	0.01	0.00
Mg	1.32	1.29	1.21	1.22	1.56	1.56	1.61	1.59	1.58	1.59	1.17	1.20	1.53	1.61
Ca	0.00	0.00	0.00	0.00	0.00	0.00	0.00	0.00	0.00	0.00	0.00	0.00	0.00	0.00
Na	0.00	0.00	0.00	0.00	0.00	0.00	0.00	0.00	0.00	0.00	0.00	0.00	0.00	0.00
K	0.00	0.00	0.00	0.00	0.00	0.00	0.00	0.00	0.00	0.00	0.00	0.00	0.00	0.00
Total	4.04	4.04	4.03	4.03	4.05	4.05	4.05	4.06	4.05	4.05	4.04	4.05	4.05	4.05
Fe/(Fe+Mg+Ca+Mn(%))	32.37	33.67	36.00	35.75	18.82	19.03	17.91	17.57	17.75	18.34	37.43	37.08	19.97	17.24
Mg/FMCM(%)	67.37	66.05	63.83	64.03	81.06	80.90	81.96	82.35	82.14	81.56	61.80	62.10	79.34	82.67
Ca/FMCM(%)	0.02	0.02	0.02	0.04	0.04	0.02	0.02	0.00	0.06	0.04	0.04	0.04	0.00	0.02
Mn/FMCM(%)	0.24	0.26	0.15	0.18	0.06	0.05	0.11	0.08	0.05	0.06	0.72	0.78	0.69	0.06
Si+Al	2.05	2.06	2.12	2.10	2.10	2.10	2.06	2.10	2.10	2.07	2.12	2.09	2.09	2.08
Fe+Mg+Mn+Ca	1.95	1.94	1.88	1.89	1.90	1.90	1.94	1.90	1.90	1.93	1.68	1.91	1.91	1.92
Fe/(Fe+Mg)	0.32	0.34	0.36	0.36	0.19	0.19	0.18	0.18	0.18	0.18	0.38	0.37	0.20	0.17

Fe: Total Fe, R-GNT: Rim adjacent to garnet, C-GNT: Core part from garnet, FINE: Fine grain, SY-SIL: Symplectite with sillimanite, F-KRN: Fine grain adjacent to hornupine

orthopyroxene type grew under different conditions with respect to pressure and temperature (Droop and Bucher-Nurminen 1984). Although iron in orthopyroxene is primarily in the  $\text{Fe}^{2+}$  state, significant amounts (0.12 - 0.03) of  $\text{Fe}^{3+}$  are calculated from stoichiometry, based on 4 cations per formulae unit (see Arima 1978).  $X_{\text{Mg}}$  of orthopyroxene from quartz-bearing rocks ranges from 0.63 to 0.68, whereas orthopyroxene from quartz-free rocks shows a significantly higher  $X_{\text{Mg}}$  (0.79-0.82).

**Cordierite :** Cordierite occurs as an early phase. Even though cordierite takes part in several mineral reactions, it is relatively homogeneous in individual grains (Table 4). The homogeneous character of cordierite has been observed from other high-grade metamorphic areas and may represent re-equilibration during retrograde metamorphism (e.g. Ellis 1980). Early cordierite that shows evidence of replacement by opx-sil-qtz, is very Mg-rich ( $X_{\text{Mg}}$ : 0.92-0.94), compatible with the inference that it formed early under high grade conditions. Similarly early cordierite coexisting with Mg-spinel is also Mg-rich ( $X_{\text{Mg}}$ : 0.92-0.94). Cordierite from garnet-bearing rocks has relatively low  $X_{\text{Mg}}$  (0.61-0.82) compared to other analyzed cordierite. Generally, cordierite in the Indian Head Range is rich in the magnesium end member and contains negligible amounts of alkalis and CaO. Cordierite

Table 4. Representative microprobe analyses and structural formulae of Cordierite

SAMPLE MINERAL CODE	S-68 Crd CORE	S-68 Crd R-SIL	SA-C-1 Crd CORE	SA-C Crd CORE	IH-46B Crd RIM	IH-46B Crd CORE	IH-46 Crd RIM	SA-C-3 Crd CORE	S-90-2 Crd CORE	S-88-1 Crd CORE
SiO <sub>2</sub>	46.12	48.71	49.22	49.24	48.99	48.62	49.15	48.76	48.16	48.75
TiO <sub>2</sub>	0.01	0.00	0.00	0.00	0.00	0.00	0.00	0.00	0.00	0.00
Al <sub>2</sub> O <sub>3</sub>	31.53	31.93	33.86	33.52	33.83	33.53	33.55	33.74	32.84	32.57
FeO	9.52	3.59	1.55	1.62	1.80	1.92	1.81	1.60	4.27	4.30
MnO	0.00	0.00	0.00	0.00	0.00	0.00	0.00	0.00	0.00	0.04
MgO	8.36	11.13	13.07	13.22	12.97	12.94	12.92	13.11	11.56	11.52
CaO	0.00	0.00	0.00	0.00	0.00	0.00	0.00	0.00	0.00	0.00
Na <sub>2</sub> O	0.01	0.85	0.11	0.14	0.13	0.16	0.17	0.26	0.18	0.26
K <sub>2</sub> O	0.00	0.00	0.00	0.00	0.00	0.00	0.00	0.00	0.00	0.00
Total	95.55	96.22	97.82	97.75	97.72	97.17	97.59	97.48	97.01	97.44
Cations on the basis of 18 oxygens										
Si	4.93	5.03	4.94	4.95	4.93	4.93	4.95	4.92	4.94	4.98
Ti	0.00	0.00	0.00	0.00	0.00	0.00	0.00	0.00	0.00	0.00
Al	3.97	3.89	4.01	3.97	4.02	4.01	3.99	4.02	3.97	3.92
Fe	0.85	0.31	0.13	0.14	0.15	0.16	0.15	0.14	0.37	0.37
Mn	0.00	0.00	0.00	0.00	0.00	0.00	0.00	0.00	0.00	0.00
Mg	1.33	1.71	1.96	1.98	1.95	1.95	1.94	1.97	1.77	1.75
Ca	0.00	0.00	0.00	0.00	0.00	0.00	0.00	0.00	0.00	0.00
Na	0.00	0.17	0.02	0.03	0.03	0.03	0.03	0.05	0.04	0.05
K	0.00	0.00	0.00	0.00	0.00	0.00	0.00	0.00	0.00	0.00
Total	11.09	11.11	11.06	11.07	11.07	11.08	11.07	11.10	11.09	11.08
Fe/(Fe+Mg+Ca+Mn)(%)	38.99	15.33	6.24	6.43	7.23	7.69	7.29	6.41	17.17	17.29
Mg/FMCM(%)	61.01	84.67	93.76	93.57	92.77	92.31	92.71	93.59	82.83	82.55
Ca/FMCM(%)	0.00	0.00	0.00	0.00	0.00	0.00	0.00	0.00	0.00	0.00
Mn/FMCM(%)	0.00	0.00	0.00	0.00	0.00	0.00	0.00	0.00	0.00	0.16
Si+Al	8.90	8.92	8.95	8.93	8.95	8.94	8.94	8.94	8.92	8.91
Fe+Mg+Mn+Ca	2.18	2.02	2.09	2.12	2.10	2.12	2.09	2.11	2.13	2.13
Fe/(Fe+Mg)	0.39	0.15	0.06	0.06	0.07	0.08	0.07	0.06	0.17	0.17

Crd : cordierite, Fe : Total Fe, R-SIL : Rim adjacent to sillimanite.

generally has totals between 96-98%. It is also optically positive with a relatively large 2V, implying that an appreciable proportion of the primary volatile content in the cordierite is CO<sub>2</sub> (Armbruster and Bloss 1980). Precise determination of the volatile composition has not been attempted due to difficulty in obtaining pure grains for determination of R.I..

**Sillimanite** : Sillimanite is fairly constant in composition and contains relatively high contents of total FeO (1-2 wt.%) and MgO (< 1 wt.%) as shown in Table 5. Similarly high contents of FeO (total) in sillimanite have also been reported from sapphirine-quartz bearing rocks from Wilson Lake and Peekskill (Caporuscio and Morse 1979; Grew 1980; Herd et al. 1987).

**Plagioclase** : Plagioclase is present as an essential phase in all mineral assemblages. The anorthite content ranges from An<sub>543</sub>, depending on the coexisting mineral assemblages. Plagioclase coexisting with sapphirine and kornerupine has a sodic character (An <30). Individual grains do not show compositional zoning.

**Spinel** : The spinels are solid solutions of Mg-spinel and

Table 5. Representative microprobe analyses of Spinel and Sillimanite.

SAMPLE MIN CODE	SA-A-1 Spl R-SPR	SA-A-1 Spl R-OPX	S-90-1 Spl INC-GNT	S-90-1 Spl INC-GNT	IH-46 Sil CORE	IH-46 Sil SY-OPX	S-68 Sil CORE	SA-C-1 Sil CORE	SA-C-1 Sil SY-OPX	S-74B Sil CORE
SiO <sub>2</sub>	0.11	0.00	0.08	0.08	35.63	35.84	35.98	35.92	36.08	35.94
TiO <sub>2</sub>	0.00	0.00	0.03	0.01	0.00	0.00	0.00	0.00	0.00	0.00
Al <sub>2</sub> O <sub>3</sub>	66.41	67.00	62.83	62.36	62.15	61.11	62.61	61.72	61.98	62.13
FeO	10.99	10.35	23.70	24.79	2.02	1.98	1.18	1.72	1.63	1.01
MnO	0.40	0.39	0.02	0.00	0.00	0.00	0.00	0.00	0.00	0.00
MgO	21.71	22.12	12.87	12.64	0.05	0.98	0.00	0.26	0.02	0.00
CaO	0.00	0.00	0.00	0.00	0.00	0.00	0.00	0.00	0.00	0.00
Na <sub>2</sub> O	0.05	0.06	0.04	0.05	0.00	0.00	0.01	0.01	0.02	0.01
K <sub>2</sub> O	0.00	0.00	0.00	0.00	0.00	0.00	0.00	0.00	0.00	0.00
Total	99.67	99.92	99.56	99.93	99.85	99.90	99.78	99.63	99.74	99.10
Si	On the basis of 4 oxygens				On the basis of 5 oxygens					
Ti	0.00	0.00	0.00	0.00	0.97	0.98	0.98	0.98	0.98	0.98
Al	0.00	0.00	0.00	0.00	0.00	0.00	0.00	0.00	0.00	0.00
Fe	1.96	1.97	1.97	1.96	2.00	1.97	2.01	1.99	1.99	2.01
Mn	0.23	0.22	0.53	0.55	0.05	0.05	0.03	0.04	0.04	0.02
Mg	0.01	0.01	0.00	0.00	0.00	0.00	0.00	0.00	0.00	0.00
Ca	0.81	0.82	0.51	0.50	0.00	0.04	0.00	0.01	0.00	0.00
Na	0.00	0.00	0.00	0.00	0.00	0.00	0.00	0.00	0.00	0.00
K	0.00	0.00	0.00	0.00	0.00	0.00	0.00	0.00	0.00	0.00
Total	3.02	3.02	3.01	3.02	3.02	3.03	3.02	3.02	3.02	3.01
Fe/(Fe+Mg+Ca+Mn)(%)	21.94	20.63	50.80	52.39	95.78	53.65	100.00	78.78	97.86	100.00
Mg/FMCM(%)	77.25	78.58	49.16	47.61	4.22	46.35	0.00	21.22	2.14	0.00
Ca/FMCM(%)	0.00	0.00	0.00	0.00	0.00	0.00	0.00	0.00	0.00	0.00
Mn/FMCM(%)	0.81	0.79	0.04	0.00	0.00	0.00	0.00	0.00	0.00	0.00
Si+Al	1.97	1.97	1.97	1.96	2.98	2.95	2.99	2.97	2.98	2.99
Fe+Mg+Mn+Ca	1.05	1.05	1.04	1.05	0.05	0.08	0.03	0.05	0.04	0.02
Fe/(Fe+Mg)	0.22	0.21	0.51	0.52	0.96	0.54	1.00	0.79	0.98	1.00

Spl : spinel, Sil : sillimanite, Fe : Total Fe, R-SPR : Rim adjacent to Sapphirine, INC-GNT : Inclusion in Garnet, SY: Symplectite.

hercynite, and contain minor amount of Mn ( <1 wt.%) (Table 5). Individual grains are homogeneous. As described in the petrography section (4-2-2), there are two types of spinel in the pelitic gneiss.  $X_{Mg}$  of grey spinel in Al-poor sapphirine bearing assemblages (3) ranges from 0.77-0.79, in contrast to a range of 0.47-0.50 measured from green spinel in quartz-bearing assemblages (1). A slight excess in the number of cations implies the presence of minor  $Fe^{3+}$ .

**Gedrite :** Relatively rare gedrite occurs as both isolated coarse grains and in a symplectite with orthopyroxene in quartz-bearing assemblage (1). Gedrite formulae were recalculated on the basis of 23 oxygens (Table 6). Total cations minus (Na + K) are commonly much higher than 15.00 implying that gedrite from the Indian Head Range contains relatively high  $Fe^{3+}$  contents (see Droop 1989). The gedrites are Al-rich (16-20 wt.%) with considerable Na-contents (2.8-3.0 wt.%).  $X_{Mg}$  ranges from 0.82 to 0.83. No compositional difference between coarse grains and grains in symplectites was detected.

**Garnet :** Garnet poikiloblasts have abundant inclusions such as spinel and sillimanite in assemblage (1) as previously described. Garnets analyzed are pyrope (31-38) -almandine (56-64) solid solutions with only minor grossular (CaO < 1 mol.%)



Table 6. Representative microprobe analyses and structural formulae of additional minerals.

SAMPLE MINERAL CODE	S-88 GED CORE	IH-45 GED CORE	IH-45 GED CORE	IH-46B COR INC-ILM	SA-A-1 BIO OLD	SA-A-1 BIO YOU	S-22 BIO YOU	S-90-2 GNT C-OPX1	S-88-2 GNT C-OPX2	S-88 PLAG CORE	SA-B-2 PLAG CORE	SA-A-2 PLAG CORE	SA-C PLAG CORE
SiO <sub>2</sub>	41.81	43.12	43.12	0.00	38.19	38.08	37.69	38.41	38.49	67.52	62.65	65.08	62.62
TiO <sub>2</sub>	0.56	0.09	0.08	0.05	2.28	2.25	2.30	0.01	0.02	0.00	0.00	0.00	0.00
Al <sub>2</sub> O <sub>3</sub>	17.20	17.55	18.37	98.37	17.32	17.12	17.05	21.67	21.85	20.01	23.36	21.66	23.07
FeO	15.44	9.44	8.75	1.71	8.10	8.39	8.86	27.74	25.08	0.08	0.20	0.30	0.06
MnO	0.15	0.08	0.10	0.00	0.00	0.00	0.00	0.62	1.78	0.00	0.00	0.00	0.00
MgO	19.26	24.56	24.75	0.00	20.48	20.37	20.27	10.74	11.74	0.00	0.09	0.13	0.00
CaO	0.09	0.14	0.08	0.00	0.00	0.00	0.00	0.21	0.57	1.15	4.58	1.38	4.27
Na <sub>2</sub> O	2.98	2.85	2.98	0.00	0.12	0.12	0.14	0.24	0.00	11.53	9.06	11.32	9.74
K <sub>2</sub> O	0.00	0.00	0.00	0.00	10.02	9.89	9.79	0.00	0.00	0.00	0.25	0.00	0.30
Total	97.28	97.63	98.22	100.14	96.50	96.23	96.10	99.86	99.53	100.29	100.20	99.87	100.08
oxygen number		23.00		3.00		22.00		12.00			8.00		
Si	6.01	6.01	5.97	0.00	5.45	5.45	5.42	2.96	2.96	2.95	2.77	2.87	2.78
Al	2.83	2.89	3.00	1.98	2.91	2.89	2.89	1.97	1.98	1.03	1.22	1.13	1.21
Fe	1.87	1.10	1.01	0.02	0.97	1.00	1.07	1.79	1.61	0.00	0.01	0.01	0.00
Mn	0.02	0.01	0.01	0.00	0.00	0.00	0.00	0.05	0.12	0.00	0.00	0.00	0.00
Mg	4.15	5.11	5.11	0.00	4.35	4.35	4.34	1.24	1.34	0.00	0.01	0.01	0.00
Ca	0.01	0.02	0.01	0.00	0.00	0.00	0.00	0.02	0.05	0.05	0.22	0.07	0.20
Na	0.83	0.77	0.80	0.00	0.03	0.03	0.04	0.04	0.00	0.98	0.78	0.97	0.84
K	0.00	0.00	0.00	0.00	1.82	1.81	1.80	0.00	0.00	0.00	0.01	0.00	0.02
Total	15.88	15.92	15.92	2.01	15.78	15.78	15.80	8.07	8.05	5.02	5.01	5.05	5.05
Fe/Fe+Mg+Ca+Mn(%)	30.86	17.88	18.49	100.00	18.16	18.77	19.70	57.82	51.68	5.15	3.21	13.05	1.08
Mg/FMCM(%)	68.60	81.86	83.12	0.00	81.84	81.23	80.30	39.89	43.11	0.00	2.58	10.07	0.00
Ca/FMCM(%)	0.23	0.34	0.19	0.00	0.00	0.00	0.00	0.56	1.50	94.85	94.21	78.88	98.92
Mn/FMCM(%)	0.30	0.15	0.19	0.00	0.00	0.00	0.00	1.73	3.71	0.00	0.00	0.00	0.00
Si+Al	8.94	8.90	8.97	1.98	8.36	8.34	8.31	4.94	4.93	Si+Al	3.99	3.99	4.00
Fe+Mg+Mn+Ca	6.04	6.24	6.14	0.02	5.32	5.35	5.41	3.10	3.12	Albite	94.78	78.16	93.69
Fe(Fe+Mg)	0.31	0.18	0.17	1.00	0.18	0.19	0.20	0.59	0.55	Anorthite	5.22	21.84	6.31

Fe: Total Fe. GED: Gedrite, COR: Corundum, INC-ILM: Inclusion in ilmenite, OLD: Old fabric, YOU: Retrograde, C-OPX: Core part from Opx.

and spessartine (MnO: 0.8-1.5 mol.%) contents. These garnets are compositionally zoned with rims of lower Mg, implying retrograde exchange between garnet and orthopyroxene.  $X_{Mg}$  is in the range 0.40 to 0.47 and always less than the magnesium number of the coexisting orthopyroxene.

**Biotite :** Biotite occurs as both a possible early and also a later phase in association with sapphirine and orthopyroxene. Individual grains are relatively homogeneous except for Ti ( $TiO_2$  : 2 -4.5 wt.%). The compositional homogeneity may reflect re-equilibration during the retrograde episode. All biotites are magnesian ( $X_{Mg}$  : 0.77-0.82), similar to coexisting orthopyroxene ( $X_{Mg}$  : 0.63-0.82). Biotites analyzed in the study have Al contents between 1.3 and 1.5 atoms per 22 oxygens. The biotite that is interpreted as a possible primary phase has the most aluminous compositions. The stoichiometric estimation of oxidation ratios in biotite is hampered by the possible presence of site vacancies in the biotite structure. However, previous workers (Chinner 1960, Stephenson 1979) have noted that average oxidation ratios are about 0.1 ( $Fe_2O_3$  : FeO). Utilizing this assumption, Fig. 59 illustrates biotite composition on Troger's (1971) diagram.

**Variation in  $X_{Mg}$  among coexisting minerals**

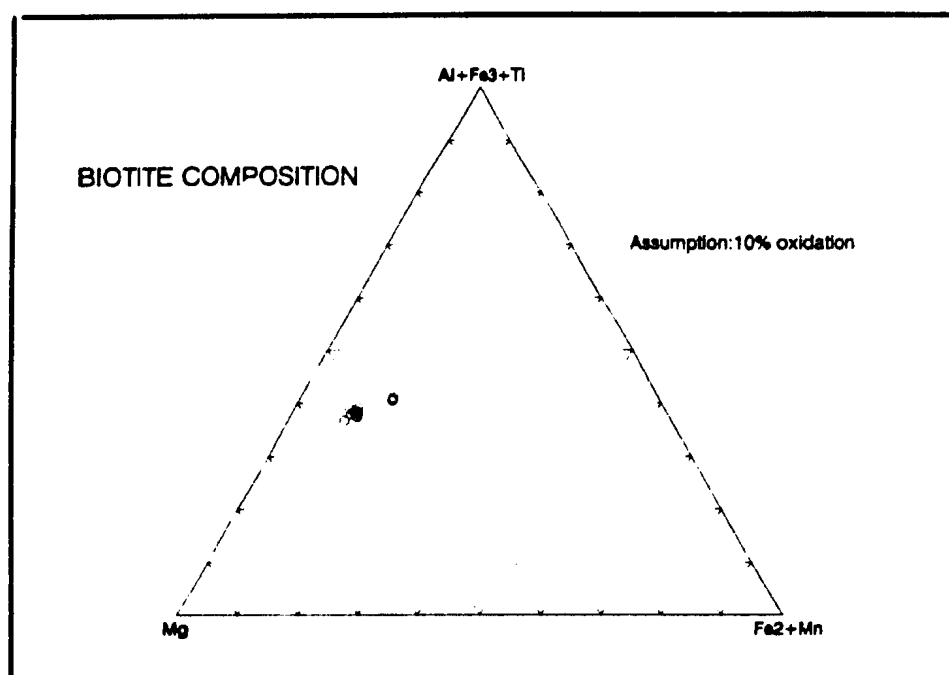


Figure 59. Biotite compositions from the pelitic gneiss in the I.H.R. plotted in Al+Fe<sub>3</sub>+Ti - Mg - Fe<sub>2</sub>+Mn diagram.

The ranking of  $X_{Mg} = (Mg/Mg+Fe)$  values among pairs of coexisting minerals is as follows :

Cordierite > Kornerupine > Gedrite > Biotite >

Orthopyroxene  $\approx$  Sapphirine > Spinel > Garnet

#### 4-2-4 Metamorphic reactions and projections

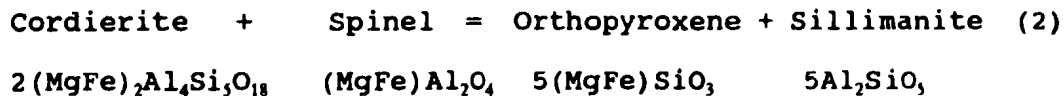
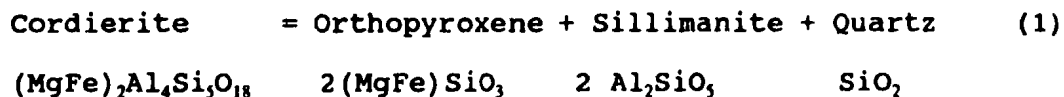
The textural relations of critical mineral assemblages, which were interpreted in the petrography section (4-2-2), attest to a sequence of metamorphic reactions which can be considered in conjunction with the measured compositions of mineral phases. The P-T conditions of reactions deduced in this manner are then approximated by comparison with the available petrogenetic grids. The model chemical systems used in the study are generally very simplified models of the real rock system (i.e. only the major elements are considered). The critical first-order components for a chemographic analysis of the assemblages in pelitic rocks are FeO, MgO, Al<sub>2</sub>O<sub>3</sub> and SiO<sub>2</sub>. Two projections are used to display the mineral assemblages in FMAS space. In the (F.M)-A-S diagram, F and M are graphed together as a single component, and the resultant diagram is very useful for evaluating the role of silica and alumina saturation in assemblages.

In the AFM diagram, the importance of MgO and FeO as separated components is enhanced. Two types of AFM diagram are used in this study. In the first, quartz is present as a phase in the assemblage, and so its activity is fixed throughout the diagram ( $a_{\text{SiO}_2} = 1$ ) (Thompson 1957). In the second type of AFM

diagram, labelled quartz-absent, quartz is not present in the assemblage, so  $a_{\text{SiO}_2} < 1$ . Although the absolute value of  $a_{\text{SiO}_2}$  is not known for each assemblage, the quartz-absent AFM projections are valid thermodynamically if  $a_{\text{SiO}_2}$  does not vary across the composition space depicted in the diagram. Inasmuch as the quartz-absent AFM diagrams represent isolated reactions in small volumes of rock that occur within FMAS reaction space, this thermodynamic validity is maintained. However direct comparisons between qtz-absent AFM diagrams are not warranted in the light of the unknown value of  $a_{\text{SiO}_2}$ .

#### (A) Sillimanite forming reactions

This reaction is characterized by formation of a sillimanite, fine-grained orthopyroxene and quartz replacing cordierite porphyroblasts, as previously described. Textural relations suggest that the following reactions (mass balanced for end member Mg or Fe compositions) ran from left to right.





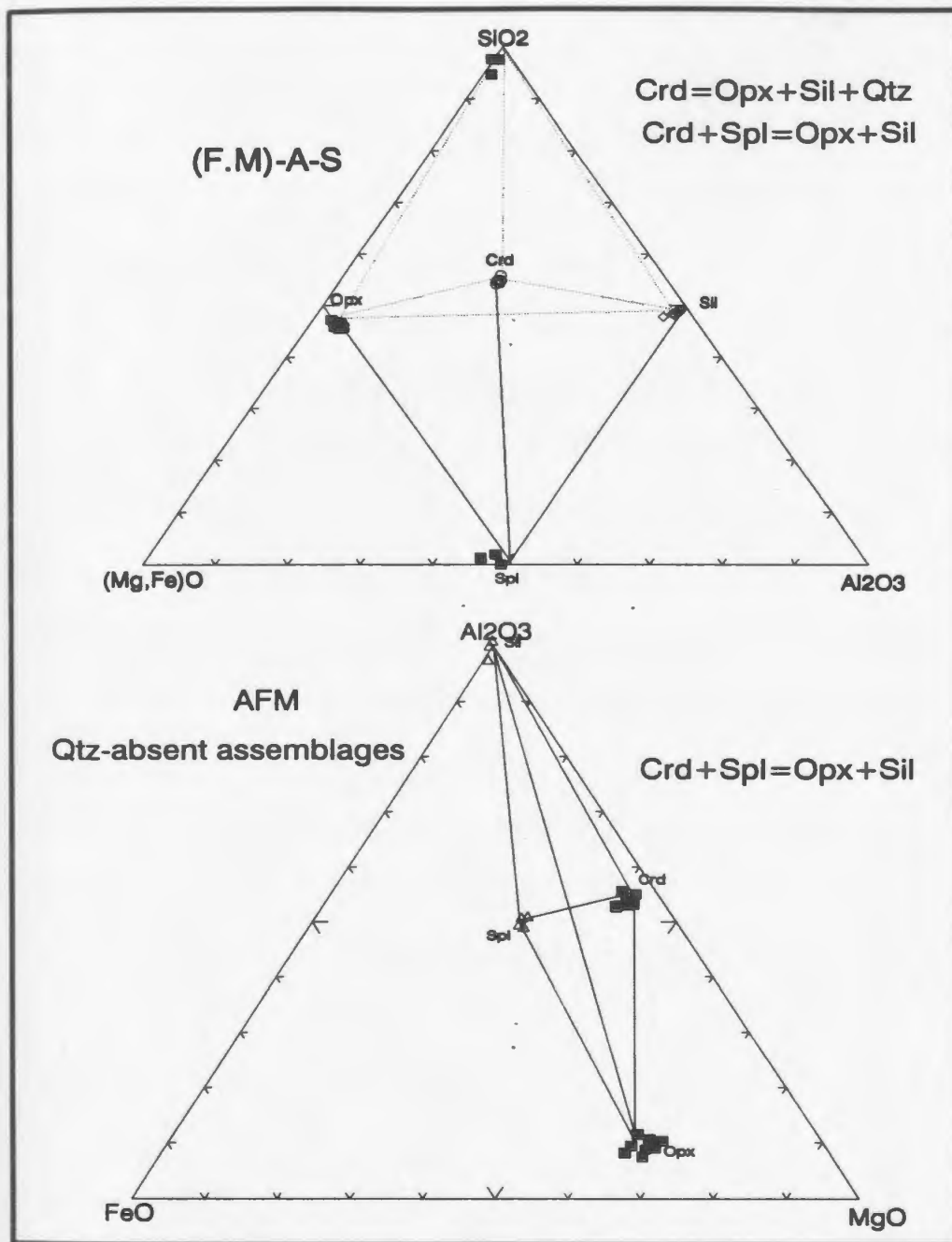


Fig. 60. (F.M)-A-S and AFM diagrams constructed from measured mineral compositions showing phase relations involving cordierite deduced from textural relationships. In the (F.M)-A-S diagram, the dotted line: Qtz-bearing assemblages, the solid line: Qtz-absent assemblages. The assemblage Opx-Crd-Sil occurs in both Qtz-bearing and Qtz-absent rocks.

Chemographic viability of reaction (1) in quartz-bearing assemblages is evident from the (Mg,Fe)O-Al<sub>2</sub>O<sub>3</sub>-SiO<sub>2</sub> diagram of Fig. 60 (a), plotted for analyzed mineral compositions in which the cordierite composition lies within the three-phase field Opx-Sil-Qtz. The assemblage crd-opx-sil-qtz is divariant in AFM space, and from the textures described earlier it is clear that the HT/LP phase cordierite is being replaced by the divariant 4 phases assemblage. The Mg-rich composition of the cordierite ( $X_{Mg}$  from 0.92-0.94) indicates the Mg-rich composition of the rocks and suggests that the reaction boundary for analyzed samples in P-T space will not be far removed from that for end-member Mg-cordierite. Similarly the viability of reaction (2) recorded in the Al rich sapphirine-bearing assemblage is also evident from the intersection of the Crd-Spl and Opx-Sil joins in the quartz-absent part of the composition space in the Al<sub>2</sub>O<sub>3</sub>-FeO-MgO diagram of Fig. 60 (b).

#### (B) Sapphirine forming reactions

Sapphirine forming reactions 3 and 4 interpreted from the temporal sequence of reaction textures are :

Fe-spinel + Orthopyroxene + O<sub>2</sub> = Mg-spinel + Magnetite



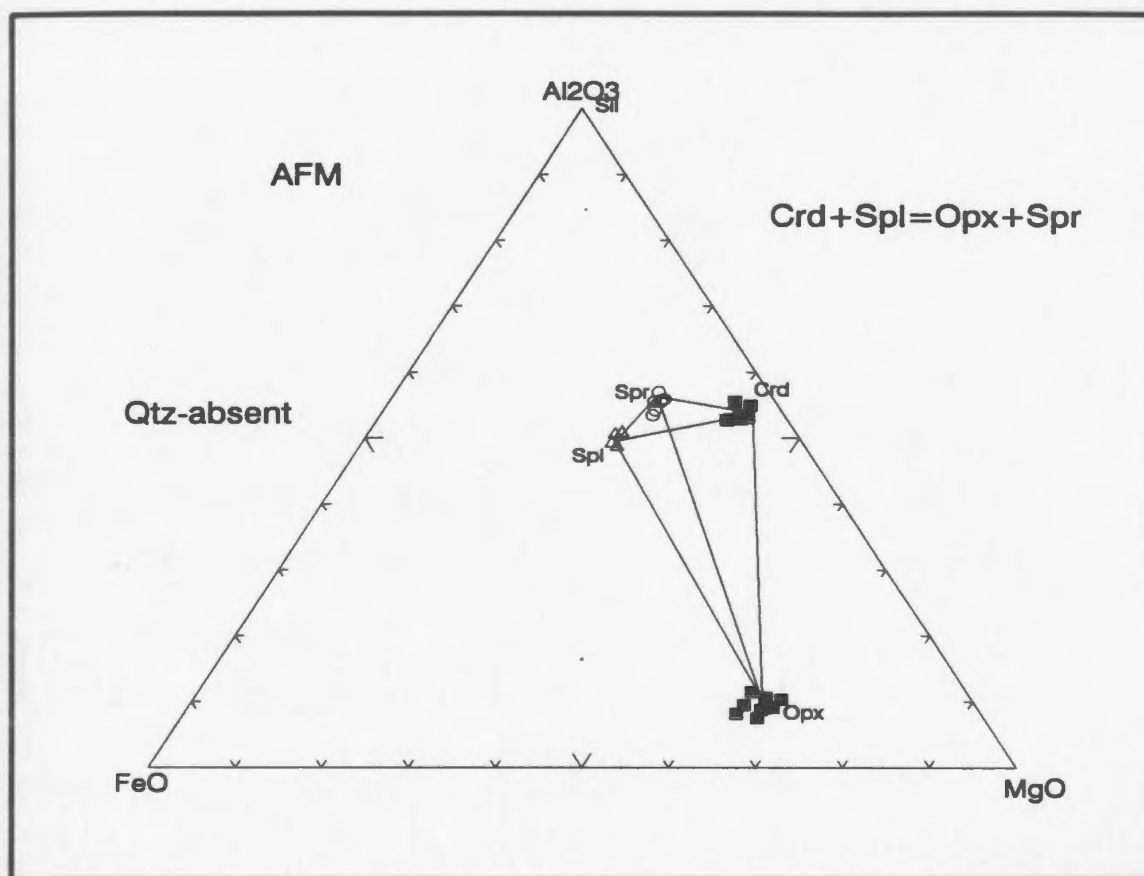
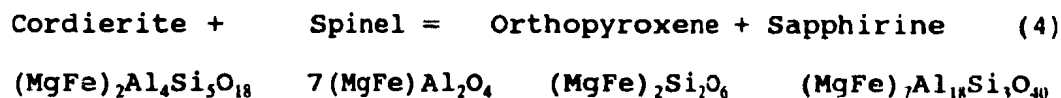
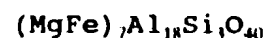


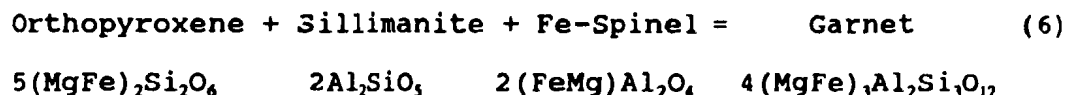
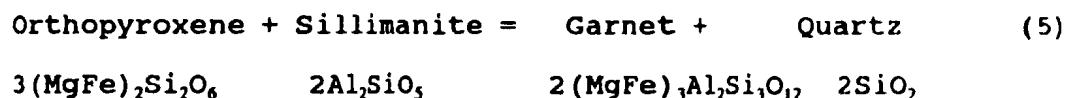
Fig. 61. AFM diagram constructed using measured mineral compositions showing phase relations for sapphirine forming reaction (4).



Reaction (3) was suggested by Herd et al. (1987), and the exact stoichiometric coefficients cannot be calculated because orthopyroxene contains variable amounts of  $\text{Al}_2\text{O}_3$ . However the reaction is supported by textural evidence (Fig. 51). Reaction (4) is deduced from the textural relations shown in Fig. 52 and is consistent with the crossing of Crd-Spl and Opx-Spr joins in the  $\text{Al}_2\text{O}_3$ -FeO-MgO diagram, as shown in Fig. 61.

### (C) Garnet forming reactions

On the basis of textural relations (Figs. 53 and 54), the following garnet-forming reactions can be inferred :



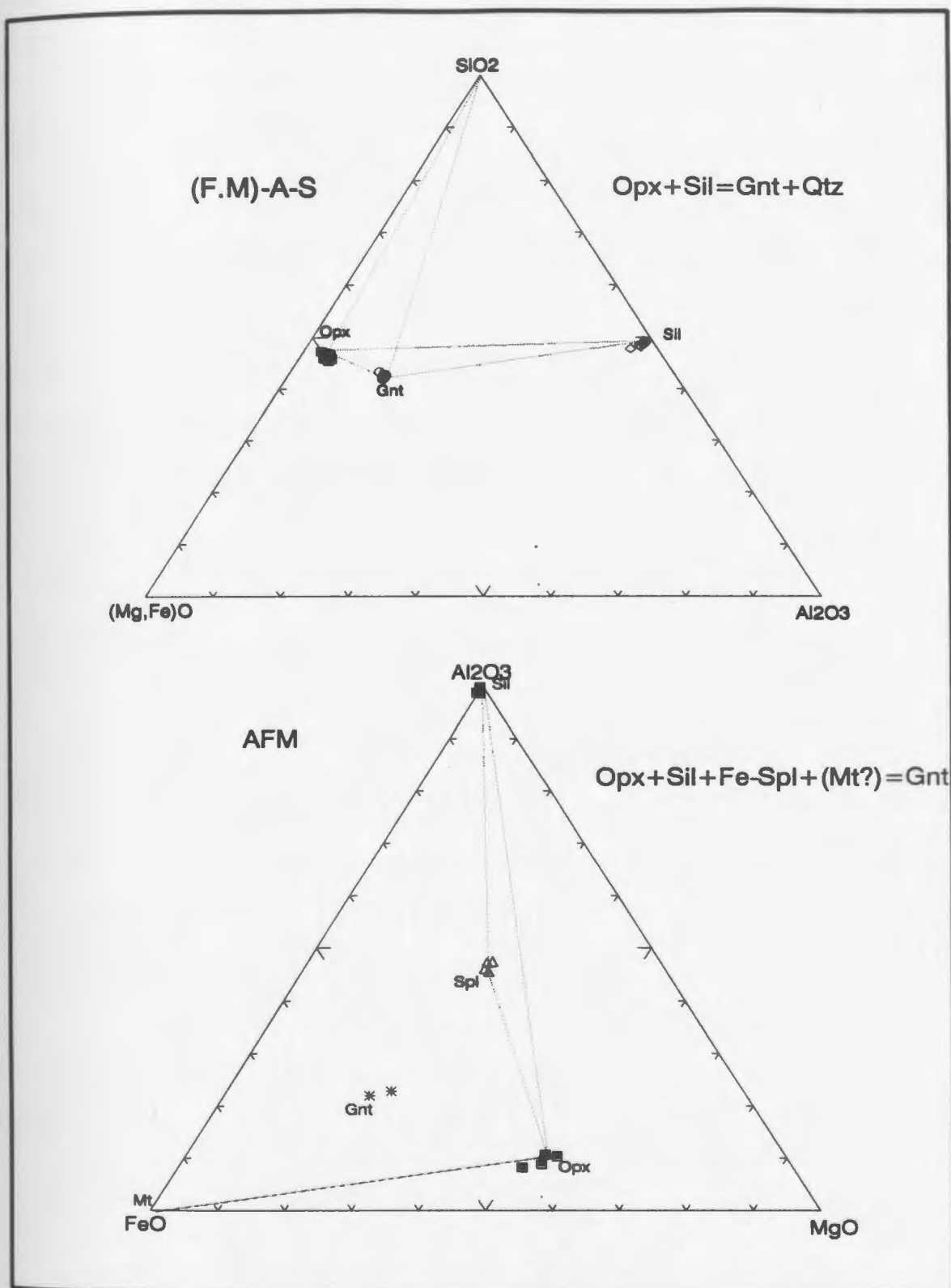


Fig. 62. (F.M)-A-S and AFM diagrams constructed from measured mineral compositions showing phase relations for garnet producing reactions.

The intersection of the two-phase assemblage Opx-Sil by Gnt-Qtz in the (F.M)-A-S system of Fig. 62 supports the inference that reaction (5) took place. Although reaction (6) is suggested on the basis of textural evidence (Fig. 53), chemographic relations in the AFM diagram of Fig. 62 are inconsistent with this reaction. An additional Fe-rich reactant phase must have been involved, the most likely candidate being magnetite which occurs as rounded inclusions in garnet.

#### (D) Kornerupine forming reactions

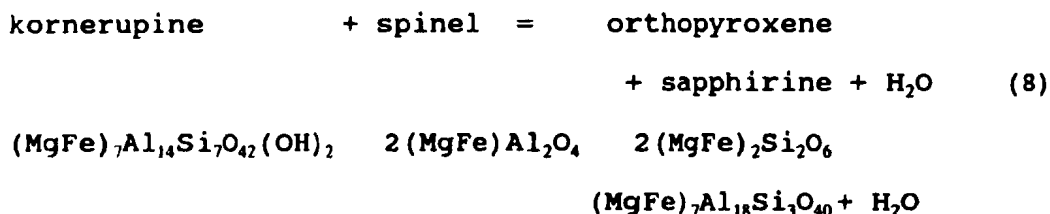
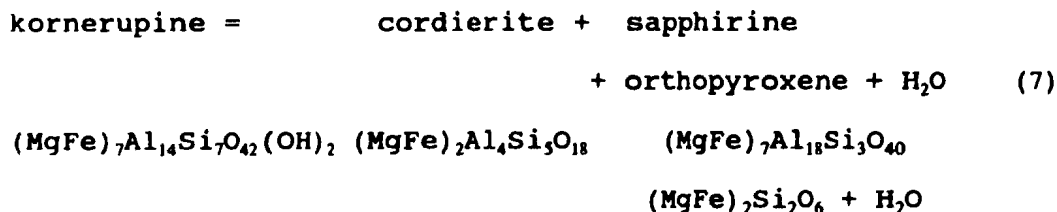
Kornerupine also occurs as porphyroblasts in mineral assemblages (1) and (2). Although reactions leading to the formation of this mineral are not clear in samples from the study area, mass balance considerations suggest that gedrite and corundum, which are considered to be early phases, may have been involved in the formation of kornerupine (see also Schreyer and Abraham 1976, Windley et al. 1984).

#### (E) Kornerupine replacement reactions

Textural interpretations suggest that kornerupine and kornerupine + spinel were replaced by the assemblages sapphirine-orthopyroxene-cordierite and sapphirine-



orthopyroxene (Fig. 55 and 56) by reactions (7) and (8).



Both these reactions were suggested by Seifert (1974, 1975). In reaction (7) the exact stoichiometric coefficients cannot be calculated for a generalized reaction because kornerupine and orthopyroxene contain variable amounts of FeO and  $\text{Al}_2\text{O}_3$ , respectively. Kornerupine compositions lie in the three-phase field Crd-Spr-Opx and the Krn-Spl join intersects the Opx-Spr join in the  $\text{Al}_2\text{O}_3$ -FeO-MgO system as shown in Fig. 63, so the inferred reactions are consistent with chemographic relations.

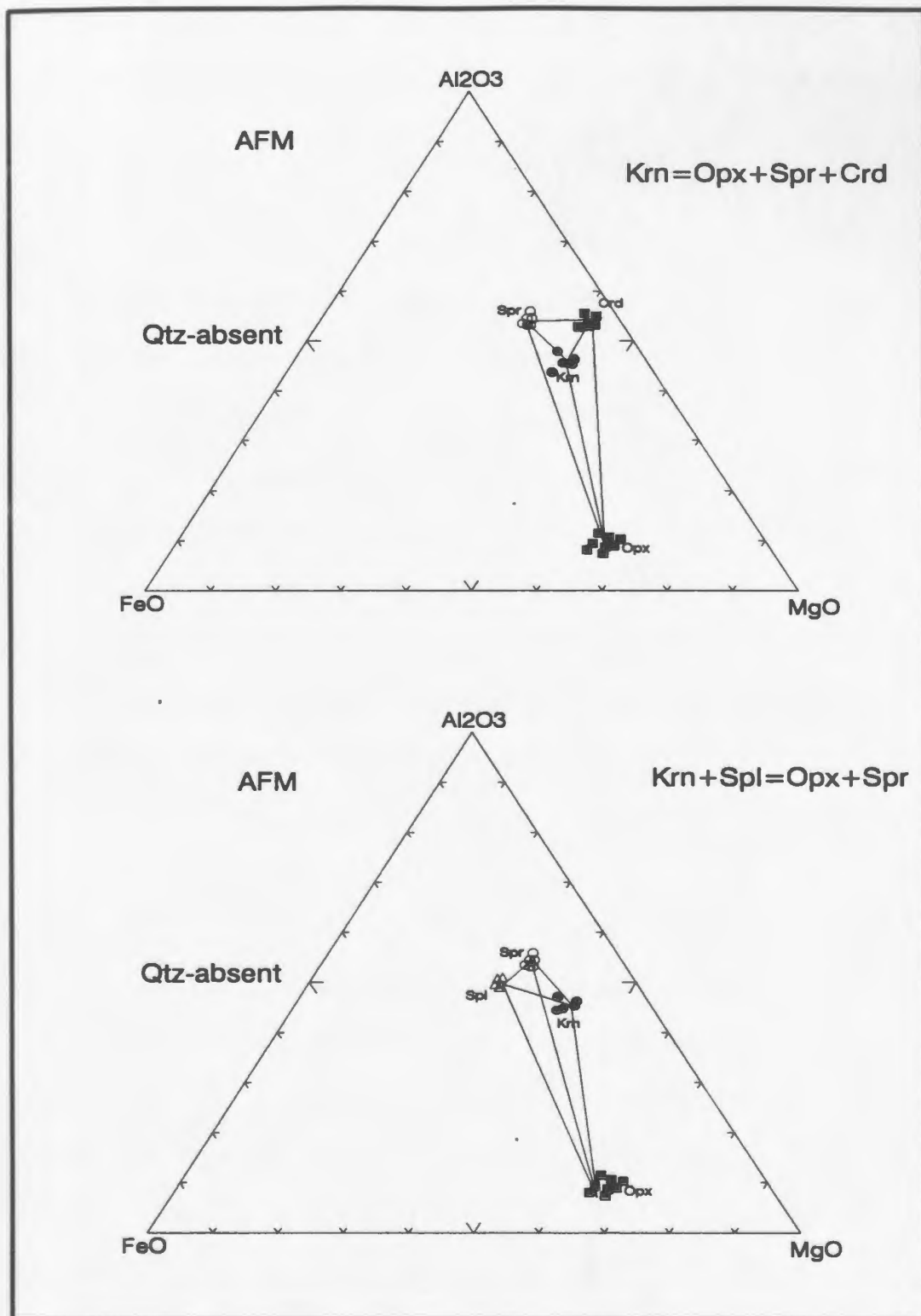


Fig. 63. AFM diagrams constructed from measured mineral compositions showing phase relations during kornepine replacement reactions.

#### 4-2-5 Estimation of P-T conditions by petrogenetic grids

In this section, the P-T conditions for each of the reactions inferred from interpretation of mineral textures are estimated with reference to available experimental data. The FeO-MgO-Al<sub>2</sub>O<sub>3</sub>-SiO<sub>2</sub>-H<sub>2</sub>O (FMAS) system (Hensen 1986, Hensen 1987) and MgO-Al<sub>2</sub>O<sub>3</sub>-SiO<sub>2</sub>-H<sub>2</sub>O (MAS) system (Seifert 1974, 1975) are very useful for this purpose. However, although such systems have produced meaningful results, caution is required because many studies have illustrated that the stability fields of certain minerals and grid topologies are distinctly modified by small amounts of minor components (Ellis et al. 1980, Bohlen and Dollase 1983, Sandiford 1985, Hensen 1986, Powell and Sandiford 1988).

As discussed above, on the basis of textural information, cordierite, spinel and orthopyroxene appear to have been stable together at an early stage in the metamorphic history. The stability field of cordierite has been the subject of several experimental investigations (Newton 1972, Green and Vernon 1974 and Newton and Wood 1979). The experimental results indicate that the upper stability limit of hydrous Mg-cordierite is up to  $\approx 12$  kbar and 1050°C for the synthetic system. These experimental results have also revealed that

hydrous cordierite is stable at higher pressures (up to 3-4 kbar higher) than anhydrous cordierite. Therefore, relatively high pressure conditions at an early stage in the metamorphic history cannot be precluded because the cordierites studied here may have significant volatile (water and/or CO<sub>2</sub>) contents as described in mineral chemistry of the section 4-2-3.

The cores of porphyroblastic orthopyroxene, which are considered to have formed relatively early during the metamorphism, have high Al contents (up to 9.5 wt.%) and coexist with spinel and cordierite. The high Al contents of orthopyroxene coexisting with the spinel-cordierite subassemblage indicate equilibration at high T (900 - 1000 °C) and moderate P ( $\approx$  8 kbar) based on solubility of Al<sub>2</sub>O<sub>3</sub> in orthopyroxene (Anastasiou and Seifert 1972). More recently, Perkins et al. (1983) suggested that this assemblage reflects somewhat lower-pressure conditions (6-8 kbar) based on their experimental studies. However, the P-T conditions inferred for the above reaction and may be affected by the existence of minor components such as ferric iron and sodium in the natural system, effects which were not taken into account in experiments performed in the Fe<sup>3+</sup> and Na free system. In summary, it is probable that the P-T conditions of peak metamorphism were less than 900 - 1000 °C and  $\sim$  8 kbar established for the end-member system, and it is deduced that

high T (  $\approx 900$  °C) and moderate P (6-8 kbar) conditions were operative to stabilize the cordierite-spinel-Al-rich orthopyroxene assemblage.

Textural evidence suggests that cordierite breakdown occurred by the reaction (1)  $\text{Crd} \rightarrow \text{Opx} + \text{Sil} + \text{Qtz}$ . This reaction, which is sensitive to pressure according to Newton (1972), results in the formation of orthopyroxene with lower Al contents (6-7 wt. %). In the pure MAS system this reaction occurs at 11.2 kbar at 1,000°C but the reaction may occur under lower P-T conditions when other components are present. The recent P-T grid of Hensen (1986) suggests that the FMAS reaction has a shallow positive slope at high  $f\text{O}_2$ , as shown in Fig 64. High oxygen fugacity conditions during the cordierite breakdown reaction in the Indian Head Range are supported by the common presence of oxides (magnetite and ilmenite) and relatively high amounts of  $\text{Fe}^{3+}$  in sapphirine and orthopyroxene from calculations based on the assumption of stoichiometry (not presented). Thus, it is likely that the mineral reactions at this stage can be approximated by Hensen's P-T grid for high  $f\text{O}_2$  conditions (Fig. 64). Additionally, secondary fine grained orthopyroxene and the rims of orthopyroxene porphyroblasts have  $\text{Al}_2\text{O}_3$  contents of 6-7 wt.%. The P-T-X grid of Hensen and Harley (1990) suggests

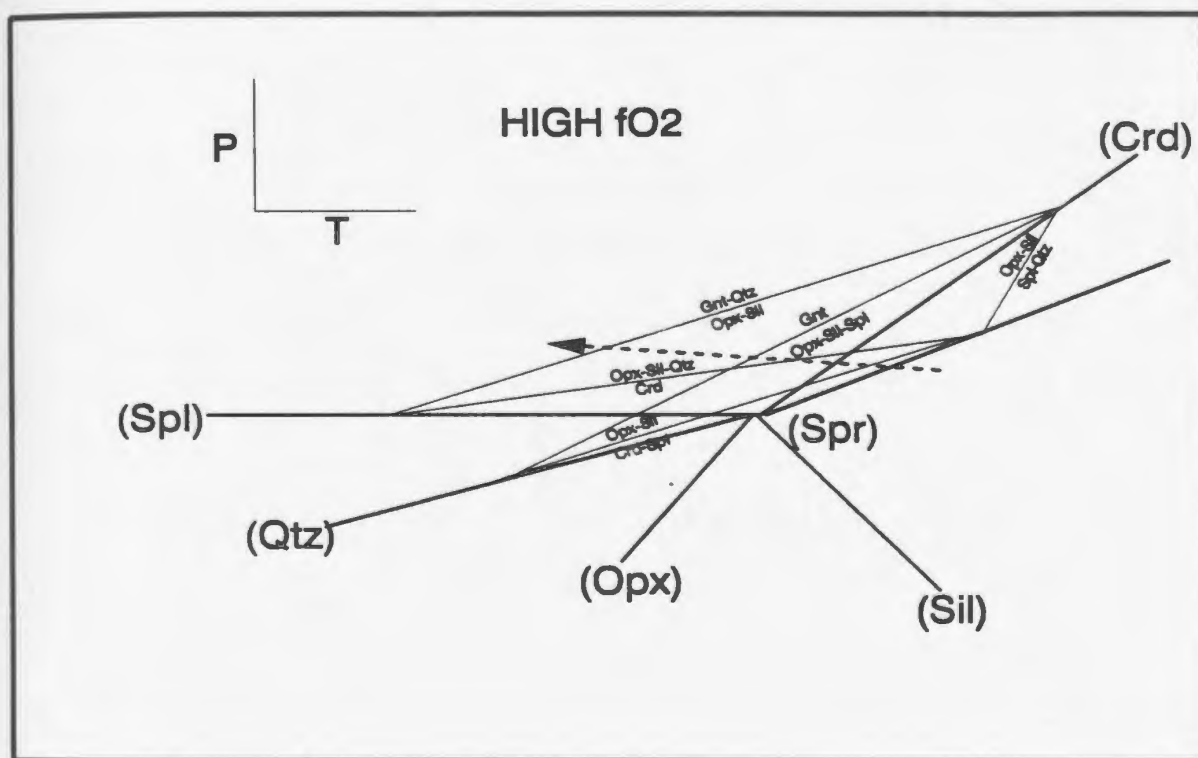


Fig. 64. Partial P-T grid for phase relations in the FMAS system for high  $fO_2$  conditions ( after Hensen 1986).

Heavy lines are univariant equilibria labelled by the absent phase.

Light lines are divariant equilibria discussed in the text. Dashed line with arrow is the inferred P-T path based on reaction textures.



that the opx-sil-qtz assemblage with a decreased  $\text{Al}_2\text{O}_3$  content (6-7 wt.%) in orthopyroxene, occurs at  $\approx 800^\circ\text{C}$  and in a pressure range of 8-10 kbar. Thus, it is inferred that the breakdown reaction of cordierite to secondary orthopyroxene and sillimanite occurred at similar or slightly increased pressure (8-10 kbar) and decreased temperature ( $\approx 800^\circ\text{C}$ ) compared with the early cordierite + high  $\text{Al}_2\text{O}_3$  orthopyroxene + spinel stability conditions. The estimates are consistent with those of Ellis (1980) and Harley (1985) for the same cordierite breakdown reaction.

The timing of sapphirine formation is not clear from mineral reaction textures. Sapphirine seems to be stable with orthopyroxene + sillimanite in quartz-free rocks based on textural relations. Based on the experimental data in the system  $\text{MgO}-\text{Al}_2\text{O}_3-\text{SiO}_2-\text{H}_2\text{O}$  by Newton (1972) and Seifert (1974), the assemblage orthopyroxene + sapphirine + hydrous cordierite can react over a broad range of pressure conditions from 3.6-11 kbars and the orthopyroxene - sapphirine assemblage (without quartz) occurs on the high pressure and low temperature side of the reaction spinel + cordierite = orthopyroxene + sapphirine (see also Arima and Barnett, 1984). This implies that sapphirine formation occurred under roughly similar conditions to sillimanite formation by cordierite

breakdown reaction (1). Furthermore, on the basis of their experimental results, Anastasiou and Seifert (1972) have suggested that the  $\text{Al}_2\text{O}_3$  contents of orthopyroxene coexisting with sapphirine and cordierite, or with spinel and cordierite, decrease with decreasing temperature and increase slightly with increasing pressure. This is compatible with changing P-T conditions during the cordierite breakdown reaction as described above and may be applicable to sapphirine-bearing assemblage (2) and (3) developed in the Indian Head Range because of similar textures, mineral assemblages, and the trend towards lower  $\text{Al}_2\text{O}_3$  contents in the rims of orthopyroxene.

Thus, P-T conditions during the breakdown of cordierite and the formation of sapphirine were probably in the range 800-900°C with pressures of 8-10 kbar, based on several experimental data, the FMAS petrogenetic grid and previous studies on analogous reactions.

The assemblage garnet - quartz - orthopyroxene - sillimanite occurs in the quartz-bearing assemblages (1). The garnets contain abundant inclusions of sillimanite, spinel and orthopyroxene. Sengupta et al. (1990) have suggested that the reaction  $\text{Opx} + \text{Sil} = \text{Gnt} + \text{Qtz}$  occurs at about 770°C, 8.3

kbar, for similar garnet compositions (pyrope 31-38, almandine 56-64) to those from the study area, and Ellis (1980) has estimated that the assemblage garnet + quartz + orthopyroxene + sillimanite formed under metamorphic conditions around 7-9 kbar and 900-980°C for their samples. However, the inferred temperature of Ellis (1980) appears to be too high because the positive slope of this reaction in P-T space (Hensen 1986, see Fig. 64) implies that this reaction takes place under falling temperature conditions following stability of the assemblage orthopyroxene-sillimanite-quartz, which is inferred to be 800-900°C.

Prismatic coarse kornerupine with abundant evidence of breakdown reactions is present in the Al-rich sapphirine bearing assemblage (2). The breakdown products of kornerupine consist of symplectic and corona phases. As described previously (reactions 7 and 8), kornerupine reacts with and without spinel to form secondary sapphirine + orthopyroxene symplectites and is replaced by cordierite + secondary sapphirine + orthopyroxene. As shown in Fig. 65, kornerupine has a relatively limited stability field (750-850 °C, 6-8 kbar) (Seifert 1974, 1975). As the kornerupine reaction grid shows in Fig. 66, Seifert (1974, 1975) has suggested that the kornerupine breakdown reaction ( $k_{rn} = crd + opx + spr$ ) occurs at 5-6 kbar at 750-800°C. On this basis, therefore, the



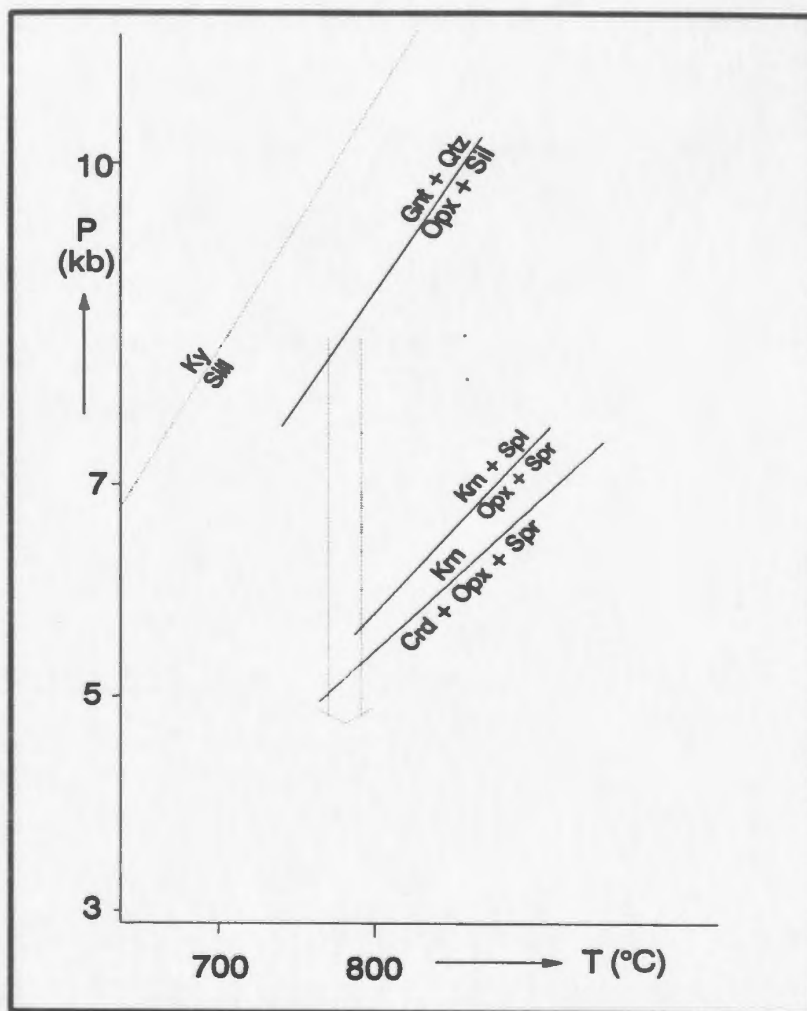


Figure 66. Inferred P-T path in the reaction grid.

kornerupine reaction in the study area occurred at significantly lower pressure (5-6 kbar) than the garnet forming reaction ( $8 \pm 1$  kbar), and a substantial isothermal decompression event has been inferred in order to connect the two.

This implies that the conditions of the kornerupine breakdown reactions (5-6 kbar and 750-800°C) are significantly changed from those of the garnet formation, especially in terms of decreased pressure as the partial P-T path shows in Fig. 66.

In summary, mineral reactions in the study area can be classified into four stages:

- Stage 1 : very early cordierite, spinel and highly aluminous orthopyroxene (up to 9.5 wt.%) formed under conditions of about 900°C and moderate pressure (6-8 kbar);
- Stage 2 : breakdown of cordierite, formation of sillimanite and secondary (Al poorer) orthopyroxene, and subsequent reaction forming Mg-spinel and sapphirine occurred under similar or slightly increased pressure (8-10 kbar) and decreasing temperature ( $\approx 800^\circ\text{C}$ );
- Stage 3 : garnet formation occurred with continued cooling

conditions at similar high pressures ( $8 \pm 1$  kbar);

**Stage 4 :** subsequently sapphirine-orthopyroxene symplectites formed from kornerupine under significantly decreased pressure (5-6 kbar, 750-800°C) following approximately isothermal decompression.



## CHAPTER 5

### Independent Geothermobarometry

#### 5-1 Introduction

In this chapter, an attempt is made to estimate quantitatively the metamorphic P-T conditions in the Indian Head Range from the compositions of coexisting minerals. Calculations are based on the standard state relation for the Gibbs free energy change of reaction :  $\Delta G^\circ = -RT \ln K$  where  $\Delta G^\circ = \Delta H^\circ - T \Delta S^\circ + (P-1) \Delta V^\circ$  and where R is the gas constant, P pressure, T the (absolute) temperature, K the equilibrium constant, and  $\Delta G^\circ$ ,  $\Delta H^\circ$ ,  $\Delta S^\circ$  and  $\Delta V^\circ$  are the free energy, enthalpy, entropy and the volume change of the reaction at 1 bar/298°K. The expression above assumes that  $\Delta H_{298}$ ,  $\Delta S_{298}$  and  $\Delta V_{1,298}$  are equal to  $\Delta H_T$ ,  $\Delta S_T$  and  $\Delta V_{P,T}$ , respectively.

Several geothermobarometers have recently been developed involving calibration of continuous equilibria. These geothermobarometers can be classified into two groups. Exchange reactions, which are used for geothermometers, comprise the interchange of two similar atoms between two or

more sites in one or two minerals, and have a small  $dP/dT$  ( $= \Delta S/\Delta V$ ) and are sensitive with respect to temperature. On the other hand, net transfer reactions, which are used for geobarometers, comprise progressive modal reduction of reactants at the expense of products and are characterized by a larger  $\Delta V$ . The general thermometric and barometric equations can be expressed from the Gibbs free energy change reaction of above:

$$T = [-\Delta H - (P-1) \Delta V] / (R \ln K - \Delta S)$$

$$P = [T \Delta S - \Delta H - RT \ln K] / \Delta V$$

Details concerning individual geothermometers and geobarometers used in this study are given in Appendix 3.

Appropriate mineral assemblages were selected in terms of exchange and net transfer reactions, from the metagabbro, noritic gneiss, dioritic gneiss and pelitic gneiss. In the selection of mineral assemblages for the calculation of quantitative P-T conditions, choice of samples was based on interpretation of textural relationships in terms of equilibrium and disequilibrium. Thus, only mineral assemblages considered to be in equilibrium were employed for geothermobarometry.

Estimates of metamorphic pressures and temperatures were made on 27 samples using the computer program of Mengel (1987) employing published calibrations of thermometers and barometers. Biotite-garnet, garnet-plagioclase-sillimanite-quartz, garnet-orthopyroxene and garnet-orthopyroxene-plagioclase-quartz mineral assemblages were chosen from the pelitic gneiss. Orthopyroxene-clinopyroxene, biotite-garnet, orthopyroxene-garnet and hornblende-garnet mineral assemblages were selected from the noritic gneiss, metagabbro and dioritic gneiss. Textures and mineral chemistry of each mineral assemblages are discussed below.

## 5-2 Mineral assemblage

### 5-2-1 Orthopyroxene-Clinopyroxene

The assemblage orthopyroxene + clinopyroxene occurs in dioritic gneiss and metagabbro units in the southern Indian Head Range. Both orthopyroxene and clinopyroxene are generally evenly distributed throughout these units and occur in contact and as grains separated by plagioclase (Fig. 67). The two pyroxenes typically display granoblastic texture with the plagioclase matrix. Contacts between the two pyroxenes are generally sharp and regular indicating an equilibrium

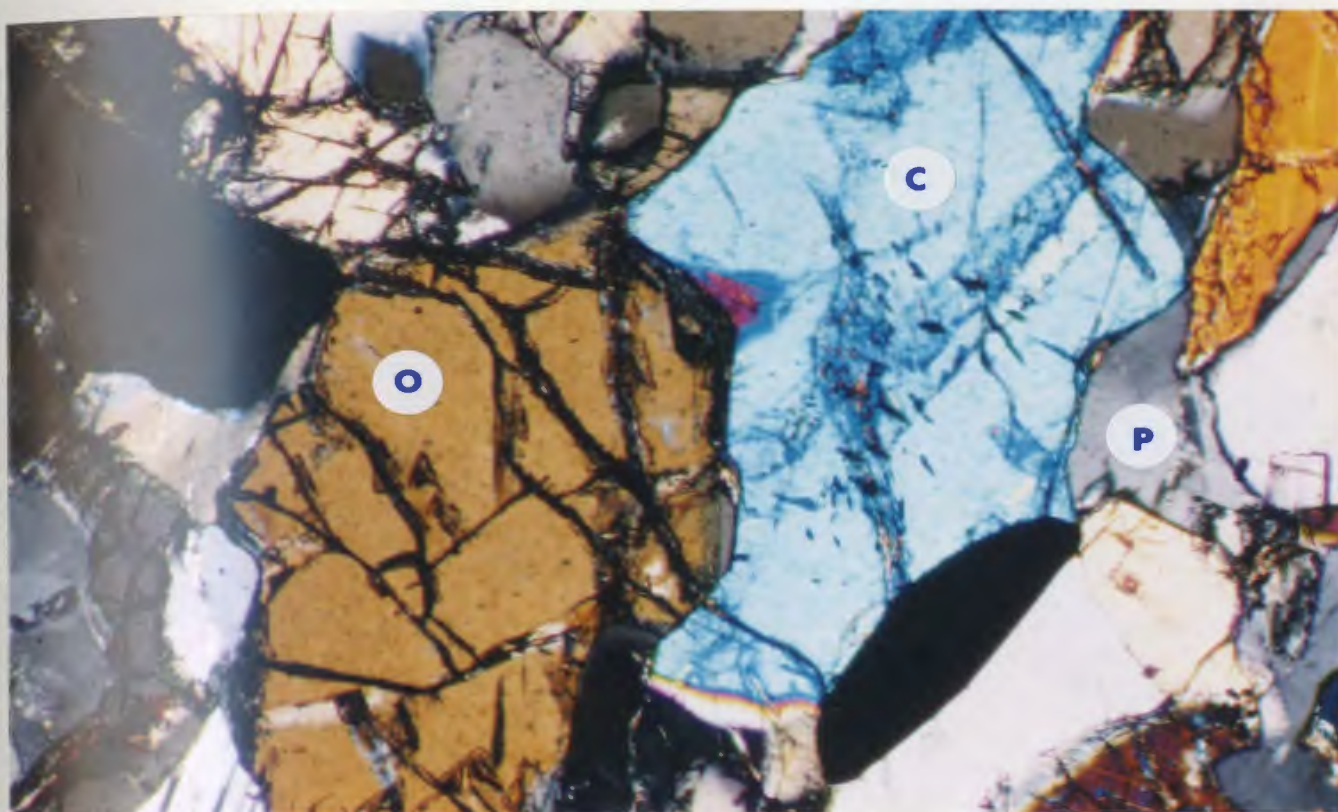


Figure 67. Photomicrograph showing equilibrium textural relationships between orthopyroxene, clinopyroxene and plagioclase in the dioritic gneiss. Width of photomicrograph : 1.6 mm. Crossed polarized light.

O: orthopyroxene, C: clinopyroxene. P: plagioclase.  
Sample# : IH-41.

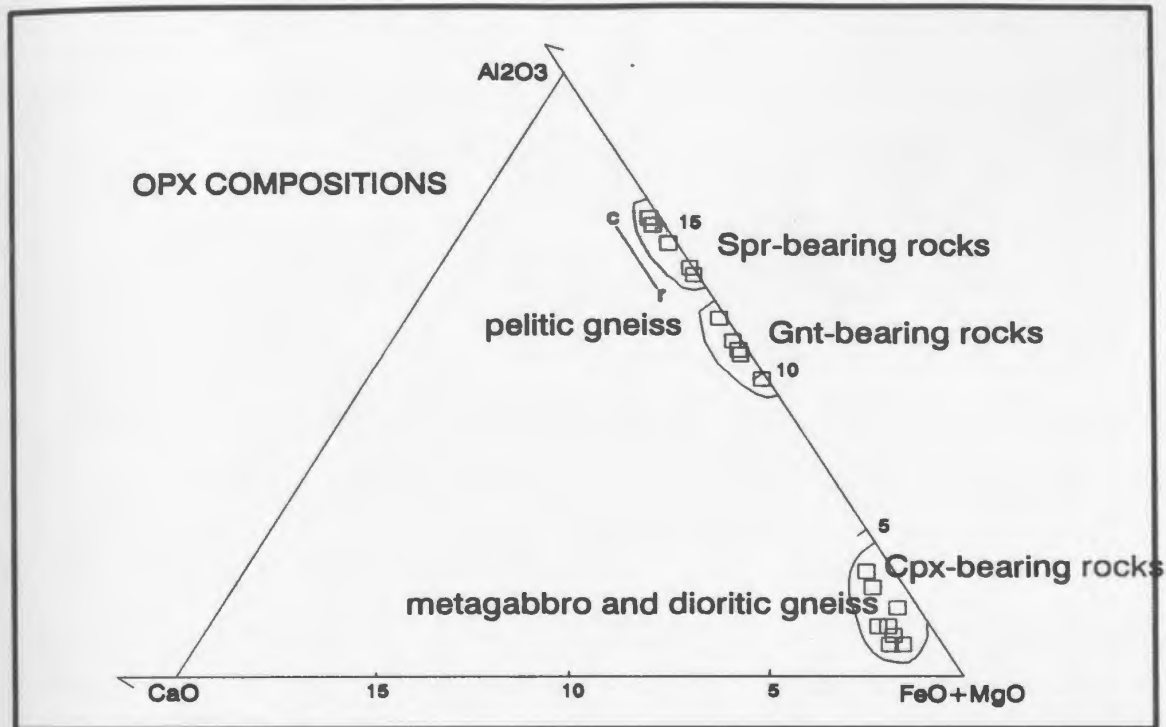


Fig. 68. Partial ternary diagram of orthopyroxene compositions from different mineral assemblages plotted in (F.M)O-CaO- $\text{Al}_2\text{O}_3$  composition space.

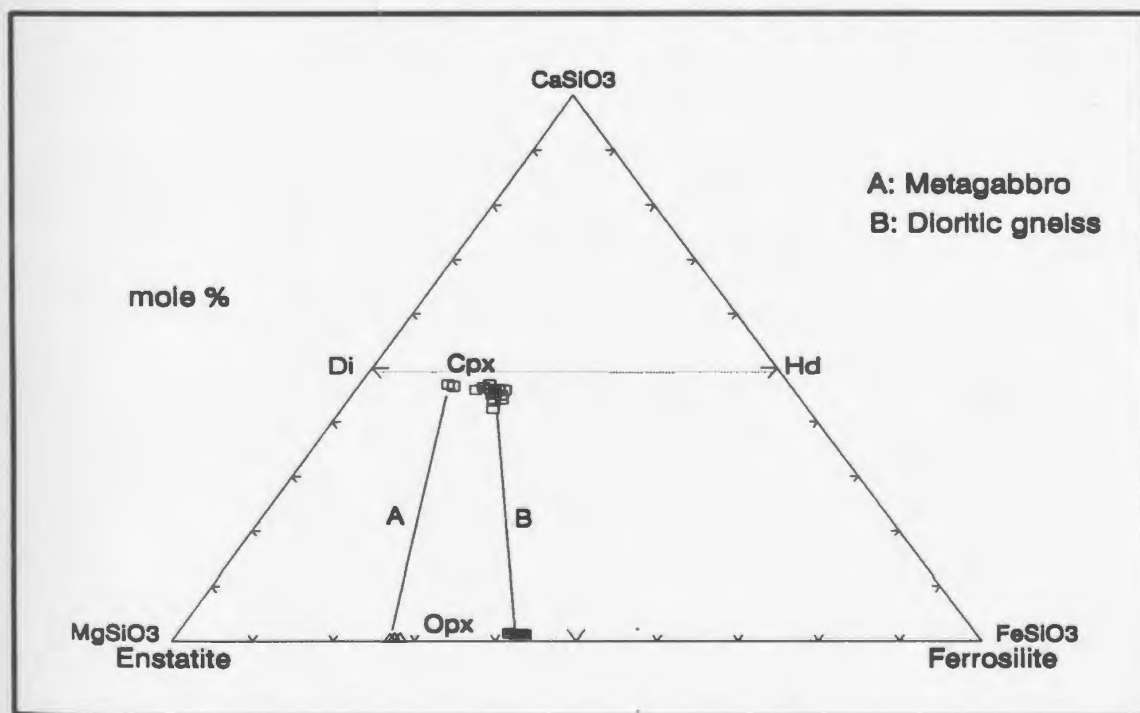


Figure 69. Compositions of coexisting orthopyroxene-clinopyroxene in the metagabbro and dioritic gneiss in the I.H.R..

relationship. The products of later alteration (such as amphibole) are common along grain boundaries and cleavages, but were avoided during analysis.

The plagioclase coexisting with the two pyroxenes is variable in composition, displaying a range of  $An_{42-74}$ . Orthopyroxenes from the metagabbro and dioritic gneiss are hypersthene with a relatively narrow range of composition, with  $Mg/(Mg+Fe)$  ranging from 0.57 - 0.66. Fig. 68 shows the compositional ranges of orthopyroxene from the metagabbro and the dioritic gneiss.  $Al_2O_3$  contents of orthopyroxenes from the two units lie in the range 1-2 wt.%. Clinopyroxenes are diopsides which also show a restricted range of composition with  $Mg/(Mg+Fe)$  ranging from 0.66 - 0.80. The typical clinopyroxene of metagabbro contains 44-50% wollastonite, 28-37% enstatite, and 13-28% ferrosilite and shows very weak zoning with Mg increasing and Ca decreasing from core toward rim. The measured range of pyroxene compositions, and tielines between coexisting orthopyroxenes and clinopyroxenes, are shown in Fig. 69.

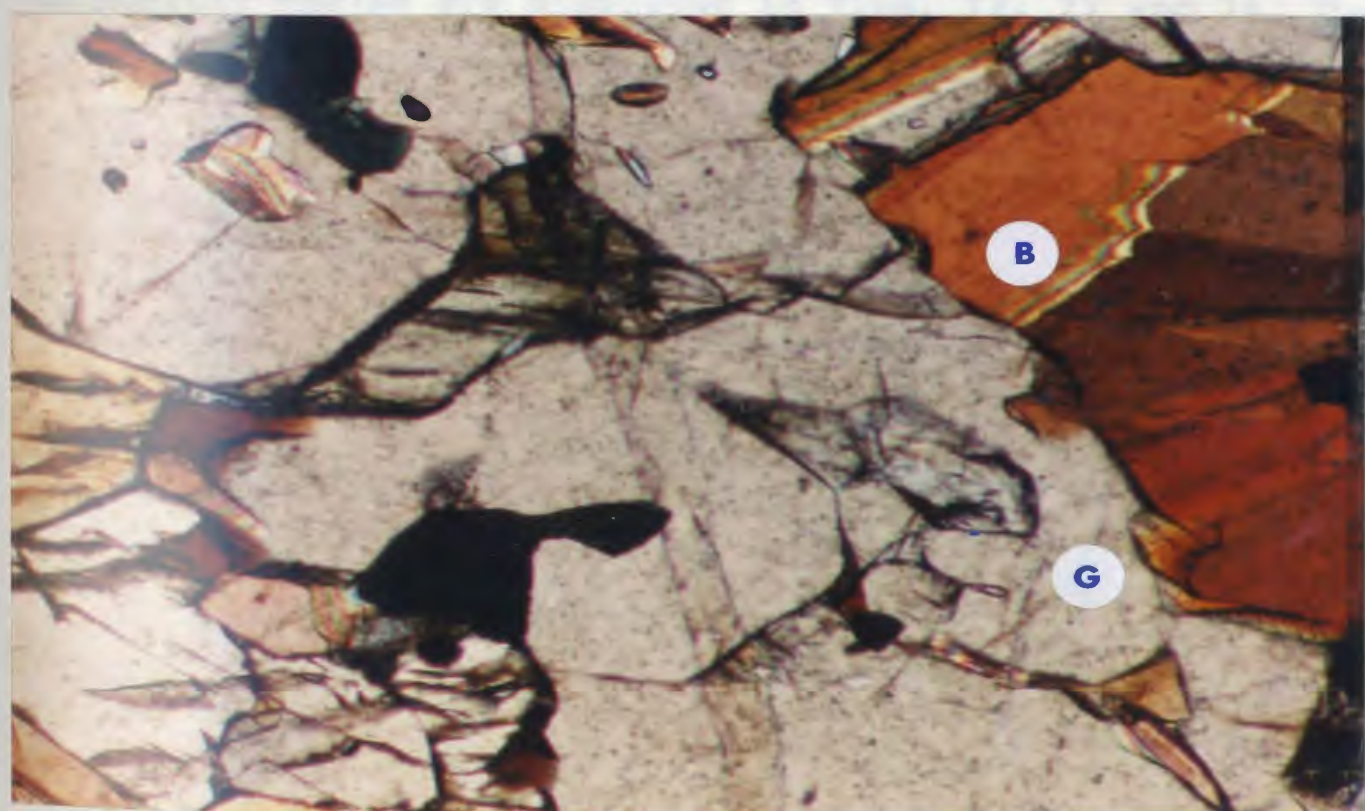
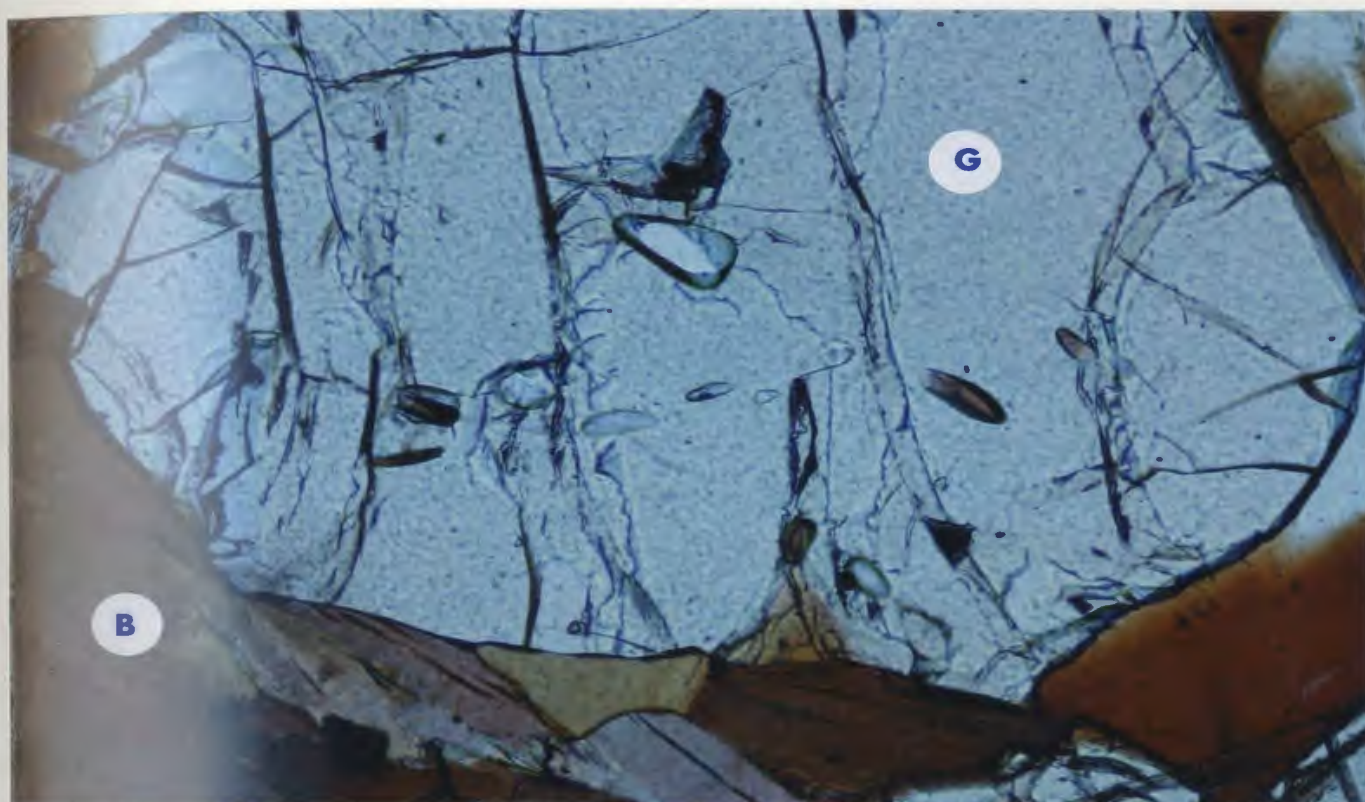
#### 5-2-2 Garnet-biotite

Garnet-biotite pairs occur in noritic gneiss and locally in

Figure 70. Photomicrograph showing garnet porphyroblast wrapped by the biotite matrix in noritic gneiss. Width of photomicrograph : 1.6 mm. Plane polarized light with blue filter. B: biotite, G: garnet. Sample# : S-127.

Figure 71. Photomicrograph showing equilibrium textural relationship between garnet and biotite in noritic gneiss. Width of photomicrograph : 1.6 mm. Plane polarized light. B: biotite, G: garnet. Sample# : S-126-1.





pelitic gneiss. Porphyroblastic garnets are locally overgrown by coarse biotite grains in the noritic gneiss (Fig. 70). On the other hand, in the pelitic gneiss inclusions of idiomorphic biotite are ubiquitous within porphyroblastic garnets, implying that garnet postdated them. Grain boundaries are generally sharp and straight, and are interpreted to be in equilibrium (Fig. 71). However, some of garnets locally show irregular contacts with biotite inclusions, and such pairs cannot be considered to be in equilibrium. Symplectic biotite-quartz intergrowths are locally developed around garnets in the noritic gneiss and are not used for geothermometry.

The characteristic garnet-biotite zoning patterns from the noritic gneiss are displayed in Figs. 72, 73 and 74. The garnets have  $X_{Mg}$  (Mg/Mg+Fe) of 0.36 - 0.47 and show distinct compositional differences between core and rim.  $X_{Mg}$  decreases and Fe increases from core to rim. Al contents of garnet do not show a distinct change between core and rim. Biotites are unzoned in individual grains but  $X_{Mg}$  is higher in biotite close to garnet than those in the matrix.

#### 5-2-3 Garnet-plagioclase-sillimanite-quartz

The garnet-plagioclase-sillimanite-quartz assemblage occurs in the pelitic gneiss. Plagioclase exhibits direct contact with

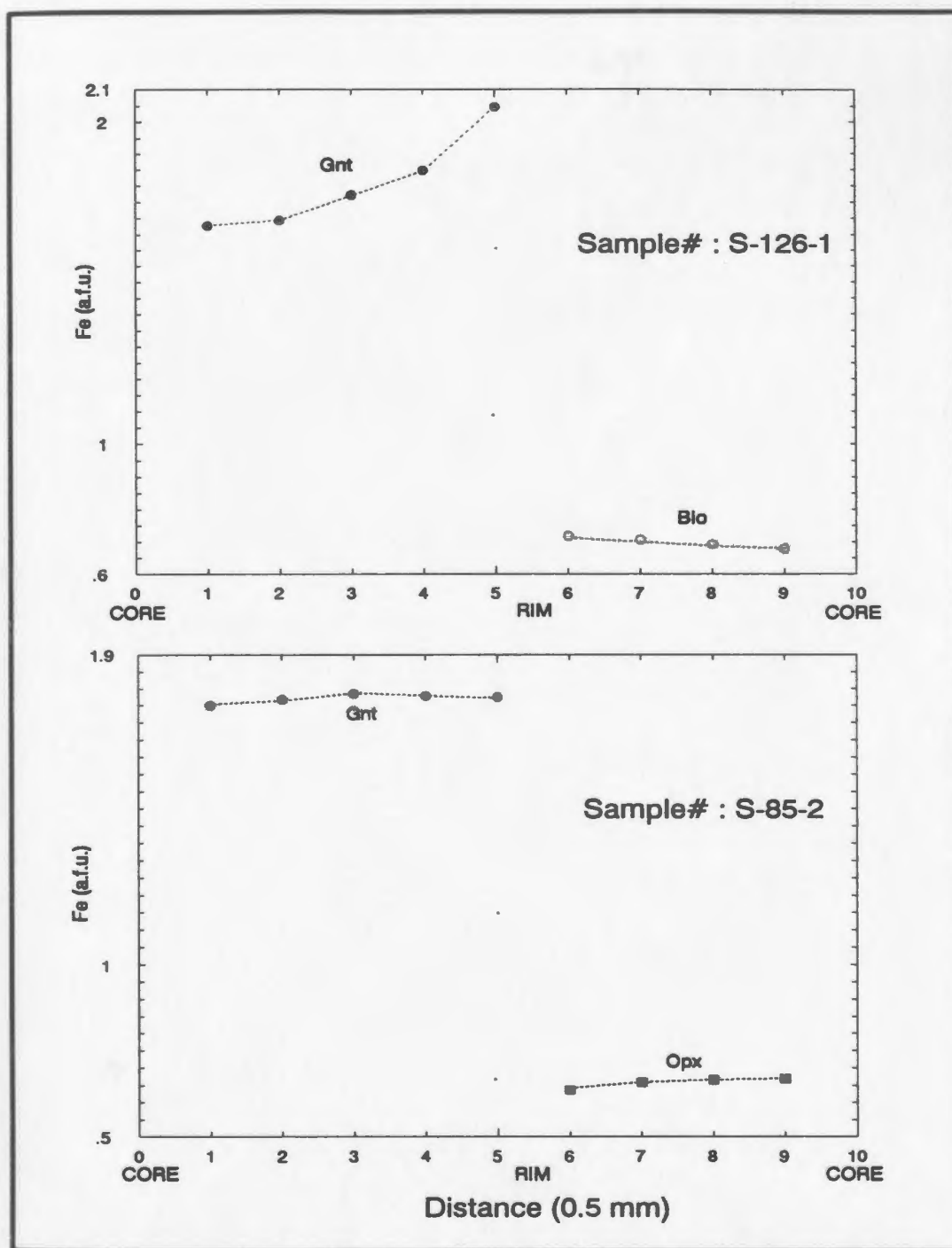


Fig. 72. Core to rim compositional profiles for Fe in garnet coexisting with biotite and orthopyroxene from the noritic gneiss in the I.H.R..

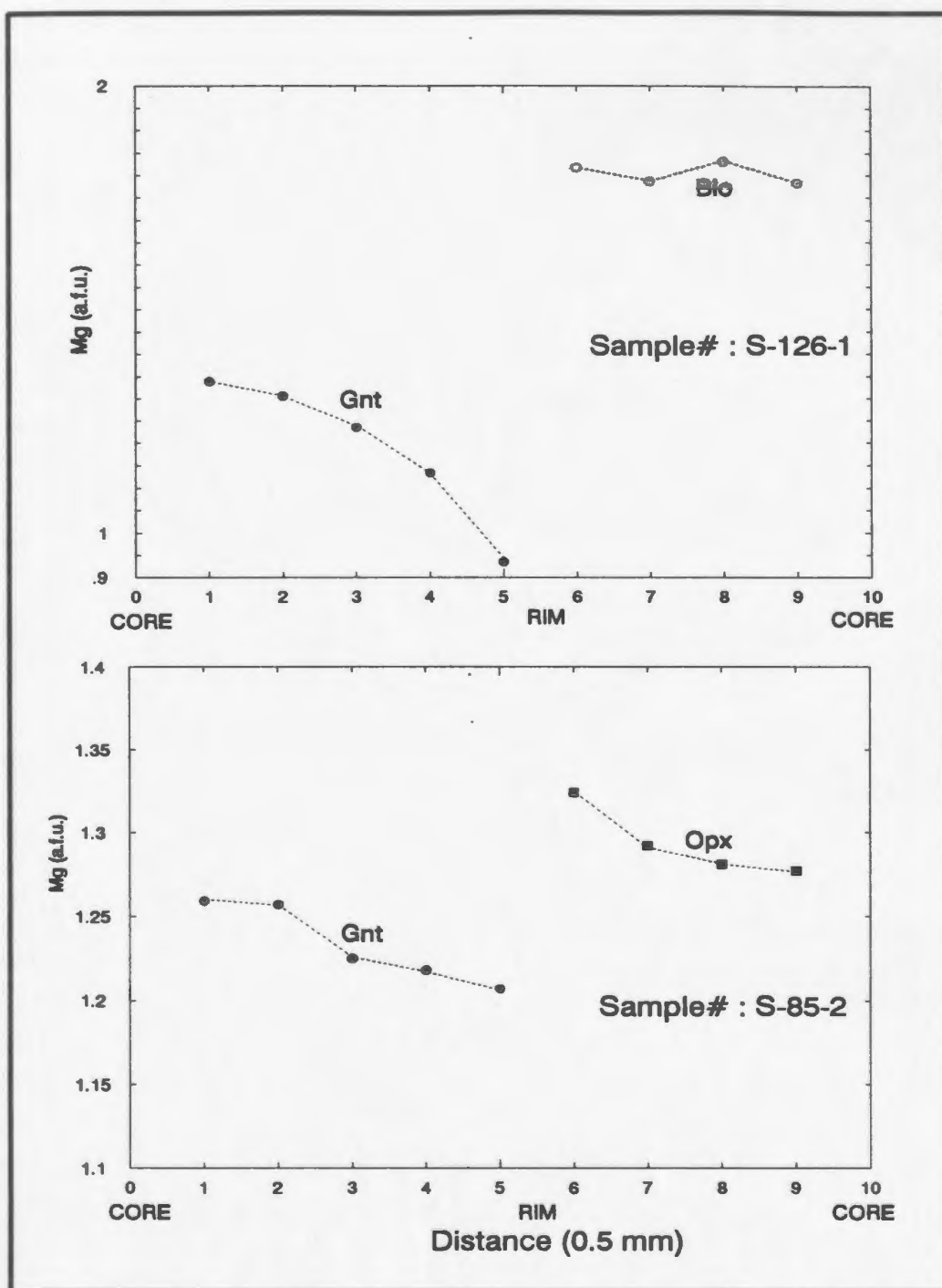


Fig. 73. Core to rim compositional profiles for Mg in garnet coexisting with biotite and orthopyroxene from the noritic gneiss in the I.H.R..

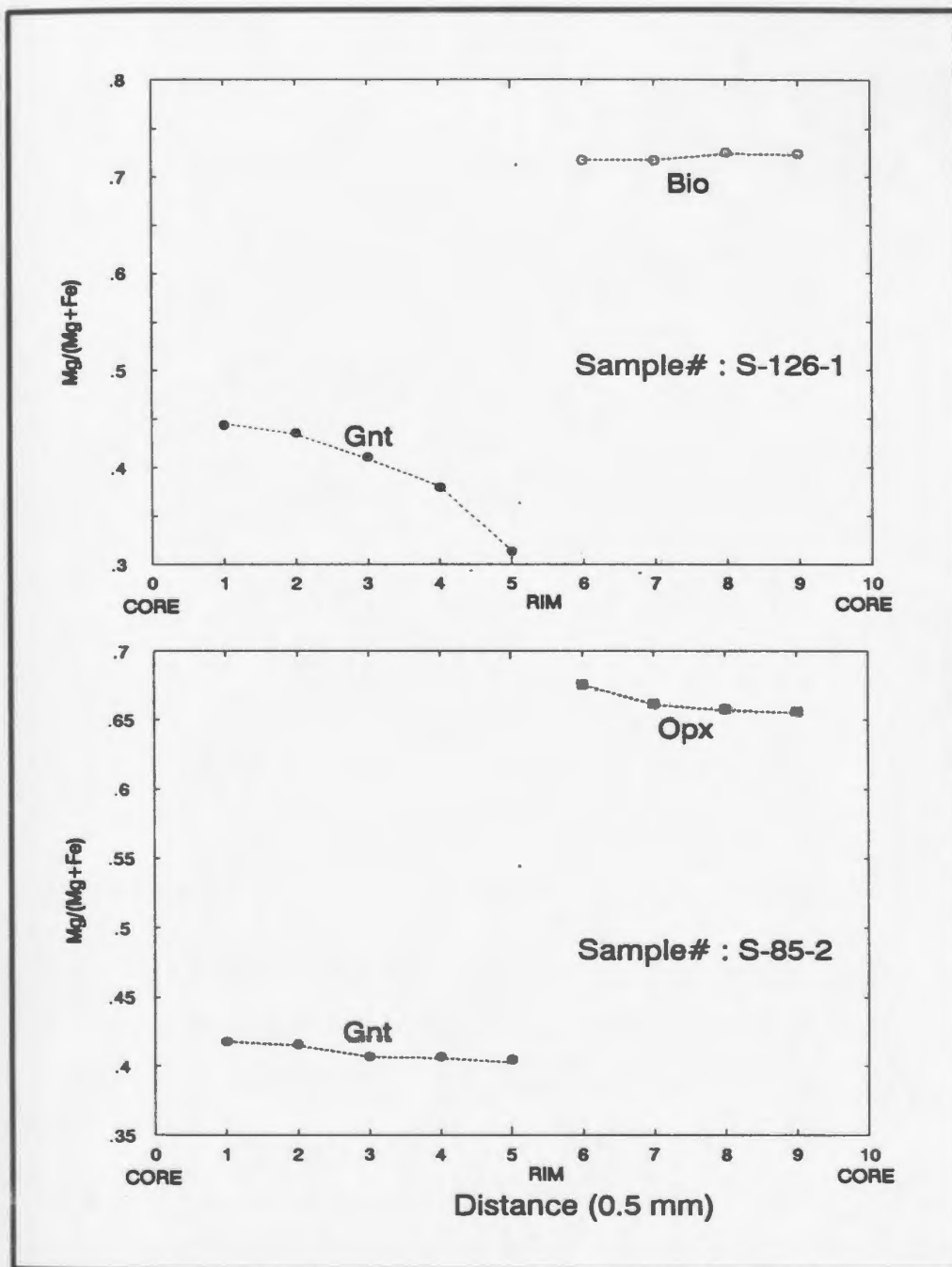


Fig. 74. Core to rim compositional profiles of the ratio  $\text{Mg}/(\text{Mg}+\text{Fe})$  in garnet coexisting with biotite and orthopyroxene from the noritic gneiss in the Indian Head Range.

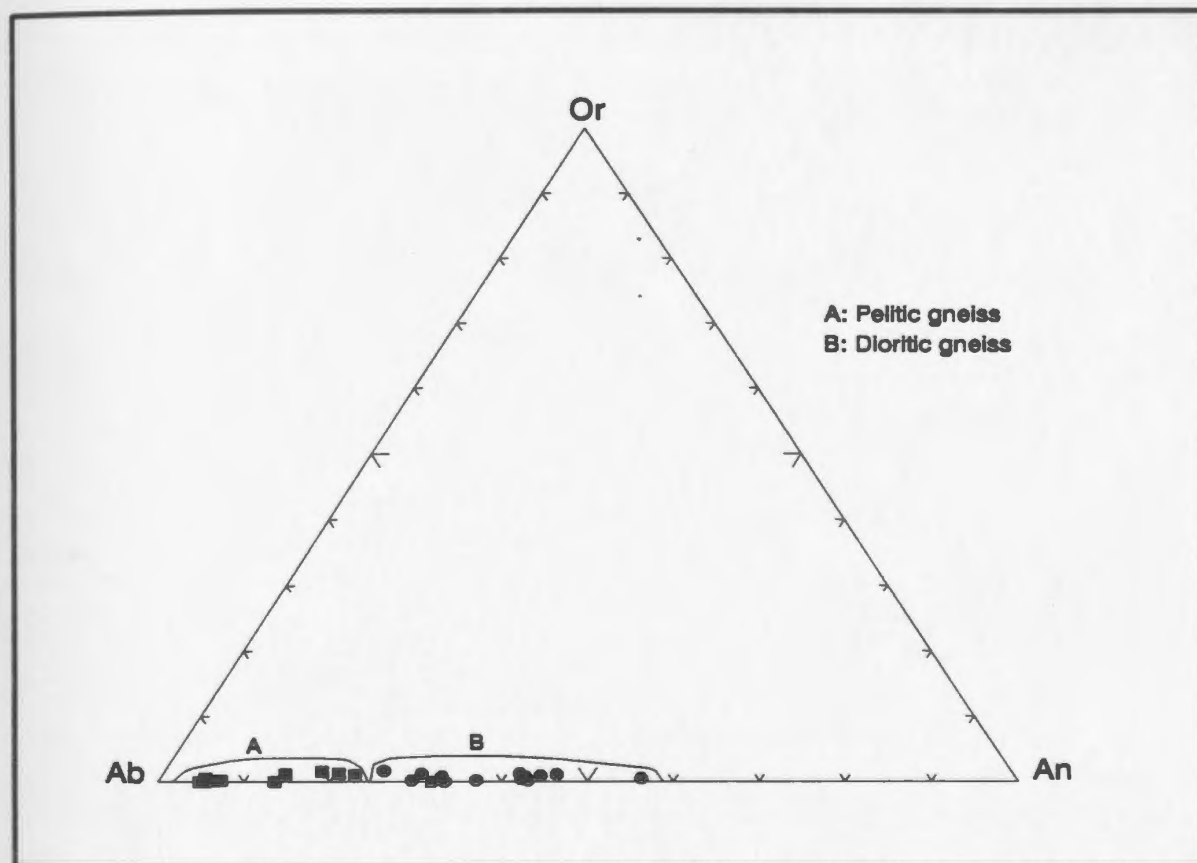
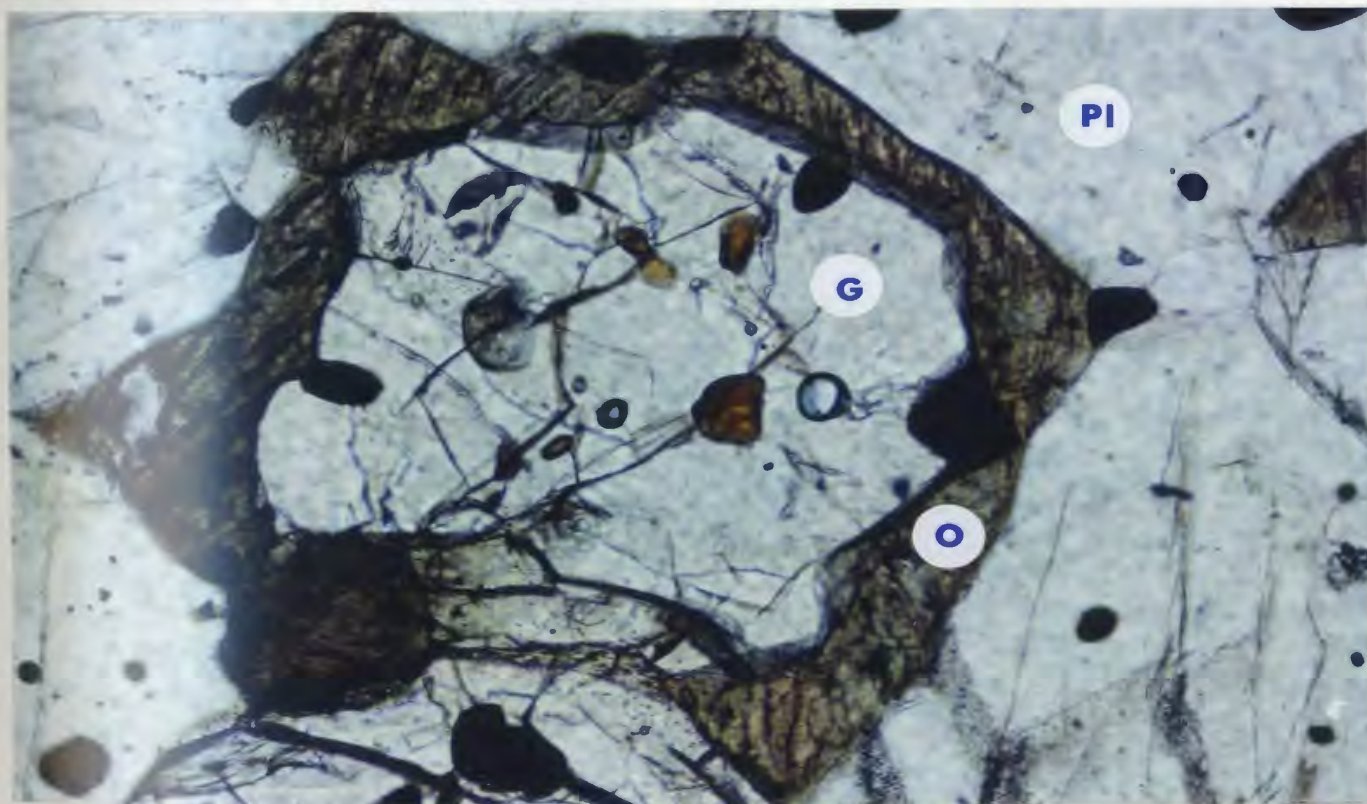
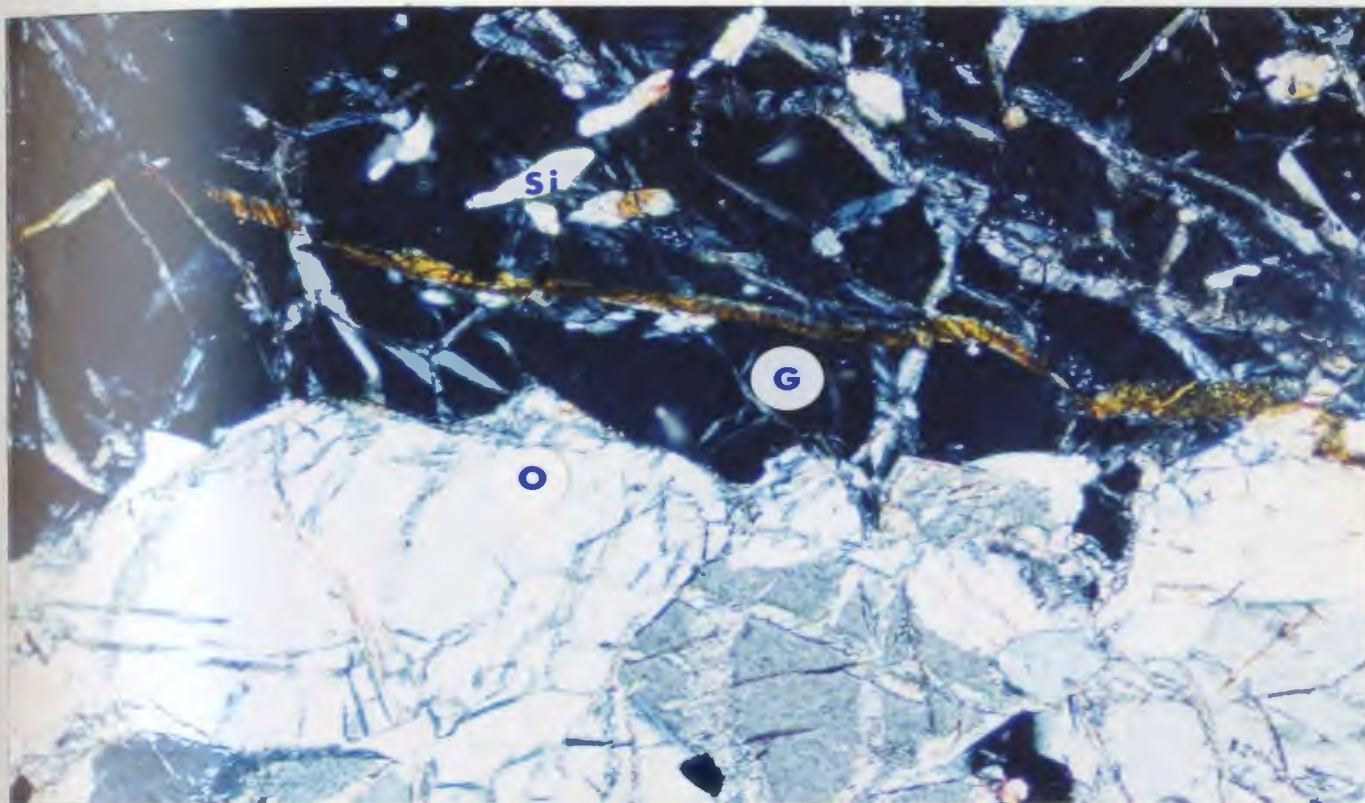


Fig. 75. Feldspar ternary diagram shows the range of plagioclase compositions from the pelitic gneiss and dioritic gneiss in the I.H.R..

Figure 76. Photomicrograph showing the textural relationship between garnet with blebby inclusions of sillimanite and adjacent orthopyroxene. Width of photomicrograph : 2.9 mm. Crossed polarized light. G: garnet, O: orthopyroxene, Si: sillimanite. Sample# : S-90-2.

Figure 77. Photomicrograph showing garnet porphyroblast with orthopyroxene corona in plagioclase matrix. Width of photomicrograph : 5.4 mm. Plane polarized light. G: garnet, O: orthopyroxene, Pl: plagioclase. Sample# : S-88-2.





garnet. The plagioclases have a limited compositional range of  $An_{11-23}$  (Fig. 75). Coexisting quartz is developed around garnet grains. The garnets analyzed here are pyrope (31-38) - almandine (56-64) solid solutions with only minor grossular ( $CaO < 1 \text{ mol.}\%$ ) and spessartine ( $MnO: 0.8-1.5 \text{ mol.}\%$ ) contents. The composition of garnets between core and rim with plagioclase does not show any zoning pattern. Sillimanite, which is present as only an inclusion phase within garnet porphyroblasts, displays elongated lamellar and blebby shapes (Fig. 76). Although textural relations are not clear as to whether sillimanite is in equilibrium with garnet or not, textures in which sillimanite has a sharp boundary with garnet were chosen for geobarometry.

#### 5-2-4 Garnet-orthopyroxene

The assemblage garnet-orthopyroxene is locally developed in the noritic gneiss and in a few samples of pelitic gneiss. Garnet-orthopyroxene contacts are sharp, reflecting equilibrium between the two phases (Fig. 77). Garnet composition is comparatively homogeneous and slightly enriched in almandine (almandine: 50-57 mol %, pyrope: 43-50 mol %). The garnets in contact with orthopyroxene do not show significant zoning. The zoning profiles of garnet from the

noritic gneiss are presented in Figs. 72, 73 and 74.  $X_{Mg}$  in garnet slightly decreases from core to rim near the contact with orthopyroxene. As noted previously, orthopyroxene from pelitic gneiss shows significantly higher Al-contents (up to 6 wt.%), compared to orthopyroxene from noritic gneiss (2-3 wt.%). The contents of Al and Fe in orthopyroxene decrease slightly from core to rim, and Mg contents increase toward the rim.

#### 5-2-5 Garnet-Hornblende

The garnet-hornblende mineral assemblage locally occurs in metagabbro. Rocks bearing this assemblage show recrystallized granoblastic textures with clear, sharp grain contacts (Fig. 44). Thus, the two minerals are considered to be texturally stable and in equilibrium. Plagioclase, showing late alteration, is ubiquitous and occurs between garnet and hornblende grains. Garnet in this assemblage is significantly different in compositions compared to that from other mineral assemblages described above (Fig. 78).  $X_{Mg}$  in garnet ranges from 0.03 - 0.05. Typical compositions of garnet are approximately 34-38 mol.% pyrope, 3-4 mol.% almandine, 36-40 mol.% grossular and 20-24 mol.% spessartine. Both garnet and hornblende are relatively homogeneous. Ti (< 0.3 mol.%) and Mg

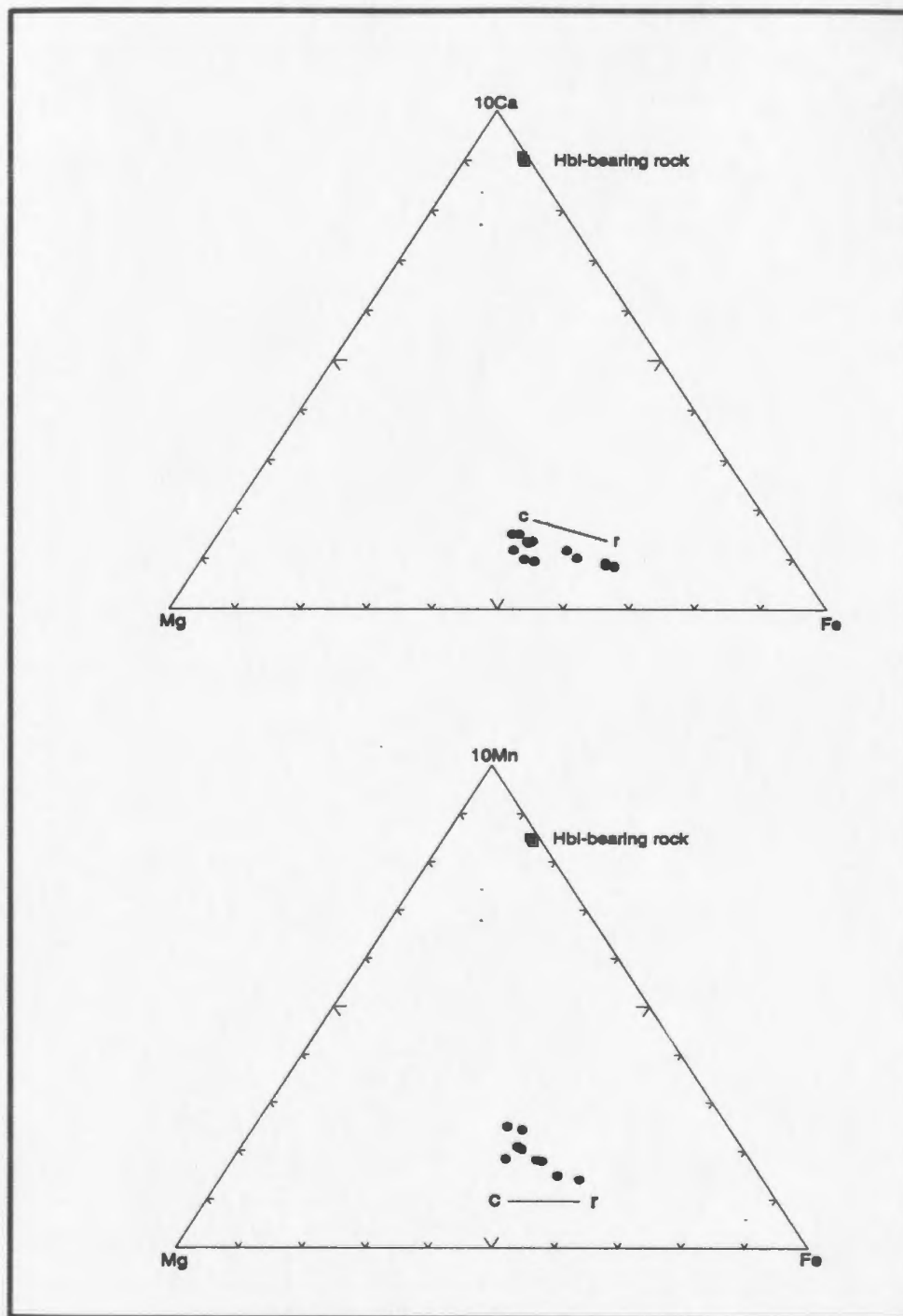


Fig. 78. Garnet compositions from the I.H.R. plotted on 10Ca-Mg-Fe and 10Mn-Mg-Fe ternary diagrams.

"c-r" shows the range of core-rim compositions.

contents (10-12 mol.%) in hornblende are lower than those from the noritic gneiss and dioritic gneiss. On the other hand, Ca (23-25 mol.%), Fe (12-13 mol.%) and Mn (1-2 mol.%) contents are much higher than those from other assemblages.  $X_{Mg}$  in hornblende is in the range 0.22 - 0.25.

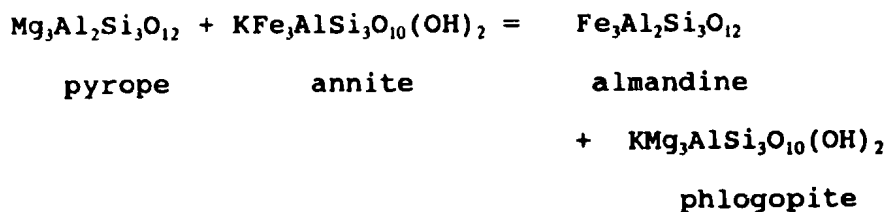
### 5-3 Geothermometry

In order to quantify temperature, the compositions of coexisting garnet-biotite, garnet-orthopyroxene, and clinopyroxene-orthopyroxene from the noritic gneiss, metagabbro, dioritic gneiss and pelitic gneiss are used.

Almost all of mineral assemblages which are considered to be in equilibrium are selected from these mafic rocks for geothermometry. A brief discussion of individual geothermometers is presented below, but a more thorough review is presented in Appendix 4.

#### 5-3-1 Garnet-Biotite Geothermometry

The distribution of Fe and Mg between garnet and biotite has been widely used to estimate temperatures of metamorphism. The cation exchange equilibrium is:



The Fe-Mg distribution, expressed as  $K_d = (Mg/Fe)_{gnt} / (Mg/Fe)_{bio}$ , is a function of temperature and is affected only to a slight degree by pressure (Thompson 1976, Goldman and Albee 1977, Ferry and Spear 1978).

For temperature estimates from garnet-biotite pairs in the study area, the thermometer of Ferry and Spear (1978), with mixing models for plagioclase and garnet by Pigage and Greenwood (1982), Hodges and Spear (1982), Indares and Martignole (1985), Perchuk and Lavrent'eva (1983) are employed.

Hodges and Spear (1982) have suggested several points which should be considered when using these garnet-biotite thermometers; in particular that " the garnet-biotite Fe-Mg-exchange geothermometer is susceptible to re-equilibration during cooling and is most accurate in medium-grade metamorphic terranes " and " the thermometer may yield unrealistically low temperatures for high-grade metamorphic terranes ". These suggestions will be considered when the results of the geothermometer are applied and interpreted in a later chapter.

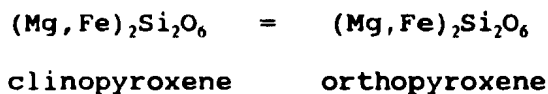
#### 5-3-2 Clinopyroxene-Orthopyroxene Geothermometry

Coexisting Ca-poor and Ca-rich pyroxenes have long been recognized as a potential geothermometer, and consequently



there have been several attempts to calibrate the temperature dependence of the solution of enstatite in diopside (Bohlen and Essene 1979).

Wood and Banno (1973) and Wells (1977) have presented data on the variation of the position and shape of the solvus with temperature in the pyroxene quadrilateral, based on the exchange reaction:



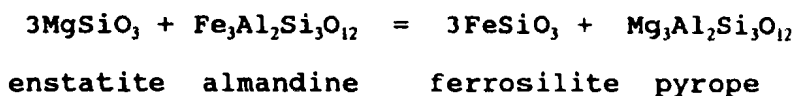
Both calibrations are based on an assumption of an ideal two-site solution model, in which a random distribution of  $\text{Fe}^{2+}$  and Mg between M2 and M1 is assumed following the allocation of Ca, Na, Mn to M2 and  $\text{Al}^{\text{vi}}$ , Cr Ti,  $\text{Fe}^{3+}$  to M1, respectively.

### 5-3-3 Garnet-Orthopyroxene Geothermometry

The equilibrium compositions of coexisting garnet and orthopyroxene have been widely recognized as potential indicators of the P-T conditions of formation of a variety of natural assemblages, especially those formed at granulite facies metamorphic conditions and in the Earth's upper mantle (Lee and Ganguly 1988).

Wood (1974), Harley and Green (1982), and Harley (1984) have experimentally calibrated the solubility of Al in orthopyroxene coexisting with garnet as a geothermobarometer.

The exchange of Fe and Mg between coexisting garnet and orthopyroxene was calibrated by Wells (1977), Lindsley (1983), Sen and Bhattacharya (1984) and Lee and Ganguly (1988) based on the equilibrium:

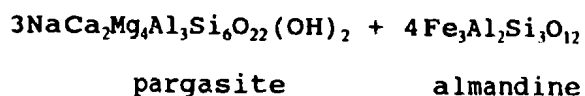
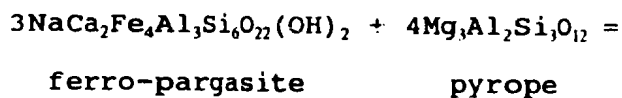


In this application, the orthopyroxene solid solution is assumed to be ideal in the temperature range for granulites and a ternary symmetrical solution model has been adopted for garnet (Sen & Bhattacharya 1984). Thermodynamic parameters for end-member solutions in garnet were taken from the data of Froese (1973) and O'Neill and Wood (1979).

#### 5-3-4 Garnet-Hornblende Geothermometry

A garnet-hornblende Fe-Mg exchange geothermometer has been presented by Graham and Powell (1984) and Powell (1985). The

exchange of Fe-Mg between garnet and hornblende may be represented by the exchange equilibrium :



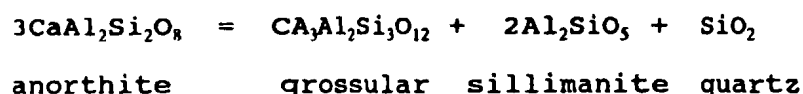
Graham and Powell (1984) have pointed out that the thermometer can be applicable below about 850 °C to rocks with Mn-poor garnet and common hornblende of widely varying chemistry metamorphosed at low  $f_{\text{O}_2}$ .

#### 5-4 Geobarometry

Metamorphic pressures were estimated using the garnet-plagioclase- $\text{Al}_2\text{SiO}_5$ -quartz geobarometers of Ghent et al. (1979), and Newton and Haselton (1981), and the garnet-orthopyroxene-plagioclase-quartz geobarometer of Perkins and Newton (1981). Additionally, the orthopyroxene-garnet geobarometry calibration of Harley and Green (1982) has been employed.

#### 5-4-1 Garnet-Plagioclase-Al<sub>2</sub>SiO<sub>5</sub>-Quartz Geobarometry

The pressure during metamorphism can be estimated from the equilibrium (Ghent 1976):



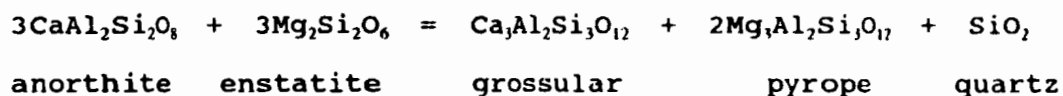
Calculations of the reaction were initially based on the assumption of ideal solid solution of garnet and plagioclase. Subsequent experimental and thermodynamic analyses have resulted in modification to the barometer (e.g. Ghent et al. 1979; Newton and Haselton 1981; Hodges and Spear 1982, Hodges and Royden 1984).

As Bohlen and Lindsley (1987) pointed out, the geobarometer has high degree of uncertainty due to the temperature-sensitivity of the end-member equilibrium and the low concentration of grossular in garnet from most pelitic assemblages. This is especially applicable to the sample in the study in which X<sub>ca</sub> garnet is lower than 0.02

#### 5-4-2 Garnet-Orthopyroxene-Plagioclase-Quartz

##### Geobarometry

Wood and Banno (1973) first experimentally calibrated the reaction of garnet with pyroxene solid solution as a geobarometer. Newton and Perkins (1982) and Perkins and Chipera (1985) have calibrated mineralogic geobarometers based on the assemblage garnet-plagioclase-pyroxene-quartz, which are applicable to granulite grade quartzofeldspathic and mafic lithologies. The equilibrium has been calibrated on the basis of the reaction :



Here, the formulations of Ganguly and Kennedy (1974) were used for the activities of the ternary garnet solid-solution and plagioclase activities were determined using the models of Kerrick and Daker (1975) and Newton et al. (1980).

In this study the choice of temperature for a pressure estimate depends on consideration of the results of appropriate mineralogic thermometers.

## 5-5 Results of Geothermobarometry

### 5-5-1 Geothermometry

On the basis of the general occurrence of high-grade mineral assemblages from mafic rocks, including the pelitic gneiss in the area, metamorphic temperatures are expected to be relatively high.

Results from the orthopyroxene-clinopyroxene geothermometer are listed in Table 7. The calibrations of Wood and Banno (1973) and Wells (1977) produce temperature estimates in the range 827-931°C. The results do not show any difference between the metagabbro and the dioritic gneiss, and there are also no significant differences arising from the use of core versus rim analyses. Thus, the temperature estimates from orthopyroxene-clinopyroxene pairs in the metagabbro and dioritic gneiss units are in good agreement with the high temperatures inferred for the pelitic gneiss using the petrogenetic grid (section 4-2-5).

Garnets from the pelitic gneiss and noritic gneiss are compositionally zoned, with rims of lower Mg, implying retrograde exchange between garnet and coexisting minerals (especially biotite) as shown in compositional zoning profile

Table 7. Temperature estimates from the opx-cpx thermometer in the metagabbro and dioritic gneiss of the Indian Head Range

Sample#	T1	T2
S-14	876	861
S-2	847	888
S-2-2	830	851
S-7	857	835
S-64A	827	851
S-103A	876	931
S-103B	849	889
T1: Wood & Banno (1973)		
T2: Wells (1979)		

Metagabbro: S-14, S-2, S-2-2, S-7

Dioritic gneiss: S-64A, S-103A, S-103B, S-36A.



of Figs. 72, 73 and 74. Application of garnet-orthopyroxene thermometry on quartz-bearing samples using Sen and Bhattacharya's (1984) thermodynamic calibration indicates that metamorphic temperatures for  $P = 8$  kbar (which is assumed on the basis of the petrogenetic grid discussed in section 4-5) are in the range of 776-805°C for core compositions (Table 8). Rim compositions yield temperatures up to 100°C lower. Lee and Ganguly's (1988) experimental calibration yields slightly higher temperatures (806-838°C). Coexisting orthopyroxene and garnet give a range of 729-754°C for core compositions using the Fe-Mg exchange thermometer of Harley (1984). The low temperature estimates from garnet-orthopyroxene pairs may represent minimum temperatures because the  $Fe^{3+}$  contents of garnet and orthopyroxene have not been calculated (Harley 1985).

Several calibrations are now available for the garnet-biotite geothermometer. The results for  $P = 8$  kbar, which is assumed on the basis of results from the petrogenetic grid, are listed in Table 9. Garnet-biotite pairs from the matrix of the noritic gneiss give temperatures of 829-689°C for garnet cores and 628-542°C for garnet rims using the calibration of Hodges and Spear (1982). The differences between the Ferry and Spear (1978) calibration and the Hodges and Spear (1982

Table 8. Temperature estimates (for 8 kbar) from garnet-orthopyroxene thermometer in mafic rocks of the Indian Head Range.

Sample#	T1	T2	T3
S-85-2(C)	804	752	835
S-85-2(R)	736	706	784
S-105 (C)	805	754	838
S-105 (R)	769	729	810
S-88-2(C)	776	729	806
S-88-2(R)	732	698	771
S-90-2(C)	794	737	807
S-90-2(R)	702	673	739

C:Core R:Rim

T1: Sen & Bhattacharya (1984)  
T2: Harley (1984)  
T3: Lee & Ganguly (1988)

\* S-85-2, S-105 : noritic gneiss  
S-88-2, S-90 : pelitic gneiss

Table 9. Temperature estimates (for P=8 kbar) from garnet-biotite thermometers in the noritic gneiss of the Indian Head Range.

Sample(S)	T1	T2	T3	T4	T5
126-2(C)	825	844	654	829	700
126-2(R)	596	611	464	600	589
127(C)	786	803	622	790	683
127(R)	623	639	482	628	604
105(C)	803	821	632	808	690
105(R)	544	558	415	548	560
85-2(C)	683	715	579	689	634
85-2(R)	535	564	450	542	555

C: Core R: Rim

T1 - Ferry and Spear (1978)  
 T2 - Pigage and Greenwood (1982)  
 T3 - Indares and Martignole (1935)  
 T4 - Hodges and Spear (1982)  
 T5 - Perchuk and Lavrent'eva (1983)

calibration are about  $\pm 25^{\circ}\text{C}$ . The correction of Pigage and Greenwood (1982) yields somewhat anomalous results. The apparent temperature difference between core and rim may reflect continued Fe-Mg re-equilibration during retrogression and record temperatures of different points on the P-T path. The Indares and Martignole (1985) calibration, which evaluated influences from Al and Ti in biotite, yields temperatures ranging from 100 to  $160^{\circ}\text{C}$  lower than those of the Hodges and Spear (1982) calibration. Estimates determined from the calibration of Perchuk and Laurent'eva (1983) also yield somewhat lower temperatures than the Ferry and Spear, Hodges and Spear, and Pigage and Greenwood calibrations.

It is likely that the calibration of Hodges and Spear (1982) is most applicable to the area because most garnet and biotites satisfy the compositional limits.

Garnet-hornblende thermometry (Graham and Powell 1984) on samples from the metagabbro unit provides temperature estimates (Table 10) in the range  $580\text{--}640^{\circ}\text{C}$ , consistent with the results from garnet-biotite rim compositions of the noritic gneiss and therefore also interpreted to represent re-equilibration during cooling.

In summary, it is likely that the best estimate of peak metamorphic temperature lies in the range of  $827\text{--}931^{\circ}\text{C}$  from

Table 10. Temperature estimates from garnet–hornblende thermometers in the metagabbro of the Indian Head Range.

Sample#	T1	T2
S-77(C)	635	618
S-77(R)	611	593
S-72(C)	631	615
S-72(R)	627	610
S-65(C)	645	629
S-65(R)	607	589

C: Core, R: Rim

T1 – Graham and Powell (1984)  
T2 – As T1, but with refinements by Powell (1985)

orthopyroxene-clinopyroxene thermometry. The temperature of garnet formation is inferred to be 750-830°C from garnet-orthopyroxene and garnet-biotite (core compositions) thermometry. The temperature from garnet-biotite (rim compositions) and garnet-hornblende thermometry is in the range of 540-640°C, which appears to indicate re-equilibration.

#### 5-5-2 Geobarometry

The absence of kyanite and andalusite in pelitic gneiss (i.e. only sillimanite occurs) implies that metamorphic pressure is moderate. Furthermore, the absence of coexisting garnet and clinopyroxene in metabasic rocks and the low jadeite contents ( $< 5$  mole %) in clinopyroxene support a moderate pressure.

Metamorphic pressures calculated from the garnet-plagioclase-sillimanite-quartz barometer for the pelitic gneiss are listed in Table 11. The temperature choice of 800°C is based on results of the geothermometry and the petrogenetic grid as described in the previous chapter.

The calibrations of Newton and Haselton (1981) (with correction by Ganguly and Saxena (1984)) yield a pressure range of 7.9-9.6 kbar at 800°C. The calibrations of Hodges and Royden (1984) yield somewhat a lower (although overlapping

Table 11. Pressure estimates (for 800°C) using the garnet–sillimanite–plagioclase–quartz barometer in pelitic gneiss of the Indian Head Range.

Sample#	P1	P2	P3	P4
S-90-1	9.6	6.1	10.3	7.7
S-90-2	9.3	5.9	10	7.5
S-88-1	8.1	5.8	8.8	7.5
S-88-2	7.9	5.7	8.6	7.4
S-45	8	5.7	8.7	7.4

P1: Newton & Haselton (1981) with Ganguly & Saxena (1984) correction  
 P2: Ghent et al. (1979)  
 P3: Ghent et al. (1979) with Kd calculated as in P1  
 P4: Newton & Haselton (1981) with Hodges & Royden (1984) correction



within error) pressure (7.4-7.7 kbar). However, both of these estimates are considered to be unreliable owing to the extremely low concentration of grossular ( $X_{\text{grossular}} < 0.02$ ) in these garnets.

The compositional parameters and calibrations of the garnet-orthopyroxene-plagioclase-quartz geobarometer for the pelitic gneiss are listed in Table 12.

The Newton and Perkins (1982) calibration (Mg-reaction) of the garnet-orthopyroxene-plagioclase-quartz geobarometer indicates a pressure range of 8.1-8.6 kbar at 800°C for the pelitic gneiss. The calibrations of Newton and Perkins (1982) and Perkins and Chipera (1985; Mg-reaction) yield similar pressures. However, the calibration of Perkins and Chipera (1985; Fe-reaction) yielded considerably higher pressures (10.8-11.8 kbar) at the same temperature.

The garnet-orthopyroxene geobarometer of Harley and Green (1984) based on alumina solubility in orthopyroxene, indicates pressures of 7.9-10.3 kbar at 800°C.

Errors associated with these geobarometers range from about  $\pm 1.0$ -1.5 kbar for garnet-orthopyroxene equilibria to at least  $\pm 2$  kbar for the garnet-plagioclase- $\text{Al}_2\text{SiO}_5$ -quartz

Table 12. Compositional parameters and pressure estimates (for 800°C) from garnet–orthopyroxene–plagioclase – quartz barometers in pelitic gneiss of the Indian Head Range.

Sample#	Opx		Gnt			Pl		P1	P2	P3
	XMg	XMg	XFe	XCu	XMn	XAn	XAn			
S-88-2(C)	0.694	0.428	0.532	0.015	0.025	0.136	0.136	8.3	8.1	11.2
S-88-2(R)	0.706	0.418	0.541	0.016	0.025	0.136	0.136	8.2	8.1	11.8
S-45(C)	0.688	0.43	0.516	0.016	0.038	0.144	0.144	8.6	8.4	10.9
S-45(R)	0.696	0.428	0.52	0.016	0.036	0.144	0.144	8.5	8.3	11.2
S-90-2(C)	0.655	0.402	0.574	0.005	0.019	0.056	0.056	8.3	8.1	10.8
S-90-2(R)	0.66	0.402	0.574	0.005	0.019	0.056	0.056	8.1	8	10.8

C: Core R: Rim

P1: Newton & Perkins (1982)

P2: Perkins & Chipera (1985; Mg–reaction)

P3: Perkins & Chipera (1985; Fe–reaction)

barometer (Bohlen and Lindsley 1987).

Thus, it can be concluded that the metamorphic pressure during garnet formation was about 8.5 kbar. This pressure estimate lies within the stability field of sillimanite at 800°C (Holdaway 1971). Although pressure estimates from geobarometers may represent later re-equilibrium conditions, they are in good agreement with the pressure estimates based on results (8-8.5 kbar) from petrogenetic grids for garnet formation.

## CHAPTER 6

### DISCUSSION AND TECTONIC IMPLICATIONS

#### 6-1 Discussion

In this chapter the P-T conditions of metamorphism obtained from petrogenetic grids are compared with the results from independent geothermobarometry discussed in the previous chapter.

The estimate from orthopyroxene-clinopyroxene geothermometers (Wood and Banno 1973, Wells 1977) from the metagabbro and dioritic gneiss in the area indicates metamorphic temperatures in the range 850-930°C. Additionally, the presence of exsolution lamellae in pyroxenes from the anorthosite and noritic gneiss supports peak metamorphic temperatures greater than 750°-820° (Ellis 1980). This result is also compatible with the presence of perthite/antiperthite in the variably foliated biotite granite.

A temperature of about 900°C is therefore assumed for the metamorphic peak. The result strongly supports the high temperature expected from the stable mineral assemblage in metapelitic rocks (highly aluminous orthopyroxene-cordierite-

spinel) of the early stage described in section 4-2-5. However, the mineral assemblages in the pelitic gneiss do not preclude the possibility of even higher temperatures (up to 1000 °C) at an early stage of metamorphism, as discussed in section 4-2-5.

Unfortunately, pressure estimates for the early stage of metamorphism in the area are not available from independent geobarometry owing to the absence of suitable mineral assemblages. Nevertheless, mineral assemblages during the early stage suggest that metamorphic pressure was moderate (6-8 kbar). The presence of the assemblage spinel-quartz supports a relatively low pressure. Sillimanite is the only aluminosilicate mineral found in the study area. It implies that pressure was not higher than about 10 kbar, even during sillimanite formation. The absence of the assemblage sapphirine + quartz indicates that the metamorphic conditions in the Indian Head Range did not exceed 10 kbar and 1000 °C.

Metamorphic temperatures during garnet formation are estimated to have been 840-800°C based on garnet-orthopyroxene thermometry (Harley 1984). Garnet-biotite geothermometry (several calibrations) yields a range of 850-800 °C for garnet core compositions. This result is broadly compatible with garnet-orthopyroxene thermometry for garnet cores. The

temperature estimates from the petrogenetic grid (Figs. 66 and 80) also yield a range near  $\approx 800^{\circ}\text{C}$ .

Garnet-orthopyroxene, garnet-orthopyroxene-plagioclase-quartz and garnet-sillimanite-plagioclase-quartz geobarometers yield estimates of 8-9 kbar maximum pressure. This is consistent with the absence of the assemblage garnet-clinopyroxene in mafic units and represents the pressure conditions during garnet formation.

The temperatures estimated from garnet-biotite rim compositions yield lower temperatures ranging from  $640-530^{\circ}\text{C}$  and are consistent with those estimated from the garnet-hornblende geothermometer ( $580-640^{\circ}\text{C}$ ) on samples from the metagabbro unit. This result may represent the temperature of the amphibolite facies metamorphism which is recognized on the basis of retrograde mineral assemblages (chapters 3 and 4).

#### P-T-t Path

The P-T-t path for the evolution of the Indian Head Range can be determined from the petrogenetic grid (Fig. 79). The mineral assemblage cpx + sil + qtz was produced by cordierite replacement on the basis of mineral reaction texture discussed in section 4-2-4. According to Hensen (1986) the slope of the

reaction is gently positive in P-T space (Fig. 64). Hensen (1987) suggested that, if the reaction occurs under conditions of high oxygen fugacity, any increase of pressure during the breakdown reaction of cordierite may be limited. Thus, pressure changes during this reaction may not be significant.

Garnet is interpreted to form by the reaction  $\text{Opx} + \text{Sil} = \text{Gnt} + \text{Qtz}$ . Continuous cooling during garnet formation is deduced from the positive slope of the mineral reaction as shown in the partial petrogenetic grid in Fig. 79. The proposed continuous cooling is supported by the geothermobarometric results discussed in chapter 5, in which the garnet-orthopyroxene thermometer yields a temperature of 750-830°C.

Kornerupine breakdown reactions produced secondary sapphirine-orthopyroxene symplectites. These reactions took place under pressure conditions of 5-6 kbar and temperature conditions of 750-800 °C as shown in Figure 66. This implies that there was a significant change in pressure between garnet formation ( from  $\approx 8$  kbar) and kornerupine replacement reactions (5-6 kbar), and may indicate nearly-isothermal decompression between these two.

Thus, an early approximately isobaric cooling history is



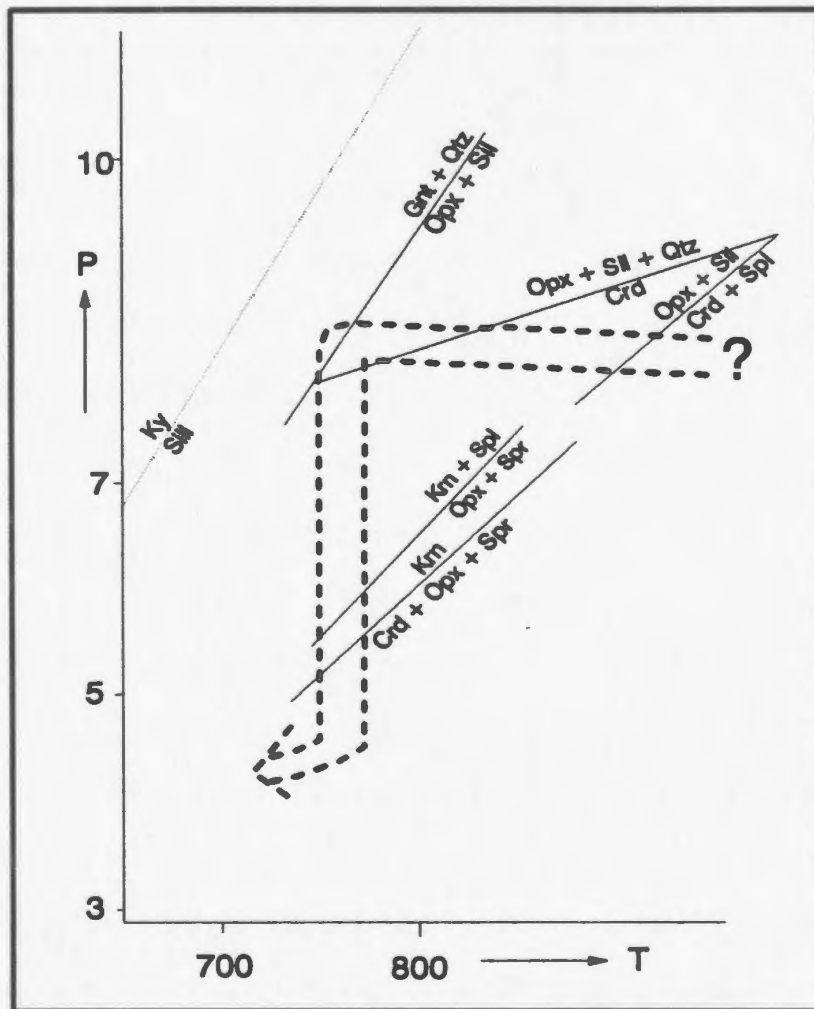


Figure 79. P-T-time trajectory from reaction grids showing successive metamorphic conditions

recognized from the textural evidence of the reaction cordierite  $\rightarrow$  orthopyroxene + sillimanite + quartz  $\rightarrow$  garnet + quartz. The reaction, kornorupine  $\rightarrow$  orthopyroxene + sapphirine + cordierite, occurred at lower P, and followed near-isothermal decompression before final cooling (Fig. 79).

Consequently, the metamorphic evolution of the Indian Head Range, as recorded by the mineral reactions, suggests a rather unusual P-T path involving discrete segments with contrasting slopes.

#### 6-2 Tectonic Implications of the P-T path

In a review of P-T paths in granulite facies terranes, Harley (1989) showed that of ninety examples, eighty six exhibited clockwise P-T paths and only four showed anticlockwise paths. Clockwise P-T paths are generally interpreted in terms of crustal thickening by overthrusting [following the numerical modelling experiments of England and Richardson (1977), England and Thompson (1984, 1986)] with an additional input of heat from either adjacent intrusion or from an enhanced mantle heat flow. The latter is necessary for the attainment of granulite facies temperatures at mid to deep-crustal pressures (6-10 kbars). In contrast, anticlockwise P-T paths, of which perhaps the best example is from the Adirondack Mountains of

the southwest Grenville Province, are characterized by a pressure increase following peak metamorphism. Such a path may have been induced by a steady increase in crustal thickness due to magmatic accretion at the base of and into the crust during metamorphism (Bohlen 1987).

Interpretation of the significance of the path determined in the IHR depends largely on the nature of the slope of the high P part of the path. This is not well constrained and may be isobaric, or may indicate a modest increase in P with decreasing T (see section 4-2-5).

If the high P part of the path is interpreted to be isobaric, then the P-T path can be considered as a clockwise loop with a high T "promontory" presumably related to the proximity of the intrusion of the anorthosite suite. In this model, isobaric cooling after intrusion of the anorthosite suite occurred before decompression (exhumation), which is interpreted to be a result of crustal thickening by thrusting. On the other hand, if the high P part of the path is interpreted to reflect increasing P during cooling, it may form part of an anticlockwise P-T path that involved modest crustal thickening during cooling, with the subsequent exhumation being caused by a later tectonic event.

With the constraints of the existing data base, it is not possible to adequately distinguish between the two models. It is noteworthy, however, that the overall shape and position of

the P-T path is quite similar to that derived for the Wilson Lake terrane in the Grenville Province of Labrador by Currie and Gittins (1988), who interpreted an origin by continent-continent collision followed by obduction of deep continental crust.

The steep, nearly isothermal decompression path (indicated by the Krn replacement reaction in IHR) has been recorded in several granulite facies terranes and is considered to be due to rapid tectonic uplift following crustal thickening due to thrusting, or to a crustal extension environment following peak metamorphic conditions (England and Thompson 1984, 1986). In this case it is apparent that if thrusting was the cause of the isothermal uplift path, it must have occurred distinctly later than the granulite facies metamorphic event. Whether such thrusting occurred during the Grenville orogeny, or during a pre-Grenvillian (1650 Ma event as suggested by Currie and Gittins for the Wilson Lake terrane) is not presently known.

Evidence of retrograde metamorphism to amphibolite facies assemblages, such as has been noted in the IHR has also been observed in the adjacent Long Range Inlier by Owen and Erdmer (1989) and Owen (1991). Owen (1991) suggested that the amphibolite facies metamorphism in the Long Range Inlier records a late Grenvillian (978 Ma) tectonothermal overprint, an interpretation which is probably also applicable to the IHR.

### 6-3 Correlations to the Long Range Mountains

Metamorphic conditions for the granulite facies rocks of the Long Range Mountain have recently been constrained by Owen and Erdmer (1989) and Owen (1991). Metamorphic conditions for the Disappointment Hill complex within the Steel Mountain terrane are also documented by Owen and Currie (1991).

Although the inferred metamorphic conditions of the Indian Head Range as determined in the study are consistent with those for granulite formation in general (see Bohlen 1991), the metamorphic conditions of the Indian Head Range exhibit relatively higher temperature than those for the adjacent Long Range Inlier (Owen 1991), and significantly higher pressure and temperature than for the Disappointment Hill complex within the Steel Mountain terrane (Owen and Currie 1991).

However, although the metamorphic conditions from these inliers are not the same, there is a consistent increase in P and T gradationally from northeast to southwestern throughout the Long Range Inlier, as pointed out by Owen and Erdmer (1989), and the regional southwestward increase in metamorphic grade of the Long Range Inlier is in good agreement with that of the Indian Head Range. Owen (1991) suggested that the difference in metamorphic conditions (especially T) along the

Long Range Inlier may be related to the distribution of heat sources such as mafic magma (e.g. the Taylor Brook gabbro complex) in the deep crust. On the other hand, although the Steel Mountain terrane has in part similar lithologies (such as anorthosite and gabbro) to the Indian Head Range and the southwestern Long Range Inlier, its metamorphism occurred under lower P-T conditions than that in the Indian Head Range and the southern Long Range Inlier.

Thus, it seems unlikely that subsurface plutons such as anorthosite and gabbro contributed to the high thermal metamorphic gradient in these inliers. As an alternative, the relatively high P-T conditions of the Indian Head Range and the southwestern Long Range Inlier may be a result of exhumation of progressively deeper crustal level towards the south during a later tectonic event (Grenvillian orogeny?).

Subsequently, Owen and Currie (1991) suggested that granulites of the Disappointment Hill complex are correlative to granulite complexes in the Indian Head Range and northern Cape Breton Island based on associations with anorthositic rocks. However, the correlation between the Disappointment Hill complex and the study area cannot be documented on metamorphic grounds.

### Future work

The present study suggests that the Indian Head Range experienced a complex metamorphic history and underwent different metamorphic conditions compared to the adjacent Grenvillian inliers. Although the present study recognizes two distinctive metamorphic (granulite and amphibolite facies) and associated deformational features, and establishes the metamorphic conditions and a possible P-T path for this area, unsolved questions remain. They stem largely from the lack of constraints on the timing of rock units and metamorphic/deformational events in the study area. Thus, geologically constrained geochronological data are indispensable to establish the evolutionary history of the Indian Head Range. Future work must be concerned with absolute age relations based on the field work of present study, and U/Pb geochronological work is in progress for the units outlined in the study.



## REFERENCES

- Anastasiou, P and Seifert, F., 1972. Solid solubility of  $\text{Al}_2\text{O}_3$  in enstatite at high temperatures and 1-5 kbar water pressure. *Contr. Mineral. Petrol.* 34, 272-287.
- Arima, M., 1978. Phase equilibria in the system  $\text{MgSiO}_3$ - $\text{Al}_2\text{O}_3$ - $\text{Fe}_2\text{O}_3$  at high temperatures and pressures with special reference to the solubility of  $\text{Al}_2\text{O}_3$  and  $\text{Fe}_2\text{O}_3$  in enstatite. *J. Fac. Sci. Hokkaido Univ. Ser. IV*, 18, 305-338.
- Arima, M., Kerrich, R. and Thomas, A., 1986. Sapphirine-bearing paragneiss from the northern Grenville province in Labrador, Canada: Protolith composition and metamorphic P-T conditions. *Geology* 14, 844-847.
- Arima, M. and Barnett, R.L., 1984. Sapphirine bearing granulites from the Sipiwesk Lake area of the late Archean Pikwitonei granulite terrain, Manitoba, Canada. *Contrib. Mineral. Petrol.* 88, 102-112.
- Armbruster, T.H. and Bloss, F.D., 1980. Channel  $\text{CO}_2$  in cordierite. *Nature* 286, 140-141.
- Bailey, E.H. and Stevens, R.E., 1960. Selective staining of K-feldspar and plagioclase on rock slabs and thin sections. *Amer. Mineral.* 45, 1020-1025.
- Barr, S.M., Raeside, R.P., and van Breeman, O., 1987. Grenvillian basement in the northern Cape Breton Highlands, Nova Scotia. *Canadian Jour. of Earth Sci.* 24, 992-997.
- Bertrand, P., Ellis, D.J. and Green, D.H., 1989. Experimental phase relationships at high pressures and temperatures in a model pelitic system. *Metamorphism and Geodynamics, Granulite Metamorphism, Program and Abstract*, IGCP-235, 9.
- Bishop, F.C and Newton, R.C., 1975. The composition of low pressure synthetic sapphirine. *Jour. of Geol.* 83, 511-517.
- Bohlen, S.R., 1987. Pressure-Temperature-Time paths and a

- tectonic model for the evolution of granulites. Jour. of Geol. 95, 617-632.
- Bohlen, S.R.**, 1991. On the formation of granulites. Jour. of metamorphic Geol. 9, 223-229.
- Bohlen, S.R. and Dollase, W.A.**, 1983. Calibration of hercynite-quartz stability. G.S.A.B.15, 529.
- Bohlen, S.R. and Essene, E.J.**, 1979. A critical evaluation of two-pyroxene thermometry in Adirondack granulites. Lithos 12, 335-345.
- Bohlen, S.R. and Lindsley, D.H.**, 1987. Thermometry and barometry of igneous and metamorphic rocks; Annual Reviews, Earth and Planetary Sciences 15, 397-420.
- Caporuscio, F.A. and Morse, S.A.**, 1978. Occurrence of sapphirine plus quartz at Peekskill, New York. Amer. Jour. of Sci. 278, 1334-1342.
- Cawood, P.A. and Williams, E.**, 1988. Acadian basement thrusting, crustal delamination, and structural styles in and around the Humber Arm allochthon, western Newfoundland. Geology 16, 370-373.
- Chatterjee, N.D. and Schreyer, W.**, 1972. The reaction enstatite + sillimanite = sapphirine + quartz in the system  $MgO-Al_2O_3-SiO_2$ . Contrib. Mineral. Petrol. 36, 49-62.
- Chinner, G.A.**, 1960. Pelitic gneisses with varying ferrous/ferric ratios from Glen Clova, Angus, Scotland. Jour. of Petrology 2, 312-323.
- Clifford, P.M. and Baird, D.M.**, 1962. Great Northern Peninsula of Newfoundland- Grenville Inlier. The Canadian Mining and Metallurgical Bulletin for March, 150-157.
- Colman-Sadd, S.P.**, 1969. Geology of the iron deposits near Stephenville, Newfoundland. Unpublished M.Sc. thesis, Memorial Univ. of NFLD.
- Connelly, J.N.**, 1991. The thermotectonic history of the Grenville Province of western Labrador (Ph.D thesis). St. John's, NFLD, Memorial Univ..

- Currie, K.L.**, 1987. A preliminary account of the geology of Harrys River map area, southern Long Range of Newfoundland; in Current Research, Part A, G.S.C., paper 87-1A, 653-662.
- Currie, K.L. and Gittins, J.**, 1988. Contrasting sapphirine parageneses from Wilson Lake, Labrador and their tectonic implications. *Jour. of Metamorphic Geol.* 6, 603- 622.
- Dallmeyer, 1978.**  $^{40}\text{Ar}/^{39}\text{Ar}$  incremental-release ages of hornblende and biotite from Grenville basement rocks within the Indian Head Range complex, southwest Newfoundland: their bearing on Late Proterozoic-Early Paleozoic thermal history. *Canadian Jour. of Earth Sci.* 15, 1374-1379.
- Davidson, A.**, 1984. Identification of ductile shear zones in the southwestern Grenville Province of the Canadian Shield. *Precambrian Tectonics Illustrated*, 263-279.
- Droop, G.T.R.**, 1989. Reaction history of garnet-sapphirine granulites and conditions of Archaean high-pressure granulite-facies metamorphism in the Central Limpopo Mobile Belt, Zimbabwe. *Jour. of Metamorphic Geol.* 7, 383- 403.
- Droop, G.T.R. and Bucher-Nurminen, K.**, 1984. Reaction textures and metamorphic evolution of sapphirine-bearing granulites from the Gruf Complex, Italian Central Alps. *Jour. of Petrology* 25, 766-803.
- Ellis, D.J.**, 1980. Osumilite-sapphirine-quartz granulites from Enderby Land, Antarctica: P-T conditions of metamorphism, implications for garnet-cordierite equilibria and evolution of the deep crust. *Contrib. Mineral. Petrol.* 74, 201-210.
- Ellis, D.J., Sheraton, J.W., England, R.N, and Dallwitz, W.B.**, 1980. Osumilite-sapphirine-quartz granulites from Enderby Land, Antarctica- Mineral assemblages and reactions. *Contrib. Mineral. Petrol.* 72, 123-143.
- Emslie, R.F.**, 1975. Pyroxene megacrysts from anorthositic rocks: new clues to the sources and evolution of the parent magmas. *Canadian Mineralogist* 13, 138-145.
- England, P.C. and Richardson, A.B.**, 1977. The influence of

erosion upon the mineral facies of rocks from different metamorphic environments. Jour. Geol. Society, London 134, 201-213.

- England, P.C. and Thompson, A.B., 1984. Pressure-temperature-time paths of metamorphism. I. Heat transfer during the evolution of regions of thickened continental crust. Jour. of Petrol. 25, 894-928.
- England, P.C. and Thompson, A.B., 1986. Some thermal and tectonic models for crustal melting in continental collision zones. In: Collisional Tectonics (eds Coward, M.P. and Ries, A.C.), 83-94. Geol. Society of London Special Publication No. 19.
- Ferry, J.M. and Spear, F.S., 1978. Experimental Calibration of the partitioning of Fe and Mg between biotite and garnet. Contrib. Mineral. Petrol. 66, 113-119.
- Froese, E., 1973. The assemblage quartz-K-feldspar-biotite-garnet-sillimanite as an indicator of  $P_{H_2O}$ -T conditions. Canadian Jour. of Earth Sci. 10, 1575-1579.
- Ganguly, J. and Kennedy, G.C., 1974. The energetics of natural garnet solid solution: I. Mixing of the aluminosilicate end members. Contrib. Mineral. Petrol. 48, 137-148.
- Ganguly, J. and Saxena, S.K., 1984. Mixing properties of aluminosilicate garnets: constraints from natural and experimental data, and applications to geothermobarometry. Amer. Mineral. 69, 88-97.
- Ghent, E.D., 1976. Plagioclase-garnet- $Al_2SiO_5$ : a potential geobarometer-geothermometer. Amer. Mineral. 61: 710-714.
- Ghent, E.D., Robbins, D.B., and Stout, M.Z., 1979. Geothermometry, geobarometry, and fluid compositions of metamorphosed calc-silicates and pelites, Mica Creek, British Columbia. Amer. Mineral. 64, 874-885.
- Gittins, J. and Currie, K.L., 1979. Petrologic studies of sapphirine-bearing granulites around Wilson Lake, Labrador. Geol. Surv. Can., Paper 79-1A, 77-82.
- Goldman, D.S. and Albee, A.L., 1977. Correlation of Mg/Fe partitioning between garnet and biotite with 180/160

partitioning between quartz and magnetite. *Am. Jour. Sci.* 277, 750-767.

- Graham, C.F. and Powell, R., 1984.** A garnet-hornblende geothermometer: calibration, testing, and application to the Pelona Schist, southern California. *Jour. of Metamorphic Geol.* 2, 13-31.
- Grant, S.M., 1989.** Tectonic implications from sapphirine-bearing lithologies, south-west Grenville province, Canada. *Jour. of Metamorphic Geol.* 7, 583-598
- Green, T.H. and Vernon, R.H., 1974.** Cordierite breakdown under high-pressure, hydrous conditions. *Contrib. Mineral. Petrol.* 46, 215-226.
- Grew, E.S., 1980.** Sapphirine + quartz association from Archean rocks in Enderby Land, Antarctica. *Amer. mineral.* 65, 821-836.
- Hanmer, S., 1987.** Granulite facies mylonites: a brief structural reconnaissance north of Stony Rapids, northern Saskatchewan; in *Current Research, Part A, G.S.C., Paper 87-1A*, 563-572.
- Hanmer, S., 1988.** Ductile thrusting at mid-crustal level, southwestern Grenville Province. *Can. Jour. Earth Sci* 25, 1049-1059.
- Harley, S.L., 1984.** An experimental study of the partitioning of Fe and Mg between garnet and orthopyroxene. *Contrib. Mineral. Petrol.* 86, 359-373.
- Harley, S.L., 1985.** Garnet-orthopyroxene bearing granulites from Enderby Land, Antarctica: metamorphic pressure-temperature-time evolution of the Archaean Napier Complex. *Jour. of Petrology* 26, 819-856.
- Harley, S.L., 1989.** The origins of granulites: a metamorphic perspective. *Geol. Magazine* 126, 215-247.
- Harley, S.L. and Green, D.H., 1982.** Garnet-orthopyroxene barometry for granulite and peridotites. *Nature* 300, 697-701.
- Harley, S.L., Hensen, B.J. and Sheraton, J.W., 1990.** Two-stage decompression in orthopyroxene-sillimanite granulites from Forefinger Point, Enderby Land, Antarctica: implications for the evolution of the

Archaean Napier Complex. Jour. of Metamorphic Geol. 8, 591-613

**Haselton, H.T. and Newton, R.C., 1980.** Thermodynamics of pyrope-grossular garnets and their stabilities at high temperatures and high pressures. Jour. Geophys. Res. 85, 6973-6982.

**Hatcher, R.D., 1983.** Basement massifs in the Appalachians: their role in deformation during the Appalachian orogenies. Geological Jour. 18, 255-265.

**Hensen, B.J., 1986.** Theoretical phase relations involving cordierite and garnet revised: the influence of oxygen fugacity on the stability of sapphirine and spinel in the system Mg-Fe-Al-Si-O. Contr. Mineral. Petrol. 92, 362-367.

**Hensen, B.J., 1987.** P-T grids for silica-undersaturated granulites in the systems MAS (n + 4) and FMAS (n + 3) - tools for the derivation of P-T paths of metamorphism. Jour. of Metamorphic Geol. 5, 255-271.

**Hensen, B.J. and Harley, S.L., 1990.** Graphical analysis of P-T-X relations in granulite facies metapelites. In: High temperature metamorphism and crustal anatexis (eds Ashworth, J.R. and Brown, M.)

**Herd, R.K., Ackermann, D., Thomas, A. and Windley, B.F., 1987.** Oxygen fugacity variations and mineral reactions in sapphirine-bearing paragneisses, E. Grenville province, Canada. Mineralogical Magazine 51, 203-206.

**Herd, R.K., Ackermann, D., Windley, B.F., and Rondot, J., 1986.** Sapphirine-garnet rocks, St. Maurice area, Quebec: petrology and implications for tectonics and metamorphism. In: The Grenville Province (eds Moore, J.M., Davidson, A. and Baer, A.J.). GAC Special Paper 31, 241-253.

**Heyl, G.R. and Ronan, J.J., 1954.** The iron deposits of Indian Head area. Geol. Surv. Can., Bull. 27, part 3, 42-65.

**Hodges, K.V. and Royden, L., 1984.** Geological thermobarometry of retrograded metamorphic rocks: an indication of the uplift trajectory of a portion of the northern Scandinavian Caledonides. J. Geophys. Res. 89, 7077-7090.

- Hodges, K.V. and Spear, F.S., 1982. Geothermometry, geobarometry and the  $\text{Al}_2\text{SiO}_5$  triple point at Mt. Moosilauke, New Hampshire. *Amer. Mineral.* 67, 1118-1134.
- Holdaway, M.J., 1971. Stability of andalusite and aluminum silicate phase diagram. *Am. Jour. Sci.* 271, 97-131.
- Horrocks, P.C., 1983. A corundum and sapphirine paragenesis from the Limpopo Mobile Belt, southern Africa. *Jour. of Metamorphic Geol.* 1, 13-23.
- Indales, A. and Martignole, J., 1985. Biotite-garnet geothermometry in the granulite facies: the influence of Ti and Al in biotite. *Amer. Mineral.* 70, 272-278.
- Kamo, S.L., Gower, C.F., and Krogh, T.E., 1989. Birth date for the Iapetus Ocean ?. A precise U/Pb zircon and baddeleyite age for the Long Range dikes, southeast Labrador. *Geology* 17, 602-605.
- Kerrick, D.M. and Darken, L.S., 1975. Statistical thermodynamic models for ideal oxide and silicate solid solutions, with application to plagioclase. *Geochimica et Cosmochimica Acta* 39, 1431-1442.
- Lal, R.K., Ackermann, D. and Upadhyay, H., 1987. P-T-X relationships deduced from Corona textures in sapphirine-spinel-quartz assemblages from Paderu, Southern India. *Jour. of Petrology* 28, 1139-1168.
- Lee, H.Y. and Ganguly, J., 1988. Equilibrium compositions of coexisting garnet and orthopyroxene: experimental determinations in the system  $\text{FeO-MgO-Al}_2\text{O}_3\text{-SiO}_2$ , and applications. *Jour. of Petrology* 29, 93-113.
- Leong, Khee Meng and Moore, J.M., 1972. Sapphirine-bearing rocks from Wilson Lake, Labrador. *Canadian Mineralogist* 11, 777-790.
- Lindsley, D.H., 1983. Pyroxene thermometry. *Amer. Mineral.* 70, 272-278.
- Lowden, J.A., 1961. Age determinations by the Geological Survey of Canada, Report 2, Isotopic Ages, Paper 61-17.
- Lowden, J.A., Stockwell, C.H., Tipper, H.W. and Wanless, R.K., 1963. Age determinations and Geological Studies. G.S.C. Paper 62-17.



- Meong, L.K. and Moore, J.M., 1972.** Sapphirine-bearing rocks from Wilson Lake, Labrador. *Canadian Mineralogist* 11, 777-790.
- Mengel, F.C., 1987.** Thermotectonic evolution of the Proterozoic-Archaeon boundary in the Saglec area, northern Labrador. Ph.D. thesis, St. John's, NFLD, Memorial Univ. P 350.
- Moore, P.B., 1968.** The crystal structure of sapphirine. *Amer. Mineral.* 54, 31-49
- Moore, P.B., and Bennett, J.M., 1968.** Kornerupine: its crystal structure: *Science* 159, 524-526.
- Morse, S.A. and Talley, J.H., 1971.** Sapphirine reactions in deep-seated granulites near Wilson Lake, central Labrador, Canada. *Earth and Planetary Science Letters* 10, 325-328.
- Motoyoshi, Y. and Hensen, B.J., 1989.** Sapphirine-quartz-orthopyroxene symplectites after cordierite in the Archaean Napier Complex, Antarctica: evidence for a counterclockwise P-T path ?. *Eur. J. Mineral.* 1, 467-471.
- Newton, R.C., 1972.** An experimental determination of the high-pressure stability limits of magnesian cordierite under wet and dry conditions. *Jour. of Geol.* 80, 398-420.
- Newton, R.C., Charlu, T.V. and Kleppa, O.J., 1980.** Thermochemistry of high structural state plagioclases. *Geochimica et Cosmochimica Acta* 44, 933-941.
- Newton, R.C. and Haselton, H.T., 1981.** Thermodynamics of the garnet-plagioclase-Al<sub>2</sub>SiO<sub>5</sub> geobarometer. In: Newton, R.C., Navrotsky, A. and Wood, B.J. (eds.) *Thermodynamics of Minerals and Melts*, Springer-Verlag, 129-145.
- Newton, R.C. and Perkins III, D., 1982.** Thermodynamic calibration of geobarometers based on the assemblages garnet-plagioclase-orthopyroxene-(clinopyroxene)-quartz. *Amer. Mineral.* 67, 203-222.
- Newton, R.C. and Wood, B., 1979.** Thermodynamics of water in cordierite and some petrologic consequences of

cordierite as a hydrous phase. Contrib. Mineral. Petrol. 68, 391-405.

- Norman, M.B., 1974. Improved techniques for selective staining of feldspar and other minerals using amaranth. Jour. of Research of the U.S. Geological Survey 2, No 1, 73-79.
- O'Neill, H.-St.C. and Wood, B.J., 1979. An experimental study of Fe-Mg partitioning between garnet and olivine and its calibration as a geothermometer. Contrib. Mineral. Petrol. 70, 59-70.
- Owen, J.V., 1991. Geology of the Long Range Inlier, Newfoundland. G.S.C. Bulletin 395.
- Owen, J.V and Currie, K.L., 1991. The Disappointment Hill complex: Proterozoic granulites in southwestern Newfoundland. Transactions of the Royal Society of Edinburgh: Earth Sciences 82, 55-63.
- Owen, J.V. and Erdmer, P., 1989. Metamorphic geology and regional geothermobarometry of a Grenvillian massif: the Long Range Inlier, Newfoundland. Precambrian Research 43, 79-100.
- Perchuk, L.L. and Lavrant'eva, I.V., 1983. Experimental investigation of exchange equilibria in the system cordierite-garnet-biotite. In: Saxena, S.K. (ed.) Kinetics and Equilibrium in Mineral Reactions, Springer-Verlag, 173-198.
- Perkins III, D. and Chipera, S.J., 1985. Garnet-orthopyroxene-plagioclase-quartz barometry: refinement and application to the English River subprovince and Minnesota River Valley. Contrib. Mineral. Petrol. 89: 69-80.
- Perkins III, D. and Newton, R.C., 1981. Charnockite geobarometers based on coexisting garnet-pyroxene-plagioclase-quartz. Nature 292, 144-146.
- Pigage, L.C. and Greenwood, H.J., 1982. Internally consistent estimates of pressure and temperature: the staurolite problem. Am. Jour. Sci. 282, 943-969.
- Powell, R., 1985. Regression diagnostics and robust regression in geothermometer/geobarometer calibration: the garnet-clinopyroxene geothermometer revisited.

Jour. of Metamorphic Geol. 90, 401-409.

**Powell, R. and Sandiford, M., 1988.** Sapphirine and spinel phase relationships in the system  $\text{FeO-MgO-Al}_2\text{O}_3\text{-SiO}_2\text{-TiO}_2\text{-O}_2$  in the presence of quartz and hypersthene. Contrib. Mineral. Petrol. 98, 64-71.

**Rivers, T., Martignole, J., Gower, C.F., and Davidson, A., 1989.** New tectonic divisions of the Grenville province, southeast Canadian shield. Tectonics 8, 63-84.

**Sandiford, M., 1985.** The metamorphic evolution of granulites at Fyfe Hills; implications for Archaean crustal thickness in Enderby Land, Antarctica. Jour. of Metamorphic Petrol. 3, 155-178.

**Saxena, S.K., 1969.** Silicate solid solution and geothermometry: 3. Distribution of Fe and Mg between coexisting garnet and biotite. Contrib. Mineral. Petrol. 22, 259-267.

**Schreyer, W. and Abraham, K., 1976.** Natural boron-free kornerupine and its breakdown products in a sapphirine rock of the Limpopo belt, southern Africa. Contrib. Mineral. Petrol. 54, 109-126.

**Schreyer, W. and Seifert, F., 1969.** Compatibility relations of the aluminous silicates in the systems  $\text{MgO-Al}_2\text{O}_3\text{-SiO}_2\text{-H}_2\text{O}$  and  $\text{K}_2\text{O-MgO-Al}_2\text{O}_3\text{-SiO}_2\text{-H}_2\text{O}$  at high pressures. Am. Jour. Sci. 267, 371-388.

**Seifert, F., 1974.** Stability of sapphirine: a study of the aluminous part of the system  $\text{MgO-Al}_2\text{O}_3\text{-SiO}_2\text{-H}_2\text{O}$ . Jour. of Geol. 82, 173-204.

**Seifert, F., 1975.** Boron-free kornerupine: a high-pressure phase. Am. Jour. Sci. 275, 57-87.

**Sen, S.K. and Bhattacharya, A., 1984.** An orthopyroxene-garnet thermometer and its application to the Madras charnockites. Contrib. Mineral. Petrol. 88, 64-71.

**Sengupta Pulak, Somnath Dasgupta, Bhattacharya, P.K., Fukuoka, M., Subrata Chakraborti and Santanu Bhowmick, 1990.** Petro-tectonic imprints in the sapphirine granulites from Anantagiri, eastern Ghats mobile belt, India. Jour. of Petrology 31, 971-996.

- Stephenson, N.C.N.**, 1979. Coexisting garnets and biotites from Precambrian gneisses of the south coast of Western Australia. *Lithos* 12, 73-87.
- Stoddard, E.F.**, 1980. Metamorphic conditions at the northern end of the northwest Adirondack Lowlands: Summary. *G.S.A.B. Part 1*, 91, 100-102.
- Streckeisen, A.**, 1976. To each plutonic rock its proper name; *Earth-Science Reviews* 13, 1-13.
- Thompson, A.B.**, 1976. Mineral reactions in pelitic rocks: II. Calculations of some P-T-X (Fe-Mg) phase relations. *Am. Jour. Sci.* 276, 425-454.
- Thompson, J.B.**, 1957. The graphical analysis of mineral assemblages in pelitic schists. *Amer. Mineral.* 42, 842-858.
- Troger, W.E.**, 1971. *Optische Bestimmung der gesteinsbildenden Minerale T.1*, Stuttgart, Schweizerbart, 259.
- Van Berkel, J.T.**, 1987. Geology of the Dashwoods Pond, St. Fintan's and Main Gut map areas, southwest Newfoundland; in *Current Research, Part A, G.S.C.*, Paper 87-1A, 399-408.
- Wardle, R.J. and Ash, C.**, 1984. Geology of the North West River Area. in *Current Research, Newfoundland Department of Mines and Energy, Mineral Development Division, Report 84-1*, 53-67.
- Wells, P.R.A.**, 1977. Pyroxene thermometry in simple and complex systems. *Contr. Mineral. Petrol.* 62, 129-139.
- Windley, B.F. Ackermann, D. and Herd, R.K.**, 1984. Sapphirine/kornerupine-bearing rocks and crustal uplift history of the Limpopo belt, south Africa. *Contrib. Mineral. Petrol.* 86, 342-358.
- Wood, B.J.**, 1974. The solubility of alumina in orthopyroxene coexisting with garnet. *Contrib. Mineral. Petrol.* 46, 1-15.
- Wood, B.J. and Banno, S.**, 1973. Garnet-orthopyroxene and orthopyroxene-clinopyroxene relationships in simple and complex systems. *Contrib. Mineral. Petrol.* 42, 109-124.

APPENDIX 1  
**STAINING METHOD**

Prior to compositional classification of granitoids from the study area, hand specimens and thin sections collected were stained for potassium feldspar and plagioclase using a substantially modified version of the sodium cobaltinitrite/amaranth procedure recommended by Bailey and Stevens (1960) and Norman (1974). This procedure is combined with the cobaltinitrite staining of K-feldspar to stain K-feldspar yellow and plagioclase red on polished hand specimen surfaces and uncovered thin sections.

A-1. Procedure for polished surfaces of hand specimens

1. In a well-ventilated hood, pour the concentrated hydrofluoric acid (52-55 %) into an etching vessel to about 1/4 of the top.
2. Place the rock specimen across the top of the etching vessel, polished surface down.
3. Cover the etching vessel and specimen with an inverted plastic cover vessel to prevent drafts, and let stand 3 minutes.

4. Remove the specimen from the etching vessel, dip in water, and dip twice quickly in and out of the barium chloride solution (5 %).
5. Rinse the specimen briefly in water and immerse it face down for 1 minute in the sodium cobaltinitrite solution (saturated).
6. Rinse the specimen by gently tilting it back and forth in tap water until the excess of cobaltinitrite reagent is removed from the surface.

The K-feldspar is stained bright yellow if the specimen has been adequately etched. If the K-feldspar is not bright yellow, remove the etch residue by rubbing the surface under water, dry, etch again for a longer period, and continue from step 4.

7. Rinse briefly with distilled water, and cover the surface with rhodizionate reagent. Within a few seconds the plagioclase becomes brick red. When the red is of satisfactory intensity, rinse the specimen in tap water to remove excess rhodizionate.

#### A-2. Procedure for uncovered thin sections

1. Place thin section for 30 seconds over the hydrofluoric

acid (52-55 %), polished surface down. A plastic ice cube tray with one segment filled almost to the top with hydrofluoric acid was recommended to be adequate for etching. Do not rinse thin section after etching.

2. Immerse the thin section in saturated sodium cobaltinitrite solution for 60 seconds. The K-feldspar is evenly stained light yellow. Rinse briefly the thin section in tap water. Rinse again in tap water. Allow to dry.
3. Re-etch the thin section for 10 seconds over hydrofluoric acid. Do not rinse.
4. Immerse the thin section for 15 seconds in saturated barium chloride solution. Rinse once in a beaker of tap water.
5. Cover the thin section with a saturated solution of amaranth using a dropper. Leave for 15 seconds. Try to make sure the solution is distributed evenly. Rinse in a beaker of tap water then run section under a gentle stream of tap water. Allow to dry and cover section as quickly as possible.

## **APPENDIX 2**

### **MICROPROBE ANALYTICAL PROCEDURE AND ANALYSES**

Almost all of mineral analyses used in the study were conducted at the Department of Geology, Dalhousie University in Halifax, using a fully automated JEOL Superprobe 733 equipped with three wavelength-dispersive spectrometers, operated with a beam current of 22 nanoamps and an accelerating voltage of 15 kV. Data were reduced using ZAF corrections. Counts were made for 30 seconds or to a maximum of 60,000. The remaining samples were analyzed at the Department of Earth Sciences, Memorial University in St. John's, Newfoundland, using a full automated JEOL JXA-50A wavelength dispersive electron microprobe with Krisel control, equipped with three wavelength spectrometers and a Digital Equipment Corporation PDP-11 computer with teleprinter. Bence-Albee corrections were employed in the data reduction, and analyses were performed using a variety of calibration standards. The majority of analyses were calibrated with clinopyroxene standard. For aluminous magnesian minerals, spinel was used for standard. These standards were also analysed routinely during operation of the microprobe.

Microprobe analyses are unable to distinguish ferric from



ferrous iron, and total iron in the analyses is expressed as FeO in this study.

Appendix 2-1 Biotite Analyses

Pelitic gneiss (unit 1) : S-45, SA-B-2.

Noritic gneiss (unit 2) : S-105, S-127, S-126-1, S-126-2,  
S-85-2.

BIO : Biotite, R-INC : Rim of inclusion, C-INC : Core of inclusion, R-GNT : Rim adjacent to garnet, C-GNT : Core adjacent to garnet, YOU : Secondary biotite, OLD : Primary biotite.

Structural formulae based on 22 oxygens.

SAMPLE MINERAL CODE	S-45 BIO R-SIL	SA-B-2 BIO YOU	SA-B-2 BIO OLD	S-105 BIO R-INC	S-105 BIO C-INC	S-105 BIO R-GNT1	S-127 BIO C-GNT2
SiO2	38.68	37.84	37.39	38.53	38.56	38.62	39.05
TiO2	1.61	2.16	2.20	4.20	4.26	4.60	4.51
Al2O3	16.57	17.24	16.77	15.39	15.18	15.43	15.38
FeO	7.35	8.58	8.15	8.12	8.49	7.74	8.29
MnO	0.01	0.00	0.00	0.01	0.00	0.00	0.00
MgO	21.30	20.29	19.96	19.78	20.09	19.93	19.82
CaO	0.00	0.00	0.01	0.00	0.00	0.00	0.00
Na2O	0.29	0.14	0.18	0.43	0.43	0.34	0.35
K2O	9.79	9.97	9.76	9.34	9.15	9.36	9.32
Total	95.79	96.22	94.42	95.79	96.17	96.00	96.71
Si	5.53	5.43	5.46	5.53	5.52	5.52	5.55
Ti	0.19	0.23	0.24	0.45	0.46	0.49	0.48
Al	2.79	2.92	2.89	2.60	2.56	2.60	2.58
Fe	0.88	1.03	0.99	0.97	1.02	0.93	0.99
Mn	0.00	0.00	0.00	0.00	0.00	0.00	0.00
Mg	4.54	4.34	4.34	4.23	4.29	4.25	4.20
Ca	0.00	0.00	0.00	0.00	0.00	0.00	0.00
Na	0.08	0.04	0.05	0.12	0.12	0.09	0.10
K	1.79	1.83	1.82	1.71	1.67	1.71	1.69
Total	15.81	15.81	15.79	15.63	15.64	15.59	15.57
Fe/Fe+Mg+Ca+Mn	16.22	19.18	18.64	18.72	19.17	17.89	19.01
Mg/FMCM	83.76	80.82	81.33	81.26	80.83	82.11	80.99
Ca/FMCM	0.00	0.00	0.03	0.00	0.00	0.00	0.00
Mn/FMCM	0.02	0.00	0.00	0.02	0.00	0.00	0.00
Si+Al	8.33	8.35	8.34	8.14	8.08	8.12	8.12
Fe+Mg+Mn+Ca	5.42	5.37	5.34	5.21	5.30	5.17	5.18
Fe/(Fe+Mg)	0.16	0.19	0.19	0.19	0.19	0.18	0.19

SAMPLE MINERAL CODE	S-127 BIO R-GNT1	S-127 BIO R-GNT2	S-127 BIO C-GNT3	S-127 BIO R-GNT1	S-127 BIO C-GNT2	S-126-2 BIO R GNT3	S 126-2 BIO C GNT4
SiO2	38.35	37.97	37.80	38.30	37.91	37.34	38.13
TiO2	3.55	3.53	3.68	4.17	4.08	5.37	5.18
Al2O3	16.31	16.27	16.00	15.94	15.85	15.18	15.38
FeO	7.89	8.20	6.09	8.33	9.15	11.34	11.19
MnO	0.00	0.00	0.00	0.00	0.00	0.00	0.00
MgO	20.07	19.60	19.36	19.53	19.01	16.80	16.48
CaO	0.00	0.00	0.00	0.00	0.00	0.01	0.00
Na2O	0.18	0.19	0.18	0.34	0.32	0.16	0.23
K2O	9.62	9.75	9.63	9.03	9.25	9.53	9.53
Total	95.97	95.51	94.73	95.64	95.56	95.72	96.13
Si	5.49	5.48	5.49	5.50	5.48	5.46	5.54
Ti	0.38	0.38	0.40	0.45	0.44	0.59	0.57
Al	2.75	2.77	2.74	2.70	2.70	2.62	2.63
Fe	0.94	0.99	0.98	1.00	1.11	1.39	1.36
Mn	0.00	0.00	0.00	0.00	0.00	0.00	0.00
Mg	4.28	4.21	4.19	4.18	4.10	3.66	3.57
Ca	0.00	0.00	0.00	0.00	0.00	0.00	0.00
Na	0.05	0.05	0.05	0.09	0.09	0.05	0.06
K	1.76	1.79	1.79	1.65	1.71	1.78	1.77
Total	15.66	15.68	15.65	15.58	15.62	15.55	15.49
Fe/Fe+Mg+Ca+Mn	18.07	19.01	19.00	19.31	21.27	27.46	27.59
Mg/FMCM	81.93	80.99	81.00	80.69	78.73	72.50	72.41
Ca/FMCM	0.00	0.00	0.00	0.00	0.00	0.03	0.00
Mn/FMCM	0.00	0.00	0.00	0.00	0.00	0.00	0.00
Si+Al	8.24	8.25	8.24	8.20	8.18	8.08	8.17
Fe+Mg+Mn+Ca	5.23	5.20	5.18	5.18	5.20	5.05	4.93
Fe/(Fe+Mg)	0.18	0.19	0.19	0.19	0.21	0.27	0.28

SAMPLE MINERAL CODE	S-126-2 BIO RIM	S-126-2 BIO CORE	S-126-2 BIO R-GNT1	S-126-2 BIO R-GNT2	S-126-1 BIO CORE	S-85-2 BIO RIM	S-85-2 BIO CORE
SiO <sub>2</sub>	37.73	38.35	37.68	37.82	37.21	38.46	38.60
TiO <sub>2</sub>	5.22	5.16	5.19	5.26	5.91	2.97	4.13
Al <sub>2</sub> O <sub>3</sub>	15.33	15.83	15.35	15.44	15.23	16.47	15.97
FeO	10.14	10.25	11.80	11.64	8.29	8.26	8.17
MnO	0.00	0.00	0.00	0.00	0.00	0.00	0.01
MgO	16.87	17.08	16.77	16.53	17.90	20.07	20.01
CaO	0.00	0.01	0.03	0.00	0.00	0.05	0.01
Na <sub>2</sub> O	0.22	0.24	0.15	0.19	0.23	0.34	0.25
K <sub>2</sub> O	9.43	9.43	9.22	9.57	9.40	9.42	9.73
Total	94.93	96.14	96.19	96.44	94.17	96.03	96.87
Si	5.52	5.54	5.48	5.49	5.45	5.50	5.49
Ti	0.57	0.56	0.57	0.57	0.65	0.32	0.44
Al	2.65	2.66	2.63	2.64	2.63	2.78	2.68
Fe	1.24	1.24	1.44	1.41	1.02	0.99	0.97
Mn	0.00	0.00	0.00	0.00	0.00	0.00	0.00
Mg	3.68	3.67	3.64	3.58	3.91	4.28	4.24
Ca	0.00	0.00	0.00	0.00	0.00	0.01	0.00
Na	0.06	0.07	0.04	0.05	0.07	0.09	0.07
K	1.76	1.74	1.71	1.77	1.76	1.72	1.76
Total	15.49	15.48	15.51	15.53	15.49	15.69	15.65
Fe/Fe+Mg+Ca+Mn	25.22	25.18	28.28	28.32	20.63	18.73	18.63
Mg/FMCM	74.78	74.78	71.63	71.68	79.37	81.12	81.32
Ca/FMCM	0.00	0.03	0.09	0.00	0.00	0.15	0.03
Mn/FMCM	0.00	0.00	0.00	0.00	0.00	0.00	0.02
Si+Al	8.17	8.20	8.11	8.13	8.09	8.28	8.16
Fe+Mg+Mn+Ca	4.92	4.91	5.08	4.99	4.93	5.28	5.21
Fe/(Fe+Mg)	0.25	0.25	0.28	0.28	0.21	0.19	0.18

SAMPLE MINERAL CODE	S-85-2 BIO RIM	S-85-2 BIO RIM	S-85-2 BIO R-GNT1	S-85-2 BIO C-GNT2	S-85-2 BIO R-GNT1	S-85-2 BIO C-GNT2	S-85-2 BIO INC
SiO <sub>2</sub>	37.79	37.68	37.37	38.01	38.15	37.89	37.19
TiO <sub>2</sub>	4.15	4.18	3.89	3.86	3.86	4.09	4.49
Al <sub>2</sub> O <sub>3</sub>	15.33	15.19	15.01	15.49	15.95	15.73	15.73
FeO	8.40	8.98	9.75	10.11	7.71	8.10	7.62
MnO	0.00	0.00	0.00	0.00	0.01	0.00	0.00
MgO	19.21	19.60	19.26	18.21	20.72	20.08	19.23
CaO	0.03	0.00	0.01	0.00	0.00	0.00	0.05
Na <sub>2</sub> O	0.22	0.33	0.08	0.15	0.33	0.31	0.57
K <sub>2</sub> O	9.32	9.42	9.39	9.89	9.30	9.53	8.62
Total	94.45	95.38	94.76	95.71	96.02	95.72	93.70
Si	5.51	5.47	5.48	5.53	5.45	5.45	5.45
Ti	0.46	0.46	0.43	0.42	0.41	0.44	0.49
Al	2.64	2.60	2.59	2.66	2.69	2.67	2.72
Fe	1.03	1.09	1.20	1.23	0.92	0.98	0.93
Mn	0.00	0.00	0.00	0.00	0.00	0.00	0.00
Mg	4.18	4.24	4.21	3.95	4.41	4.31	4.20
Ca	0.00	0.00	0.00	0.00	0.00	0.00	0.01
Na	0.06	0.09	0.02	0.04	0.09	0.09	0.18
K	1.73	1.74	1.76	1.84	1.70	1.75	1.65
Total	15.61	15.69	15.69	15.66	15.68	15.69	15.61
Fe/Fe+Mg+Ca+Mn	19.69	20.45	22.12	23.75	17.27	18.46	18.16
Mg/FMCM	80.22	79.55	77.85	76.25	82.71	81.54	81.68
Ca/FMCM	0.09	0.00	0.03	0.00	0.00	0.00	0.15
Mn/FMCM	0.00	0.00	0.00	0.00	0.02	0.00	0.00
Si+Al	8.15	8.07	8.07	8.18	8.14	8.12	8.18
Fe+Mg+Mn+Ca	5.21	5.33	5.40	5.18	5.34	5.28	5.14
Fe/(Fe+Mg)	0.20	0.20	0.22	0.24	0.17	0.18	0.18

Appendix 2-2 Clinopyroxene Analyses

Metagabbro (unit 3) : S-7, S-2, S-2-2, S-14,

Dioritic gneiss (unit 5) : S-103B, S-64A, S-103A, S-36A.

CPX : clinopyroxene, C-OPX : cpx core adjacent to  
orthopyroxene, R-OPX : rim adjacent to orthopyroxene,

Structural formulae based on 6 oxygens.

SAMPLE MINERAL CODE	S-7 CPX CORE	S-7 CPX CORE	S-7 CPX CORE	S-7 CPX CORE	S-7 CPX CORE	S-2 CPX C-OPX1	S-2 CPX R-OPX2
SiO <sub>2</sub>	51.59	51.59	52.69	51.53	51.75	51.81	52.25
TiO <sub>2</sub>	0.21	0.21	0.14	0.23	0.17	0.19	0.14
Al <sub>2</sub> O <sub>3</sub>	3.04	2.99	2.82	3.11	2.53	2.24	1.78
FeO	7.45	7.41	6.01	7.41	6.98	9.65	9.33
MnO	0.40	0.34	0.34	0.41	0.39	0.23	0.26
MgO	14.17	14.57	16.82	14.70	15.15	13.30	13.92
CaO	23.03	23.01	22.66	22.82	23.34	22.51	22.64
Na <sub>2</sub> O	0.60	0.65	0.65	0.63	0.56	0.71	0.63
K <sub>2</sub> O	0.00	0.00	0.00	0.00	0.00	0.00	0.00
Total	100.49	100.78	102.13	100.83	100.86	100.65	100.95
Si	1.91	1.91	1.91	1.90	1.91	1.93	1.94
Ti	0.01	0.01	0.00	0.01	0.00	0.01	0.00
Al	0.13	0.13	0.12	0.14	0.11	0.10	0.08
Fe	0.23	0.23	0.18	0.23	0.22	0.30	0.29
Mn	0.01	0.01	0.01	0.01	0.01	0.01	0.01
Mg	0.78	0.80	0.91	0.81	0.83	0.74	0.77
Ca	0.91	0.91	0.88	0.90	0.92	0.90	0.90
Na	0.04	0.05	0.05	0.05	0.04	0.05	0.05
K	0.00	0.00	0.00	0.00	0.00	0.00	0.00
Total	4.04	4.04	4.05	4.04	4.05	4.04	4.04
Fe/Fe+Mg+Ca+Mn	11.90	11.72	9.20	11.71	10.86	15.46	14.71
Mg/FMCM	40.33	41.08	45.86	41.41	42.00	37.97	39.12
Ca/FMCM	47.13	46.65	44.42	46.22	46.52	46.20	45.75
Mn/FMCM	0.65	0.54	0.53	0.66	0.61	0.37	0.42
Si+Al	2.05	2.04	2.03	2.04	2.02	2.03	2.02
Fe+Mg+Mn+Ca	1.94	1.95	1.98	1.95	1.98	1.95	1.97
Fe/(Fe+Mg)	0.23	0.22	0.17	0.22	0.21	0.29	0.27



SAMPLE MINERAL CODE	S-2-2 CPX CORE	S-2-2 CPX CORE	S-14 CPX CORE	S-103B CPX C-OPX1	S-103B CPX R-OPX1	S-103B CPX CORE	S-103B CPX C-OPX1
SiO <sub>2</sub>	52.10	51.90	51.50	51.84	52.37	50.85	51.30
TiO <sub>2</sub>	0.19	0.19	0.22	0.25	0.19	0.23	0.21
Al <sub>2</sub> O <sub>3</sub>	1.95	2.23	1.95	2.20	2.01	2.27	2.16
FeO	9.33	9.89	10.53	11.08	11.26	11.48	10.84
MnO	0.24	0.23	0.59	0.37	0.30	0.38	0.36
MgO	13.82	13.50	12.98	12.16	13.14	12.63	12.61
CaO	22.53	22.15	21.59	21.62	19.95	21.21	22.10
Na <sub>2</sub> O	0.57	0.69	0.77	0.74	0.54	0.79	0.76
K <sub>2</sub> O	0.00	0.00	0.00	0.00	0.00	0.00	0.00
Total	100.72	100.79	100.12	100.25	99.75	99.85	100.35
Si	1.94	1.93	1.94	1.95	1.97	1.93	1.93
Ti	0.01	0.01	0.01	0.01	0.01	0.01	0.01
Al	0.09	0.10	0.09	0.10	0.09	0.10	0.10
Fe	0.29	0.31	0.33	0.35	0.35	0.36	0.34
Mn	0.01	0.01	0.02	0.01	0.01	0.01	0.01
Mg	0.77	0.75	0.73	0.68	0.74	0.71	0.71
Ca	0.90	0.88	0.87	0.87	0.80	0.86	0.89
Na	0.04	0.05	0.06	0.05	0.04	0.06	0.06
K	0.00	0.00	0.00	0.00	0.00	0.00	0.00
Total	4.03	4.04	4.04	4.02	4.00	4.04	4.04
Fe/Fe + Mg + Ca + Mn	14.79	15.81	17.01	18.22	18.60	18.65	17.49
Mg/FMCM	39.05	38.46	37.36	35.63	38.68	36.57	36.25
Ca/FMCM	45.77	45.36	44.67	45.54	42.22	44.15	45.68
Mn/FMCM	0.39	0.37	0.97	0.62	0.50	0.63	0.59
Si + Al	2.02	2.03	2.03	2.05	2.06	2.03	2.03
Fe + Mg + Mn + Ca	1.96	1.95	1.95	1.91	1.90	1.95	1.95
Fe/(Fe + Mg)	0.27	0.29	0.31	0.34	0.32	0.34	0.33

SAMPLE MINERAL CODE	S-103B CPX C-OPX2	S-103B CPX R-OPX3	S-64A CPX R-OPX1	S-64A CPX C-OPX2	S-64A CPX CORE	S-64A CPX RIM	S-103A CPX R-OPX
SiO2	51.18	51.58	52.03	51.46	51.21	51.92	50.98
TiO2	0.19	0.18	0.17	0.25	0.27	0.20	0.18
Al2O3	2.10	2.05	2.28	2.21	2.30	2.11	2.44
FeO	10.97	10.79	11.24	11.25	10.01	9.70	11.02
MnO	0.33	0.34	0.31	0.36	0.22	0.20	0.29
MgO	12.57	12.84	12.33	12.70	13.05	13.32	13.02
CaO	21.93	21.84	20.53	21.43	22.95	22.61	20.77
Na2O	0.68	0.67	0.54	0.72	0.61	0.60	0.59
K2O	0.00	0.00	0.00	0.00	0.00	0.00	0.05
Total	99.96	100.30	99.44	100.38	100.61	100.67	99.33
Si	1.93	1.94	1.96	1.94	1.92	1.94	1.93
Ti	0.01	0.01	0.00	0.01	0.01	0.01	0.01
Al	0.09	0.09	0.10	0.10	0.10	0.09	0.11
Fe	0.35	0.34	0.35	0.35	0.31	0.30	0.35
Mn	0.01	0.01	0.01	0.01	0.01	0.01	0.01
Mg	0.71	0.72	0.69	0.71	0.73	0.74	0.74
Ca	0.89	0.88	0.83	0.86	0.92	0.90	0.84
Na	0.05	0.05	0.04	0.05	0.04	0.04	0.04
K	0.00	0.00	0.00	0.00	0.00	0.00	0.00
Total	4.04	4.03	4.00	4.03	4.04	4.03	4.03
Fe/Fe+Mg+Ca+Mn	17.75	17.40	18.79	18.23	15.92	15.49	18.03
Mg/FMCM	36.24	36.91	36.72	36.68	36.98	37.91	37.96
Ca/FMCM	45.46	45.13	43.96	44.50	46.75	46.27	43.53
Mn/FMCM	0.54	0.56	0.52	0.59	0.35	0.32	0.48
Si+Al	2.03	2.03	2.07	2.03	2.02	2.03	2.04
Fe+Mg+Mn+Ca	1.95	1.95	1.89	1.94	1.97	1.95	1.94
Fe/(Fe+Mg)	0.33	0.32	0.34	0.33	0.30	0.29	0.32

SAMPLE MINERAL CODE	S-103A CPX R-OPX	S-103A CPX CORE	S-103A CPX C-OPX1	S-103A CPX C-OPX2	S-36A CPX C-OPX3	S-36A CPX R-OPX4
SiO <sub>2</sub>	51.68	50.82	51.08	51.32	51.63	51.67
TiO <sub>2</sub>	0.20	0.27	0.24	0.21	0.18	0.17
Al <sub>2</sub> O <sub>3</sub>	1.85	2.22	2.26	2.10	1.91	1.87
FeO	10.58	12.42	11.38	11.43	10.87	10.34
MnO	0.32	0.40	0.34	0.37	0.30	0.29
MgO	13.06	12.72	12.64	12.66	12.84	13.14
CaO	21.96	20.81	21.55	21.56	22.07	22.43
Na <sub>2</sub> O	0.59	0.69	0.71	0.67	0.67	0.63
K <sub>2</sub> O	0.00	0.00	0.00	0.00	0.00	0.00
Total	120.23	100.35	100.18	100.33	100.48	100.54
Si	1.94	1.92	1.93	1.93	1.94	1.94
Ti	0.01	0.01	0.01	0.01	0.01	0.00
Al	0.08	0.10	0.10	0.09	0.08	0.08
Fe	0.33	0.39	0.36	0.36	0.34	0.32
Mn	0.01	0.01	0.01	0.01	0.01	0.01
Mg	0.73	0.72	0.71	0.71	0.72	0.73
Ca	0.88	0.84	0.87	0.87	0.89	0.90
Na	0.04	0.05	0.05	0.05	0.05	0.05
K	0.00	0.00	0.00	0.00	0.00	0.00
Total	4.03	4.05	4.04	4.04	4.04	4.04
Fe/Fe + Mg + Ca + Mn	16.98	19.98	18.40	18.44	17.44	16.47
Mg/FMCM	37.35	36.47	36.41	36.39	36.71	37.29
Ca/FMCM	45.15	42.90	44.63	44.56	45.36	45.77
Mn/FMCM	0.52	0.65	0.56	0.60	0.49	0.47
Si + Al	2.02	2.02	2.03	2.03	2.02	2.02
Fe + Mg + Mn + Ca	1.96	1.97	1.95	1.95	1.96	1.97
Fe/(Fe + Mg)	0.31	0.35	0.34	0.34	0.32	0.31

**Appendix 2-3 Hornblende Analyses**

Metagabbro (unit 3) : S-77, S-72, S-7.

Dioritic gneiss (unit 5) : S-103B, S-116, S-116B.

Hornblende granodiorite (unit 8) : S-109.

HBL : Hornblende, C-GNT : hbl core adjacent to garnet, R-PLA  
: Rim adjacent to plagioclase.

Structural formulae based on 23 oxygens.

SAMPLE MINERAL CODE	S-77 HBL	S-77 HBL	S-77 HBL	S-72 HBL	S-72 HBL	S-72 HBL	S-72 HBL
	C-GNT1	C-GNT2	R-GNT3	R-GNT1	C-GNT2	R-GNT1	C-GNT2
SiO <sub>2</sub>	47.53	48.33	48.48	48.22	48.08	48.86	48.00
TiO <sub>2</sub>	0.41	0.27	0.35	0.43	0.46	0.42	0.45
Al <sub>2</sub> O <sub>3</sub>	3.45	2.56	2.93	2.81	3.43	2.71	3.20
FeO	16.03	15.28	15.65	16.64	16.58	16.02	16.48
MnO	1.76	1.93	1.72	1.92	1.77	1.62	1.79
MgO	7.37	7.82	7.75	7.28	7.15	7.77	7.21
CaO	22.00	22.08	22.32	22.31	22.02	22.21	21.97
Na <sub>2</sub> O	0.79	0.99	0.69	0.67	0.88	0.70	0.86
K <sub>2</sub> O	0.00	0.00	0.00	0.00	0.00	0.00	0.00
Total	99.34	99.25	99.88	100.28	100.36	100.32	99.96
Si	7.19	7.30	7.27	7.25	7.21	7.30	7.23
Ti	0.05	0.03	0.04	0.05	0.05	0.05	0.05
Al	0.62	0.46	0.52	0.50	0.61	0.48	0.57
Fe	2.03	1.93	1.98	2.09	2.08	2.00	2.08
Mn	0.23	0.25	0.22	0.24	0.22	0.20	0.23
Mg	1.66	1.76	1.73	1.63	1.60	1.73	1.62
Ca	3.57	3.57	3.59	3.59	3.54	3.55	3.54
Na	0.23	0.29	0.20	0.20	0.26	0.20	0.25
K	0.00	0.00	0.00	0.00	0.00	0.00	0.00
Total	15.57	15.59	15.53	15.55	15.56	15.52	15.56
Fe/Fe+Mg+Ca+Mn	27.11	25.70	26.17	27.67	27.95	26.72	27.80
Mg/FMCM	22.21	23.44	23.09	21.57	21.48	23.09	21.67
Ca/FMCM	47.67	47.58	47.82	47.53	47.55	47.48	47.48
Mn/FMCM	3.01	3.29	2.91	3.23	3.02	2.74	3.08
Si+Al	7.81	7.78	7.79	7.75	7.82	7.76	7.80
Fe+Mg+Mn+Ca	7.48	7.51	7.50	7.56	7.44	7.49	7.47
Fe/(Fe+Mg)	0.55	0.52	0.53	0.56	0.57	0.54	0.56

SAMPLE MINERAL CODE	S-72 HBL C-GNT2	S-72 HBL CORE	S-7 HBL CORE	S-7 HBL CORE	S-65 HBL CORE	S-65 HBL CORE	S-103B HBL CORE
SiO <sub>2</sub>	47.95	48.73	42.30	42.48	42.33	42.43	40.09
TiO <sub>2</sub>	0.46	0.40	1.33	1.29	1.98	2.05	2.21
Al <sub>2</sub> O <sub>3</sub>	3.14	2.77	11.35	11.33	11.80	12.01	11.53
FeO	16.62	16.08	11.16	11.09	12.19	11.86	17.65
MnO	1.82	1.79	0.21	0.14	0.44	0.46	0.18
MgO	7.11	7.52	14.69	15.00	13.59	13.92	9.52
CaO	21.94	21.89	12.34	12.24	11.67	11.48	11.72
Na <sub>2</sub> O	0.73	0.86	1.37	1.54	2.63	2.70	1.11
K <sub>2</sub> O	0.00	0.00	2.28	2.12	0.66	0.60	2.15
Total	99.76	100.01	97.02	97.22	97.29	97.52	96.17
Si	7.24	7.31	6.31	6.32	6.29	6.27	6.23
Ti	0.05	0.05	0.15	0.14	0.22	0.23	0.26
Al	0.56	0.49	2.00	1.99	2.07	2.09	2.11
Fe	2.10	2.01	1.39	1.38	1.51	1.47	2.29
Mn	0.23	0.23	0.03	0.02	0.06	0.06	0.02
Mg	1.60	1.68	3.27	3.32	3.01	3.07	2.20
Ca	3.55	3.52	1.97	1.95	1.86	1.82	1.95
Na	0.21	0.25	0.40	0.44	0.76	0.77	0.33
K	0.00	0.00	2.43	0.40	0.13	0.11	0.43
Total	15.54	15.53	15.95	15.97	15.90	15.89	15.84
Fe/Fe+Mg+Ca+Mn	28.05	27.07	20.91	20.67	23.53	22.88	35.43
Mg/FMCM	21.39	22.59	49.06	49.83	46.75	47.85	34.05
Ca/FMCM	47.45	47.28	29.63	29.23	28.86	28.37	30.14
Mn/FMCM	3.11	3.06	0.40	0.26	0.66	0.90	0.37
Si+Al	7.80	7.80	8.31	8.30	8.36	8.37	8.34
Fe+Mg+Mn+Ca	7.48	7.44	6.66	6.67	6.44	6.41	6.47
Fe/(Fe+Mg)	0.57	0.55	0.30	0.29	0.33	0.32	0.51

SAMPLE MINERAL CODE	S-116 HBL	S-116B HBL	S-116B HEL	S-116B HBL	S-109 HBL	S-109 HBL
	R-PLA1	C-PLA2	C-PLA2	CORE	CORE	CORE
SiO <sub>2</sub>	43.42	43.68	44.25	43.66	44.62	44.65
TiO <sub>2</sub>	1.76	1.74	1.60	1.64	1.45	1.52
Al <sub>2</sub> O <sub>3</sub>	10.03	9.90	9.74	10.01	9.91	9.67
FeO	12.53	12.52	12.21	12.34	11.29	11.42
MnO	0.25	0.26	0.25	0.25	0.11	0.11
MgO	14.32	14.44	14.71	14.15	14.98	15.23
CaO	11.87	11.73	11.91	11.81	11.73	11.88
Na <sub>2</sub> O	1.80	1.84	1.82	1.77	2.06	2.01
K <sub>2</sub> O	1.22	1.18	1.12	1.07	0.91	1.04
Total	97.20	97.28	97.59	96.70	97.08	97.52
Si	8.46	8.49	8.54	8.51	8.58	8.57
Ti	0.20	0.19	0.18	0.18	0.16	0.17
Al	1.76	1.73	1.70	1.76	1.72	1.68
Fe	1.56	1.56	1.51	1.54	1.39	1.40
Mn	0.03	0.03	0.03	0.03	0.01	0.01
Mg	3.18	3.20	3.24	3.15	3.29	3.34
Ca	1.89	1.87	1.88	1.89	1.85	1.87
Na	0.52	0.53	0.52	0.51	0.59	0.57
K	0.23	0.22	0.21	0.20	0.17	0.20
Total	15.83	15.83	15.80	15.78	15.78	15.81
Fe/(Fe+Mg+Ca+Mn)	23.42	23.38	22.64	23.31	21.25	21.19
Mg/FMCM	47.69	48.06	48.60	47.63	50.25	50.36
Ca/FMCM	28.42	28.07	28.29	28.58	28.29	28.24
Mn/FMCM	0.47	0.49	0.47	0.48	0.21	0.21
Si + Al	8.22	8.22	8.23	8.27	8.30	8.24
Fe + Mg + Mn + Ca	6.66	6.65	6.66	6.61	6.55	6.63
Fe/(Fe + Mg)	0.33	0.33	0.32	0.33	0.30	0.30

**Appendix 2-4 Plagioclase Analyses**

Pelitic gneiss (unit 1) : S-45, S-88-1, S-88-2, S-90-2.

Metagabbro (unit 3) : S-77, S-7, S-5.

Dioritic gneiss (unit 5) : S-116, S-103B, S-64A.

Hornblende granodiorite (unit 8) : S-109.

PLAG : Plagioclase.

Structural formulae based on 8 oxygens.



SAMPLE MINERAL CODE	S-45 PLAG CORE	S-88-1 PLAG CORE	S-88-2 PLAG CORE	S-88-2 PLAG CORE	S-90-2 PLAG CORE	S-90-2 PLAG CORE	S-77 PLAG CORE
SiO <sub>2</sub>	65.58	63.48	64.62	65.39	66.20	66.13	61.06
TiO <sub>2</sub>	0.00	0.00	0.00	0.00	0.00	0.00	0.00
Al <sub>2</sub> O <sub>3</sub>	19.74	22.79	21.79	21.60	21.28	20.89	24.81
FeO	0.00	0.12	0.08	0.25	0.00	0.00	0.24
MnO	0.00	0.00	0.00	0.00	0.00	0.00	0.00
MgO	0.00	0.00	0.00	0.00	0.00	0.00	0.00
CaO	0.13	3.32	3.13	2.87	1.09	1.27	6.29
Na <sub>2</sub> O	2.72	10.42	10.25	10.09	11.73	11.73	7.57
K <sub>2</sub> O	12.04	0.14	0.22	0.00	0.00	0.00	0.00
Total	100.20	100.27	100.10	100.20	100.31	100.03	99.97
Si	2.97	2.80	2.85	2.87	2.90	2.91	2.71
Ti	0.00	0.00	0.00	0.00	0.00	0.00	0.00
Al	1.05	1.19	1.13	1.12	1.10	1.08	1.30
Fe	0.00	0.00	0.00	0.01	0.00	0.00	0.01
Mn	0.00	0.00	0.00	0.00	0.00	0.00	0.00
Mg	0.00	0.00	0.00	0.00	0.00	0.00	0.00
Ca	0.01	0.16	0.15	0.14	0.05	0.06	0.30
Na	0.24	0.89	0.88	0.86	1.00	1.00	0.65
K	0.70	0.01	0.01	0.00	0.00	0.00	0.00
Total	4.97	5.05	5.03	5.00	5.05	5.05	4.97
Fe/Fe + Mg + Ca + Mn	0.00	2.74	1.96	6.37	0.00	0.00	2.89
Mg/FMCM	0.00	0.00	0.00	0.00	0.00	0.00	0.00
Ca/FMCM	100.00	97.26	98.04	93.63	100.00	100.00	97.11
Mn/FMCM	0.00	0.00	0.00	0.00	0.00	0.00	0.00
Si + Al	4.03	3.99	3.99	3.99	4.00	3.99	4.01
Albite	97.43	84.76	85.56	86.42	95.12	94.35	68.53
Anorthite	2.57	15.24	14.44	13.58	4.88	5.65	31.47

SAMPLE MINERAL CODE	S-77 PLAG CORE	S-7 PLAG CORE	S-5 PLAG CORE	S-5 PLAG CORE	S-116 PLAG CORE	S-116 PLAG CORE	S-103B PLAG CORE
SiO2	58.21	54.21	59.07	59.03	60.99	60.29	59.25
TiO2	0.00	0.00	0.00	0.00	0.00	0.00	0.00
Al2O3	28.48	28.78	25.85	25.26	24.73	24.58	25.70
FeO	0.17	0.13	0.13	0.05	0.10	0.12	0.13
MnO	0.00	0.00	0.00	0.00	0.00	0.00	0.00
MgO	0.00	0.00	0.00	0.00	0.00	0.09	0.04
CaO	9.10	11.89	7.33	7.11	6.49	6.65	7.88
Na2O	6.75	5.11	8.10	8.34	8.42	8.01	7.46
K2O	0.14	0.09	0.00	0.00	0.12	0.17	0.00
Total	100.83	100.18	100.47	99.79	100.85	99.90	100.45
Si	2.59	2.45	2.83	2.65	2.70	2.69	2.64
Ti	0.00	0.00	0.00	0.00	0.00	0.00	0.00
Al	1.39	1.53	1.36	1.33	1.29	1.29	1.35
Fe	0.01	0.00	0.00	0.00	0.00	0.00	0.00
Mn	0.00	0.00	0.00	0.00	0.00	0.00	0.00
Mg	0.00	0.00	0.00	0.00	0.00	0.01	0.00
Ca	0.43	0.58	0.35	0.34	0.31	0.32	0.38
Na	0.58	0.45	0.70	0.72	0.72	0.69	0.64
K	0.01	0.01	0.00	0.00	0.01	0.01	0.00
Total	5.01	5.01	5.04	5.05	5.02	5.01	5.01
Fe/Fe+Mg+Ca+Mn	1.44	0.85	1.37	0.55	1.19	1.36	1.26
Mg/FMCM	0.00	0.00	0.00	0.00	0.00	1.82	0.69
Ca/FMCM	98.56	99.15	98.63	99.45	98.81	96.81	98.05
Mn/FMCM	0.00	0.00	0.00	0.00	0.00	0.00	0.00
Si+Al	3.98	3.98	3.99	3.98	3.98	3.98	3.98
Albite	57.31	43.75	66.66	67.98	70.13	68.55	63.14
Anorthite	42.69	56.25	33.34	32.02	29.87	31.45	36.86

SAMPLE MINERAL CODE	S-64A PLAG CORE	S-109 PLAG CORE
SiO <sub>2</sub>	58.61	61.54
TiO <sub>2</sub>	0.00	0.00
Al <sub>2</sub> O <sub>3</sub>	26.33	24.01
FeO	0.26	0.11
MnO	0.00	0.00
MgO	0.00	0.00
CaO	8.64	5.44
Na <sub>2</sub> O	6.81	8.60
K <sub>2</sub> O	0.07	0.30
Total	100.93	100.01
Si	2.60	2.74
Ti	0.00	0.00
Al	1.38	1.26
Fe	0.01	0.00
Mn	0.00	0.00
Mg	0.00	0.00
Ca	0.42	0.26
Na	0.59	0.74
K	0.00	0.02
Total	5.00	5.01
Fe/Fe + Mg + Ca + Mn	2.24	1.55
Mg/FMCM	0.00	0.00
Ca/FMCM	97.76	98.45
Mn/FMCM	0.00	0.00
Si + Al	3.98	3.99
Albite	58.23	74.10
Anorthite	41.77	25.90

Appendix 2-5 Orthopyroxene Analyses

Pelitic gneiss (unit 1) : SA-B-3, SA-A-1, IH-46, SA-C-3, S-22,  
S-90-2, S-45, S-88-2.

Noritic gneiss (unit 2) : S-85-2, S-105, S-85.

Metagabbro (unit 3) : S-14, S-2, S-2-2.

Dioritic gneiss (unit 5) : S-103B, S-64A, S-103A, S-36A.

OPX : orthopyroxene, R : Rim, C : Core, R-CPX : Rim adjacent to clinopyroxene, C-CPX : Core adjacent to clinopyroxene, FINE : fine grain, SY-SIL : Symplectite with sillimanite, SY-SA : Symplectite with sapphirine, F-KOR : fine grain adjacent to kornervupine.

Structural formulae based on 6 oxygens.

SAMPLE MINERAL CODE	SA-B-3 OPX R-KOR	SA-B-3 OPX CORE	SA-A-1 OPX R-SA	IH-46 OPX SY-OPX	IH-46 OPX SY-SIL	IH-46 OPX CORE	IH-46 OPX SY-SA
SiO <sub>2</sub>	50.50	50.58	50.51	50.59	50.70	49.40	50.26
TiO <sub>2</sub>	0.00	0.02	0.00	0.02	0.01	0.00	0.04
Al <sub>2</sub> O <sub>3</sub>	8.33	8.23	7.28	6.93	6.56	8.28	7.54
FeO	11.00	11.17	12.93	13.56	13.74	13.74	12.40
MnO	0.04	0.03	0.45	0.11	0.08	0.08	0.03
MgO	30.81	30.36	29.12	29.34	28.60	27.99	29.72
CaO	0.02	0.04	0.01	0.00	0.01	0.01	0.01
Na <sub>2</sub> O	0.03	0.03	0.02	0.01	0.01	0.03	0.02
K <sub>2</sub> O	0.00	0.00	0.00	0.00	0.00	0.00	0.00
Total	100.74	100.48	100.31	100.57	99.70	99.51	100.01
Si	1.77	1.78	1.80	1.80	1.82	1.78	1.79
Ti	0.00	0.00	0.00	0.00	0.00	0.00	0.00
Al	0.34	0.34	0.31	0.29	0.28	0.35	0.32
Fe	0.32	0.33	0.39	0.40	0.41	0.41	0.37
Mn	0.00	0.00	0.01	0.00	0.00	0.00	0.00
Mg	1.61	1.59	1.55	1.56	1.53	1.50	1.58
Ca	0.00	0.00	0.00	0.00	0.00	0.00	0.00
Na	0.00	0.00	0.00	0.00	0.00	0.00	0.00
K	0.00	0.00	0.00	0.00	0.00	0.00	0.00
Total	4.06	4.05	4.05	4.05	4.04	4.05	4.05
Fe/Fe+Mg+Ca+Mn	16.67	17.08	19.80	20.56	21.20	21.57	18.98
Mg/FMCM	83.23	82.79	79.48	79.27	78.65	78.29	80.97
Ca/FMCM	0.04	0.08	0.02	0.00	0.02	0.02	0.02
Mn/FMCM	0.06	0.05	0.70	0.17	0.13	0.13	0.05
Si+Al	2.12	2.12	2.10	2.09	2.10	2.13	2.10
Fe+Mg+Mn+Ca	1.94	1.92	1.94	1.96	1.94	1.92	1.95
Fe/(Fe+Mg)	0.17	0.17	0.20	0.21	0.21	0.22	0.19

SAMPLE MINERAL CODE	SA-C-3 OPX R-SA	S-22 OPX C-SA	S-22 OPX R-SA	S-90-2 OPX CORE	S-90-2 OPX RIM	S-90-2 OPX C-1	S-90-2 OPX R-2
SiO <sub>2</sub>	49.38	50.17	50.45	49.17	49.18	48.52	50.03
TiO <sub>2</sub>	0.04	0.01	0.00	0.09	0.07	0.08	0.05
Al <sub>2</sub> O <sub>3</sub>	8.70	7.86	7.58	5.49	5.65	6.06	4.93
FeO	12.66	13.47	13.06	20.73	21.38	21.40	19.98
MnO	0.01	0.40	0.42	0.17	0.16	0.19	0.12
MgO	29.15	28.66	28.66	23.57	23.24	22.77	24.64
CaO	0.01	0.01	0.00	0.03	0.01	0.01	0.01
Na <sub>2</sub> O	0.01	0.02	0.04	0.18	0.03	0.06	0.01
K <sub>2</sub> O	0.00	0.00	0.00	0.00	0.27	0.00	0.00
Total	99.96	100.60	100.21	99.44	99.98	99.08	99.77
Si	1.76	1.79	1.80	1.83	1.83	1.82	1.65
Ti	0.00	0.00	0.00	0.00	0.00	0.00	0.00
Al	0.37	0.33	0.32	0.24	0.25	0.27	0.21
Fe	0.38	0.40	0.39	0.65	0.67	0.67	0.62
Mn	0.00	0.01	0.01	0.01	0.01	0.01	0.00
Mg	1.55	1.52	1.52	1.31	1.29	1.27	1.36
Ca	0.00	0.00	0.00	0.00	0.00	0.00	0.00
Na	0.00	0.00	0.00	0.01	0.00	0.00	0.00
K	0.00	0.00	0.00	0.00	0.01	0.00	0.00
Total	4.06	4.05	4.04	4.05	4.05	4.05	4.04
Fe/Fe+Mg+Ca+Mn	19.59	20.74	20.23	32.93	33.95	34.42	31.21
Mg/FMCM	80.38	78.62	79.11	66.73	65.77	65.25	68.58
Ca/FMCM	0.02	0.02	0.00	0.06	0.02	0.02	0.02
Mn/FMCM	0.02	0.62	0.66	0.27	0.26	0.31	0.19
Si+Al	2.13	2.12	2.12	2.07	2.08	2.09	2.06
Fe+Mg+Mn+Ca	1.93	1.93	1.92	1.96	1.96	1.95	1.98
Fe/(Fe+Mg)	0.20	0.21	0.20	0.33	0.34	0.35	0.31

SAMPLE MINERAL CODE	S-45 OPX CORE	S-45 OPX CORE	S-88-2 OPX R-1	S-88-2 OPX C-2	S-88-2 OPX R-1	S-88-2 OPX C-2	S-88-2 OPX CORE
SiO <sub>2</sub>	49.03	46.71	50.02	49.58	50.26	50.37	47.89
TiO <sub>2</sub>	0.05	0.08	0.04	0.04	0.04	0.04	0.05
Al <sub>2</sub> O <sub>3</sub>	6.06	7.84	5.34	5.60	5.15	5.07	7.92
FeO	21.45	22.47	19.42	19.55	18.83	19.53	21.25
MnO	0.17	0.48	0.19	0.20	0.21	0.21	0.39
MgO	23.18	21.46	25.02	24.50	25.38	24.80	22.47
CaO	0.00	0.01	0.02	0.04	0.02	0.02	0.02
Na <sub>2</sub> O	0.00	0.01	0.01	0.03	0.00	0.00	0.00
K <sub>2</sub> O	0.00	0.00	0.00	0.00	0.00	0.00	0.00
Total	99.94	99.05	100.06	99.55	99.90	100.04	99.99
Si	1.82	1.77	1.84	1.83	1.84	1.85	1.78
Ti	0.00	0.00	0.00	0.00	0.00	0.00	0.00
Al	0.27	0.35	0.23	0.24	0.22	0.22	0.35
Fe	0.87	0.71	0.60	0.60	0.58	0.60	0.66
Mn	0.01	0.02	0.01	0.01	0.01	0.01	0.01
Mg	1.28	1.21	1.37	1.35	1.39	1.36	1.24
Ca	0.00	0.00	0.00	0.00	0.00	0.00	0.00
Na	0.00	0.00	0.00	0.00	0.00	0.00	0.00
K	0.00	0.00	0.00	0.00	0.00	0.00	0.00
Total	4.04	4.06	4.05	4.04	4.04	4.04	4.05
Fe/Fe + Mg + Ca + Mn	34.09	36.71	30.24	30.81	29.29	30.53	34.43
Mg/FMCM	65.84	62.48	69.42	68.79	70.34	69.09	64.88
Ca/FMCM	0.00	0.02	0.04	0.08	0.04	0.04	0.04
Mn/FMCM	0.27	0.79	0.30	0.32	0.33	0.33	0.64
Si + Al	2.09	2.12	2.07	2.08	2.07	2.07	2.13
Fe + Mg + Mn + Ca	1.96	1.94	1.97	1.96	1.97	1.97	1.92
Fe/(Fe + Mg)	0.34	0.37	0.30	0.31	0.29	0.31	0.35

SAMPLE MINERAL CODE	S-88-2 OPX R-1	S-88-2 OPX R-2	S-88-2 OPX C-3	S-85-2 OPX CORE	S-85-2 OPX RIM	S-85-2 OPX R-1	S-85-2 OPX C-2
SiO <sub>2</sub>	49.29	49.76	49.18	48.31	50.05	49.17	48.37
TiO <sub>2</sub>	0.06	0.06	0.08	0.06	0.03	0.05	0.02
Al <sub>2</sub> O <sub>3</sub>	6.12	5.67	6.00	6.22	5.60	5.49	6.18
FeO	19.29	19.38	19.65	18.57	18.26	21.42	22.08
MnO	0.35	0.39	0.36	0.36	0.39	0.17	0.15
MgO	24.78	24.58	24.30	24.27	25.73	23.30	22.65
CaO	0.03	0.02	0.02	0.03	0.03	0.03	0.01
Na <sub>2</sub> O	0.00	0.01	0.00	0.02	0.04	0.07	0.13
K <sub>2</sub> O	0.00	0.00	0.00	0.00	0.00	0.00	0.00
Total	99.91	99.88	99.58	97.84	100.11	99.69	99.60
Si	1.82	1.83	1.82	1.81	1.83	1.83	1.81
Ti	0.00	0.00	0.00	0.00	0.00	0.00	0.00
Al	0.27	0.25	0.26	0.28	0.24	0.24	0.27
Fe	0.59	0.60	0.61	0.58	0.56	0.87	0.69
Mn	0.01	0.01	0.01	0.01	0.01	0.01	0.00
Mg	1.36	1.35	1.34	1.36	1.40	1.29	1.26
Ca	0.00	0.00	0.00	0.00	0.00	0.00	0.00
Na	0.00	0.00	0.00	0.00	0.00	0.01	0.01
K	0.00	0.00	0.00	0.00	0.00	0.00	0.00
Total	4.05	4.04	4.05	4.05	4.05	4.05	4.06
Fe/(Fe+Mg+Ca+Mn)	30.22	30.47	31.02	29.84	28.29	33.92	35.27
Mg/FMCM	69.17	68.87	68.36	69.51	71.04	65.75	64.47
Ca/FMCM	0.06	0.04	0.04	0.06	0.06	0.06	0.02
Mn/FMCM	0.56	0.62	0.58	0.59	0.61	0.27	0.24
Si+Al	2.08	2.08	2.08	2.09	2.07	2.07	2.08
Fe+Mg+Mn+Ca	1.97	1.96	1.96	1.95	1.97	1.97	1.96
Fe/(Fe+Mg)	0.30	0.31	0.31	0.30	0.28	0.34	0.35



SAMPLE MINERAL CODE	S-85-2 OPX CORE	S-105 OPX RIM	S-105 OPX CORE	S-85 OPX RIM	S-85 OPX CORE	S-7 OPX CORE	S-7 OPX CORE
SiO <sub>2</sub>	48.79	50.48	48.99	50.13	48.83	52.84	53.04
TiO <sub>2</sub>	0.05	0.03	0.06	0.08	0.07	0.05	0.04
Al <sub>2</sub> O <sub>3</sub>	6.10	5.97	6.58	5.97	7.23	1.98	1.63
FeO	21.13	18.48	19.45	18.86	19.64	17.96	17.94
MnO	0.15	0.34	0.32	0.27	0.36	1.05	0.95
MgO	23.28	25.06	24.08	24.59	23.17	25.56	26.38
CaO	0.02	0.03	0.02	0.02	0.03	0.43	0.39
Na <sub>2</sub> O	0.06	0.02	0.02	0.00	0.00	0.02	0.00
K <sub>2</sub> O	0.00	0.00	0.00	0.00	0.00	0.00	0.00
Total	99.55	100.41	100.53	99.91	99.34	99.87	100.37
Si	1.82	1.84	1.83	1.84	1.81	1.94	1.93
Ti	0.00	0.00	0.00	0.00	0.00	0.00	0.00
Al	0.27	0.28	0.28	0.26	0.32	0.09	0.07
Fe	0.66	0.56	0.59	0.58	0.61	0.55	0.55
Mn	0.00	0.01	0.01	0.01	0.01	0.03	0.03
Mg	1.29	1.36	1.31	1.34	1.28	1.40	1.43
Ca	0.00	0.00	0.00	0.00	0.00	0.02	0.02
Na	0.00	0.00	0.00	0.00	0.00	0.00	0.00
K	0.00	0.00	0.00	0.00	0.00	0.00	0.00
Total	4.05	4.03	4.03	4.03	4.03	4.02	4.03
Fe/Fe + Mg + Ca + Mn	33.67	29.09	31.02	29.95	32.02	27.58	27.01
Mg/FMCM	66.05	70.30	68.43	69.58	67.32	69.94	70.79
Ca/FMCM	0.04	0.06	0.04	0.04	0.06	0.85	0.75
Mn/FMCM	0.24	0.54	0.52	0.43	0.59	1.63	1.45
Si + Al	2.09	2.10	2.11	2.10	2.13	2.02	2.00
Fe + Mg + Mn + Ca	1.96	1.94	1.92	1.93	1.90	2.00	2.03
Fe/(Fe + Mg)	0.34	0.29	0.31	0.30	0.32	0.28	0.28

SAMPLE MINERAL CODE	S-14 OPX R-CPX	S-14 OPX C-CPX	S-2 OPX C-CPX1	S-2 OPX R-CPX2	S-2-2 OPX C-CPX1	S-2-2 OPX R-CPX2	S 103B OPX R CPX1
SiO <sub>2</sub>	51.01	50.84	51.75	52.09	51.64	51.85	51.83
TiO <sub>2</sub>	0.07	0.08	0.06	0.05	0.04	0.09	0.05
Al <sub>2</sub> O <sub>3</sub>	0.72	1.16	1.21	1.14	1.13	1.28	0.93
FeO	26.71	27.26	25.16	25.12	24.47	24.53	26.48
MnO	0.88	0.81	0.69	0.67	0.69	0.65	0.87
MgO	19.42	19.16	20.66	21.06	21.51	21.55	19.23
CaO	0.52	0.67	0.61	0.57	0.50	0.57	0.53
Na <sub>2</sub> O	0.01	0.04	0.04	0.02	0.02	0.02	0.00
K <sub>2</sub> O	0.00	0.00	0.00	0.00	0.00	0.00	0.00
Total	99.34	100.02	100.16	100.73	100.02	100.54	99.92
Si	1.96	1.95	1.95	1.96	1.95	1.95	1.97
Ti	0.00	0.00	0.00	0.00	0.00	0.00	0.00
Al	0.03	0.05	0.05	0.05	0.05	0.06	0.04
Fe	0.86	0.87	0.79	0.79	0.77	0.77	0.84
Mn	0.03	0.03	0.02	0.02	0.02	0.02	0.03
Mg	1.11	1.09	1.16	1.18	1.21	1.21	1.09
Ca	0.02	0.03	0.02	0.02	0.02	0.02	0.02
Na	0.00	0.00	0.00	0.00	0.00	0.00	0.00
K	0.00	0.00	0.00	0.00	0.00	0.00	0.00
Total	4.02	4.03	4.02	4.02	4.03	4.02	4.00
Fe/Fe+Mg+Ca+Mn	42.48	43.21	39.65	39.21	38.15	38.14	42.50
Mg/FMCM	55.04	54.12	58.02	58.59	59.76	59.70	55.00
Ca/FMCM	1.06	1.36	1.23	1.14	1.00	1.14	1.09
Mn/FMCM	1.42	1.30	1.10	1.06	1.09	1.02	1.41
Si+Al	1.99	2.00	2.01	2.01	2.00	2.00	2.02
Fe+Mg+Mn+Ca	2.02	2.02	2.00	2.01	2.02	2.02	1.99
Fe/(Fe+Mg)	0.44	0.44	0.41	0.40	0.39	0.39	0.44

SAMPLE MINERAL CODE	S-103B OPX C-CPX2	S-64A OPX CORE	S-64A OPX C-CPX1	S-64A OPX R-CPX2	S-103A OPX R-CPX1	S-103A OPX R-CPX2	S-36A OPX R-CPX3
SiO <sub>2</sub>	51.91	51.25	51.02	51.80	51.14	50.80	51.02
TiO <sub>2</sub>	0.07	0.06	0.09	0.06	0.06	0.08	0.08
Al <sub>2</sub> O <sub>3</sub>	1.11	1.24	1.31	1.08	0.93	1.02	1.04
FeO	25.60	26.44	26.40	25.97	27.50	27.17	27.25
MnO	0.96	0.55	0.53	0.57	0.82	0.78	0.74
MgO	20.21	20.07	20.07	20.50	19.31	19.08	19.08
CaO	0.69	0.52	0.63	0.56	0.55	0.62	0.62
Na <sub>2</sub> O	0.03	0.02	0.05	0.04	0.00	0.01	0.03
K <sub>2</sub> O	0.00	0.00	0.00	0.00	0.00	0.00	0.00
Total	100.57	100.14	100.11	100.58	100.32	99.55	99.86
Si	1.96	1.95	1.94	1.95	1.95	1.95	1.96
Ti	0.00	0.00	0.00	0.00	0.00	0.00	0.00
Al	0.05	0.06	0.06	0.05	0.04	0.05	0.05
Fe	0.81	0.84	0.84	0.82	0.88	0.87	0.87
Mn	0.03	0.02	0.02	0.02	0.03	0.03	0.02
Mg	1.14	1.14	1.14	1.15	1.10	1.09	1.09
Ca	0.03	0.02	0.03	0.02	0.02	0.03	0.03
Na	0.00	0.00	0.00	0.00	0.00	0.00	0.00
K	0.00	0.00	0.00	0.00	0.00	0.00	0.00
Total	4.02	4.02	4.03	4.02	4.02	4.02	4.02
Fe/Fe+Mg+Ca+Mn	40.33	41.69	41.57	40.71	43.34	43.32	43.40
Mg/FMCM	56.74	56.39	56.31	57.26	54.24	54.15	54.15
Ca/FMCM	1.39	1.05	1.27	1.12	1.11	1.27	1.26
Mn/FMCM	1.53	0.88	0.85	0.90	1.31	1.26	1.19
Si+Al	2.01	2.00	2.00	2.00	2.00	2.00	2.00
Fe+Mg+Mn+Ca	2.00	2.02	2.02	2.01	2.03	2.02	2.01
Fe/(Fe+Mg)	0.42	0.43	0.42	0.42	0.44	0.44	0.44

SAMPLE MINERAL CODE	S-36A OPX C-CPX4
SiO <sub>2</sub>	51.11
TiO <sub>2</sub>	0.08
Al <sub>2</sub> O <sub>3</sub>	1.06
FeO	27.07
MnO	0.81
MgO	19.14
CaO	0.66
Na <sub>2</sub> O	0.00
K <sub>2</sub> O	0.00
Total	99.93
Si	1.96
Ti	0.00
Al	0.05
Fe	0.87
Mn	0.03
Mg	1.09
Ca	0.03
Na	0.00
K	0.00
Total	4.02
Fe/Fe+Mg+Ca+Mn	43.08
Mg/FMCM	54.27
Ca/FMCM	1.35
Mn/FMCM	1.31
Si+Al	2.00
Fe+Mg+Mn+Ca	2.01
Fe/(Fe+Mg)	0.44

**Appendix 2-6 Garnet Analyses**

Pelitic gneiss (unit 1) : S-88-1, S-88-2, S-90-1, S-90-2,  
S-45.

Noritic gneiss (unit 2) : S-85-1, S-85-2, S-126-1, S-126-2,  
S-105, S-127.

Metagabbro (unit 3) : S-77, S-65, S-72.

GNT : garnet, C-OPX : core part from orthopyroxene, R-OPX :  
rim adjacent to orthopyroxene, C-BIO : core adjacent to  
biotite, R-BIO : rim adjacent to biotite, C-HBL : core  
adjacent to hornblende, R-HBL : rim adjacent to hornblende.

Structural formulae based on 12 oxygens.

SAMPLE MINERAL CODE	S-88-1 GNT CORE	S-88-1 GNT R-OPX	S-88-2 GNT C-OPX1	S-88-2 GNT R-OPX3	S-88-2 GNT C-OPX1	S-88-2 GNT C-OPX2	S-88-2 GNT C-OPX3
SiO2	39.09	38.69	38.57	38.48	38.58	38.61	38.71
TiO2	0.02	0.02	0.02	0.03	0.04	0.02	0.03
Al2O3	21.73	21.89	22.01	22.00	21.92	22.05	21.99
FeO	25.40	25.80	25.72	25.98	25.70	25.92	26.19
MnO	1.19	1.09	1.22	1.16	1.20	1.15	1.24
MgO	11.54	11.59	11.72	11.41	11.62	11.58	11.56
CaO	0.58	0.59	0.58	0.57	0.56	0.59	0.57
Na2O	0.02	0.02	0.00	0.00	0.00	0.00	0.00
K2O	0.00	0.00	0.00	0.00	0.00	0.00	0.00
Total	99.58	99.70	99.83	99.64	99.60	99.92	100.28
Si	2.99	2.97	2.95	2.96	2.96	2.96	2.96
Ti	0.00	0.00	0.00	0.00	0.00	0.00	0.00
Al	1.96	1.98	1.99	1.99	1.98	1.99	1.98
Fe	1.63	1.65	1.65	1.67	1.65	1.66	1.67
Mn	0.08	0.07	0.08	0.08	0.08	0.07	0.08
Mg	1.32	1.32	1.34	1.31	1.33	1.32	1.32
Ca	0.05	0.05	0.05	0.05	0.05	0.05	0.05
Na	0.00	0.00	0.00	0.00	0.00	0.00	0.00
K	0.00	0.00	0.00	0.00	0.00	0.00	0.00
Total	8.03	8.05	8.05	8.05	8.05	8.05	8.05
Fe/Fe+Mg+Ca+Mn	53.01	53.40	52.94	53.88	53.17	53.47	53.69
Mg/FMCM	42.92	42.75	42.99	42.17	42.84	42.57	42.23
Ca/FMCM	1.55	1.56	1.53	1.51	1.48	1.56	1.50
Mn/FMCM	2.52	2.29	2.54	2.44	2.51	2.40	2.57
Si+Al	4.95	4.94	4.94	4.95	4.94	4.94	4.94
Fe+Mg+Mn+Ca	3.07	3.10	3.11	3.10	3.10	3.10	3.12
Fe/(Fe+Mg)	0.55	0.56	0.55	0.56	0.55	0.56	0.56

SAMPLE MINERAL CODE	S-88-2 GNT C-OPX4	S-88-2 GNT R-OPX5	S-90-1 GNT C-OPX1	S-90-1 GNT C-OPX2	S-90-1 GNT C-OPX3	S-90-1 GNT C-OPX4	S-90-1 GNT R-OPX5
SiO2	38.32	39.31	39.27	39.02	39.01	39.02	39.00
TiO2	0.03	0.03	0.02	0.01	0.02	0.03	0.01
Al2O3	22.05	20.95	21.69	21.63	21.75	21.71	21.75
FeO	26.02	25.53	27.42	27.59	27.88	27.71	27.62
MnO	1.19	1.09	0.86	0.88	0.91	0.84	0.88
MgO	11.28	12.84	11.07	11.02	10.74	10.66	10.55
CaO	0.61	0.51	0.19	0.18	0.20	0.18	0.19
Na2O	0.00	0.04	0.00	0.01	0.00	0.02	0.01
K2O	0.00	0.00	0.00	0.00	0.00	0.00	0.00
Total	99.50	100.31	100.52	100.34	100.51	100.17	100.02
Si	2.95	2.99	3.00	2.99	2.99	2.99	3.00
Ti	0.00	0.00	0.00	0.00	0.00	0.00	0.00
Al	2.00	1.88	1.95	1.95	1.96	1.96	1.97
Fe	1.67	1.62	1.75	1.77	1.78	1.78	1.77
Mn	0.08	0.07	0.06	0.06	0.06	0.05	0.06
Mg	1.29	1.46	1.26	1.26	1.22	1.22	1.21
Ca	0.05	0.04	0.02	0.01	0.02	0.01	0.02
Na	0.00	0.01	0.00	0.00	0.00	0.00	0.00
K	0.00	0.00	0.00	0.00	0.00	0.00	0.00
Total	8.05	8.07	8.03	8.04	8.03	8.03	8.02
Fe/Fe + Mg + Ca + Mn	54.09	50.89	56.82	57.06	57.85	57.99	58.08
Mg/FMCM	41.78	45.61	40.87	40.62	39.71	39.75	39.53
Ca/FMCM	1.62	1.30	0.50	0.48	0.53	0.48	0.51
Mn/FMCM	2.51	2.20	1.80	1.84	1.91	1.78	1.87
Si + Al	4.95	4.87	4.95	4.94	4.95	4.96	4.96
Fe + Mg + Mn + Ca	3.10	3.19	3.08	3.10	3.08	3.07	3.05
Fe/(Fe + Mg)	0.56	0.53	0.58	0.58	0.59	0.59	0.60

SAMPLE MINERAL CODE	S-90-2 GNT C-OPX1	S-90-2 GNT R-OPX3	S-90-2 GNT C-OPX1	S-90-2 GNT C-OPX4	S-45 GNT C-OPX1	S 45 GNT R OPX4	S 85 GNT C OPX1
SiO2	38.24	38.03	38.12	38.20	38.33	38.30	38.95
TiO2	0.00	0.00	0.00	0.00	0.05	0.02	0.03
Al2O3	21.75	21.74	21.73	21.90	21.83	21.86	21.58
FeO	27.48	27.84	27.91	27.76	27.39	27.25	24.85
MnO	0.89	0.89	0.90	0.83	0.85	0.82	1.65
MgO	10.89	10.68	10.50	10.80	10.85	10.75	11.61
CaO	0.22	0.21	0.21	0.21	0.19	0.20	0.61
Na2O	0.19	0.13	0.03	0.05	0.00	0.00	0.00
K2O	0.00	0.00	0.00	0.00	0.00	0.00	0.00
Total	99.66	99.53	99.40	99.74	99.48	99.20	99.28
Si	2.95	2.95	2.96	2.95	2.96	2.97	2.99
Ti	0.00	0.00	0.00	0.00	0.00	0.00	0.00
Al	1.96	1.99	1.99	1.99	1.99	2.00	1.95
Fe	1.78	1.80	1.81	1.79	1.77	1.76	1.60
Mn	0.06	0.06	0.06	0.05	0.06	0.05	0.11
Mg	1.25	1.23	1.21	1.24	1.25	1.24	1.33
Ca	0.02	0.02	0.02	0.02	0.02	0.02	0.05
Na	0.03	0.02	0.00	0.01	0.00	0.00	0.00
K	0.00	0.00	0.00	0.00	0.00	0.00	0.00
Total	8.07	8.07	8.05	8.06	8.04	8.04	8.03
Fe/Fe+Mg+Ca+Mn	57.17	57.95	58.39	57.69	57.27	57.38	51.78
Mg/FMCM	40.37	39.61	39.14	40.00	40.42	40.34	43.11
Ca/FMCM	0.59	0.56	0.56	0.56	0.51	0.54	1.63
Mn/FMCM	1.88	1.88	1.91	1.75	1.80	1.75	3.48
Si+Al	4.94	4.93	4.94	4.94	4.95	4.96	4.95
Fe+Mg+Mn+Ca	3.11	3.11	3.10	3.11	3.09	3.07	3.08
Fe/(Fe+Mg)	0.59	0.59	0.60	0.59	0.59	0.59	0.55



SAMPLE MINERAL CODE	S-85-1 GNT C-OPX2	S-85-1 GNT R-OPX3	S-85-1 GNT C-BIO1	S-85-1 GNT R-BIO2	S-85-2 GNT C-BIO1	S-85-2 GNT C-BIO2	S-85-2 GNT R-BIO3
SiO2	38.92	39.11	39.00	38.98	38.48	38.58	38.60
TiO2	0.00	0.01	0.01	0.04	0.00	0.00	0.01
Al2O3	21.56	21.56	21.83	21.78	22.00	22.04	22.09
FeO	24.86	24.88	25.12	25.36	24.35	24.91	24.83
MnO	1.73	1.70	1.74	1.78	1.85	1.78	1.81
MgO	11.63	11.61	11.89	11.46	12.19	11.94	11.71
CaO	0.58	0.54	0.59	0.55	0.59	0.59	0.60
Na2O	0.01	0.02	0.02	0.01	0.01	0.02	0.01
K2O	0.00	0.00	0.00	0.00	0.00	0.00	0.00
Total	99.29	99.42	100.19	99.95	99.48	99.85	99.66
Si	2.99	3.00	2.97	2.98	2.95	2.95	2.96
Ti	0.00	0.00	0.00	0.00	0.00	0.00	0.00
Al	1.95	1.95	1.96	1.96	1.99	1.99	1.99
Fe	1.60	1.60	1.60	1.62	1.56	1.59	1.59
Mn	0.11	0.11	0.11	0.12	0.12	0.12	0.12
Mg	1.33	1.33	1.35	1.31	1.39	1.36	1.34
Ca	0.05	0.04	0.05	0.05	0.05	0.05	0.05
Na	0.00	0.00	0.00	0.00	0.00	0.00	0.00
K	0.00	0.00	0.00	0.00	0.00	0.00	0.00
Total	8.03	8.03	8.05	8.04	8.06	8.06	8.05
Fe/Fe + Mg + Ca + Mn	51.71	51.85	51.45	52.52	50.00	51.10	51.41
Mg/FMCM	43.10	43.12	43.39	42.29	44.60	43.65	43.20
Ca/FMCM	1.55	1.44	1.55	1.46	1.55	1.55	1.59
Mn/FMCM	3.64	3.59	3.61	3.73	3.85	3.70	3.80
Si + Al	4.94	4.95	4.93	4.94	4.94	4.94	4.95
Fe + Mg + Mn + Ca	3.09	3.08	3.11	3.09	3.12	3.12	3.09
Fe/(Fe + Mg)	0.55	0.55	0.54	0.55	0.53	0.54	0.54

SAMPLE MINERAL CODE	S-85-2 GNT C-OPX1	S-85-2 GNT R-OPX2	S-85-2 GNT C-BIO1	S-85-2 GNT R-BIO4	S-126-1 GNT C-BIO	S-126-1 GNT C-BIO	S-126-1 GNT C-BIO1
SiO2	38.82	38.55	38.35	38.04	38.45	38.19	39.07
TiO2	0.00	0.00	0.00	0.00	0.00	0.08	0.02
Al2O3	22.16	22.14	21.84	21.79	21.80	21.70	21.67
FeO	24.55	24.34	26.70	26.98	26.95	26.96	26.24
MnO	1.91	1.90	1.70	1.73	0.67	0.74	0.75
MgO	12.11	12.29	10.99	10.61	10.89	10.63	11.76
CaO	0.59	0.54	0.62	0.59	0.44	0.37	0.39
Na2O	0.03	0.01	0.03	0.07	0.01	0.03	0.02
K2O	0.00	0.00	0.00	0.00	0.00	0.00	0.00
Total	100.16	99.75	100.24	99.82	99.20	98.70	99.91
Si	2.95	2.94	2.95	2.94	2.97	2.97	2.99
Ti	0.00	0.00	0.00	0.00	0.00	0.00	0.00
Al	1.99	1.99	1.98	1.99	1.99	1.99	1.95
Fe	1.56	1.55	1.72	1.75	1.74	1.75	1.68
Mn	0.12	0.12	0.11	0.11	0.04	0.05	0.05
Mg	1.37	1.40	1.26	1.22	1.25	1.23	1.34
Ca	0.05	0.04	0.05	0.05	0.04	0.03	0.03
Na	0.00	0.00	0.00	0.01	0.00	0.00	0.00
K	0.00	0.00	0.00	0.00	0.00	0.00	0.00
Total	8.05	8.06	8.07	8.07	8.04	8.03	8.04
Fe/Fe+Mg+Ca+Mn	50.29	49.82	54.71	55.75	56.62	57.21	54.15
Mg/FMCM	44.20	44.83	40.13	39.07	40.77	40.20	43.25
Ca/FMCM	1.55	1.42	1.63	1.56	1.18	1.01	1.03
Mn/FMCM	3.96	3.94	3.53	3.62	1.43	1.59	1.57
Si+Al	4.94	4.94	4.93	4.93	4.96	4.96	4.94
Fe+Mg+Mn+Ca	3.11	3.12	3.14	3.13	3.08	3.06	3.10
Fe/(Fe+Mg)	0.53	0.53	0.58	0.59	0.58	0.59	0.56

SAMPLE MINERAL CODE	S-126-2 GNT C-BIO2	S-126-2 GNT C-BIO3	S-126-2 GNT C-BIO4	S-126-2 GNT R-BIO5	S-105 GNT C-BIO1	S-105 GNT C-BIO2	S-105 GNT C-BIO3
SiO2	39.19	38.93	38.70	38.28	39.08	38.98	39.18
TiO2	0.02	0.04	0.03	0.04	0.02	0.02	0.03
Al2O3	21.49	21.31	21.27	20.94	21.81	21.67	21.58
FeO	26.39	27.48	28.46	31.11	25.86	25.93	26.52
MnO	0.71	0.64	0.70	0.77	0.76	0.72	0.76
MgO	11.43	10.75	9.80	7.99	12.13	11.87	11.46
CaO	0.37	0.42	0.43	0.37	0.41	0.36	0.38
Na2O	0.02	0.00	0.00	0.00	0.01	0.01	0.01
K2O	0.00	0.00	0.00	0.00	0.00	0.00	0.00
Total	99.63	99.58	99.40	99.50	100.09	99.55	99.91
Si	3.00	3.00	3.01	3.01	2.98	2.99	3.00
Ti	0.00	0.00	0.00	0.00	0.00	0.00	0.00
Al	1.94	1.94	1.95	1.94	1.96	1.96	1.95
Fe	1.69	1.77	1.85	2.05	1.65	1.66	1.70
Mn	0.05	0.04	0.05	0.05	0.05	0.05	0.05
Mg	1.31	1.24	1.13	0.94	1.38	1.35	1.31
Ca	0.03	0.03	0.04	0.03	0.03	0.03	0.03
Na	0.00	0.00	0.00	0.00	0.00	0.00	0.00
K	0.00	0.00	0.00	0.00	0.00	0.00	0.00
Total	8.02	8.03	8.02	8.02	8.04	8.04	8.03
Fe/Fe + Mg + Ca + Mn	55.03	57.46	60.32	66.76	53.02	53.72	55.02
Mg/FMCM	42.48	40.06	37.01	30.55	44.32	43.82	42.37
Ca/FMCM	0.99	1.13	1.17	1.02	1.08	0.96	1.01
Mn/FMCM	1.50	1.36	1.50	1.67	1.58	1.51	1.60
Si + Al	4.95	4.94	4.95	4.95	4.93	4.94	4.94
Fe + Mg + Mn + Ca	3.07	3.08	3.06	3.06	3.11	3.09	3.08
Fe/(Fe + Mg)	0.56	0.59	0.62	0.69	0.54	0.55	0.56

SAMPLE MINERAL CODE	S-105 GNT C-BIO4	S-105 GNT R-BIO5	S-127 GNT C-BIO1	S-127 GNT C-BIO2	S-127 GNT C-BIO3	S-127 GNT R-BIO4	S 77 GNT R HBL1
SiO2	39.06	38.63	39.25	38.92	38.58	38.59	37.81
TiO2	0.03	0.05	0.00	0.02	0.04	0.04	0.19
Al2O3	21.50	21.36	22.02	21.66	21.75	21.74	17.82
FeO	26.81	29.11	25.09	25.34	25.87	26.76	18.26
MnO	0.73	0.77	1.86	1.81	1.69	1.85	10.46
MgO	10.88	9.45	11.87	11.41	10.86	10.13	0.98
CaO	0.42	0.39	0.58	0.59	0.57	0.55	14.36
Na2O	0.01	0.01	0.01	0.02	0.00	0.01	0.03
K2O	0.00	0.00	0.00	0.00	0.00	0.00	0.00
Total	99.44	99.76	100.70	99.76	99.35	99.66	99.90
Si	3.01	3.00	2.97	2.98	2.98	2.98	3.06
Ti	0.00	0.00	0.00	0.00	0.00	0.00	0.01
Al	1.95	1.95	1.97	1.96	1.98	1.98	1.70
Fe	1.73	1.89	1.59	1.62	1.67	1.73	1.23
Mn	0.05	0.05	0.12	0.12	0.11	0.12	0.72
Mg	1.25	1.09	1.34	1.30	1.25	1.17	0.12
Ca	0.03	0.03	0.05	0.05	0.05	0.05	1.24
Na	0.00	0.00	0.00	0.00	0.00	0.00	0.00
K	0.00	0.00	0.00	0.00	0.00	0.00	0.00
Total	8.02	8.02	8.04	8.04	8.03	8.03	8.08
Fe/Fe+Mg+Ca+Mn	56.47	61.64	51.34	52.51	54.28	56.47	37.27
Mg/FMCM	40.84	35.66	43.28	42.13	40.60	38.09	3.56
Ca/FMCM	1.13	1.06	1.52	1.57	1.53	1.49	37.55
Mn/FMCM	1.56	1.65	3.85	3.80	3.59	3.95	21.62
Si+Al	4.96	4.95	4.94	4.94	4.95	4.96	4.76
Fe+Mg+Mn+Ca	3.06	3.07	3.10	3.09	3.08	3.06	3.31
Fe/(Fe+Mg)	0.58	0.63	0.54	0.55	0.57	0.60	0.91

SAMPLE MINERAL CODE	S-77 GNT R-HBL2	S-77 GNT C-HBL3	S-77 GNT C-HBL1	S-77 GNT R-HBL3	S-65 GNT R-HBL1	S-65 GNT CORE	S-72 GNT C-HBL1
SiO2	37.83	38.06	37.77	37.37	37.93	37.86	37.82
TiO2	0.19	0.20	0.21	0.17	0.21	0.18	0.19
Al2O3	17.94	18.03	17.91	17.82	17.92	17.78	17.78
FeO	17.94	17.97	18.14	17.88	17.97	17.86	17.56
MnO	11.22	11.24	10.79	10.42	10.78	11.09	10.44
MgO	1.07	1.08	1.01	0.86	0.98	1.03	0.86
CaO	13.62	13.57	14.25	15.12	14.25	13.64	14.93
Na2O	0.03	0.02	0.01	0.03	0.02	0.01	0.00
K2O	0.00	0.00	0.00	0.00	0.00	0.00	0.00
Total	98.84	100.16	100.10	99.87	100.06	99.46	99.57
Si	3.06	3.06	3.05	3.03	3.06	3.07	3.06
Ti	0.01	0.01	0.01	0.01	0.01	0.01	0.01
Al	1.71	1.71	1.70	1.71	1.70	1.70	1.70
Fe	1.21	1.21	1.22	1.21	1.21	1.21	1.19
Mn	0.77	0.77	0.74	0.72	0.74	0.76	0.72
Mg	0.13	0.13	0.12	0.10	0.12	0.12	0.10
Ca	1.18	1.17	1.23	1.32	1.23	1.19	1.30
Na	0.00	0.00	0.00	0.00	0.00	0.00	0.00
K	0.00	0.00	0.00	0.00	0.00	0.00	0.00
Total	8.08	8.07	8.09	8.11	8.08	8.07	8.08
Fe/Fe + Mg + Ca + Mn	36.87	36.93	36.93	36.24	36.75	36.90	35.99
Mg/FMCM	3.92	3.95	3.66	3.11	3.57	3.79	3.14
Ca/FMCM	35.86	35.73	37.16	39.26	37.34	36.10	39.20
Mn/FMCM	23.35	23.39	22.25	21.39	22.33	23.21	21.67
Si + Al	4.77	4.78	4.75	4.74	4.76	4.77	4.76
Fe + Mg + Mn + Ca	3.29	3.28	3.32	3.35	3.30	3.28	3.30
Fe/(Fe + Mg)	0.90	0.90	0.91	0.92	0.91	0.91	0.92

SAMPLE MINERAL CODE	S-72 GNT R-HBL2
SiO <sub>2</sub>	38.08
TiO <sub>2</sub>	0.18
Al <sub>2</sub> O <sub>3</sub>	17.67
FeO	17.54
MnO	10.28
MgO	0.84
CaO	14.98
Na <sub>2</sub> O	0.01
K <sub>2</sub> O	0.00
Total	99.57
Si	3.08
Ti	0.01
Al	1.68
Fe	1.19
Mn	0.70
Mg	0.10
Ca	1.30
Na	0.00
K	0.00
Total	8.07
Fe/Fe+Mg+Ca+Mn	35.06
Mg/FMCM	3.08
Ca/FMCM	39.46
Mn/FMCM	21.41
Si+Al	4.76
Fe+Mg+Mn+Ca	3.29
Fe/(Fe+Mg)	0.92

**APPENDIX 3****GEOOTHERMOBAROMETRY****3-1 Garnet-Biotite**

The partitioning of Fe and Mg between garnet and biotite is a temperature sensitive equilibrium affected only to a slight degree by pressure. The relationship between the Fe-Mg distribution coefficient and temperature has been empirically calibrated as a thermometer by Saxena (1969), Thompson (1976) and Goldman and Albee (1977). Experimental calibrations have been presented by Ferry and Spear (1978) and Perchuk and Lavrent'eva (1983).

The exchange reaction is :



Initial calibrations assumed that the solid solutions were ideal. Subsequently, several calibrations have been presented, which attempt to correct for the non-ideality in garnet caused by mixing of Fe and Mg and other elements, by introducing additional correction factors to the expression of

Ferry and Spear (1978) (e.g. Hodges and Spear (1982); Pigage and Greenwood (1982); Ganguly and Saxena (1984)). The effect of Ca and Mn on the garnet Fe-Mg binary solution used in the Ferry and Spear (1978) calibration is taken into account by Pigage and Greenwood (1983). Indares and Martignole (1985) also presented an empirical calibration which in addition evaluated influences from Al and Ti in biotite.

The expression of Ferry and Spear (1978) calibration is  

$$0 = 12454 - 4.662T(^{\circ}\text{K}) + 0.057P(\text{bars}) + RT(\text{K})\ln K$$

$$T(^{\circ}\text{K}) = (2089 + 9.56P) / (\ln K + 0.782)$$

where  $K = (\text{Fe/Mg})_{\text{garnet}} / (\text{Fe/Mg})_{\text{biotite}}$ .

The expression of Hodges and Spear (1982) calibration is

$$T(^{\circ}\text{K}) = (2089 + 9.56P + 1661X^{\text{Ca}}) / (\ln K + 0.782 + 0.755X^{\text{Ca}})$$

where  $X^{\text{Ca}} = \text{Ca} / \text{Ca} + \text{Mg} + \text{Fe} + \text{Mn}$  in garnet.

The expression of Pigage and Greenwood (1982) calibration is :

$$T(^{\circ}\text{K}) = 1586X^{\text{Ca}} + 1308X^{\text{Mn}} + 2089 + 0.00956P(\text{bars}) / 0.78198 - \ln K$$

where  $X^i = i / \text{Mg} + \text{Fe} + \text{Ca} + \text{Mn}$  in garnet.



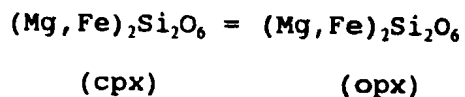
The expression of the Indares and Martignole (1985) calibration is :

$$T(^{\circ}\text{K}) = [12454 + 0.057P(\text{bars}) + 3(mX^{\text{Al}} + nX^{\text{Ti}} - (W_{\text{Ca}}X^{\text{Ca}} + W_{\text{Mn}}X^{\text{Mn}}))] / [4.662 - 0.9616 \ln K_{\text{D}}]$$

where  $K_{\text{D}} = (\text{Fe/Mg})_{\text{garnet}} / (\text{Fe/Mg})_{\text{biotite}}$  and  $n$  and  $m$  are interaction parameters depending on the model adopted for the non-ideality in garnet.

### 3-2 Orthopyroxene-Clinopyroxene

Wood and Banno (1973) and Wells (1977) have investigated experimentally and theoretically temperature variations of the position and shape of the solvus in the pyroxene quadrilateral. The exchange reaction is :



Wood and Banno's (1973) calibration is based on the approximation that the solubility of enstatite in diopside co-existing with orthopyroxene is an ideal solution.

Well (1977)'s calibration is a semi-empirical formulation

derived from available experimental data for the diopside - enstatite miscibility gap. The solubility of  $\text{Fe}^{2+}$  in the pyroxene solution has been calibrated empirically using experimental data for multicomponent pyroxenes.

The thermometric expressions of the calibrations of Wood and Banno (1973) and Wells (1977) are :

Wood and Banno (1973) :

$$T(^{\circ}\text{K}) = -10,202 / [(\ln K - 7.65X^{\text{Fe}} + 3.88(X^{\text{Fe}})^2) - 4.6]$$

Wells (1977) :

$$T(^{\circ}\text{K}) = 7341 / [3.355 + 2.44(X^{\text{Fe}}) - \ln K]$$

where  $X^{\text{Fe}}$  is  $\text{Fe}/\text{Fe}+\text{Mg}$  in orthopyroxene.  $K$  is  $a^{\text{en(cpx)}} / a^{\text{en(opx)}}$ , where the activities of enstatite ( $\text{Mg}_2\text{Si}_2\text{O}_6$ ) in clinopyroxene and orthopyroxene are calculated following the ideal mixing on sites model outlined in Powell (1978).

### 3-3 Garnet-Orthopyroxene

Wood (1974), Harley and Green (1982), and Harley (1984) have experimentally calibrated the solubility of Al in orthopyroxene coexisting with garnet. The Fe-Mg exchange between coexisting garnet and orthopyroxene has also been calibrated as a geothermometer based on experiments in the CFMAS system (Harley 1984) and on thermodynamic analysis of

available data formulated for granulite facies conditions (Sen and Bhattacharya 1984). The thermometric expressions are :

Harley (1984) :

$$T(^{\circ}\text{K}) = (3740 + 1400X^{\text{Ca}} + 0.02286P) / (1.96 - 1.987\ln K)$$

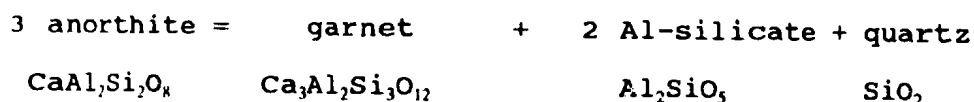
Sen and Bhattacharya (1984) :

$$T(^{\circ}\text{K}) = [2713 + 0.022P + 3300X^{\text{Ca}} + 195(X^{\text{Fe}} - X^{\text{Mg}})] / (-1.9872\ln K + 0.787 + 1.5X^{\text{Ca}})$$

where  $X'$  is  $\text{Ca}/\text{Ca}+\text{Fe}+\text{Mg}$ ,  $\text{Fe}/\text{Ca}+\text{Fe}+\text{Mg}$ , and  $\text{Mg}/\text{Ca}+\text{Fe}+\text{Mg}$  in garnet,  $P$  is in bars, and  $K$  is  $(\text{Fe}/\text{Mg})^{\text{opx}} / (\text{Fe}/\text{Mg})^{\text{grt}}$ . Sen and Bhattacharya (1984) assumed ideal solution for orthopyroxene, and take into account the non-ideality from Fe-Mg and Ca-Mg interactions for garnet ( $W_{\text{FeMg}}$  from O'Neill and Wood (1979),  $W_{\text{CaMg}}$  from Haselton and Newton (1980)).

### 3-4 Garnet-Plagioclase- $\text{Al}_2\text{SiO}_5$ -Quartz

Ghent (1976) developed the reaction :



as geobarometer, on the basis of the assumption of ideal solid

solution of garnet and plagioclase. The degree of non-ideality of grossular solid solution in garnet has estimated from calculations using the activity coefficients of anorthite in plagioclase and the kyanite-sillimanite curve as a limiting case for kyanite and sillimanite-bearing assemblages (Ghent et al. 1979). The equilibrium can be expressed by :

$$0 = -3272/T(^{\circ}\text{K}) + 8.3969 - 0.3448(P-1)/T(^{\circ}\text{K}) + \log a_{\text{Ca}}^{\text{gr}} - 3\log a_{\text{Ca}}^{\text{pl}} \text{ (kyanite)}$$

$$0 = -2551.4/T(^{\circ}\text{K}) + 7.1711 - 0.2842(P-1)/T(^{\circ}\text{K}) + \log a_{\text{Ca}}^{\text{gr}} - 3\log a_{\text{Ca}}^{\text{pl}} \text{ (Sillimanite)}$$

where  $a_{\text{Ca}}^{\text{gr}} = (X_{\text{Ca}}^{\text{gr}})^3 (\gamma_{\text{Ca}}^{\text{gr}})^3$  and  $a_{\text{Ca}}^{\text{pl}} = (X_{\text{Ca}}^{\text{pl}})^3 (\gamma_{\text{Ca}}^{\text{pl}})^3$

$$X_{\text{Ca}}^{\text{gr}} = \text{Ca} / \text{Ca} + \text{Mg} + \text{Fe} + \text{Mn} \text{ and } X_{\text{Ca}}^{\text{pl}} = \text{Ca} / \text{Ca} + \text{Na} + \text{K}$$

$$\gamma_{\text{Ca}}^{\text{gr}} = \exp[(3300 - 1.5T) * (X_{\text{py}} + X_{\text{al}}X_{\text{py}} + X_{\text{py}}X_{\text{spn}}) / RT]$$

$$\gamma_{\text{Ca}}^{\text{pl}} = \exp[(X_{\text{ab}}^2 (2025 + 9442X_{\text{an}}) / RT]$$

Subsequently, the barometer was refined by experiments and thermodynamic analysis (Newton and Haselton 1981; Hodges and Royden 1984). Among them, Newton and Haselton (1981) applied recent solution and low temperature calorimetry in addition to experimental phase equilibrium data on garnet and plagioclase solid solution. The result was a more precise, experimental determination of the Garnet - Plagioclase -

$\text{Al}_2\text{SiO}_5$  - Quartz assemblage, making possible a major improvement on non-ideal formulations.

Ganguly and Saxena (1984) revised the end member calculations for the garnet - plagioclase -  $\text{Al}_2\text{SiO}_5$  - quartz barometer proposed by Newton and Haselton (1981). The calibrated geobarometer is expressed as :

$$0 = 13352 - 36.709T(^{\circ}\text{K}) + V(P-1) + 1.9872T(^{\circ}\text{K}) \ln(a_{\text{gr}}^{\text{gr}}/a_{\text{m}}^{\text{pl}})$$

(with kyanite)

$$0 = 10055 - 31.101T(^{\circ}\text{K}) + V(P-1) + 1.9872T(^{\circ}\text{K}) \ln(a_{\text{gr}}^{\text{gr}}/a_{\text{m}}^{\text{pl}})$$

(with sillimanite)

where  $V$  and  $P$  are expressed in cal/bar and kbar, respectively.

### 3-5 Garnet-Orthopyroxene-Plagioclase-Quartz

The reaction of garnet with pyroxene solid solutions was first calibrated from experimental phase equilibrium studies as a geobarometer by Wood and Banno (1973). Newton and Perkins (1982) calibrated two mineralogic geobarometers based on the assemblage garnet-plagioclase-pyroxene-quartz, which are applicable to granulite grade quartzofeldspathic and basic lithologies. The Mg equilibrium has been calibrated on the

**DAI Note:**

**Page missing from  
bound thesis.**

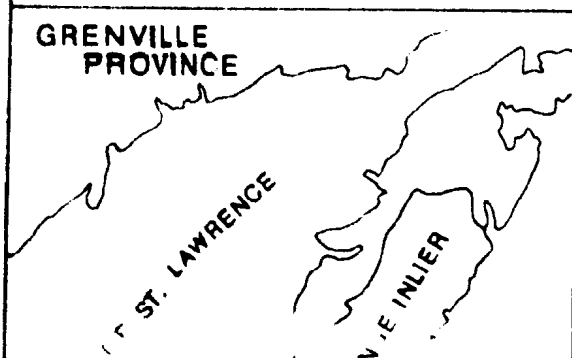
# G E O L O G I



Unmap

46° 33'

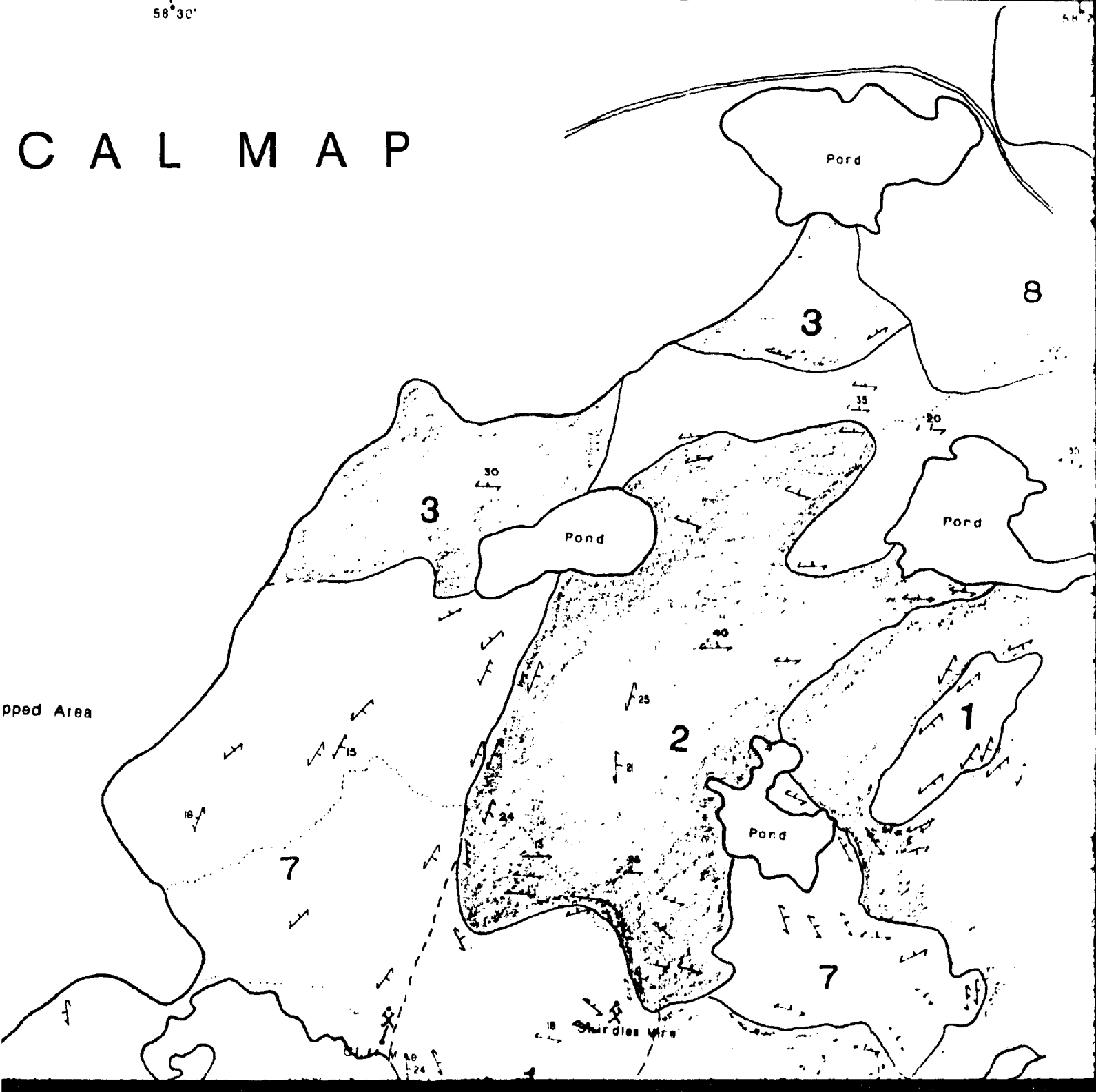
## INDEX MAP



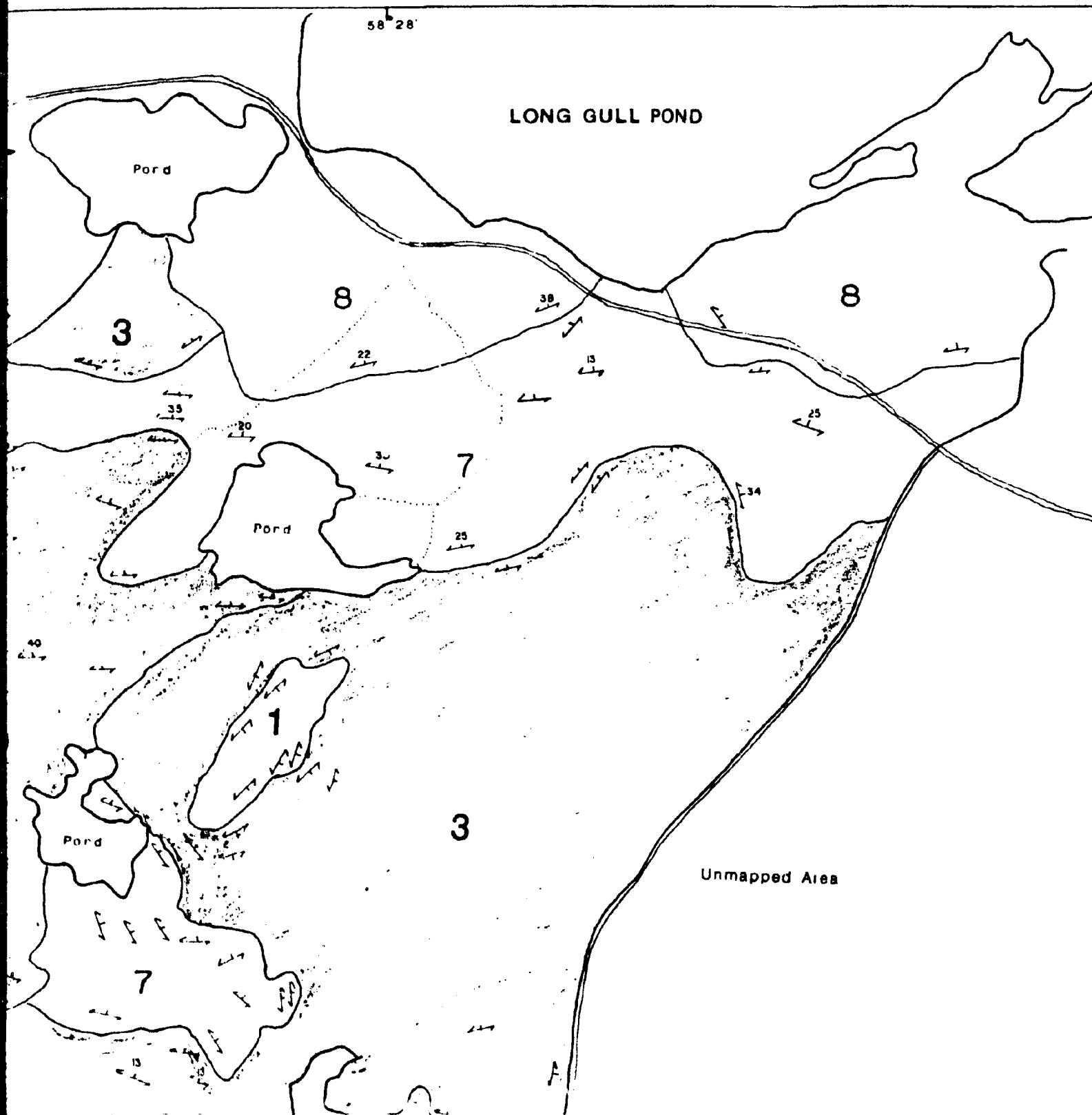
58° 30'

58° 2'

# CALMAP







58° 26'

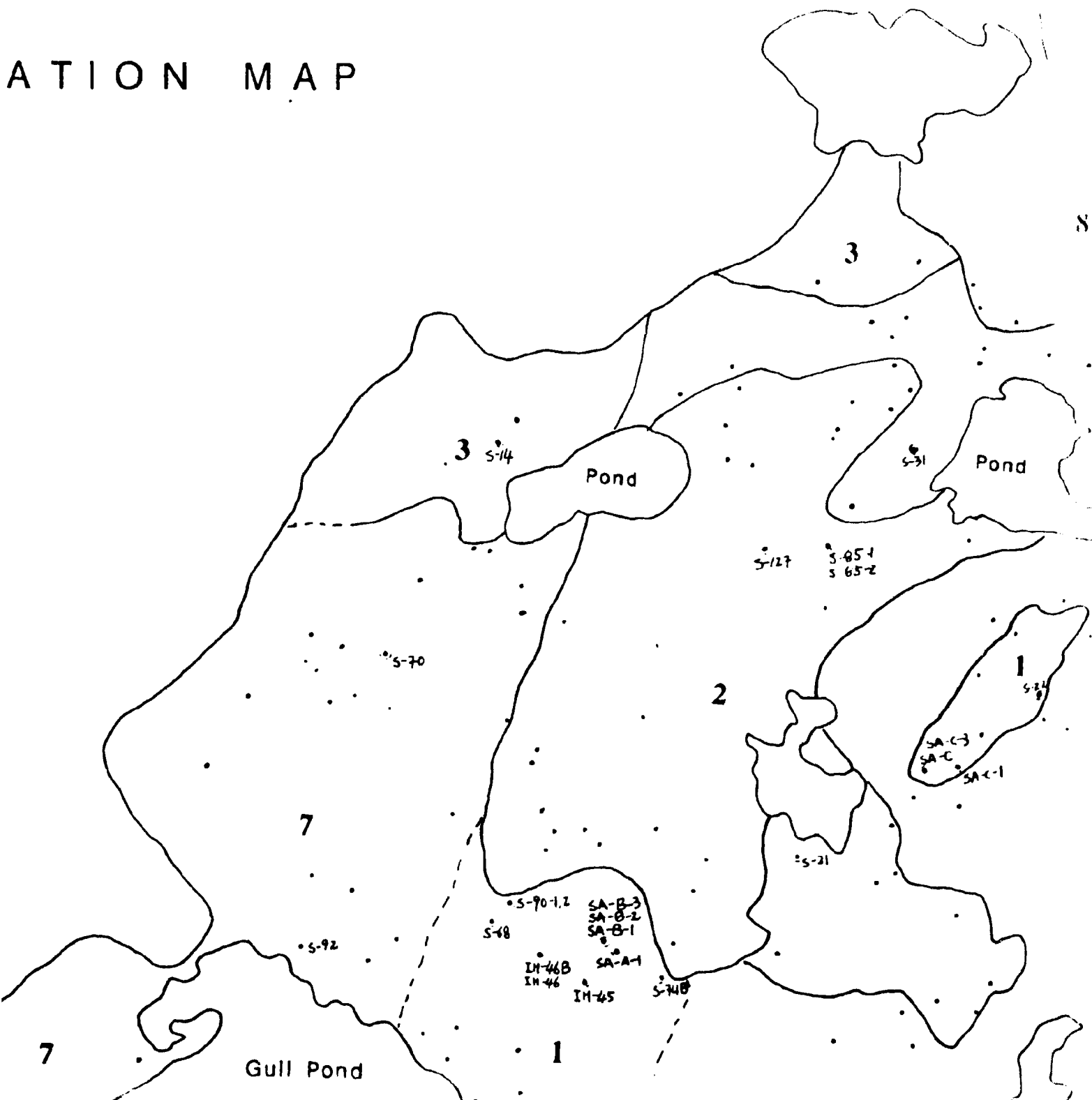


SAMPLE LOC



48 33'

# ATION MAP



Long Gulf Pond

3

8

S-32

IW-14

8

IW-19

IW-18

S-37

7

S-31

Pond

S-47

S-127

S-85-1  
S-85-2

S-65

2

1

S-33

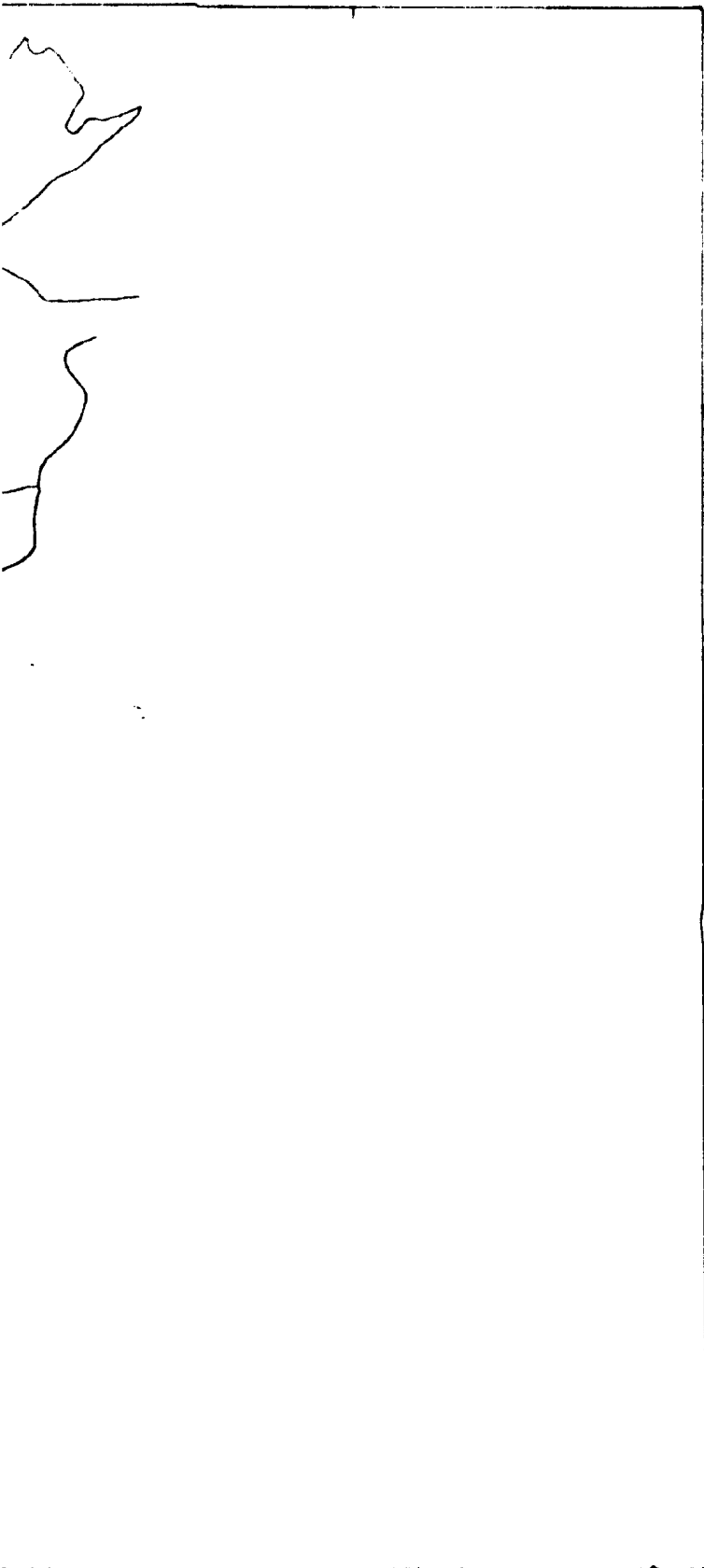
SA-C-3

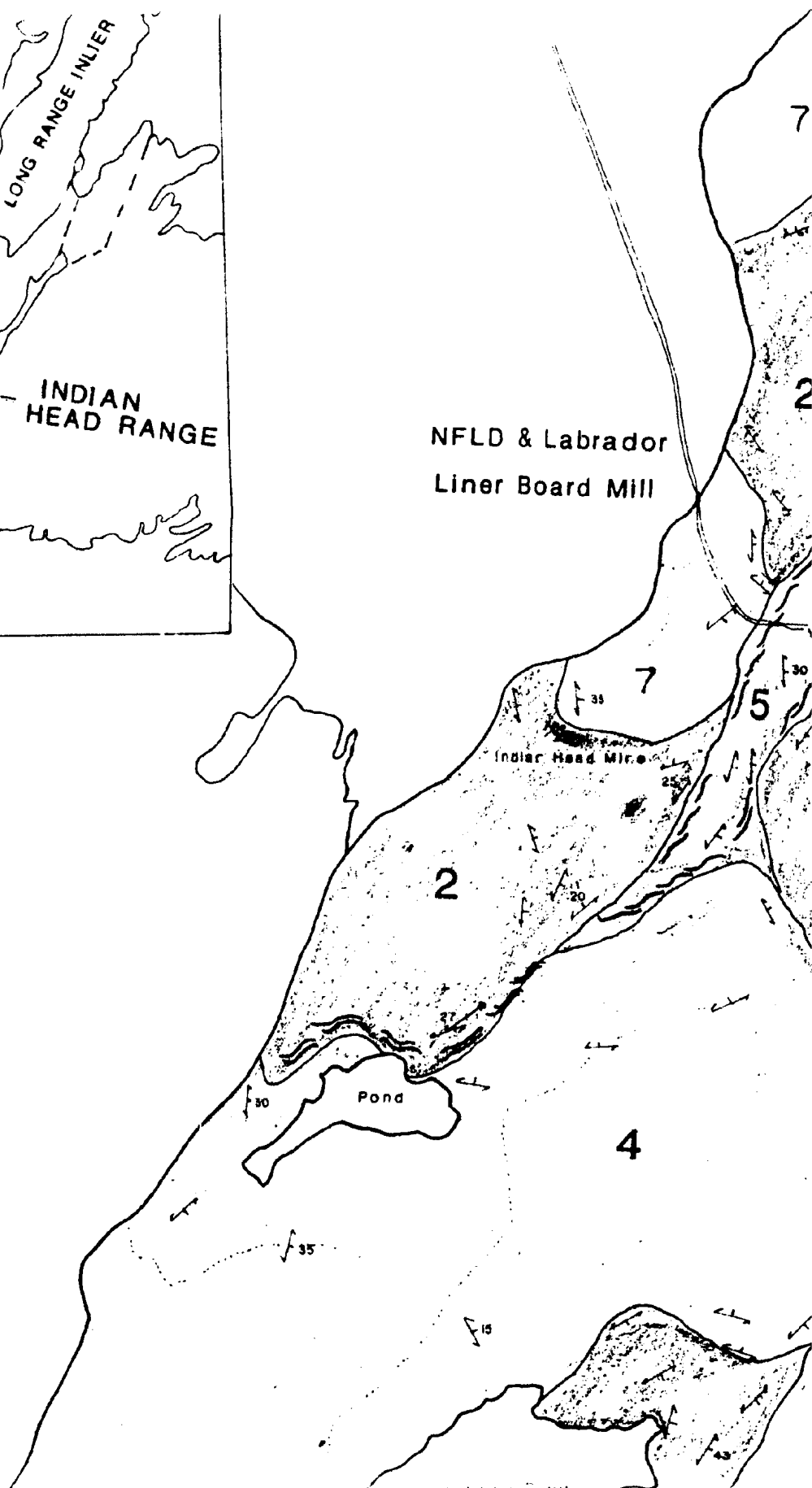
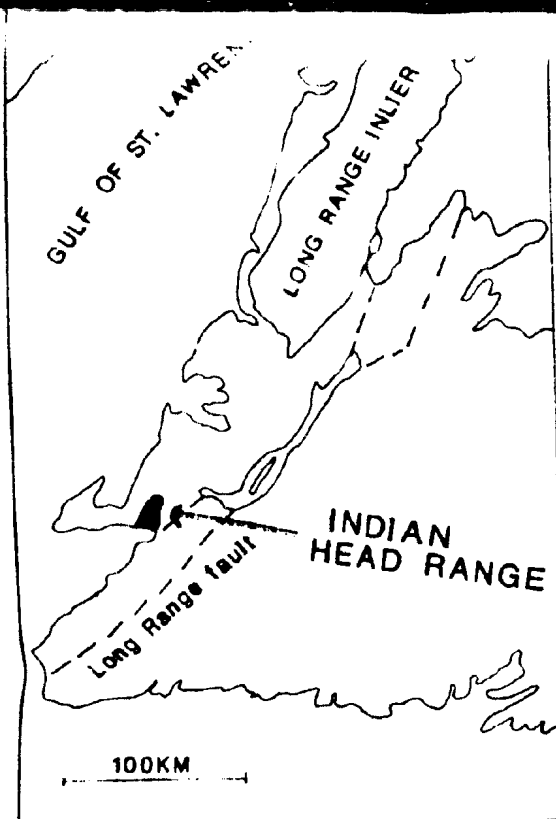
SA-C

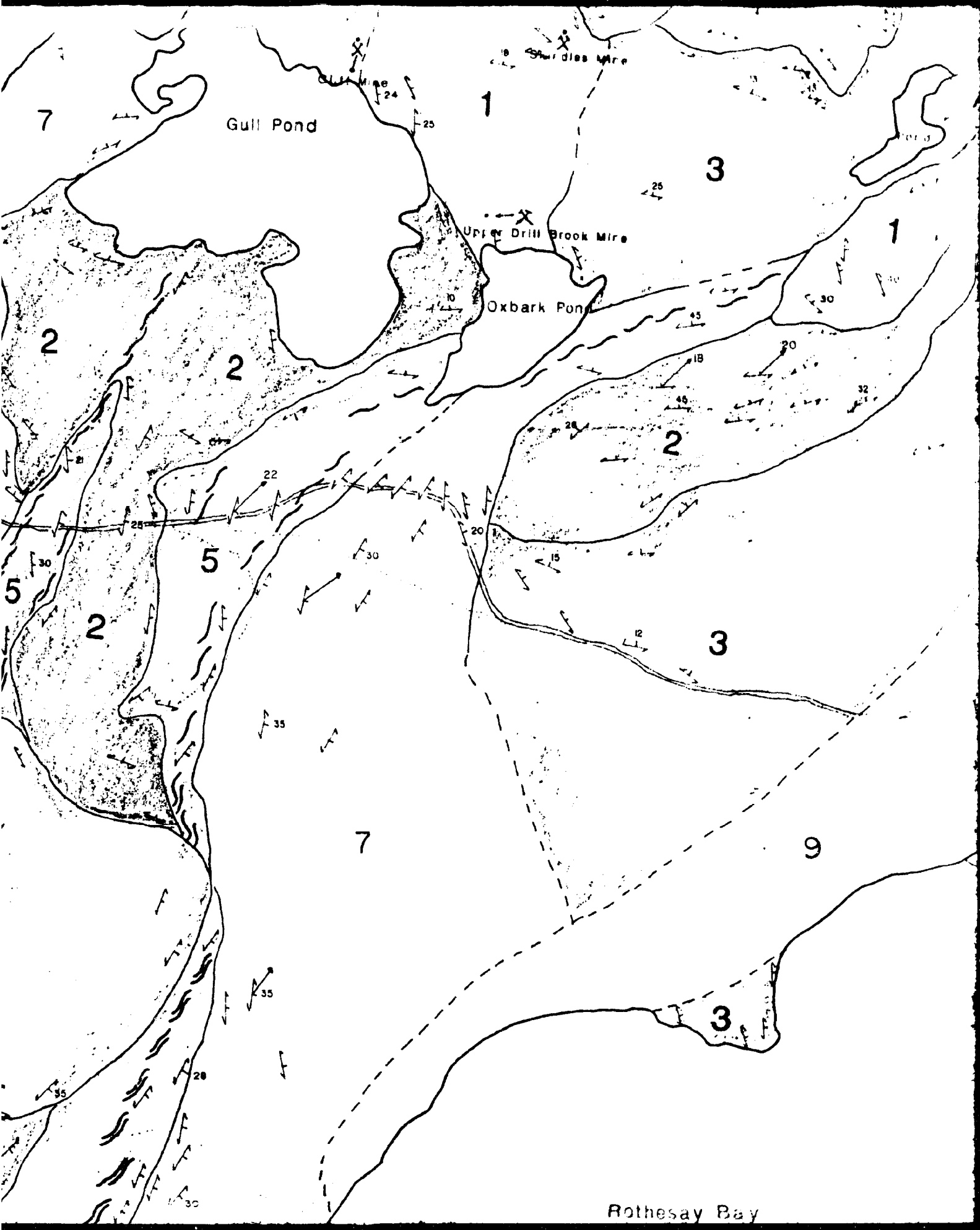
SA-C-1

3

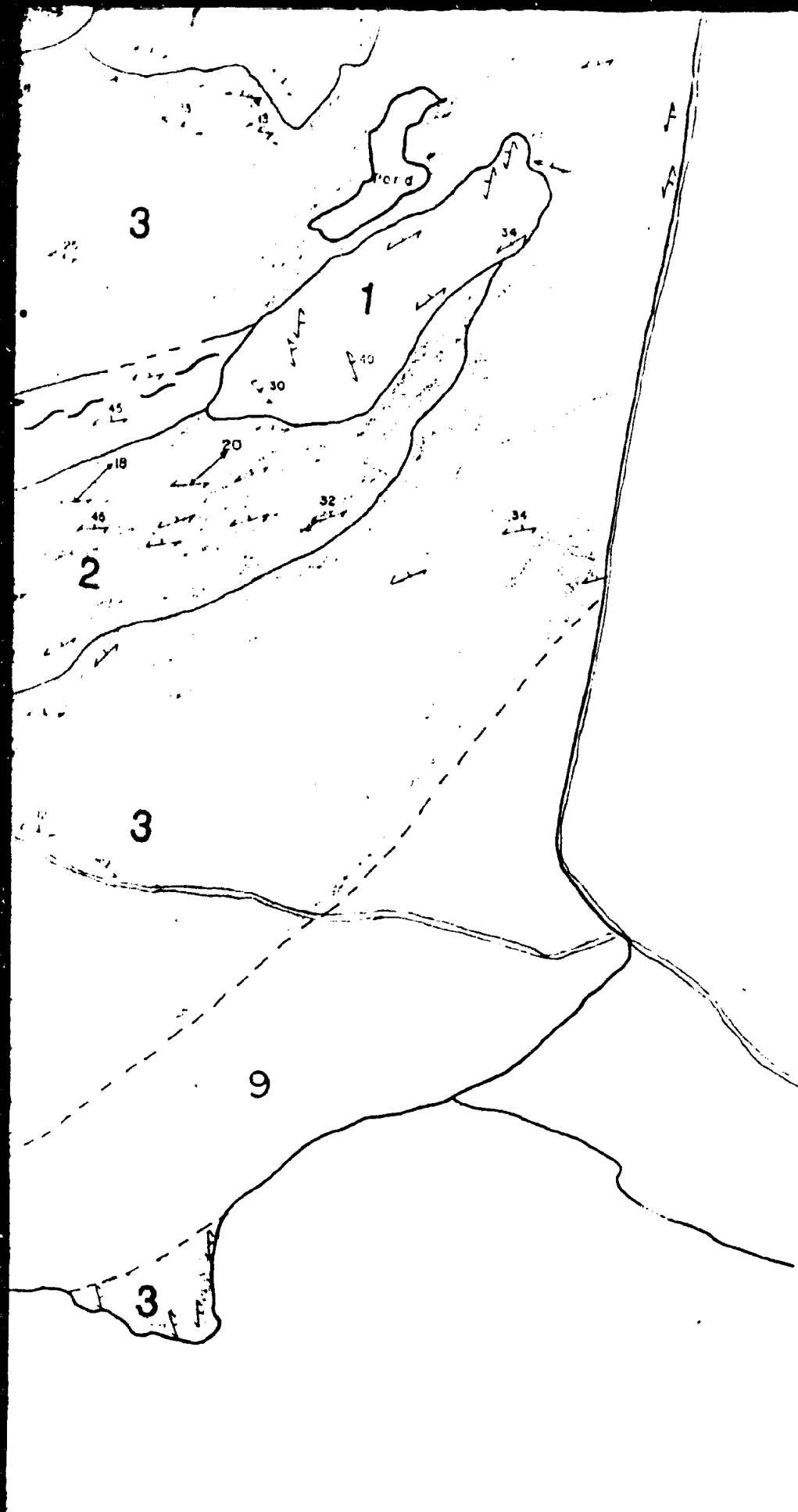
S-21











# LEGEND

- 10 MAFIC DIKE
- 9 PALEOZOIC ROCKS
- 8 Foliated HORNBLende GNEISS
- 7 Variably foliated BIOTITE GRANITE
- 6 LHERZOLITE
- 5 Strongly foliated DIORITIC GNEISS
- 4 Weakly foliated ANORTHOSITE
- 3 Weakly foliated METAGABBRO
- 2 Strongly deformed NORITIC GNEISS
- 1 Variably deformed PELITIC GNEISS

PROTEROZOIC

- Lithological boundary
- Inferred lithological boundary
- Foliation orientation
- Lination orientation
- Mine

KS (undivided)

---

GRANODIORITE

d  
E

ed to mylonitic

t to massive

t

med

med

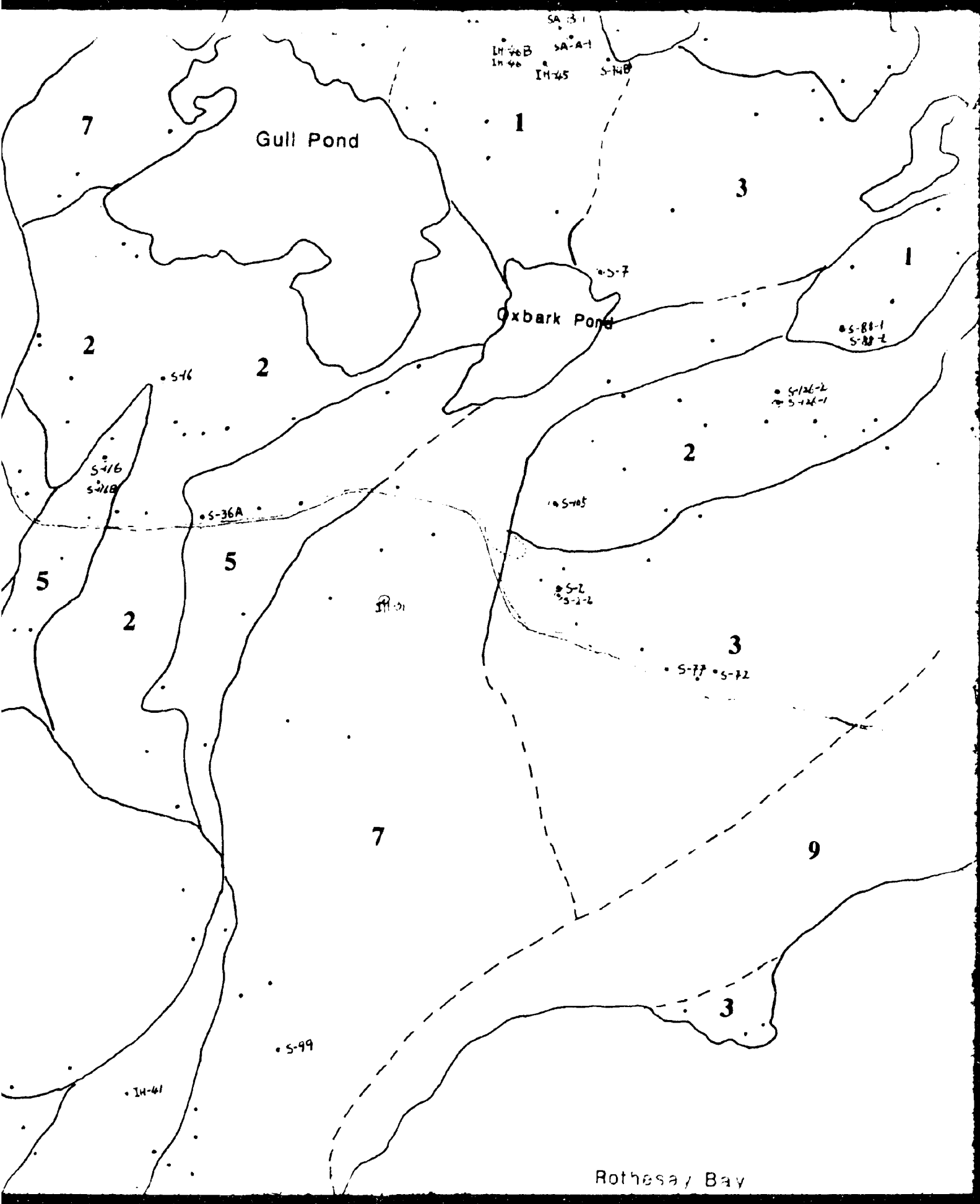
ndary

gical boundary

ation

tation





SA-31

IN-46B  
IN-46

SA-A-1

IN-45

S-148

7

Gull Pond

1

3

2

2

S-16

Oxbark Pond

S-7

S-81-1  
S-81-2

S-126-2  
S-126-1

2

S-16  
S-16

S-36A

S-105

5

5

2

IN-41

S-2  
S-2-2

3

S-77 S-72

7

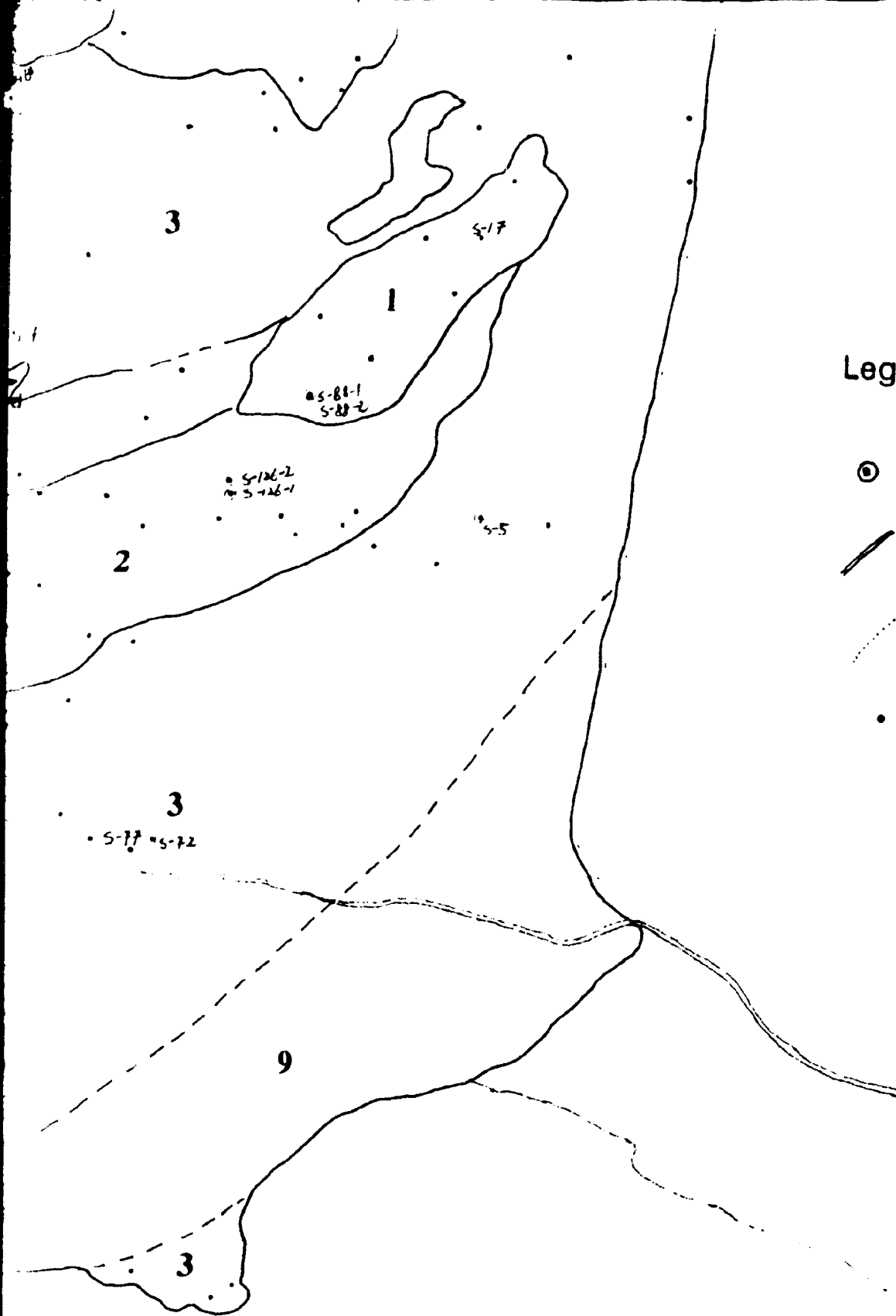
9

S-99

IN-41

3


Rothsay Bay



Legend is the same as

⊙ Sample Location

 Main Road

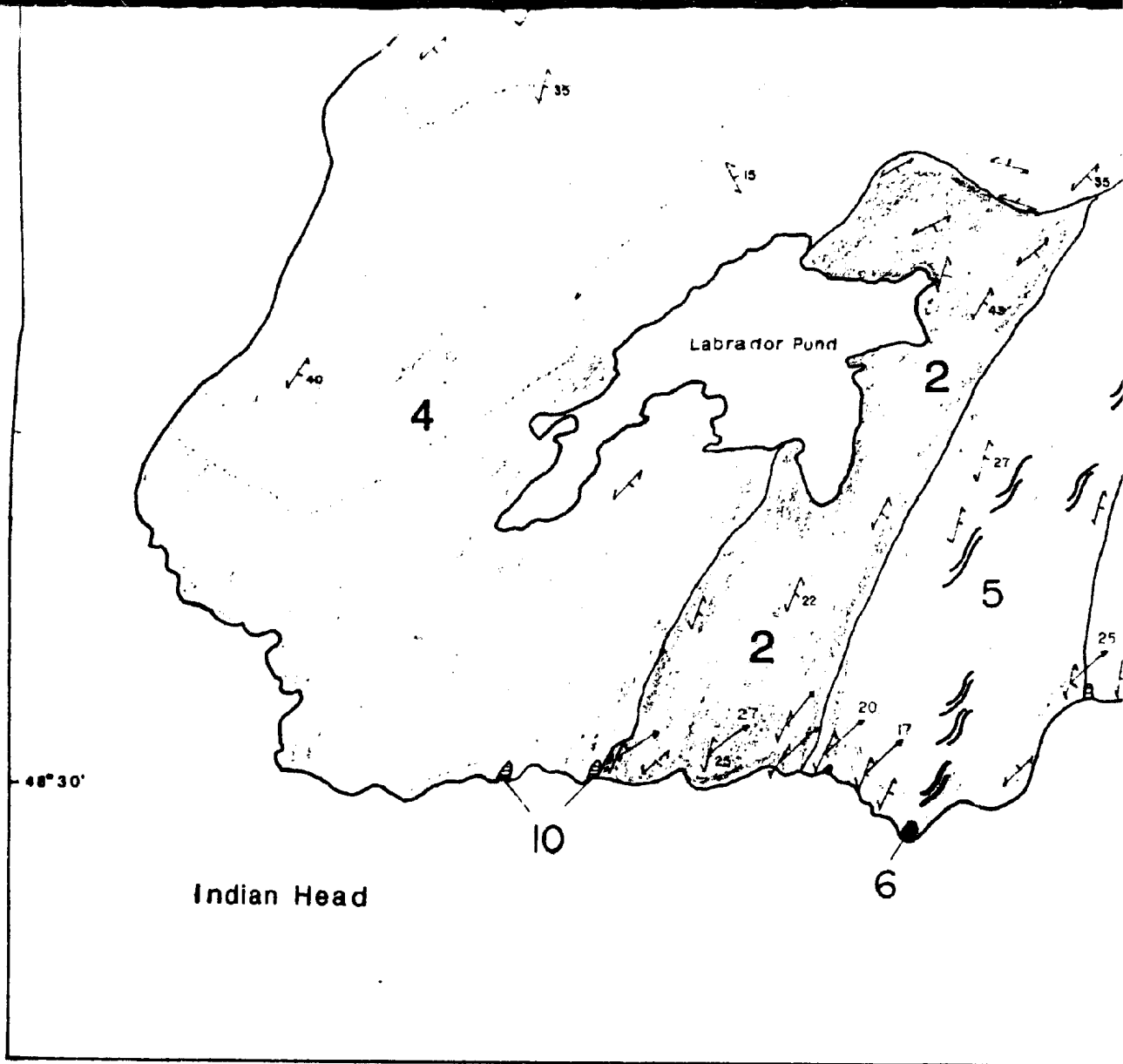
 Trail

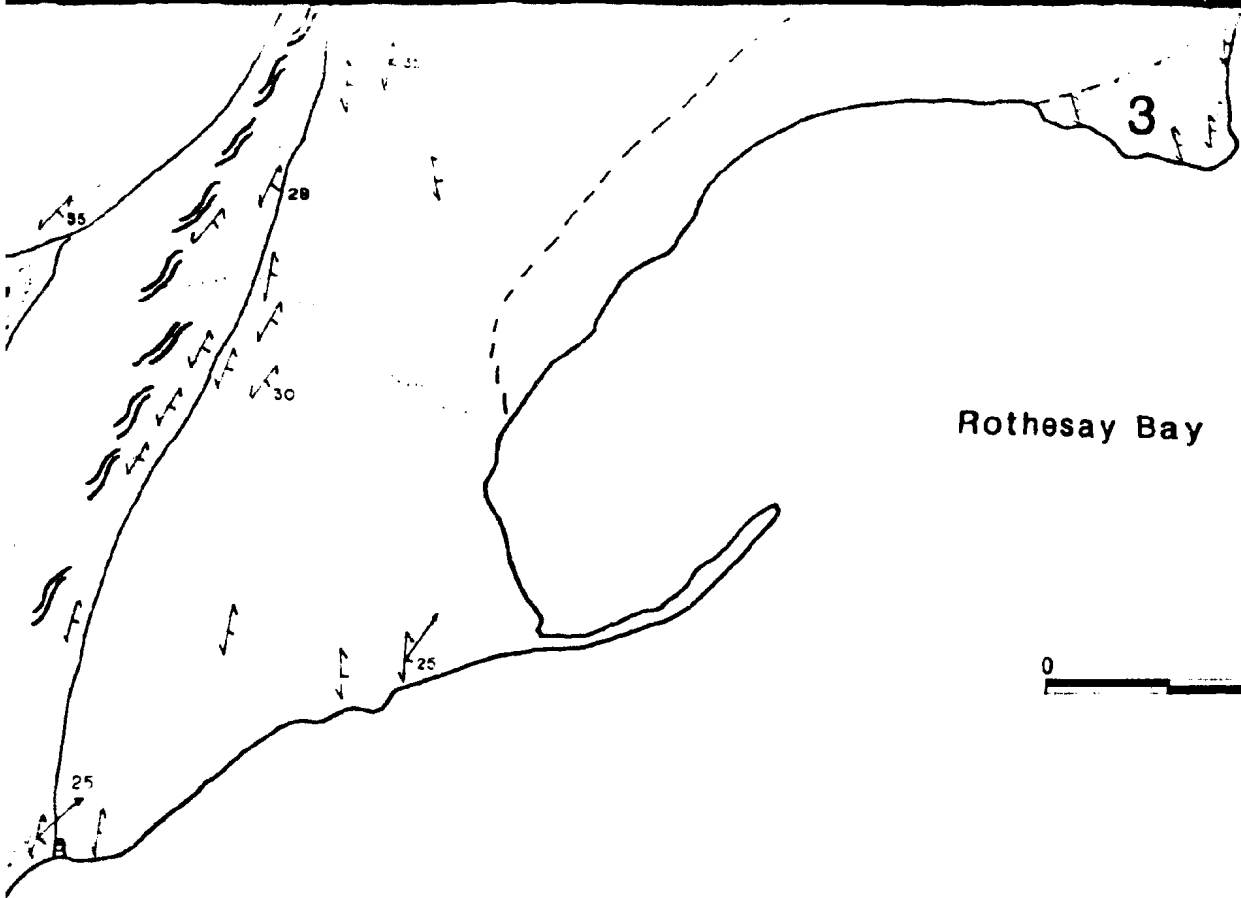
• Sample Location

ne as the geological map.

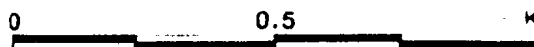
ation (referred in thesis)

ation (not referred in thesis)





Rothesay Bay





3

esay Bay

0.5 1 Km

- Lithological bounda
- Inferred lithological
- Foliation orientation
- Lineation orientatio
- Mine
- Shear Zone
- Main Road
- Trall

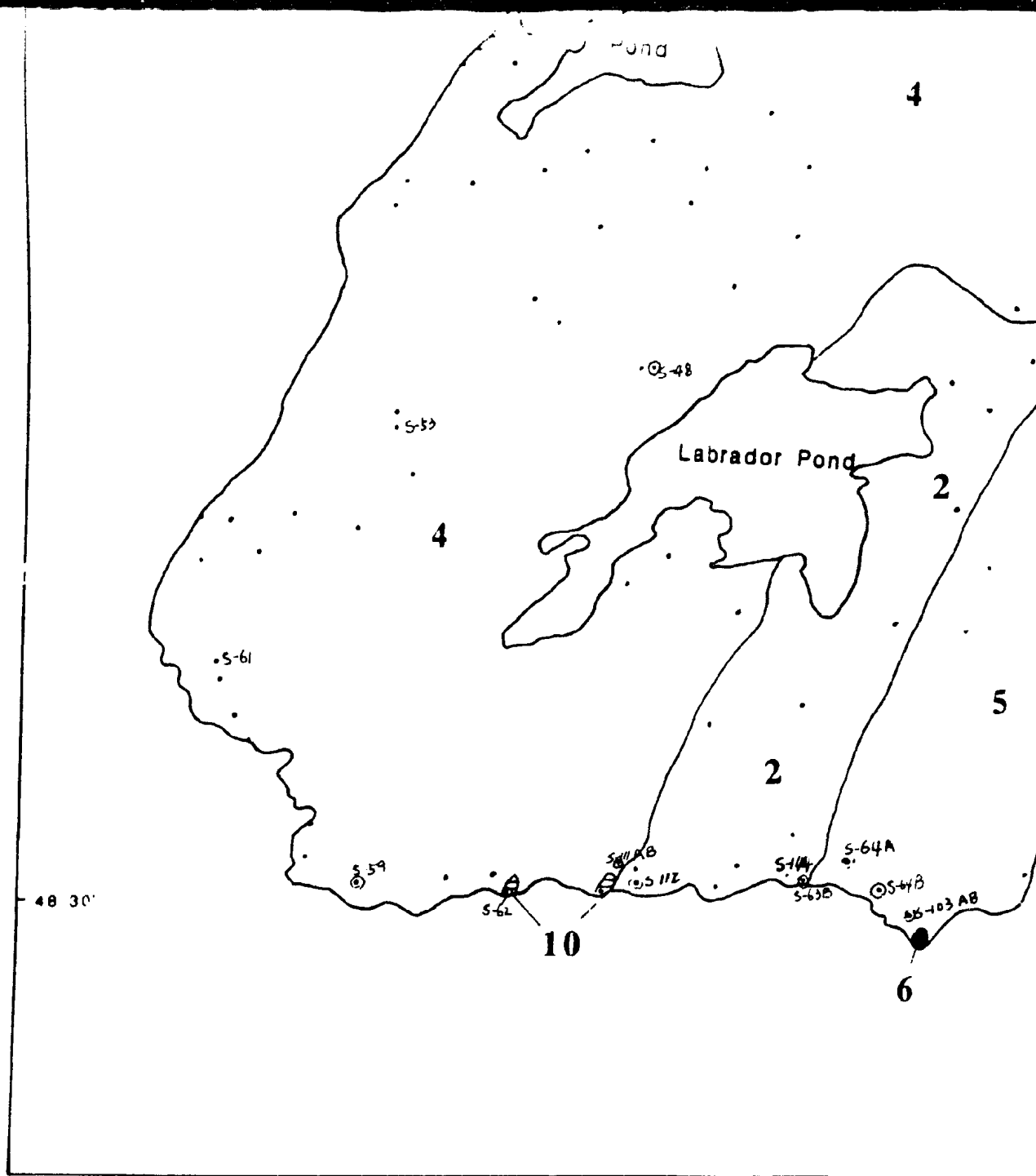
GEOLOGICAL

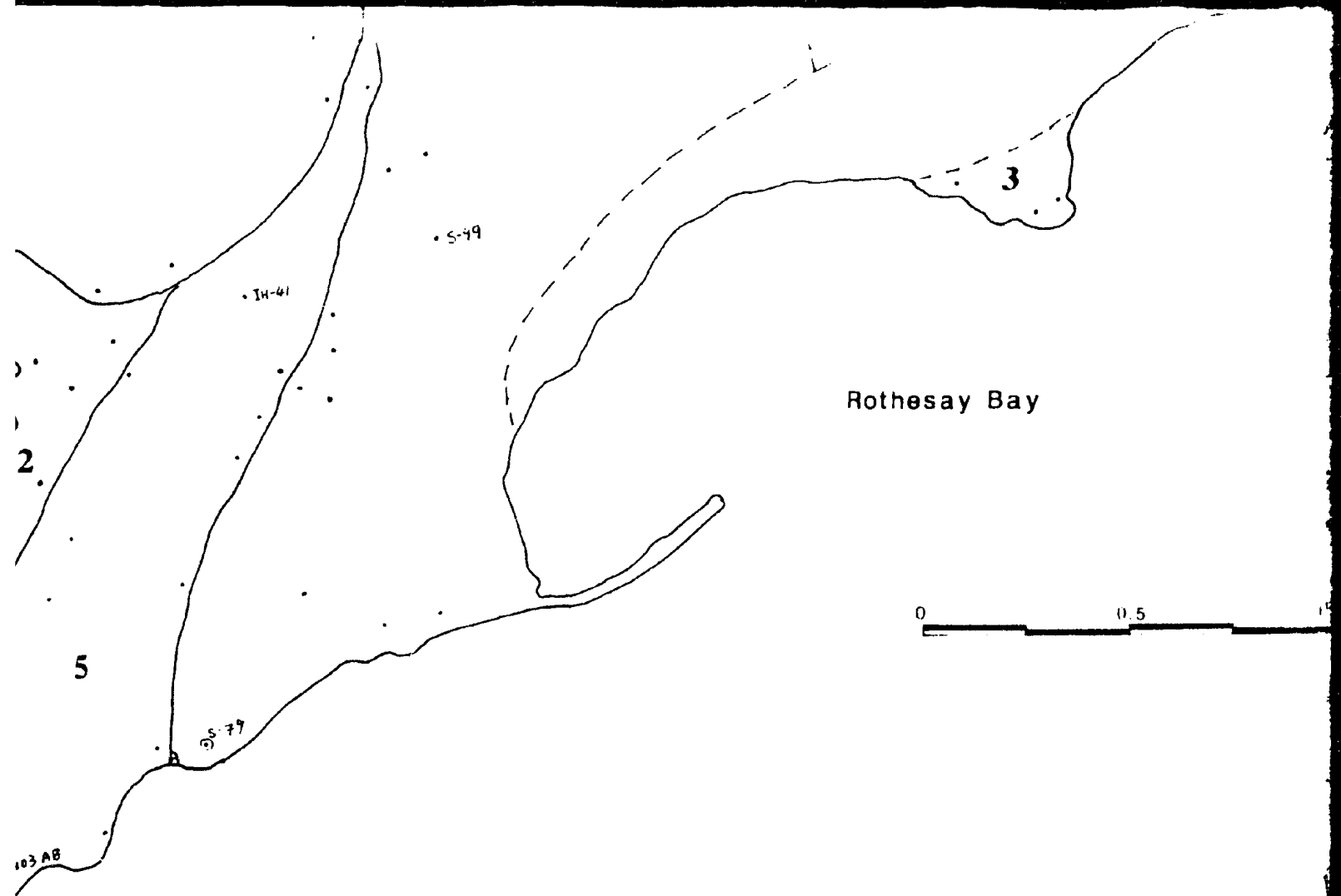
1992

boundary  
ogical boundary  
itation  
ntation

AL MAP OF THE INDIAN  
HEAD RANGE

BY G. W. SUNG







Rothsay Bay

